

**The application of let-through-energy protection in multi-
source interconnected utility networks**

by

Martin Johannes Slabbert

Submitted in partial fulfilment of the requirements for the degree
Doctor of Philosophy (Electrical Engineering)

in the

Department of Electrical, Electronic and Computer Engineering
Faculty of Engineering, Built Environment and Information Technology

UNIVERSITY OF PRETORIA

Nov 2020

SUMMARY

THE APPLICATION OF LET-THROUGH ENERGY PROTECTION IN MULTI-SOURCE INTERCONNECTED UTILITY NETWORKS

by

Martin Johannes Slabbert

Supervisor: Prof. R. Naidoo
Co-supervisor: Prof. R. C. Bansal
Department: Electrical, Electronic and Computer Engineering
University: University of Pretoria
Degree: Philosophiae Doctor (Electrical Engineering)
Keywords: Protection, let-through energy, overcurrent, IDMT, energy-area, energy-volume, medium voltage, overhead lines, renewable generation, distributed generation, interconnected network, multi-source

Medium voltage feeders are evolving from traditional radial topologies to interconnected feeders with distributed generation. For a feeder with a source at either end, the circuit breakers at both ends have to open to isolate a fault on the feeder. The type of overcurrent protection applied to these networks are predominantly of the inverse definite minimum time type.

To evaluate if a feeder conductor is protected from the thermal effect of conducting fault current, let-through energy can be considered. Let-through energy refers to the I^2t heating effect of the fault current for a certain time period and the absorption of this energy as an adiabatic process. The hypothesis that is tested in this thesis shows that it is possible to evaluate conductor let-through energy in a multi-source interconnected network. To evaluate

a conductor's let-through energy exposure, the network has to be considered from a holistic perspective as a circuit breaker operation in a multi-source interconnected network will result in fault current redistributing. This change in fault current will change the protection operating time. The change in fault current and exposure time creates different let-through energy levels over time and at different positions on a faulted feeder. With this change in measured fault current a discrete version of the traditional inverse definite minimum time relay equations have to be used to determine the relay operating time. An average disk speed relay model was also created in this research.

A full evaluation application was developed for evaluating the hypothesis and feeder let-through energy exposure. A new three-dimensional surface and heat map of let-through energy-to-distance-to-time was created within this full evaluation application. The time component of this surface allows other circuit breakers in the network to operate and the fault current to redistribute. The change in conductor let-through energy exposure is captured in the current that is measured at either end of the feeder and the relay operating time (time to trip). To assist with the evaluation the volume under the let-through energy graph is determined so as to provide a single quantifiable comparable number. The hypothesis was proven by means of case studies. Three case studies were used, the first a radial feeder application where elements that influence let-through energy were shown. The second and third case studies were for a multi-source interconnected feeder; one with a strong and weak source and the other with two similar sources at either end of the feeder. Some of the protection elements that were evaluated are high-set elements, auto reclosing and different operating curves. In the case studies it was shown that this full evaluation method works well for evaluating the conductor exposure in both radial and multi-source interconnected networks. This holistic evaluation method assists with identifying elements that influence let-through energy and supports optimising protection settings with the aim of minimising conductor let-through energy exposure.

ACKNOWLEDGEMENT

The University of Pretoria has provided the means to advance myself, learn to think and become a greater asset to the society. This assistance was not only in the form of knowledge but also financial assistance from the university and its generous affiliates. For this I will always be grateful.

Thanks to my two study leaders, Raj (Prof Raj Naidoo) and Ramesh (Prof Ramesh Bansal). The two of you became more than just mentors and study leaders. You knew how to challenge me with opportunity, when to guide me and when to tell me I must look up towards the goal! These are lessons that I would like to pass on to others someday. Thank you Helena Gous, for your friendly and extremely competent assistance and support in administration matters.

Stuart van Zyl, Anura Perera, Paul Keller and Hans Bekker, thank you for the countless debates and exchanging of ideas. These were some of the greatest, constructive sessions I had during this study period. I am appreciative for these sessions and time we have spent together.

To my parents, without your many sacrifices, believe, motivation and care, I would not have been able to reach this milestone. This is a reflection of how you have raised me and the work ethics you have installed in me.

Almari my wife, words cannot state how much I appreciate your unwavering love, support, and patience through all the years of study. Finally, we can go on vacation without me having to study...

I am humbled by the Lord Jesus Christ for gracing me with this achievement.

Martin Johannes Slabbert

July 2021

LIST OF ABBREVIATIONS

AC	Alternating current
AR	Auto-recloser
ARC	Auto-reclose
CB	Circuit breaker
CT	Current transformer
COMTRADE	Common Format for Data Exchange
CRS	Central receiver system
CSP	Concentrated solar power
DC	Direct current
DFIG	Double-fed-induction-generator
DG	Distributed generation
DSL	DigSilent Simulation Language
DSP	Digital signal processor
DT	Definite time
EF	Earthfault
EI	Extremely inverse
ETAP	Electrical Power Systems Analysis and Operation Software
HV	High voltage
IDMT	Inverse definite minimum time
L-G	Line-to-ground
L-L	Line-to-line
L-L-G	Line-to-line-ground
LTE	Let-through energy
LTI	Long time inverse

LV	Low voltage
MAIFI	Momentary average interruption frequency index
MV	Medium voltage
NI	Normal inverse
N/O	Normal open
OC	Overcurrent
PSCAD	Power System Computer Aided Design
PSS	Power System Simulation and Modelling Software
PU	Pick-up
PV	Photovoltaic
RMS	Root mean square
SAIDI	System average interruption duration index
TM	Time multiplier
UN	United Nations
US	United States
VI	Very inverse
VT	Voltage transformer

TABLE OF CONTENTS

CHAPTER 1	INTRODUCTION	1
1.1	PROBLEM STATEMENT	1
1.1.1	Background to the problem.....	1
1.1.2	Research gap	6
1.2	HYPOTHESIS AND RESEARCH METHODOLOGY	9
1.3	RESEARCH GOALS	11
1.4	RESEARCH CONTRIBUTION	11
1.5	OVERVIEW OF THE THESIS	12
1.6	CHAPTER SUMMARY	14
CHAPTER 2	LITERATURE STUDY ON THE EFFECT OF DG ON PROTECTION	15
2.1	CHAPTER OVERVIEW	15
2.2	EXISTING NETWORKS AND EQUIPMENT	15
2.3	DISTRIBUTED GENERATION AND STORAGE.....	20
2.4	DRAWBACKS OF NEW DISTRIBUTED GENERATION	22
2.5	PROTECTING INTERCONNECTED MULTI-SOURCE FEEDERS.....	28
2.6	EXISTING INTERCONNECTION STANDARDS.....	38
2.7	CHAPTER SUMMARY	39
CHAPTER 3	FEEDER OVERCURRENT PROTECTION PHILOSOPHY AND ELEMENTS.....	40
3.1	CHAPTER OVERVIEW	40
3.2	MV FEEDER PROTECTION PHILOSOPHY.....	41
3.3	RADIAL NETWORK LAYOUT	46

3.4	PROTECTION ELEMENTS AND FUNCTIONS	48
3.4.1	Operating curves and equations	48
3.4.2	Maximum time function	53
3.4.3	Reset curve	54
3.4.4	High-set element	54
3.5	AUTO-RECLOSING	57
3.5.1	The number of attempts	58
3.5.2	Dead and reclaim time	60
3.6	PROTECTION ELEMENT APPLICATION	62
3.7	CHAPTER SUMMARY	68
CHAPTER 4	LTE APPLICATION IN DISTRIBUTION NETWORKS.....	69
4.1	CHAPTER OVERVIEW	69
4.2	LET-THROUGH ENERGY DEFINITION	70
4.2.1	Conductor limit and damage	70
4.2.2	Let-through energy	75
4.2.3	Maximum and minimum network conditions	77
4.3	RESISTANCE BACKGROUND	79
4.4	CONDUCTOR SHORT TIME AND LET-THROUGH ENERGY LIMIT	81
4.5	NETWORK CONFIGURATIONS	91
4.5.1	Radial medium voltage network	91
4.5.2	Multi-source medium voltage network	94
4.6	FAULT CURRENT AND DISTRIBUTION	96
4.7	OVERCURRENT RELAY MODEL	99
4.8	CURVE SELECTION	105
4.9	MULTIPLE CONDUCTOR TYPES AND CIRCUIT BREAKERS	109
4.10	THE EFFECT OF THE AUTO-RECLOSE FUNCTION	111
4.10.1	A radial network	111
4.10.2	A multi-source interconnected network	113
4.11	ENERGY-AREA AND ENERGY-VOLUME	119
4.12	CHAPTER SUMMARY	120
CHAPTER 5	APPLICATIONS FOR EVALUATING LTE PROTECTION ...	122
5.1	CHAPTER OVERVIEW	122
5.2	AIM OF THE SOFTWARE APPLICATIONS	122

5.3 FULL EVALUATION APPLICATION.....	123
5.3.1 Defining the primary plant model.....	125
5.3.2 Define the secondary plant model.....	128
5.3.3 Create the required relay model.....	129
5.3.4 Create the required simulation code	136
5.3.5 Set the specific parameters for study	143
5.3.6 Data extraction application	144
5.3.7 Result calculation and presentation	147
5.3.8 Output from the full evaluation application.....	153
5.4 SIMPLIFIED EVALUATION APPLICATION.....	155
5.5 CASE STUDY RESULTS: SIMPLIFIED EVALUATION APPLICATION.....	160
5.6 CHAPTER SUMMARY	162

CHAPTER 6 RESULTS AND DISCUSSION OF LTE PROTECTION

APPLICATION	164
6.1 CHAPTER OVERVIEW	164
6.2 CASE STUDY OVERVIEW	164
6.3 CASE STUDY 1 – RADIAL FEEDER APPLICATION	165
6.3.1 The objective of the case study.....	165
6.3.2 The case study setup	165
6.3.3 Protocol.....	166
6.3.4 Experimental parameters	167
6.3.5 Case study 1 step 2 results – control case	168
6.3.6 Case study 1 step 3 results – source impedance	172
6.3.7 Case study 1 step 4 results – ARC and high-set	175
6.3.8 Case study 1 step 5 results – NI and EI operating curves.....	179
6.4 CASE STUDY 2 – INTERCONNECTED MULTI-SOURCE NETWORK (WEAK AND STRONG SOURCE).....	183
6.4.1 The objective of the case study.....	183
6.4.2 The case study setup	183
6.4.3 Protocol.....	186
6.4.4 Experimental parameters	187
6.4.5 Case study 2 step 2 results – control case	189
6.4.6 Case study 2 step 3.1 results – operating time increase.....	192
6.4.7 Case study 2 step 3.2 results – operating time increase with ARC.....	193

6.4.8 Case study 2 step 3.3 results – operating time increase with ARC and high-sets.....	195
6.4.9 Case study 2 step 4.1 results – deadtime 4 s and 1 s applied.....	197
6.4.10 Case study 2 step 4.2 results – deadtime 0.3 s and 1 s applied.....	198
6.5 CASE STUDY 3 – INTERCONNECTED MULTI-SOURCE NETWORK (STRONG SOURCES)	199
6.5.1 The objective of the case study.....	199
6.5.2 The case study setup	200
6.5.3 Protocol.....	202
6.5.4 Experimental parameters	203
6.5.5 Case study 3 step 2 – control case	204
6.5.6 Case study 3 step 3 – high-set application.....	208
6.5.7 Case study 3 step 4 – reduction in ARC attempts.....	210
6.6 FULL EVALUATION APPLICATION RESULT GENERATION.....	211
6.7 RESULTS: HYPOTHESIS AND RESEARCH QUESTIONS	212
6.8 CHAPTER SUMMARY	220
CHAPTER 7 CONCLUSION	221
7.1 SUMMARY OF THE WORK	221
7.2 SUMMARY OF THE RESULTS AND THE DISCUSSION.....	224
7.3 SUGGESTIONS FOR FUTURE WORK.....	226
REFERENCES	229
ADDENDUM A CASE STUDY INFORMATION	244
A.1 CASE STUDY 1 FEEDER DATA	244
A.2 CASE STUDY 2 FEEDER DATA	244
A.3 CASE STUDY 1 FEEDER DATA	245

CHAPTER 1 INTRODUCTION

1.1 PROBLEM STATEMENT

1.1.1 Background to the problem

Energy. Everybody needs it, when they need it, at minimum cost, as reliable as possible and presently there is pressure to reduce the impact or harm to the environment when generating electricity.

The United Nations (UN) has shown that the energy generation mix within the world is changing [1] and [2]. For the year 2014 to 2017, generation from combustible fuels increased by 6.1 % to that of renewable energy sources of 28.8 % [1]. For the six-year period from 2011 to 2017 the following can be observed for the UN energy mix statistics if it is normalised to the values in 2011. Combustible fuels and nuclear generation stayed fairly constant over the six-year period whereas wind and solar generation showed significant changes. When comparing the different regions of the world the change in wind and solar is most prominent for all the different regions in the world (Africa, North America, South America, Asia, Europe and Oceania).

There was a big change in the installed solar capacity for the South American continent starting at just 7 MW in 2011 and reaching 3523 MW in 2017 [1], [2]. A similar trend is also observed in Asia with an installed capacity of 8411 MW in 2011 and reaching an installed capacity of 218169 MW by 2017 [1], [2]. The installed capacity of wind generation on the Asian continent increased from 67.8 MW to 217.8 MW from 2011 to 2017. In Europe, wind generation increased from 95 MW to 170.8 MW. The greatest increase in generation

capability is within Asia. In 2001, close to 70 % of all electricity that was generated in the United States came from fossil fuels and 30 % was from sources such as hydroelectric and nuclear plants [3]. A very small amount was from other generation types. The United States of America have set a goal of 20 % wind energy generation by 2030 [4]. The UN statistics for North America is indeed showing a significant change towards renewable sources, supporting the drive towards renewables [1], [2].

An article that was published in CBS News indicated that the levelized cost of energy in 2018 for a wind farm was between \$ 29 to \$ 56 per megawatt [5], [6]. For a solar farm this was reported at \$ 31 to \$ 44 per megawatt [5]. A cost of \$ 36 to \$ 46 per megawatt for a solar farm was reported in [6]. The cost of a coal plant was placed between \$ 27 and \$ 45 per megawatt [5], [6]. This shows that it is becoming better to invest in renewable generation technologies as compared to traditional coal generation. The reduction in cost is supported by the increase in wind and solar generation types when considering Figure 1.1.

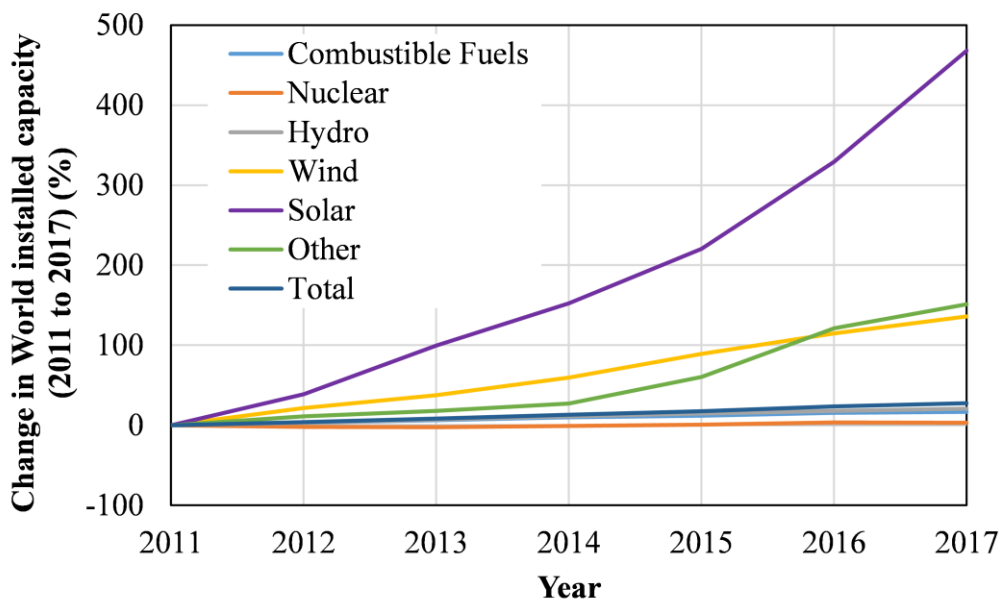


Figure 1.1. Worldwide generation type capacity change from 2011 to 2017.

Figure 1.1 shows how the worldwide energy mix has changed over the period from 2011 to 2017 [1], [2]. The biggest increase is within the renewables. This renewables category includes generation such as wind, solar and other (tide, wave and geothermal marine). From

Figure 1.1, the reduction in levelized costs for renewables and government drives towards cleaner energy (e.g. US target of 20 % wind), it can be predicted that the installation of renewable generation is only going to increase into the future. Over the period shown all the generation types have increased except nuclear that have decreased below zero during certain periods.

In 2019 the commissioned DG (and related technologies) reached a value of 51 GW, an increase of 10 % in one year [7]. Projections for the global market in DG are set to reach a value of US\$ 183 billion in 2025 [8]. For the decade of 2020 to 2030 the total investment into DG is set to reach US\$ 846 billion [7]. Solar photovoltaic (PV) is set to account for the majority of the generation with 88.2 % of the funding allocated for it [7]. It is projected that the top three areas for DG installations will be Asia at 48 %, North America at 17.5 % and Europe at 16 % [7]. The global installed capacity of DG is set to account for 10 % of the generation at a value of 1182 GW by 2030 [7]. Generation installed at consumers premises are set to change the industry. The cost of energy storage is also forecast to reduce by 35 % from 2020 to 2030 [7]. This will promote the installation of this technology into the grid.

In the initial electricity networks, the generation was installed close to the load, but as AC transmission was developed, the generation was moved further away from the load [9]. For the power system network in Figure 1.2, generation is done in large quantities where natural resources (fuel) are present and this energy is then transported to load centres [10]. This bulk power is moved over large distances using high and extra HV transmission lines [9], [11]-[13]. Transmission lines are normally constructed in relatively straight lines whereas distribution feeders tend to follow roads [11]. This helps with the maintainability and initial construction of the distribution feeders [11].

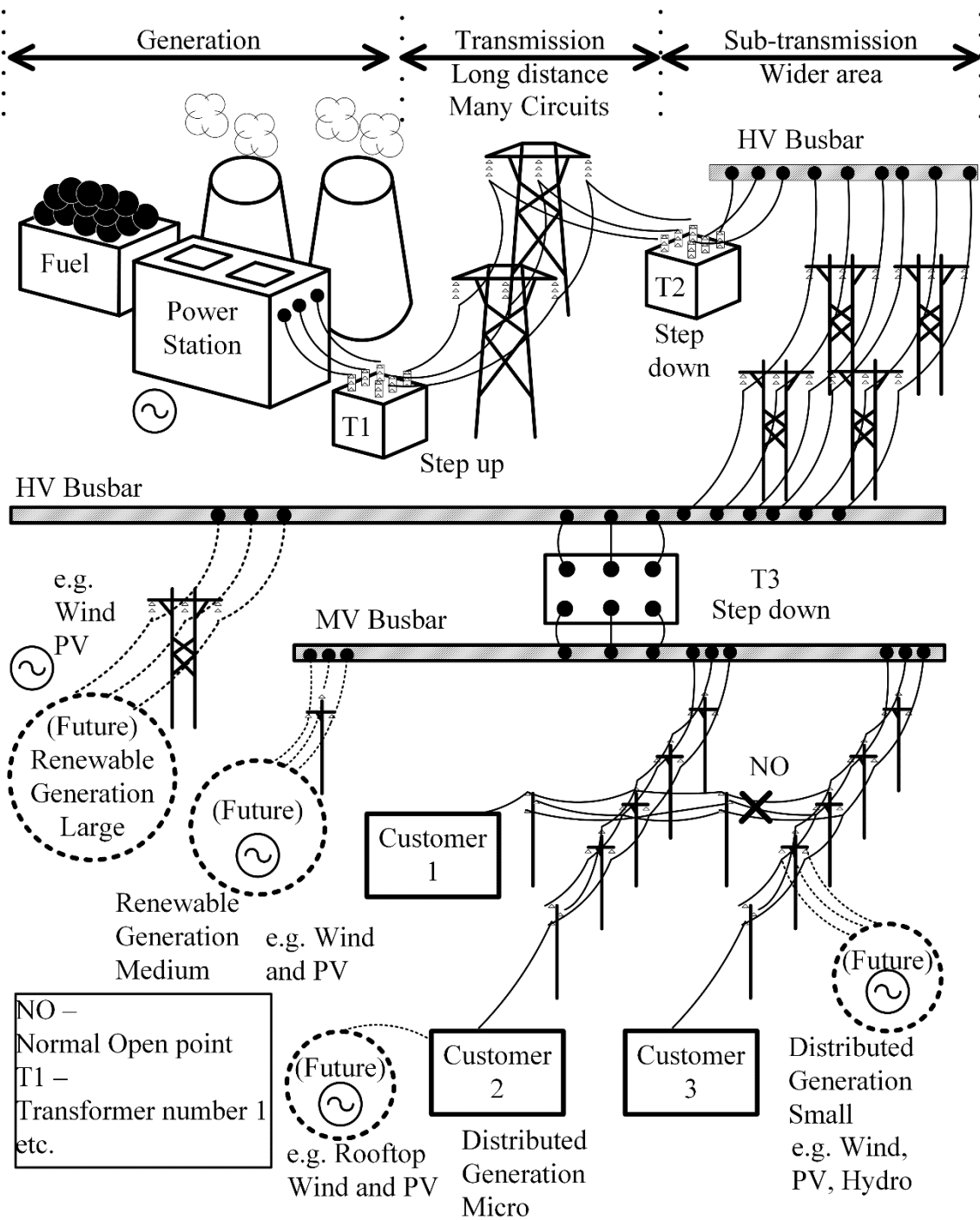


Figure 1.2. General power system network layout.

From these transmission substations the voltage is changed to lower values (step down) for the purpose of further distributing the power over shorter distances. Then, this sub-transmission level is further reduced to distribution level voltages such as medium voltage (MV) and finally to levels for use at the loads itself such as low voltage (LV). The

transmission lines will normally cover a large distance but a small geographical area. Distribution lines will normally cover shorter distances. The distribution feeders do cover a wide area and may have a complicated layout [12]. The MV distribution feeders are traditionally radial in nature [9], [13]. It is found that 97 % of the world population live within a radius of 10 km of an MV feeder [11]. MV is defined by the IEEE as voltages ranging from 1 kV (including) to 100 kV (less than) [14]. The IEC defines this as voltages ranging from 1 kV (excluding) to 35 kV (including) [15]. Within South Africa the distribution code defines this as voltages as ranging from 1 kV (excluding) to 44 kV (less than) [16].

The generation, transmission and distribution of electricity is very inefficient with roughly only a third of the input energy actually being consumed by the customer. The rest of these are accounted for in losses in the transmission and distribution system, inhouse supplies at power stations and the loss in converting fuel to electricity [3]. Larger scale renewable generation wind and solar PV farms can connect to high voltage (HV) busbars due to the magnitude of power that have to be transmitted. By increasing the voltage, the I^2Rt losses are reduced. Medium scale generation can be connected to the MV system directly. Distributed generation (DG) can also be connected to the MV feeder directly. With the reduction in cost of wind and PV generation, increased pressure on governments to invest in green or cleaner energies and the global increase in demand for energy the distributed energy model as shown in Figure 1.2 with all the future generation sources connected is fast becoming a reality for a much wider spectrum of countries. This installation of DG is changing the once uncomplicated radial feeder into a new configuration resembling an HV network.

There are many types of DG that can be implemented on a small scale. Some of these are hydroelectric, biomass, wind, solar, gas or liquid fuel [17]-[19]. Electric vehicles may also start to backfeed into the grid at low voltage levels when they are parked (or docked). The vehicles become an energy storage device in the network under certain conditions [12]. At present, the two most common technology types used are wind and solar. Wind and solar generation can be implemented on scales ranging from a panel placed on a rooftop to a large

farm covering square kilometres. With the generation being so versatile, it is possible to implement different scales of these generating plants that can be used for private generation or then to feed back into the supply grid (small and micro generation in Figure 1.2). This can keep the cost of electricity down if the generation is close to the load centre [20]. By having the generation close to the load, the efficiency of the power system is improved as the losses associated with transporting the power from the traditional large base load power station via the transmission lines and transformers are removed (see Figure 1.2) [20]-[22].

1.1.2 Research gap

MV distribution networks are generally radial in nature due to the simplicity and cost effectiveness of this design [12], [23]-[26]. For a radial network, fault current will always be unidirectional, flowing from the source to the fault (no other infeeds). Customer 1 to 3 in Figure 1.2 are supplied on two radial feeders if the additional DG (small and micro) are removed.

A radial feeder allows the network to be protected using an uncomplicated method of measuring current and operating in a certain time if the current is above a threshold [17], [24], [26]-[33]. This form of protection is called overcurrent (OC) protection. This method of protecting a network has drawbacks in that it is generally slow and not as selective when it comes to isolating a fault (compared to impedance and differential protection). But it is a much less expensive relay. When comparing the cost of an OC and earthfault (EF) relay to a basic impedance and differential relay from one manufacturer it was found to be 44 % cheaper. If a transmission substation is taken offline (due to a fault), it can result in a larger number of customers being influenced than when a distribution station is taken offline. It does make sense in designing a system that is less expensive for distribution MV feeders and a system that is more secure for HV feeders. This can be seen in the relay technology (available functions) and price thereof.

There are many philosophies and approaches available for protecting a MV network. All of these philosophies have criteria that can be defined in terms of sensitivity, selectivity,

security, speed and dependability [21], [34], [35]. These are the main building blocks of any protection philosophy. When setting the devices, the philosophy is providing the guidance on what should be considered as acceptable protection settings for the applied protection elements. For OC protection there are a number of settings that can be set per protection relay that should reflect the philosophy. These are the operating curve, the pick-up (PU) current, the time multiplier (TM), the time delay (depending on curve), the application of auto-reclose (ARC) cycles and perhaps additional operating curves.

The MV OC protection will have to be set to provide the required sensitivity and selectivity. For traditional radial MV feeders there is normally no main protection (e.g. differential) as the MV feeders can branch significantly. As the MV networks are evolving with the application of DG and more interconnectivity between feeders using normal open (N/O) points, the MV feeders are starting to resemble transmission and sub-transmission networks.

Additional generation or interconnections to other feeders does however create a new set of challenges in the traditional radial MV networks. With additional DG being implemented close to the load or on the MV feeder there is now an opportunity for bidirectional powerflow on the feeder [9], [13]. It may be possible for the feeder to island itself from the supply grid under certain conditions. Fault current can also be supplied from the DG (depends on generation type and applied protection). This may change the fault levels [9], [13]. This change in fault levels and bidirectional powerflow can influence the protection operating times (speed), the sensitivity of the protection, the selectivity (coordination) and security (e.g. sympathetic trips).

The main focus of this thesis is to introduce the concept of let-through energy (LTE) protection, show why and how this should be considered in a multi-source or interconnected network. If this statement is broken down into components, we can see that it consists of a number of key concepts. These are LTE, protection, multi-source and interconnected networks. LTE has both a fault current and time component. Both of these are influenced by the DG or interconnected network topology. There are many forms of protection, but OC protection is the predominant type used on MV feeders. To isolate a fault in a multi-source

interconnected feeder, it may require multiple CBs to open as compared to a radial feeder where a single CB can isolate the fault.

As current passes through a material (such as a conductor), the material is heated due to the internal resistance of the material. This heat can alter and weaken the conductor material. If this is the case, the material can then be damaged if the current magnitude is high enough and it is present for a long enough period [10]. The protection equipment should break the fault current prior to this conductor damage occurring, this is LTE protection. Mention is made of LTE protection in the literature [10], [36]. Some guidance towards the application on a radial feeder is provided in [37]. In general, little application information is available for reducing conductor LTE exposure. No mention of the application or philosophy for the application of LTE protection in multi-source or interconnected networks (or a combination of both) are made in the literature. The conventional protection of radial and multi-source networks is discussed in the literature. New developments in these fields extends towards using optimisation techniques to determine the required OC protection settings. The optimisation technique then uses the applicable philosophy (speed, selectivity etc.) to set the constraints. The LTE element has not been used as a constraint in this optimisation techniques for interconnected or multi-source networks. Other forms of protection such as impedance, differential and travelling wave methods are also being applied on newer feeders for the protection thereof.

There are many types of faults that can be found on an overhead feeder. These are three-phase faults, Line-to-Line faults (L-L), Line-to-ground (L-G) and Line-Line-to-Ground (L-L-G) faults [38], [39]. The work done in this thesis is limited to phase OC protection for faults not involving an earth path, thus phase faults only (three-phase and L-L). For the three-phase and L-L faults only positive and negative sequence currents are expected to flow [38], [39].

The philosophy of applying LTE still has to be determined for this changing network towards interconnectivity and multiple generation points. That is the focus of this work.

1.2 HYPOTHESIS AND RESEARCH METHODOLOGY

As the access to small scale renewable generation is becoming more accessible, the electricity industry is changing with generation to be implemented in MV networks. These MV networks also have the ability to be interconnected to other MV networks or feeders for improved security of supply, thus creating another possible source of supply to the MV feeder. Most of the existing MV networks are radial in nature. The feeder interconnections and additional generation is changing the radial nature of these feeders. The protection and protection philosophy applied to these feeders are still predominantly current based IDMT type protection. The hypothesis to be tested in this research is:

A method can be developed to evaluate conductor LTE protection on a MV feeder within an interconnected network and with distributed generation installed.

The main objective of this protection is to develop a method that can be used to ensure the feeder conductor is actually protected in a MV multi-source interconnected network. It was found that LTE protection is a key component of phase overcurrent (OC) protection in radial MV feeders [40], [41]. This research is expanded towards including this new generation of MV feeders (multi-source, interconnected). The main focus of this philosophy is similar to the main focus areas that was used for a radial feeder [41]. For an ideal philosophy, these key points in order of priority are the following:

- The risk at the fault position can be removed.
- Faults will not damage primary plant equipment.
- Load demands can be met indefinitely.

Risk can take the form of risk to life and then the risk to primary plant [42]. Life includes all life, human, fauna and flora. If primary plant gets damaged, this can influence the ability of the utility to meet load demands and this can have far reaching impacts on economies and revenue streams.

From the problem statement provided in Section 1.1 and the objectives that were identified to test the hypothesis, the following research questions are presented:

- What are the fundamental protection relay elements used to protect a MV feeder?
- How can the conductor LTE limit be calculated?
- What protection elements influence the conductor LTE exposure?
- Determine what present methods or philosophies are used to protect multi-source MV networks?

To test the hypothesis comparative case studies will be used based on information gathered while addressing the research questions with guidance taken from the research objectives. Thus, the result validation will be as follows:

- The results are to be verified using comparative case studies.
- A radial feeder will be used as reference.
- A test feeder is to be created. DG and/or multiple sources are too added to this network (feeder is part of this network).
- Case studies will be created for comparison on the same feeder with the same protective devices. A fault will be placed in the network and the protection devices will be required to operate accordingly.
- Utilize the present conventional method of setting the devices.
- An evaluation method will be developed for the results that includes a visual component for fast holistic conclusions. This is required to evaluate the application of LTE to these multi-source interconnected networks.

A network simulation package will be used to develop a model for simulation purposes. Both the network and protection devices will be modelled in the software. The network simulation software will be used to generate raw data (current and time). This raw data will be used in MATLAB where an evaluation application will be created. This evaluation application will be visual in nature.

1.3 RESEARCH GOALS

The following research goals are set to obtain a favourable outcome towards the application and then evaluation of LTE protection in multi-source interconnected networks.

- To develop a holistic evaluation method for phase OC protection applied to MV feeders with DG or multiple sources of supply.
- To determine if LTE protection can be applied to these new generation of MV feeders.
- To develop an evaluation method for the interconnected multi-source network when LTE protection is applied.

1.4 RESEARCH CONTRIBUTION

The contribution that this research will add to the body of knowledge in the gap that exists with the application of LTE protection to MV interconnected multi-source network. The same concept and method can also be applied to HV networks as these networks are already in the form of interconnected multi-source networks. In the literature mention is only made of applying LTE application, but it is not mentioned for the new generation of networks with DG and interconnections. This research will pioneer the application of this LTE protection on these new types of networks and develop a visual method of evaluating if the network is protected. This evaluation method will also be applicable to existing radial networks. Further, this evaluation method can be applied to existing networks that evolve into multi-source interconnected networks.

Outputs from this research:

Patent Application M. J. Slabbert, R. C. Bansal and R. Naidoo, “A method of evaluating circuit protection of a power network”, have been approved by the University of Pretoria for a patent search. Patent application in RSA. Application No. 2020/06849

- Journal M. J. Slabbert, R. C. Bansal and R. Naidoo, "Application of let-through energy to back-up over-current protection on high-voltage feeders," in *IET Generation, Transmission & Distribution*, vol. 12, no. 19, pp. 4341-4347, Oct., 2018, doi: 10.1049/iet-gtd.2018.6190
- Book chapter M. J. Slabbert, R. Naidoo and R. C. Bansal, "Medium Voltage Phase Overcurrent Feeder Protection," in *Power System Protection in Smart Grid Environment*, 1st ed., Taylor & Francis, NY, USA, 2019, ch. 6, pp.197-272.
- Conference M. J. Slabbert, R. Naidoo, and R. C. Bansal, "The application of let-through energy protection to the main and back-up protection elements on high voltage overhead feeders," in *CIGRE Conf.*, Paris, France, 26-31 Aug. 2018.
- Conference M. J. Slabbert, R. Naidoo, and R. C. Bansal, "Adaptive Protection Settings for Medium Voltage Feeders," in *SAIEE Smart Grid Conf.*, Jhb., RSA, Feb., 2016.

1.5 OVERVIEW OF THE THESIS

The research in this thesis is discussed in seven chapters with additional case study information provided in appendix A.

This first chapter is the research methodology where background information with the problem statement is provided. This is also where the hypothesis, objectives, research questions and goals are set to ensure a reasonable scientific method is applied in the course of this thesis.

In Chapter 2 a literature survey is done to determine what the benefits of DG are, what constraints are being introduced towards the traditional protection and what has been done regarding the protection of MV feeders with DG installed. This is with a focus towards identifying the application of LTE protection on these multi-source interconnected feeders.

Chapter 3 discusses the general protection philosophy applied for protecting a MV feeder. The chapter also identifies the basic elements that are used for existing OC protection of MV feeders. This lays the groundwork to understand the typical OC protection elements that are applied to MV feeders, how they are set and what influence the element.

The concept and application of LTE protection is discussed in Chapter 4. This includes the definition thereof and determining conductor limits. Results of determining conductor limits are provided here. The LTE application is discussed from a radial feeder perspective first and then the concept is applied to an interconnected multi-source network. The fault current contribution of dominant renewable generation is also discussed. This is with the aim of characterising the generation when the model is developed for simulation purposes. The effect of changing measured fault current is discussed on relay operating time and a rotating new disc relay model is introduced. This relay model is verified using simulation and calculations.

In Chapter 5 the software tools that are developed to generate results and evaluation methods are discussed in detail. This is done by means of flow diagrams, inputs and expected outputs from the software tools. The simplified evaluation application is applied to an interconnected HV circuit (supply at both ends) as a proof of concept case study.

Chapter 6 is the main result and discussion chapter. This chapter includes three case studies where the main evaluation tool (or method) has been applied to a radial and multi-source interconnected network. The radial feeder application is creating a reference result and shows how the full evaluation application can be used. The results of these three case studies are discussed at each case study. A general result discussion is also included where all the case study results (Chapter 6), research question and hypothesis are evaluated and discussed.

Finally, Chapter 7 serves to summarise the work, draw a conclusion and highlight future research that can be conducted from this work in this field of study.

1.6 CHAPTER SUMMARY

In Section 1.1 the problem statement is defined. At present the electricity industry is changing with the reduction in cost of renewable generation. Traditional MV networks are radial in nature and the protection philosophies applied to them are fit for radial networks. But with the networks evolving towards multi-source interconnected networks, the protection philosophy will have to adapt so as to meet the change in network topology. The hypothesis, research questions and methodology are expressed in Section 1.2. LTE protection is not a new concept, but the application thereof to multi-source interconnected networks are. The hypothesis that is tested here states that LTE can be used to evaluate if a conductor is protected in these new evolving networks. This hypothesis will be tested by means of case studies. Section 1.3 states the goals that are set for this research. The approach is to develop a holistic evaluation approach. Section 1.5 provided an overview of the thesis and what is contained within each chapter.

CHAPTER 2 LITERATURE STUDY ON THE EFFECT OF DG ON PROTECTION

2.1 CHAPTER OVERVIEW

In Chapter 1 it was shown that the traditional radial networks are changing with the growing application of DG. In doing this literature survey there was not any application found on the topic of applying LTE protection to a multi-source or interconnected network. Mention was made in the literature on the equipment that should be protected and some mention is made towards the application of this on a radial feeder, but even this is not detailed extensively. In this chapter a literature review is done on the impact of DG on existing MV network protection. In Section 2.2 the existing radial MV network layout and protection equipment are introduced. An interconnected multisource network is also defined in this section. Section 2.3 presents the various types of DG and storage that are applied to feeders. The negative effect of these new DG units on existing installed protection is explored in Section 2.4. Section 2.5 introduces the various methods used to protect a network that have DG or interconnections installed. Finally, various operating standards are shared in Section 2.6 that are used to govern the operation and installation requirements for DG interconnections.

2.2 EXISTING NETWORKS AND EQUIPMENT

Traditional distribution networks are radial by design [9], [17], [20], [23], [24], [28]-[30], [32], [33], [43]-[50]. Radial can be defined as a network that consists of a single source (or

connection to the supply grid) where one or multiple loads are supplied from this source [9], [17], [20], [26], [28], [29], [45]. Current direction (or powerflow) is only in one direction away from the source [9], [26], [17], [30], [46], [47]. Fault levels are generally high close to the source (or utility grid connection) and then reduce as the fault position is moved further into the radial feeder (away from source) [30], [51]. The protection equipment applied to radial distribution feeders are normally uncomplicated [26]. The protection equipment applied to radial feeders are auto-reclosers (AR), fuses and sectionalisers [23], [28]-[30], [45], [52]-[54]. Substation based relays with dedicated circuit breakers (CB) and current transformers are also used [29], [53]. The actual protection elements and associated settings for these devices are covered in the next chapter.

A radial feeder with various loads is shown in Figure 2.1. This circuit is radial, but with multiple circuit ends (e.g. at load ‘P’, ‘R’ and ‘S’) [34]. On this radial feeder there are three CBs ‘K’, ‘L’ and ‘M’. OC protection is commonly applied to radial feeders in a distribution network [17], [26], [28]-[32], [55]. This is both OC and EF protection. The CBs in Figure 2.1 can be ARs. For the work done in this thesis a focus is placed on faults not involving an earth path.

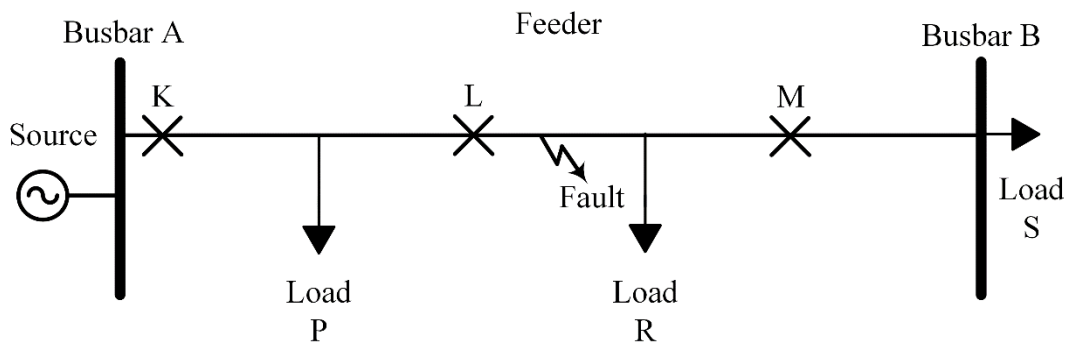


Figure 2.1. A radial medium voltage feeder.

For a radial feeder the fault levels are expected to be at its greatest at the source (Busbar A end) and at its lowest at a point furthest away from the source [29], [30], [51]. This can be Busbar B. If a fault were to occur on the radial feeder of Figure 2.1, the fault current will be supplied by the source and will be measured by CB ‘K’ and ‘L’. CB ‘M’ will not measure any current as there are no other sources on the feeder beyond the fault.

For this fault on the radial feeder of Figure 2.1 coordination can be maintained by grading the network. A coordinated network means that the CB closest to the fault will operate first and if this fails, the next upstream CB will operate (main and backup) [22]. Thus, maintaining selectivity between the main and backup protection. To grade the protection on the feeder the fault has to be evaluated in maximum network conditions [54], [56]-[58]. The maximum network conditions are also used to determine the equipment rating [57]. When determining the sensitivity of the protection element the PU must be set in minimum network conditions [25], [56]-[58]. Minimum and maximum network conditions will be applied in Chapter 3 and 4. To isolate this fault, CB 'L' will have to operate. This can be classified as main protection [26], [32], [35], [42], [58]. If CB 'L' fails to operate, CB 'K' will operate. CB 'K' will be providing backup protection for CB 'L' [22], [26], [32], [35], [42], [58]. CB 'M' does not have to operate as it will not measure any fault current from the source.

If the fault in Figure 2.1 was a bolted three-phase fault with no fault resistance, the voltage at the fault position will be zero as well. The voltage from the fault position back to the source will be a function of Ohm's law based on the product of fault current and the feeder impedance. The duration of the voltage dip is a function of the protection operating time [40], [59]. All the feeders connected to the same source busbar (Busbar A) will experience the same voltage dip due to the fault [40], [41], [59]. Voltage dips may be classified into different types using the NRS-048-2 standard [60].

There may be a number of traditional MV feeders radiating from the same substation (does not have to be the same substation). Between these feeders they may have a N/O point that allows the two feeders to be connected together for a period of time. This N/O point can cause current to be redistributed within the feeder [28], [50]. This results in an interconnected feeder. Parallel feeders terminating on the same remote (far) end busbar can cause the same phenomenon [34]. An interconnected feeder can also be called a multi-loop or loop feeder [50], [61], a meshed network [32] or a ring feeder [48]. By closing this CB (parallel feeders) a loop is created and this improves the reliability of the feeder [23]. Interconnected feeder in the context of this work is defined as a feeder that has more than one point of supply to a

fault on the feeder. When a traditional radial feeder is changed to a ring feeder, it may introduce difficulties with the protection setup [48]. There may be a protection device such as an AR applied at this N/O point to facilitate the switching. This may also have protection elements (e.g. OC protection) applied to it. If another generator is placed on the feeder, this can have the same effect with this generator being another source of current on the feeder [30]. Distribution networks are changing towards becoming more interconnected and having more DG installed [51]. Figure 2.2 shows a feeder with a N/O point and additional generation in the form of a distributed generator. The additional generation has its own protection and CB ‘J’.

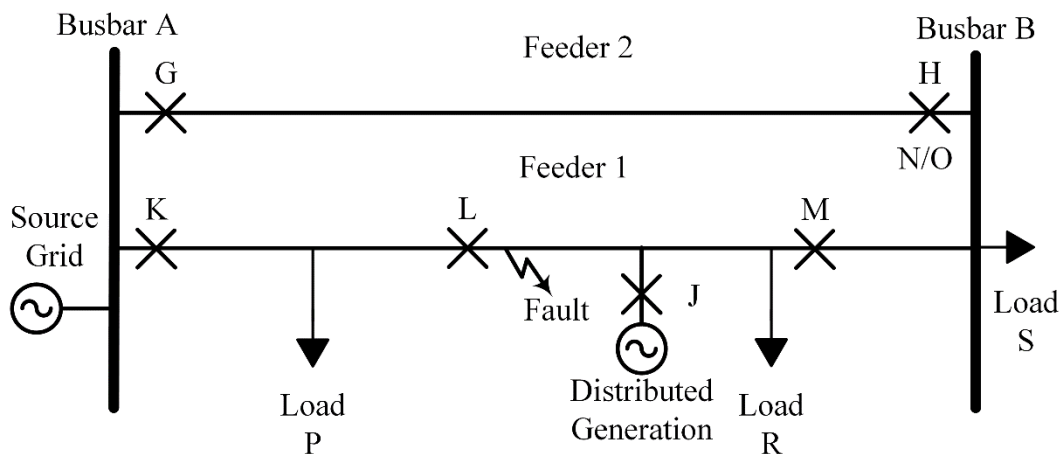


Figure 2.2. A medium voltage feeder with a normal open point and distributed generation.

The literature provides many benefits for installing DG on a feeder. DG is changing power generation from traditional large fossil fuel-based sources to decentralised units [21], [43], [62]. Fossil fuel-based generation produces water and gasses such as CO₂ and SO₂ when the fuel is burned. When renewable generation is installed it is a more environmentally friendly form of energy generation [18], [19], [22], [24], [30], [63], [64]. It aids with the world movement towards decarbonisation [18], [31], [45], [62], [65]. Many governments are providing incentives towards installing renewable generation in the grid [44], [45]. The reliability of the network is increased with the additional DG [18], [20], [22], [31], [43], [64]. The reliability can be defined in terms of improving the availability of supply with redundant generation available for breakdowns [53]. The DG can improve the loss on the feeder [21], [22], [24], [31]. This reduction in loss is due to the DG being installed close to the load centre

[20]-[22], [45], [50], [63], [66]. This network design minimises the power loss when transporting it from the traditional large fossil fuel power stations. The feeder can also support more load with congestion being reduced as generation is installed closer to the load [31]. An interconnected feeder with additional generation improves the stability of the network as there is more generation available to supply the load [53]. Additional generation will also improve the availability of supply with redundant generation available for breakdowns [53].

The voltage profile of the traditional radial feeder is improved when DG is installed [21], [66]. On a traditional radial feeder, there will be a HV close to the source busbar and this will then decrease to a lower level at the end of the feeder. In South Africa acceptable levels are provided in the NRS-048 standard [60]. The DG assists with levelling the voltage profile and can provide voltage support on the feeder.

The penetration of DG refers to how much generation is installed compared to the load on that part of the network [52]. As was shown in Chapter 1 there is an increase in DG installations. With this increase in installations the penetration level of the distribution generators is increasing. This can lead to a scenario where part of the feeder (or network) can operate as an island [17], [52]. Islanded operation may be caused by a fault or the switching of plant (planned and unplanned) [30], [46], [67]. Consider Figure 2.2 without the fault. If CB L is open with the N/O point at CB H open and the generation is capable of supplying Load R and S, that network is being operated in an island mode [18]. That is, independent from the source grid. If the load is much larger than the installed generation, the generation will not be able to sustain the loads and will remove itself from the network.

The literature does indicate that islanded operation was normally not permitted (anti-island protection may be applied) [28], [29], [47], [48], [52], [54], [68]. This was due to safety (electrocution) and technical constraints (closing CB out of phase) [28], [47]. Unintentional islanding can occur [24], [44] and the protection should be able to detect this [26]. There are three broad categories of anti-islanding protection, active, communication based and passive protection [28], [47]. Where the DG penetration is high, there has been a shift toward

allowing part of the network to island [43], [46]. This islanded network can also be called a microgrid. A microgrid is more applicable to a LV network [22], but the use of the concept works well for MV networks as they are evolving to independent grids (similar to HV networks).

A philosophy was proposed in [20] where the DG should remove itself from the grid before any other CB can operate. This may minimise the coordination problem associated with these feeders where DG is installed as the feeder is changed back to a radial feeder (no connection to another feeder in the example). A concept of multi-microgrids are also mentioned where a microgrid can be divided further into smaller pockets [22]. In a microgrid or islanded network the fault levels may be different from the when the network is connected to the grid [22], [30], [46], [50]. This can create difficulties in coordinating the protection for both these network conditions [50]. It may also be difficult for conventional OC protection to function with the low fault currents [22].

2.3 DISTRIBUTED GENERATION AND STORAGE

There are many types of embedded generation that can be connected to a MV feeder. These include small scale fossil fuel plants, solar power plants, biomass plants, micro hydro plants, fuel cells and wind generation [3], [17], [19], [22]. Some of these can be broken down further into subcategories. If we take small scale fossil fuel plants this can be divided into technology such as gas turbines of simple-cycle or combined cycle [3]. There can also be piston driven internal combustion engines that are used to drive an AC generator [3]. There can also be engines where energy is added to a medium outside the engine and this primed medium is then used to drive the engine. An example of this is a steam engine that is driving pistons [3]. When solar power plants are considered, there are essentially three types. The first is concentrated solar power (CSP), the second is a solar central receiver system (CRS) and the third is PV cells [3]. A CSP and CRS plant are another form of a Sterling engine (such as a steam engine) where a medium is primed outside the engine using sunlight and a dish [3]. In a CRS and CSP plant the medium can be water, nitrate salts or air (emerging technology) [3]. Wind generation can be divided into four types based on the generator and interface with

the grid [4], [69]-[71]. As wind at PV generation is most common, they will be considered in more detail in Chapter 5 where their fault current contribution is evaluated for different types of generators.

For hydro plants it can be a pump storage (energy storage), conventional generator constructed below a dam or a generator placed within a river [53]. When considering a pumped storage or conventional hydro plant, the available energy is a function of potential energy or head (this is the vertical height above the generator) and the flow rate that can be achieved [3], [53]. The generators are normally of a synchronous machine type [3], [53].

Fuel cells convert chemical energy into electricity. There are many forms of fuel that can be used, these include methanol, natural gas, hydrogen, etc [3]. Fuel cells do not produce CO₂ and SO₂ which make it more environmentally friendly [3]. Fuel cells have a high efficiency rating [3]. Fuel cells can be supplied by the electrolysis of water and this can be driven by a wind generator [3]. With present sizes ranging between 30 W and 250 kW [3], they may be more readily applied as an embedded generator.

Biomass generation makes use of plant material that is burned to generate a syngas. Most biomass generation work on a steam-Rankine cycle [3]. This plant material can be from forestry waste, the waste from agriculture and certain municipal wastes [3].

There are various forms and variations of DG. There may be slight differences between a CRS plant using salts vs. a plant using water. The generation can be divided into two main groups, one group where the generator is connected to the network directly such as a synchronous machine. The other is where the generator (does not have to be a rotating machine) is connected to the grid through power electronic devices e.g. PV generation. Each of these groups have certain trades that are similar when considering their fault current contribution. The focus in this work is not on the differences, but more that there are many types and their efficiencies and characteristics may differ. In the approach we are proposing, these differences will be captured in the network model used in the network simulation package. This package is used to generate the fault current results.

Renewable generation such as wind and PV generation is not dispatchable [72]. This promotes the need for a storage medium. Storage mediums can be used to improve the effective time use of the renewable DG. Storage mediums can include battery banks, super capacitors, fuel cells superconducting magnetic energy storage, pumped hydro's and flywheels [9], [22], [50], [73]. These energy storage devices can again change the fault currents in the network based on the type of storage [50]. When considering the network diagram of Figure 2.2, an energy storage device may be added next to the distributed generator to improve its availability [9]. Storage devices can however be costly [50].

2.4 DRAWBACKS OF NEW DISTRIBUTED GENERATION

DG is changing many aspects of traditional radial feeders. Traditional distribution feeders were not designed to accommodate DG or interconnections [19]. The operation and maintenance strategies of feeders with DG is changing [62]. Having DG installed on a feeder also changes the network design approach, protection, control of the network and the operation thereof [45], [47]. In this section a focus is placed on the effect that DG has on the protection applied to traditional radial feeders as it has a major effect on this [26], [31], [44]. There may be other influences such as voltage regulation [9] and the effect on metering, but these are not the focus of this work.

In a radial feeder current is flowing in one direction. When DG is introduced there is the possibility of bidirectional current flow [9], [18], [21], [22], [26], [28], [30]-[32], [43], [45]-[50], [65], [67]. Bidirectional current flow on a feeder in principle is not a problem as it is simply current flowing through a conductor. The problem arises when there is a fault on this conductor. To isolate a fault on a radial feeder only one CB has to open. When this feeder has DG or a N/O point that is closed (while circuit is energised), then two CBs have to open to isolate the fault. A traditional radial feeder with newly installed DG is shown in Figure 2.3. If we consider the network of Figure 2.3 and a fault at 'X' without the generation installed, fault current will be flowing from the source grid through CB 'K' in the forward direction to the fault. CB 'L', 'M' and 'N' will not measure any fault current. Forward is seen as the

direction towards the plant that is being protected under normal conditions. For CB 'K', 'L', 'M' and 'N' this would be away from the source grid at Busbar A towards Busbar B. reverse would be in the direction from busbar B to Busbar A. When the DG is connected, CBs 'K', 'L' and 'M' will measure fault current for a fault at 'X'. CB 'K' will measure it in the forward direction. CB 'L' and 'M' will measure it in the reverse direction. CB 'N' will still not measure any current. If the fault was at position 'Y' then CB 'K', 'L' and 'M' would measure the fault current in the forward direction and CB 'N' would not measure any current. If the fault was placed at position 'Z' then all the CBs will measure the fault current in the forward direction. The direction of current flow is dependent on where the fault is, where the embedded generation is installed and where the protection is installed. For the fault at 'Z' the selectivity between CB 'N' and the upstream protection may be improved as 'N' should measure more current than the upstream protection devices [28].

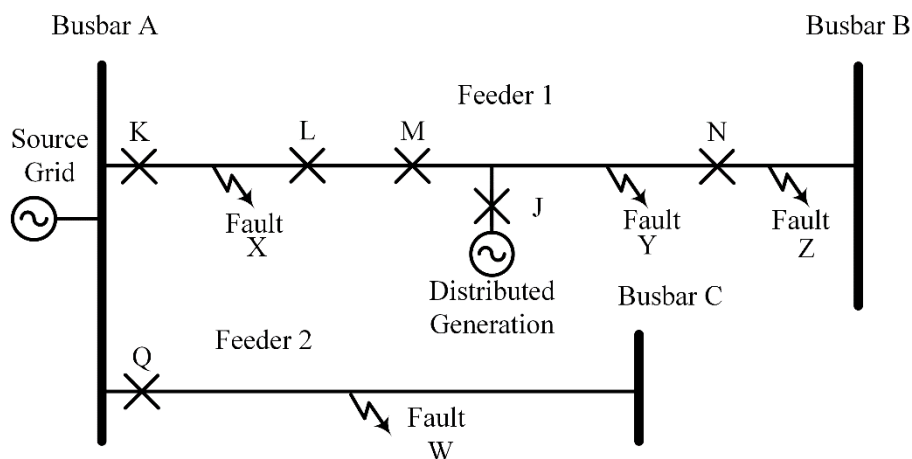


Figure 2.3. A medium voltage feeder with distributed generation installed.

The protection on a radial feeder will be coordinated in a direction (forward) as fault current will normally only flow from the source grid to the fault. When the grid is coordinated, it means that the protection applied to the CBs are graded in both time and current. A graded circuit entails the CB closest to the fault will trip first and then the next upstream CB will trip (slower). If we consider the fault at 'X' and the network being graded from Busbar A to Busbar B, CB 'M' may trip before CB 'L' (CB 'K' will also trip). This is a loss of coordination. There are many aspects that are considered when determining the protection settings that should be applied to the relay. Some of these aspects and elements are covered

in Chapter 3. What is important here is that there may be a loss of coordination between the CBs when DG is installed [20]-[22], [24], [28]-[31], [43], [44], [46], [52], [65], [66]. If a N/O point is closed in a radial network changing the feeder to a multi-source network this loss of coordination may also occur if the feeder was graded for radial operation (in one direction).

In a radial feeder with one supply grid connection the fault current will be high at the source end of the feeder and decrease as the fault moves further away from the supply grid [30]. When DG is installed it can produce a constant fault current that is close to its rated value irrespective of where the generation is connected to the grid. This can influence the coordination when the coordination was based on the reduction in fault current [30].

When DG is installed on a feeder it may reduce the measured fault current [9], [20], [28], [29], [43], [44], [46], [48]. It may reduce the current to such a level that the protection is unable to detect the fault, the protection is thus blinded [9], [21], [24], [26], [28]-[30], [43]-[45], [50]. This may lead to an increased risk to life and damage to the environment (e.g. veldt fire) [28]. Let's consider the feeder in Figure 2.3. For a fault at 'Y' the protection at CB 'L' and 'M' is expected to isolate the fault as main and backup protection devices. This will happen in a coordinated way. If the DG is installed on this feeder then the fault current passing through CB 'K', 'L' and 'M' may reduce. This translates into a reduction in the sensitivity of the protection to faults (protection philosophy is covered in Chapter 3). This reduction in sensitivity can also be called an underreaching effect of the OC element [31]. It is a function of the size of the DG installed relative to the source grid, the fault location and the installed location of the distributed generator [45]. The reason for this phenomenon is that the DG may provide voltage support to the grid at its point of connection which will reduce the current flowing from the source grid. Depending on the operating curves applied to the protection relays, the protection may become slow in clearing the fault [9], [26], [29], [46]. This can result in a loss of coordination with further upstream protection. If this reduction in fault current is to such a degree that the upstream protection at 'K', 'L' and 'M' is not able to detect the fault, the protection is said to be blinded. A possible solution to the new blind areas is to have lower PUs applied with different operating curves [29]. This lower

PU approach may cause new challenges [29]. The currents from motors and rotating DG during start-up may cause a trip. This is increasing the likelihood of a sympathetic trip. There may also be trips due to load.

It is not uncommon for distributed generators to disconnect themselves from the network when a fault occurs [65]. Most grid operators have prescribed a fault ride through time for the distributed generators based on the voltage that is measured by the distributed generator. This fault ride through is to aid in protecting the network, rather than protecting the distributed generator [74]. In the South African Grid code for renewable power plants different categories of generation are specified. These categories are category A1 to A3, category B and category C generators [75]. Category A1 to A3 are for small generators connected at LV ranging in size from 0 to 1 MVA (category 3A is from 100 kVA to 1 MVA). Category B is for generators connected at MV levels ranging from 1 MVA to 20 MVA. Category C generators are for generators larger than 20 MVA. The South African grid code graphs provide the fault ride through requirements for these categories of generators [75].

Figure 2.4 shows the minimum voltage ride through requirements for the types of generation. From this graph, if a category B generator was connected to the grid and the voltage were to drop to 0.4 p.u. then it would be required to stay connected to the grid for one second. For the DG in Figure 2.3, the generator protection at CB 'J' would be expected to open, removing the generator from the feeder. Similar generator ride through criteria is also specified for generation in New Zealand in the Electricity Industry Participation Code – Part 8 [76]. The New Zealand code does not provide a curve for lower voltages, only for 110 kV and 220 kV. Different curves are however specified between the North and South Islands of New Zealand.

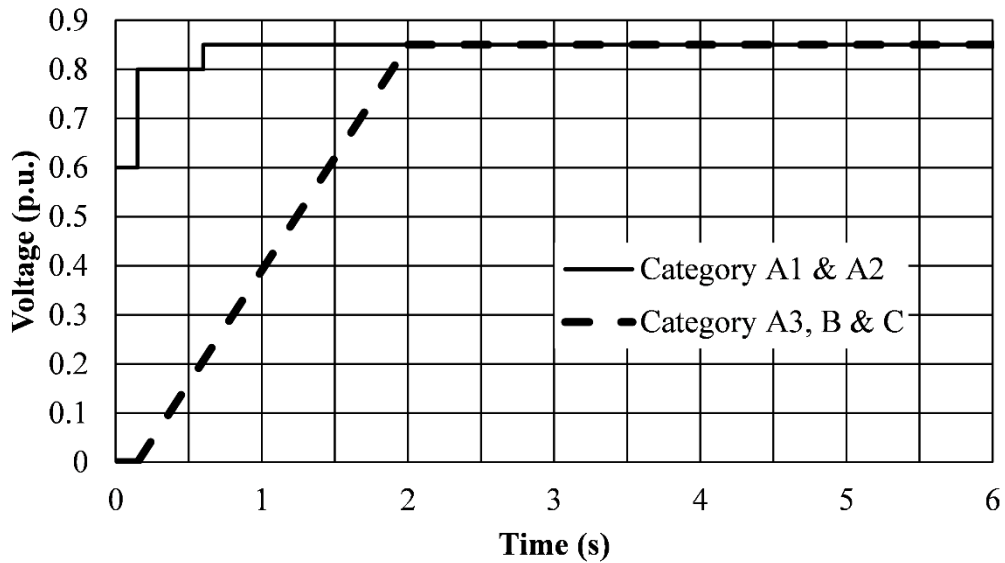


Figure 2.4. Fault ride through criteria for generators in the South African Grid code.

What should be seen from the fault ride through curves is that there are requirements for generators to stay connected. While they are connected the generators are contributing fault current. Once they have removed themselves from the grid, the fault current passing through the network may change again. Elements that were previously blinded may start to PU and others that were not measuring the full complement of fault current may speed up. This therefore has an impact on the protection operating time and coordination.

When DG is installed with ARs and fuses in the network, the coordination between these protection elements may be impacted [30]. This is the case when ARC strategies are used that involve fuse save and fuse blow philosophies [30]. This can be due to the change in fault current and the bidirectional fault current flow.

When a CB operates for a fault elsewhere in the network where it was not designated as main or backup protection (its own circuit is healthy), it is deemed to be a sympathetic trip [9], [21], [24], [26], [29]-[31], [43], [45], [48], [52], [54], [59]. Sympathetic tripping may also be known as false tripping [21], [24], [31], [43], [45]. Sympathetic trips are normally the result of a voltage dip due to a fault [59]. It may also be caused by inrush conditions [54]. When DG is installed on a feeder, it may result in sympathetic tripping for faults on adjacent

feeders [9], [28], [29], [30], [48], [52]. This may happen when non-directional relays are installed [28], [29], [45]. When considering a fault at ‘W’ on Feeder 2 in Figure 2.3, the current from the distributed generator may flow back towards Busbar A and to the fault on Feeder 2 [30]. This may result in the tripping of CBs ‘K’, ‘L’ and ‘M’. Also, the DG may remove itself by opening CB ‘J’.

DG can influence auto-reclosing [26]. Auto-reclosing is applied to improve the availability of the network [20], [29], [58], [65]. This is due to most faults being transient in nature [20], [24], [25], [28], [29], [49]. Let’s consider a transient fault at position ‘Y’ on Feeder 1 of Figure 2.3. If the DG was not connected to the feeder (radial feeder), then the protection at CB ‘M’ would detect the fault, open, allow the air insulation to reassert itself during the ARC deadtime (see Chapter 3) and energise the feeder again (close CB ‘M’). If the DG is connected to the feeder, it may continue to supply the fault, thus maintaining the arc [26], [28]. This will result in an unsuccessful ARC attempt with the fault current still flowing [44]. It may also result in increased damage to the network and risk. This risk can be electrocution and veldt fires [28]. The DG influences the required deadtime setting for the ARC element. The IEEE standard 1547 and Australian standard 4777.3 states that if passive anti-island protection is applied, the generator should disconnect itself within two seconds if the connection to the grid is lost [68], [77]. Auto reclosing may also require synchronisation of the distributed generator to the grid [49], [52]. Even with auto reclosing applied, the CB may fail to close when DG is installed [29], [45]. Even worse, the circuit may close out of phase or unsynchronised [24]. Restoring a network after an outage may be complicated when DG is active within a network [52].

If the DG is of a synchronous machine type, there may be shaft damage to the distributed generator if network faults take a long time to clear [52]. This can happen when synchronisation is lost. A scenario where the electrical and mechanical power on the generator is out of synchronism. This can also lead to stability problems on the network [26].

Not only will the fault current decrease at certain parts of the network, but it may also increase in other parts of the network when DG is installed [21], [26], [29]-[31], [43]-[45],

[48], [66]. Consider the faults at ‘Y’ and ‘Z’ in Figure 2.3. The fault current passing to faults there will be the sum of currents from the source grid and the DG. This increase in current may increase the risk of equipment damage [43], [58]. This increase in fault current may lead to saturated current transformers [30]. CBs will have to be rated for breaking this increased fault current [74]. This increased fault current can also increase fire risk as more pieces of molten conductor can be expelled at the fault position to the surrounding area [78], [79].

Many of the concerns raised in this section are influenced by the type of DG, its installed location in the network and the type of network it is installed in (interconnected vs. radial) [31].

It was found in the literature that damage is not one of the major elements of concern when DG is connected to a feeder. The greater concern was leaning towards the loss of coordination, protection blinding (can lead to damage) and sympathetic trips. The IEEE standard 1547 does mention that embedded generation should not adversely affect the operation of the feeder [68]. The literature does not provide guidance on how to check for damage in an interconnected network. For this work conductor damage is considered and LTE is used as the measure. No application of LTE protection in a multi-source interconnected network was found in the literature. The use of LTE as a conductor damage evaluation method is encountered in [37], [40], [80], [81]. The application of LTE will be covered in Chapters 4 to Chapter 6.

2.5 PROTECTING INTERCONNECTED MULTI-SOURCE FEEDERS

For each of the protection methods or types (e.g. impedance protection) that will be discussed there are vast amounts of literature available. This is normally based on the protection concept. The philosophy of how to apply this protection to evolving networks (e.g. security vs. sensitivity of protection) is the basis of much discussion. In this part of the literature survey the various methods used to protect interconnected multi-source networks are identified. It is found that there may be slight differences between two applications of

differential protection where one application may have added a voltage element for security as an example. In general, the main types used to protect these networks are listed as there are too many subtle differences to list all of the approaches.

With most MV distribution networks being radial in nature there is most likely only OC protection applied [29]. OC protection is applied to protect networks with DG [18]. OC protection is not ideal for protecting networks that have inverter based DG installed [18], [28]. With inverter-based generators not being able to supply significant fault current an energy storage device such as a flywheel can be implemented with the distributed generator to increase the inertia of the ‘source’ [28]. The same holds for networks that are evolving into interconnected networks where current can flow in multiple directions. A complete redesign of protection strategies is required [28]. As the distribution network is evolving, it is resembling a transmission network [28].

The protection applied to the CBs may be directionalised [18], [21], [28], [30], [31], [45], [52], [54], [74]. Directional protection is very often applied to distribution networks where DG is being installed based on its relative low cost and effectiveness [21]. In Figure 2.5 a feeder with directional protection is shown. To make protection directional two quantities have to be measured. In Figure 2.5 these are the voltage and current using a voltage transformer (VT) and a current transformer (CT). This allows for one to be used as a reference (or polarising quantity) and the other as a direction element [31], [54], [82]. Voltage is used as the polarising element as it does not change its phasor position as compared to the current [31]. The direction is thus determined by the product of the polarising element and directional element and the cosine angle between them [31], [83], [84]. The traditional OC element is actually supervised by a directional element in the relay [83]. Based on this there are two regions defined, the first is forward and the second reverse. Forward is normally towards the protected object and reverse away from it. If another protection relay and CB were to be installed at Busbar B on the feeder, it may see forward as towards Busbar A if another source is connected to Busbar B (similar to Figure 2.2 with the N/O point closed). There are a number of methods to achieve directional protection. One

classical method is using a quadrature measurement [31], [83], [84]. The other more modern method involves using sequence components [82]-[84].

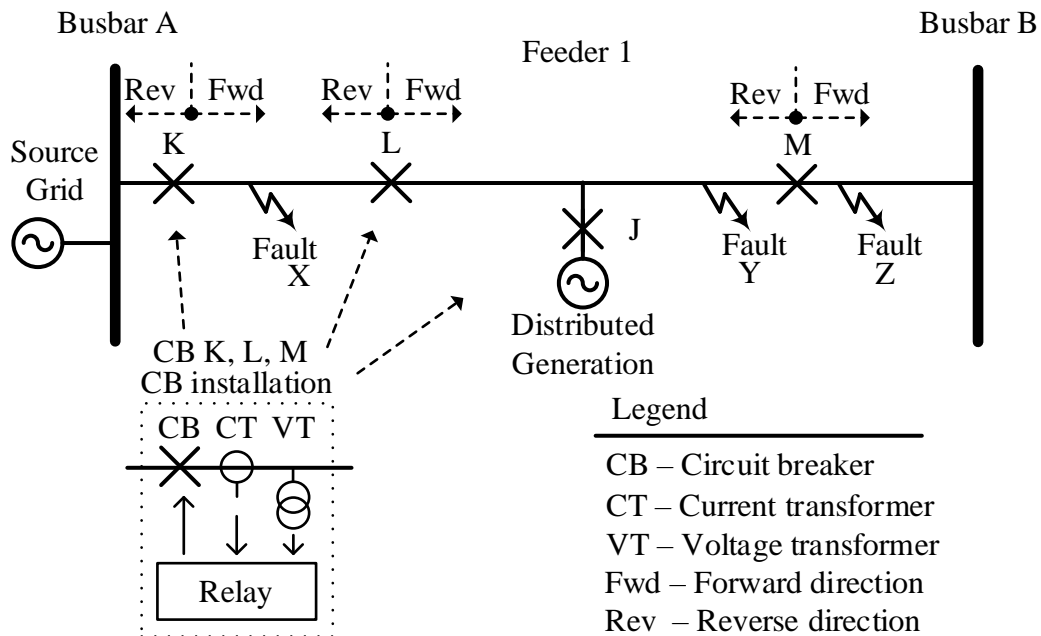


Figure 2.5. Directional protection applied on a feeder.

OC protection can only be graded in one direction if it is non directional. This means that the relay will not distinguish between a current flowing in the forward or reverse direction. The relay will operate in a coordinated way for current flowing in the graded direction. For radial networks this is adequate. When the network becomes interconnected (or looped) directional protection is required [45], [84]. If DG is installed directional protection is also required as it will result in bidirectional current flow [28], [30]. If the protection is Figure 2.5 is graded in the forward and reverse direction, the protection should clear a fault at 'Z' in the sequence of CB 'M', 'L' and then 'K' (excluding DG). All of this protection should see the direction as forward. If the fault is at position 'X' then CB 'K' will see the fault as forward, 'L' will see the fault as reverse and 'M' will not measure any current (no source or interconnection from Busbar B). The OC protection can be set to block for a reverse fault (e.g. CB 'L') or it can be set to operate on different protection settings when the fault is in the reverse direction. The protection can thus be set to grade in a forward and reverse direction.

There are constraints however when implementing directional protection. There may be a loss of polarising element that can render the protection ineffective. The polarising quantity may be too small to measure for closeup faults, rendering the directional element ineffective [82]. Memory voltage has been introduced to allow for closeup fault clearance, but the memory voltage may be ineffective when slow protection is applied [82], [84].

There is no requirement for a communication medium to other parts of the network when an OC element is directionalised. This makes it a very uncomplicated and cost effective first step to improve protection performance on a traditional radial feeder where the network is changing towards an interconnected multi-source network. This also assists with sympathetic trips.

The protection applied to an interconnected multi-source feeder can be made adaptive [18], [21], [22], [26], [28], [30], [44]-[46], [50]. Adaptive protection means the protection may change depending on network conditions or elements being measured (voltage, current sequence components, etc). This adaptive protection may make the protection faster and more selective [44]. In the previous paragraph directional protection was introduced and this allowed different protection elements to be applied to each CB for a fault in the forward and a fault in the reverse direction. This directionality principle is allowing adaptive protection to be applied [50]. Adaptive protection can be applied without the need of a communication medium [50]. This makes it a good approach to minimise costs for existing radial networks with capable relays that are evolving. Other forms require communication [21], [26], [44], [45]. There are various forms in which adaptive protection can be implemented. This can be in the form of just changing certain elements on a relay (e.g. desensitising a PU) [85], selecting different protection groups on a relay (e.g. group forward vs. reverse) [54], [86]-[88] and obtaining new settings from a central computer based on network conditions [22], [50]. These new protection settings can be based on predefined conditions (evaluated offline) or it can be made to determine the settings based on actual real time network conditions [50]. The predefined method is more likely to be implemented [87]. A method of applying different predefined group settings for islanded and normal grid connection was proposed in [21], [46]. A drawback of predefined network conditions is that the fault current may not

flow as predicted [44]. This can influence the protection performance again. Parallel feeders may be tied together using a tie CB [54]. This can be done either remotely or from a local control unit. This will change the fault levels and current flow direction again.

An adaptive scheme consisting of a central controller and relay sensing (installed on the feeder) are mentioned [28]. This scheme made use of OC protection where the protection settings applied to the relays installed on the feeder are changed based on the network configuration. Predefined network conditions are identified for this scheme. Communication infrastructure is required for this scheme to function. A similar approach is also mentioned in [22].

There are numerous constraints when implementing adaptive protection [50]. Not all the protection relays used in the existing feeder may be capable of adaptive protection. It may be difficult to upgrade them to enable adaptive protection. To determine the protection settings, all the possible network operating modes, possible fault types and fault positions have to be determined before the scheme is applied. Determining these fault currents can prove to be difficult for all conditions. It may be costly to implement a communication scheme if the adaptive protection scheme requires one.

Differential protection can be applied [18], [28], [30], [50]. There are a number of forms of differential protection, this can be based on current measurements, voltage measurements or a combination thereof [34]. This can be used for a phase comparison scheme, directional comparison or a distance protection scheme using teleprotection [34]. In this section the focus is placed on the current differential which is a directional comparison method based on the complete phasor (magnitude and phase) at each end [34].

Current differential protection is based on the principle of current that enters a node has to leave a node. If there is a mismatch (above a minimum limit), then there has to be a fault on the node [34], [50]. The node in this case is the protected feeder. The differential protection concept is shown in Figure 2.6. The protection is bound by the physical current transformer

measurement positions. For the differential protection to work, it requires a communication medium between the relays [18], [28], [30].

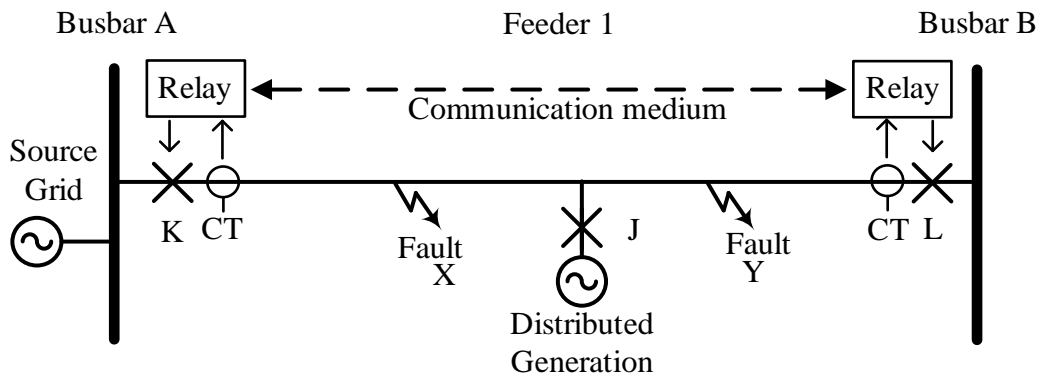


Figure 2.6. Differential protection applied on a feeder.

Differential protection is fairly immune against fault level changes and bidirectional current flow (resulting from DG and interconnections) [30], [50]. This is due to the differential nature of the protection. Differential protection can be set sensitive as they are limited by instrument transformer errors [34]. These errors can be as a result of external transients [34], [50]. The bias is used to improve the sensitivity and security of the differential scheme as it is a function of the fault current measured [34]. If DG is applied to the feeder of Figure 2.6, the generator should also be included into the differential calculation. This may require similar relays at each end of the feeder and at the generator point of connection. This protection may also be adequate during islanded operation of the network (e.g. source grid at Busbar A trips). The differential protection may clear faults in the region of 50 ms [50]. This is a combination of CB operating time and relay time. A relay operating time of 5 ms is provided in [18]. For the feeder in Figure 2.6, whether the fault is at “X” or ‘Y’, it will operate at the same speed. With the fast operation for faults in the protected region, and the ‘no operation’ for faults outside the protected region, grading is not a concern for differential protection [34]. Differential protection can be set sensitive as it is not as susceptible to load currents (bias setting and comparing measurement at both ends) when comparing it to OC protection. There are deviations from the classical differential method where it is combined with symmetrical components to provide better selectivity for different fault types [89].

There are however a number of drawbacks when applying differential protection to a feeder [50]. Another form of backup protection is required if the communication medium fails. This may be OC protection at a distribution level. The required communication medium and associated infrastructure may be costly to implement. When comparing the differential scheme to an OC relay it is substantially more expensive [30]. When connecting and disconnecting DG it can create transients that may influence the protection [34], [50].

Impedance protection may be applied to feeders [18], [28], [30], [50]. Impedance protection can also be named distance protection as the distance to the fault is a function of the impedance measured [34], [50]. Impedance protection in its basic form is non unit protection, but when it is combined with a communication medium and protection at the remote end, it may be considered unit protection [34]. Impedance protection allows for fast fault clearance (region of 40 ms) and can provide remote backup protection [34]. Impedance protection that uses an admittance principle can operate when the network is in islanded and grid connected modes [18]. A feeder with impedance protection is shown in Figure 2.7. In its fundamental form impedance protection is based on Ohms's Law with measured voltage being divided by measured current [34].

Different zones of protection may be set on an impedance relay. This can include a zone 1 instantaneous element set to cover in the region of 80 % of the feeder (can be a bit more or less depending on relay technology) [34]. This zone is set less than 100 % to allow for errors. These errors include measurement errors, inaccurate network data and relay errors [34]. The zone 1 reach will thus not reach past the remote (or far end) busbar (Busbar B in Figure 2.7). Zone 2 is normally set to cover 100 % of the line and then an allowance is made for the same errors of zone 1 resulting in a minimum setting of 120 % of the feeder impedance [34]. As this is overreaching the feeder, a time delay is added to slow down the zone 2 element to allow for selectivity with downstream protection (protection beyond Busbar B) [34]. This delay can be in the region of 200 to 500 ms [34]. The zone 2 time delay can vary in more complex network arrangements. In Figure 2.7 fault 'X' will be cleared by the zone 1 element and zone 2 will clear a fault at 'Y'. Other zones may also be set, such as reverse reaching (towards Busbar A) and far overreaching zones (towards Busbar C) in an interconnected

power system [34]. There are various impedance characteristic curves that can be applied to the relay. These include mho (with variations) and quadrilateral operating regions or characteristics [34]. A directional element may also be applied to the impedance measurement [34].

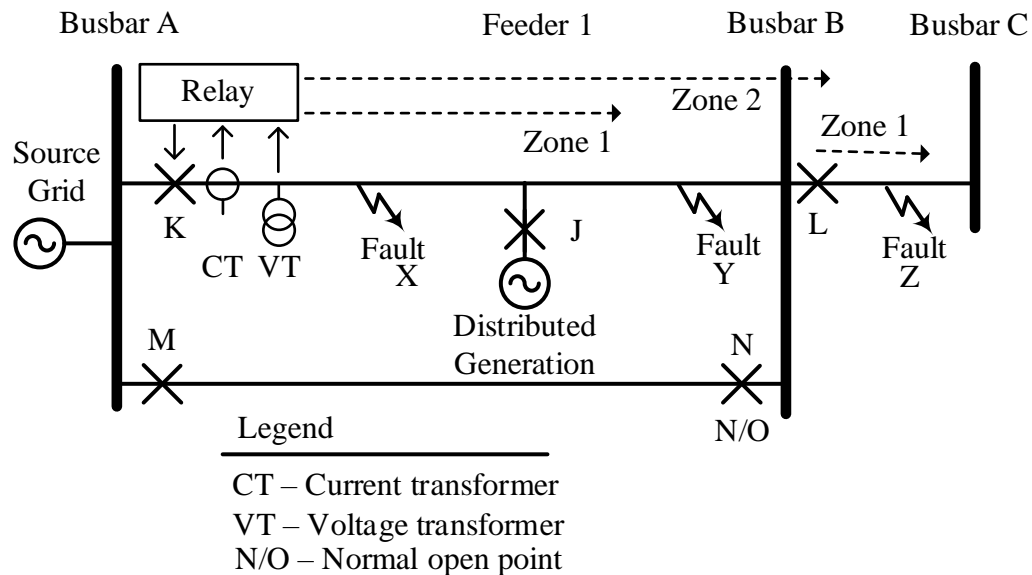


Figure 2.7. Impedance protection applied on a feeder.

Constraints that can be encountered when applying these relays are the following. Fault resistance can influence the measured impedance [50]. Short lines may not be of suitable for impedance measurements [34], [50]. The voltage at the relay measuring point may be too low to measure the impedance accurately (memory voltage may be applied under certain conditions) [34]. The additional voltage transformer can increase the costs of this scheme [28]. Transients may influence the relay accuracy when obtaining the measured signal fundamental components [50]. Remote infeed may cause the relay to underreach (not detect the fault as measured impedance is greater) [30], [34], [43]. This happens if additional DG is added to the feeder such as in Figure 2.7. Underreaching may cause the impedance element not to operate or be delayed (e.g. operate on another slower zone reach setting) [30]. Overreaching (measuring a smaller impedance than the expected) of the impedance element can also occur [9], [34], [43]. This is for parallel lines where one is taken out of service. If the N/O point in Figure 2.7 is closed and the relay is set to detect faults at ‘Z’ under this network condition, the impedance relay can measure faults beyond the next line section

zone 1 setting (CB 'L' zone 1) if the N/O point is opened [34]. For impedance protection elements fault resistance and load current can also influence the directional determination [84].

If there are lines in close proximity to each other, the feeder may be subject to mutual coupling which influence the measured impedance [34]. Mutual coupling may be more common at higher voltages or on circuits that share the same structure. Mutual coupling may influence the reach settings of the impedance zones. For the network of Figure 2.7, if impedance protection is applied to CB 'K' with a blocking or permissive overreach scheme active and the N/O point closed at 'N' there can be a situation called current reversal for a fault on feeder 2 [34]. In this phenomenon both Feeder 1 and 2 will be tripped (incorrectly). There is additional current reversal protection that can be applied. Determining the protection settings for the impedance elements may be more demanding than the OC elements [28].

Protection schemes centred around a voltage measurement are also used [18], [50], [67]. In [67] a method is proposed where the measured voltage at the embedded generator is used. This voltage is transformed from an 'abc' voltage to the 'dq' reference frame. Using this reference frame, the protection scheme was able to detect short circuits and if the fault was within or outside of the protected zone. An adaptive protection scheme was mentioned in [28] that allows for protection against voltage sags. In this scheme voltage and current thresholds are used and depending on the levels measured, the relays will trip either instantaneously or on a time delay. In [64] a method for detecting faults in both islanded and grid connection mode was suggested based on the busbar voltages and direction of current flow. Some challenges for voltage-based protection were identified in [50]. These challenges included the required communication medium, the costs involved, the possible network contingencies have to be known before the voltage scheme is implemented and the present fleet of protection relays will have to be replaced to meet the voltage-based protection scheme requirements. More variations of these voltage-based schemes are mentioned in [50].

Other voltage-based protection schemes are centred around the harmonic content of the measured voltage [28]. The total harmonic distortion in the voltage signal at the point of

connection is measured. If the value is above a level, it will trip the local CB. The measured values at each of the distributed generators are also compared. Another protection scheme for radial feeders with DG installed (not a radial feeder anymore) are proposed in [90]. In this approach fault detection modules are used, with traditional OC protection, directionality is applied and voltage measurements are used on top of this.

Development was also made towards improving normal OC protection by including sequence components into the protection design [28], [30], [50]. The aim of this was to improve the performance of the OC protection during islanded mode. In [89] negative sequence and zero sequence components were used to improve performance with regards to L-L and L-G faults. This was done using a communication scheme, staged tripping and adaptive protection settings.

The use of blocking signals with OC and sequence components is mentioned in [28]. These signals can assist distribution networks in maintaining redundancy and selectivity. This does require a communication medium.

Travelling wave methods are mentioned in [28]. In this method the polarity of the reflected wave is compared to determine if the fault is in or out of zone. Fault clearing using this method is faster than traditional methods. This method may be susceptible to disturbances and discrimination between an actual fault and a disturbance may have to be evaluated further.

Similar challenges as sympathetic trips, unscheduled islanding, protection blinding, selectivity and change in fault levels are also reported for LV networks [91]. LV networks are also traditionally radial in nature with OC protection and DG have a similar impact.

There may be some variants on these protection schemes where certain elements are supervised by another. It is recommended that the approach towards protecting a multi-source interconnected network should be from a holistic perspective [28]. Communication infrastructure is required for most of the protection methods [28]. Other network protection

elements such as phasor measurement units may be required at distribution level [30]. This can create a real time wide area monitoring protection scheme for these distribution networks with DG installed [30]. This is recommended as compulsory for a smart grid [30]. It is recommended by [9] that smart grid technologies such as adaptive protection be applied when DG is installed. There are many variants available for the mentioned protection functions in this section. In some cases, these are combined to improve either selectivity or sensitivity. In [52] it is said that the installation of DG may cause damage to customer and network equipment. An investigation into the effect on coordination and protection device ratings are requested in [20]. In general, damage is not mentioned often or at all, a focus is placed on the items mentioned within Section 2.4 and 2.5 of this chapter. The determination of optimal OC settings by means of a genetic algorithm was applied in [92]. In this application the damage curve of a cable was considered and was added to the objective function.

When OC protection is applied to an interconnected multi-source network it can be very difficult to determine suitable protection settings. This is evident if one considers all the constraints that are introduced when a normally radial feeder is transformed in this way. The literature indicates that optimisation techniques are used very often to solve this [32]. Various techniques have been applied. This includes a dual simplex algorithm [61], cuckoo search algorithm [32], Firefly algorithm [32], Simulated Annealing [32], JAYA algorithm [32] and a Genetic Algorithm [32]. There may be more methods available that may have been applied.

2.6 EXISTING INTERCONNECTION STANDARDS

Utilities normally specify how DG may connect to the distribution feeders [52]. This protection is generally related to the point of common coupling (PCC) between the grid and the DG. At this PCC this interconnection standard normally specifies how the protection should behave. This can include the generator having to disconnect itself during a fault and that the protection at this PCC should be able to protect the utility grid and the generator from damage (transient over voltage and fault current) [52]. This behaviour can influence

when and how much current is being allowed to flow on the faulted feeder. The IEEE 1547-2 standard for interconnecting distributed resources with electric power systems with its amendment 1 is used as a reference point in much of the literature [68], [93]. The author of [63] compared many of the interconnection standards available. These include the following standards: British standards that govern the interconnection are the BS EN 50438 of 2013, Requirements for the interconnection of micro-generating in parallel with public low-voltage distribution networks [94]. In Germany there is a guideline published in 2008 named VDR-AR-N-4105 Power generation system connected to LV distribution network [95]. In China the interconnection standard is Q/GDW 480-2010 Technical rule for distributed resources connected to power grid [96]. These standards are only mentioned here to show that there are numerous interconnection standards available. There are more standards available that may address certain parts of the network interconnection.

2.7 CHAPTER SUMMARY

Section 2.2 defined the traditional radial feeder and interconnected multisource feeder. The two main differences are the possible directions of current flow and number of CBs required to isolate a fault. Benefits of this interconnected multisource feeder was shared. In this chapter the traditional radial feeder was transformed to an interconnected multi-source feeder. Section 2.3 identified forms of DG. This included wind, hydro, CSP, CRS, PV and biomass generation. Storage of energy on distribution networks was shared in Section 2.3. Storage mediums included flywheels and batteries among others. The constraints of installing DG on a traditional radial network was shared in Section 2.4. This included elements such as protection blinding, bi-directional current flow, loss of coordination and changes in fault levels. These constraints focused on the protection system where traditional OC protection is normally applied. The various ways of protecting these interconnected multisource feeders have been shared in Section 2.5. The protection is still predominantly OC based with additional elements such as directionality, security (sequence components) and adaptability that are added. Other methods such as impedance and differential protection are also applied. Finally, standards used to govern the installation and operation of DG on feeders are mentioned.

CHAPTER 3 FEEDER OVERCURRENT PROTECTION PHILOSOPHY AND ELEMENTS

3.1 CHAPTER OVERVIEW

Traditionally overhead MV networks are designed to be radial [97]. Designing a radial network is relatively uncomplicated, starting with the source and then meeting the load requirements further down at various positions on this feeder. The protection philosophy and technology were also uncomplicated [97]. CBs (with relays), ARs and fuses are used to protect these networks. As fault current only flows in one direction, there is no need for directionality and as such grading a network (or then feeder) is fairly uncomplicated.

In this chapter, protection philosophy and protection element application for an overhead MV feeder in a MV network is discussed. This protection is limited to phase OC protection. The concept of protection philosophy is discussed in Section 3.2 and this can be understood well by using radial networks. Section 3.3 defines a typical layout of a radial feeder with the expected protection devices applied. The key protection elements and functions that can be enabled on ARs (and substation-based relays) are introduced in Section 3.4. The typical application of these protection elements (such as the choice of operating curve) is shared in Section 3.5 in an example application on a radial feeder with a top-down grading method.

3.2 MV FEEDER PROTECTION PHILOSOPHY

A feeder cannot be designed that is not susceptible to faults [54]. Hence, the necessity for protection and the protection philosophy. Protection philosophy forms the basis for how the complete protection system should perform within a certain physical section in the network, type of network or for equipment specific protection. The main protection philosophy building blocks are reliability, sensitivity, selectivity, speed, and security [6], [21], [31], [34], [35].

When defining a protection philosophy, the details pertaining to these building blocks have to be defined. Speed indicates how fast the protection system can detect and then clear or isolate a fault in the network. Generally, a protection system should clear a fault as fast as possible [21], [31], [32], [34], [42], [44], [58], [59], [98]. This will reduce damage and promote safety [25]. The speed of the protection system is influenced by a multitude of factors: type of relay technology, type of protection element, operating curve, actual settings of the protection element, magnitude of fault current and fault resistance. The relays can be divided into four time categories, namely instantaneous (no time delay), time delay (introduce delay time before trip signal), high speed (relay sends trip signal in less than 50 ms) and ultra-high speed (relay send trip signal in less than 4 ms) [42]. Having faster protection operating times will reduce the effect of the fault on the power quality of other healthy equipment [99].

The sensitivity of the protection system indicates at what current level the protection system operation will be initiated, in other words, how sensitive or insensitive is the specific protection element to the detection of a fault. The protection should be sensitive to faults [21], [31], [100]. The sensitivity of the protection is influenced by the protection philosophy, the relay technology, magnitude of fault current, and fault resistance. The protection philosophy influences the sensitivity of the PU by determining what level of plant should be removed to determine minimum fault levels and to what degree other protection should provide backup. If the protection system is selective, protective devices will be graded with

CHAPTER 3 FEEDER OVERCURRENT PROTECTION PHILOSOPHY AND ELEMENTS

each other to allow the device closest to the fault to try and clear the fault first [31], [44]. If this device (closest) fails, the upstream device will then have cleared the fault. This selectivity ensures that the smallest portion of the network will be interrupted [54], [101].

The reason for keeping the interrupted part of the network to the smallest portion possible is because the number of customers interrupted has an impact on energy sales. An interruption can also influence the utility's image, and this can have an impact on the investments in that country or on the utility for obtaining loans and the interest associated with the capital. This interruption can also influence customer processes (manufacturing) or the ability for utility customers to provide services to their customers in the retail and commercial environment. Thus, customer satisfaction is influenced [29].

The reliability of the protection system can be defined as the protection system will operate every time it is required to do so [34]. Protection systems are human-made, and hence they will fail at some stage. This is similar to network faults; a network cannot be designed that is immune against faults [54]. Regular maintenance of the power system protection equipment can prolong the times between these failures, but it will not completely prevent them. The maintenance strategy for these devices can be scheduled-based maintenance or condition-based maintenance. The security of the protection system can be defined as the protection system should not operate when it is not called on to operate [42]. In laypeople's terms, the protection relay should not just trip randomly (no fault present). The security of the protection system can be influenced by aging of the protection equipment (from experience with old relays in the network), and then changes in the network that change the network configuration and fault levels.

Reliability can be seen as a combination of dependability and security [34], [42]. Dependability refers to the ability of the protections scheme to operate when it is asked to do so [34], [42]. Between security and dependability, a greater emphasis should be placed on dependability when the level of backup protection is not deep. A greater emphasis on dependability is preferred in [42], [58]. As an example, a wrong trip is more acceptable than a "no trip" from a safety perspective. Where the level of backup protection is high and a

CHAPTER 3 FEEDER OVERCURRENT PROTECTION PHILOSOPHY AND ELEMENTS

wrong trip can result in a wide area incident, protection security has a higher priority. An example of this is extra HV buszone protection where an incorrect trip can result in a complete loss of supply to a large region consisting of multiple substations and backup is provided by dual main protection schemes and overreaching remote end protection schemes.

When developing the philosophy for protecting the network, many of these philosophy building blocks have to be weighed against each other. The protection philosophy cannot be such that 100 % of all the building blocks are present. As an example, sensitivity and security may be conflicting [101], [102]. Priority of the philosophy elements are important. If sensitivity is the main priority, then setting the OC PU to a minimum value (e.g. zero ampere) means that the protection element will be able to detect any current (fault and load) flowing in the protected circuit. This will compromise the security of the protection as the protection can trip for current that is not due to a network fault (e.g. load current). A low PU can also compromise selectivity (between series devices) when current grading is considered. By raising the PU to a high or maximum value, it will make the device secure in that it will not trip for any current, but it will also not trip for any fault current. The protection can be set to operate as fast as possible (e.g. zero second time delay), but then selectivity with downstream protection devices may not be obtained. Hence a balance is required between the various building blocks. In general, protection systems are designed to be more dependable than secure [42]. From this discussion, it can be seen that the protection philosophy forms the basis for any protection system as it will govern which protection functions should be active, how they should be set, and on which faults the protection should operate. It can also influence the protection scheme design and choice of required hardware (e.g., type of protection relay).

The main objectives of protection for MV feeders (in terms of priority) are to preserve life, protect equipment, reduce the risk of fire, promote the reliability and quality of supply and reduce life cycle cost [37]. The first and most important objective is to safeguard life (also safety) [58], [103], [104]. This includes not only human life but life in general. Animals can get electrocuted if they make contact with low hanging conductors. It is not always possible to save the first life that makes contact with live apparatus [58], but a protection system

CHAPTER 3 FEEDER OVERCURRENT PROTECTION PHILOSOPHY AND ELEMENTS

enables one to avoid further incidents and avoid subsequent loss of life. Very often there is a larger focus placed on selectivity (grading), rather than sensitivity and protecting life [103]. A study represented in [105] shows that 65 % of the participating utilities take grading with upstream protection into consideration when designing protection settings. In the same study 63 % take downstream grading into consideration and 44 % is looking at security towards load. Only 39 % included far end fault levels for reach settings and 51 % took the conductor thermal withstand into consideration. The protection system should protect the equipment installed in the network [103]. Failures of equipment can lead to lengthy outages and difficult fault-finding exercises in large networks. In resistively grounded networks such as those used in Australia and South Africa, a fault (i.e. clashing conductors with arcing) can lead to heated pieces of conductor being thrown around the faulted position [78], [103], [104], [106]. If the conditions are conducive to the development of veldt fires (dry, windy, presence of vegetation, etc.), a fault on a conductor in a resistively grounded network can lead to the ignition of veldt fires [104]. The expelled particles can be in the region of 0.5 to 2.5 mm in size [104]. The temperature of this melted drop of aluminium is approximately 2300 K [104]. This can again endanger life, damage the environment and have financial implications. The way in which the protection is set can affect the behaviour of the protection during network faults. It can unnecessarily affect the quality of supply, for example, with excessive voltage dips (also called voltage sags) when trying to clear a fault [107], [108]. Similarly, if the selectivity is not maintained, it can lead to larger parts of the network being without supply for a single fault. Then finally, by reducing the time and frequency of equipment fault exposure, the life expectancy of the equipment can be prolonged. An example of this is the cumulative damage to supply transformers as a result of through faults in the MV network [109]. Supply transformers that supply distribution feeders are subjected to an increased amount of through faults [110].

To combat relay failures and to improve the protection system's dependability, the concept of backup protection is introduced. The individual relay's dependability is not improved; rather, the protection system as a whole is improved. Two concepts are thus introduced: main and backup protection. Main protection is faster than backup protection and is normally functional in a smaller or equal area (sensitivity to faults) in the network. In a classic HV

CHAPTER 3 FEEDER OVERCURRENT PROTECTION PHILOSOPHY AND ELEMENTS

feeder, there would be main protection in the form of impedance or differential protection and backup in the form of OC relays (both phase and EFs). Main protection responds quickly to faults on the feeder as the fault position or boundary is known (e.g., on the feeder) and which protection is required to clear the fault. Backup protection relays provide protection in case the main protection fails to detect the fault [9]. The backup protection will be sensitive to faults at or beyond the reach of the main protection and as such can lead to a loss of selectivity for faults beyond the protected feeder. Because of this, they are generally set slower than the main protection to allow for main protection on and beyond the feeder to clear the fault first. In MV feeders, there is traditionally only current-based protection; hence they have to be set in a certain way to provide this backup functionality to the system. The word set refers to their physical position on the feeder and their applied protection settings in software. It is not required for main and backup protection to be installed at the same physical location in the network [42].

The protection settings that are applied to protective devices are based on the protection philosophy. The philosophy should be such that it is robust. The robustness means that if the network conditions change, the applied protection settings are still valid or effective. The relay does not know if the fault levels in the network changed e.g. a transformer being faulted or out for maintenance. Or, if a downstream CB operated thus changing the intended reach of the protective devices. This status update can be created by means of an automation system in a smart grid environment. In a smart grid system, the protection system (and relays) can then adjust itself to meet the reconfigured network. Even when the system is then reconfigured, the new applied protection settings should still reflect the protection philosophy. To achieve the robustness the protection functions, have to be set under minimum and maximum network conditions [54]. For current based protection, minimum network conditions refer to a network contingency that will result in the minimum fault current passing through the device that is being set for a specific fault. Maximum network conditions refer to maximum fault current that will pass through the device being set for a specific fault. For radial feeders, minimum and maximum network conditions are achieved by changing the source impedance such as switching in and out source transformers [54].

CHAPTER 3 FEEDER OVERCURRENT PROTECTION PHILOSOPHY AND ELEMENTS

Maximum network conditions are normally easy to define with all source transformers in service [54]. Minimum network conditions can be complicated when considering loading and probabilities of network plant out of service. For a radial network it is normally set by removing source transformers and setting minimum load [54]. If the minimum or maximum network condition is too extreme, it can hamper the way in which the protection functions are set and the expected performance from the feeder. For these extreme conditions, compromises, mitigation strategies or additional protection equipment or elements might be required to meet an acceptable application level of the protection philosophy.

A number of network performance indicators can be used to measure the performance of the MV feeder and then the network in general. These indicators are a good feedback loop when evaluating actual feeders and then to check for improvements on the feeder performance. Reliability indices that can be used are specified in the IEEE Std 1366 [111]. This can include indices such as system average interruption duration index (SAIDI) and momentary average interruption frequency index (MAIFI) among others. The momentary indices are generally more relevant to protection performance.

3.3 RADIAL NETWORK LAYOUT

Figure 3.1 shows a radial MV feeder with a substation-based feeder CB, ARs, a sectionaliser, fuses and a number of loads on this feeder. The use of inline fuses on MV feeders is not recommended [37] because it can lead to bad network availability (long outages), many customers being affected by one backbone fuse operation, extra labour hours for replacing the fuses when they are blown (and they can be replaced with the wrong type of fuse, which is a human error), they are not visible to a control centre (SCADA system), fault finding in the network is difficult and the risk to utility personnel increases as they have to go out to the actual fuse installation to replace the fuse [42]. Fuses can have a negative impact on protection performance indicators such as SAIDI [111].

A sectionaliser can be described as an intelligent isolator or disconnecter [52]. A disconnecter cannot break load or fault current; thus, it can only be opened when there is no

current flowing through the disconnector. The same applies to a sectionaliser [112]. A sectionaliser is thus used in conjunction with a normal CB upstream from its position [52], [54], [109], [113]. This allows for a smaller portion of the network to be sectionalised if the fault is downstream from the sectionaliser. For the feeder in Figure 3.1, sectionaliser 1 is used with AR 3. For the protection philosophy covered in this chapter, inline fuses and sectionalisers are not going to be considered as part of the network. The work can be extended, towards including these protective devices if required.

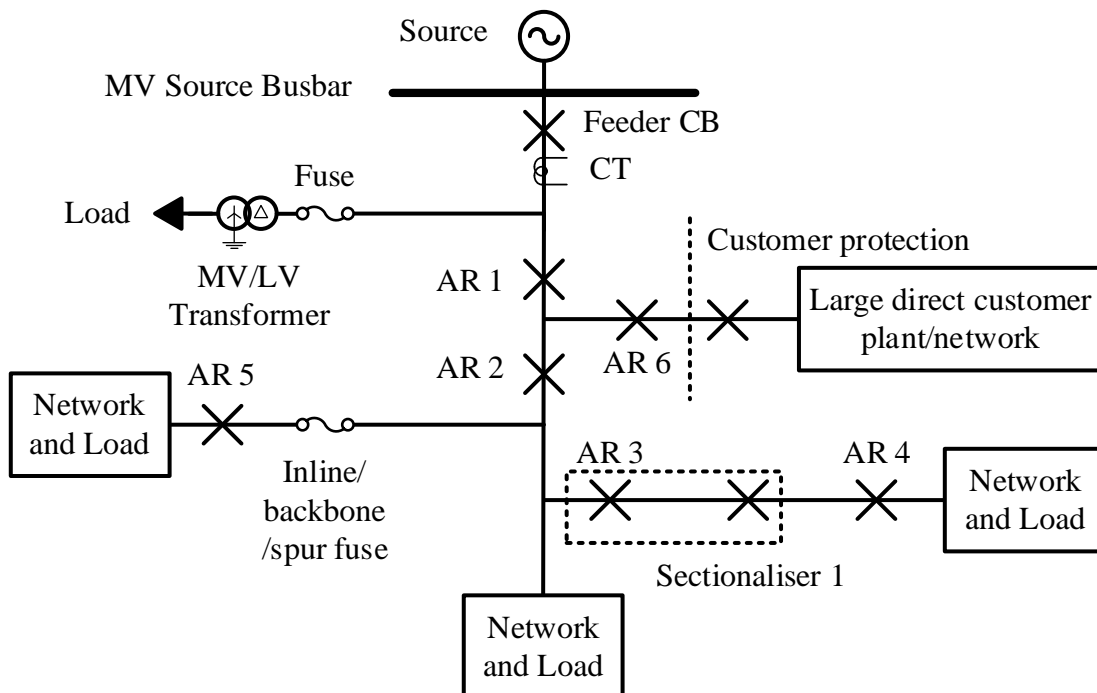


Figure 3.1. A radial medium voltage feeder showing commonly applied protective devices.

Fuses are used at the MV/LV transformers to improve the network availability. They are not installed to protect the MV/LV transformer. This means that if there is a fault on the MV/LV transformer, its own protection should protect the unit and the fuse should remove the transformer unit from the network, thus promoting the continuity of supply to the rest of the non-faulty feeder. Protection is required to isolate only a limited (faulted) portion of the network [114]. These fuses are sized to be insensitive to transients such as transformer inrush and lightning, and also the continuous current rating (load current estimate) of the downstream MV/LV transformer (security element of philosophy).

In the context of this thesis, the feeder CB protection technology can be seen similar to that of an AR. In an actual substation, the feeder CB protection is normally a dedicated relay with a much larger variety of protection functions and capabilities than the AR.

3.4 PROTECTION ELEMENTS AND FUNCTIONS

In the previous section, various types of protection equipment and their typical positions on a radial MV feeder were introduced. Details on typical protection elements, operating characteristics and functions are provided in this section. These operating characteristics refer to how they can be set to isolate faults in the network. All of the functions are not always enabled and it depends on the type of protective device, the network layout, fault levels and protection philosophy that are applied.

There are various types of relay technology that are present in power system networks. They can be placed into four categories [34]. These are electromechanical relays, static relays, digital relays, and numerical relays. Each type or generation of relays have their own characteristics. For this thesis, the relay technology is set to numeric relays. Electromechanical devices are very limited in functionality and many of the static relays are being replaced in existing networks. The difference between a digital and numeric relay is in its processing capability. Numeric relays make use of digital signal processors (DSP). These are processors that are optimised towards signal processing and this has improved the speed of the relay [34]. There are more functions in one of the modern relays (e.g. numeric) as compared to the electromechanical relays [42]. With numeric relays the relay functionality and operation (user definable logic with other relays) are very customisable.

3.4.1 Operating curves and equations

IDMT operating curves are well suited for use in a power system as the protection will trip quickly during high fault currents and slowly during low fault currents [52], [115]. This is excellent for coordinating multiple protection devices in series, but can result in long operating times [115]. The operation of current based protection relays is governed by the

 CHAPTER 3 FEEDER OVERCURRENT PROTECTION PHILOSOPHY AND ELEMENTS

selection of a time current operating characteristic or curve. Depending on the relay technology (as discussed in the previous section) the relay might only have one operating curve or it can have multiple. In both cases there will be some parameters that can be set to move the characteristic curve around in the time-current plane. There are a large variety of curves available. In modern relays these curves can be combined or set to operate simultaneously. Some relays also allow for customisable curves [116]. The IEEE and IEC define standard IDMT operating curves and their equations for the industry in their respective IEEE std. C37.112 and IEC 60255-3 standards [25], [34], [117]. The standard curves are named differently between the two standards, but the same approach is applied to both. Both have a standard inverse curve which are then changed to become more inverse in other defined curves. For this work the IEC curves are applied. The curves are named normal (or standard) inverse (NI), very inverse (VI) and extremely inverse (EI) curves. There are other curves such as the long-time inverse (LTI) curve but these are not considered for this thesis. The method that is developed here can be extended to include the other curves. The constant time adder functionality has not been included in the curve equations below.

$$\text{NI curve} \quad OT = \frac{0.14 \cdot TM}{\left(\frac{If}{PU}\right)^{0.02} - 1} \quad (3.1)$$

$$\text{VI curve} \quad OT = \frac{13.5 \cdot TM}{\left(\frac{If}{PU}\right) - 1} \quad (3.2)$$

$$\text{EI curve} \quad OT = \frac{80 \cdot TM}{\left(\frac{If}{PU}\right)^2 - 1} \quad (3.3)$$

For (3.1) to (3.3) If refers to the fault current (A), PU is the relay PU current (A), TM is the TM (unit less) and OT is the relay operating time (s). This relay operating time is the programmed delay time based on the applied protection settings and when this time is reached, the relay will issue a trip signal to the CB. The TM and PU values are user selectable settings for each curve. The operating curve can be moved right (more secure) on the time-

 CHAPTER 3 FEEDER OVERCURRENT PROTECTION PHILOSOPHY AND ELEMENTS

current graph by increasing the PU and left (more sensitive) by decreasing the PU [58]. The operating curve can be moved up (increase time delay) on the time-current graph by increasing the TM and down (decrease time delay) by decreasing the TM [58]. At a certain fault current value (I_f in (3.1) to (3.3)) for the curve) the relay will reach a straight line in terms of operating time. This means that irrespective of fault current, as long as it is more than this value, the relay will have a constant trip time. The rationale behind this is based on the relay limitations. As an example, for an electromechanical relay the disc can only turn that fast (the electromagnet gets saturated) [118], [119]. In a numeric relay the algorithm execution time takes a certain time or the closing of contacts to energise the trip circuit. This can also be seen as a saturation level for the curve based on the magnitude of the current passing through the relay. This part of the curve is called the minimum definite time section of the curve. A definite time (DT) curve can also be selected as an operating curve. The equation for a DT operating curve is provided in (3.4).

$$\text{DT curve} \quad OT = \begin{cases} TD, & |I_f| > PU \\ \infty, & |I_f| \leq PU \end{cases} \quad (3.4)$$

where OT is the operating time (s), TD is the time delay of the curve (s), I_f is the fault current (A) and PU is the PU current setting (A) of the curve. The DT curve is well suited for networks where there is a significant change in source impedance (results in changing fault levels) which will result in mal-grading when IDMT relays are used [34].

A combination of curves can be created where the DT and IDMT curves are combined. The DT curve can be applied as a high-set or instantaneous curve. This high-set will have a time delay set to zero seconds. A time delay can be applied to allow for selectivity with downstream devices if the required level of security for the element cannot be attained. The operating curves for (3.1) to (3.4) are shown in Figure 3.2 with no saturation for high currents. The graphs show the relay operating time (after which a trip signal is sent) to fault current values.

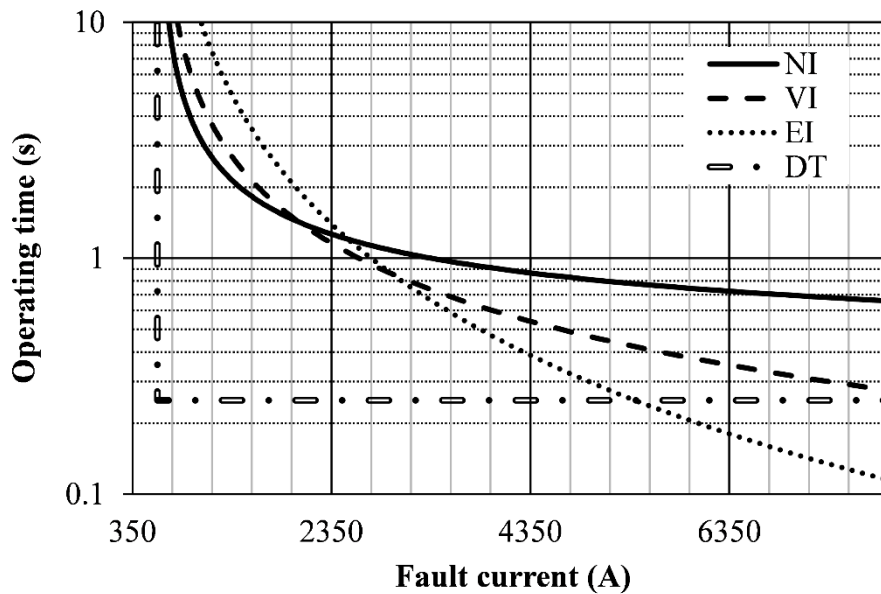


Figure 3.2. Relay IDMT operating curves.

In Figure 3.3 a radial feeder with high and low fault current regions is shown. There are CBs (or AR) applied to this feeder. There is a relay controlling each of the CBs. In this thesis, when the term CB is used, it implies the complete CB with protection relay controlling the CB except if reference is made to a specific element (e.g. relay). A NI and EI operating curve are applied to the feeder CB. The operating times for the relay operating curves are superimposed on to the feeder at the various CB positions. The operating time axis is shown on the left with time increasing away from the feeder and zero time at the feeder. The grading margin between upstream and downstream devices are also indicated.

The curves shown in Figure 3.2 are all set with the same PU of 600 A and TM of 0.25. The inverse nature of the curves shows the fast fault clearance at high fault currents and the longer operating times at low fault currents (also illustrated in Figure 3.3) [26]. When comparing the EI curve to the NI curve it can be seen that there is benefit in using the EI curve on feeders where there are high fault levels as the operating time will be reduced. The reduction in operating time will improve power quality (voltage dip), reduce the damage and risk at the fault position [59], [107]. The reduction in operating time and subsequent reduction in voltage dip time will also decrease the probability of a sympathetic trip [59]. It

CHAPTER 3 FEEDER OVERCURRENT PROTECTION PHILOSOPHY AND ELEMENTS

may increase the risk of losing selectivity with downstream devices as the curve is moving down in the time-current plot.

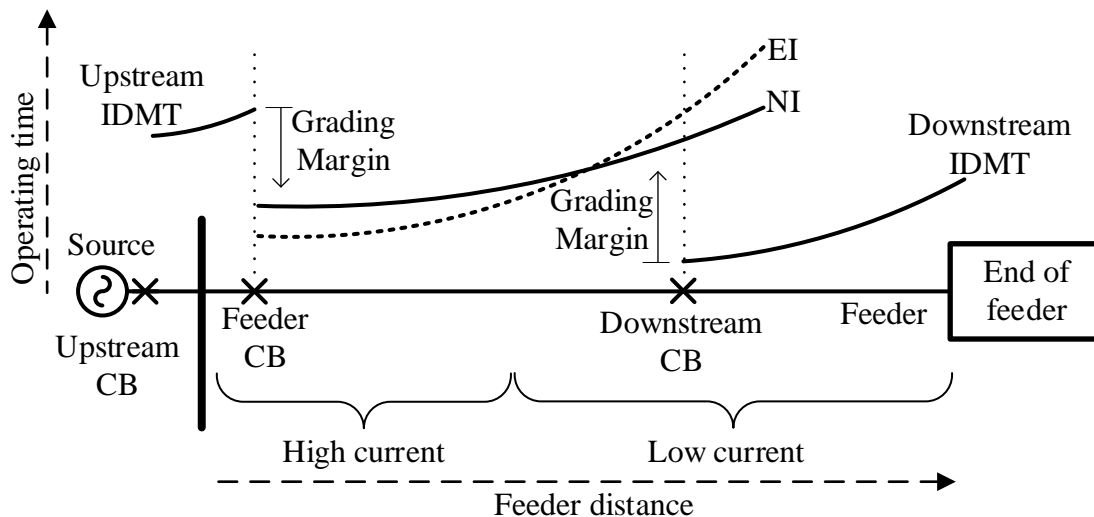


Figure 3.3. A radial feeder showing protection operating times, grading margins, high current and low current regions.

An example of damage at the fault position can be on the conductor where pieces of molten aluminium (conductor) is expelled (mechanical damage) [120]. This welding effect of the conductor material is a function of the current magnitude and exposure time ($I-t$ effect) [120]. Risk refers to fire risk such as the starting of veldt fires or plantation fires. This is due to the hot conductor pieces being expelled at the fault position [79], [120]. This veldt fire can result in this being classified as an environmental incident. Fast fault clearing will assist with reducing the damage due to the thermal effect of the fault current that the healthy equipment needs to carry [28], [34], [114]. The reduced operating time can increase the grading margin (promote selectivity) with the upstream protection (see Figure 3.3). The drawback of using a curve that is more inverse (compared to NI) is that the rate at which the operating time increases down the feeder is also increased. This can make the protection operation slow in clearing a fault, perhaps violating the speed philosophy element of Section 3.2. If both these curves were set to operate in 1 s with the same PU applied in the high fault current region, the more inverse curve would require a larger TM to slow it down. The opposite would be

true at low fault levels. For inverse curves, as the ratio of fault current to PU gets closer to a value of one, the operating time can become infinitely high with the asymptote being the PU current applied [121]. This is due to this ratio residing in the denominator of (3.1) to (3.3).

If reducing risk in the network is the protection priority, then this increase in operating time at low fault levels is a drawback. However, if selectivity for downstream devices is the priority, then the potential grading margin is improved (increased) with the downstream protection devices. This then becomes a benefit. From this discussion, it can be seen that the priority of the philosophy elements is important and this dictates the way in which protection elements are set and the choice of operating curve can aid in this configuration. Different utilities may have a different approach to each of these.

3.4.2 Maximum time function

When IDMT curves are applied on long feeders where the fault level reduces to a small value at the end of the feeder compared to the relay PU, the operating time can become excessively high. This can be seen in Figure 3.2 in low current region (350 A-1000 A) and is also illustrated in Figure 3.3 for faults towards the end of the device reach (towards low current). To counter this effect, a DT curve can be applied to the relay with the same PU current value as the IDMT curve but with a time delay set to the desired maximum operating time. Equation (3.4) and Figure 3.2 show that the DT curve will operate at the same time, irrespective of the fault current it measures. The measured fault current simply has to be bigger than the relay set PU current to initiate the tripping sequence (time delay). This second DT curve is normally not available on electromechanical devices. For electromechanical devices a separate relay will have to be installed. A number of OC elements may be available on newer microprocessor and numerical relays. It is good practice to apply this DT curve with an IDMT curve to create an upper bound for the operating curve. This limits the detectable fault exposure time to a fixed value. Clearing (or isolation) times in the range of 0.6 s to three seconds are common in distribution networks [122]. It is recommended that a fault should be interrupted within 5 s [51]. Some manufactures do have specific functions (e.g. maximum time function) on the relay (or AR) that do perform this function [116]. Other

utilities specify a maximum time for each trip event as a final time setting. Transpower have applied a value of 2.4 s for MV networks of 33 kV and below [102].

3.4.3 Reset curve

For a modern relay the reset characteristic of the relay can be programmed [54]. This reset characteristic refers to the relays behaviour once the relay has detected a fault and the measured fault current is removed. When considering an electromechanical relay, the disk will take a period of time to return to its original starting position (resting position). For modern relays this can simply be a register inside the relay that is cleared or, it can be set to reset on a certain curve such as to emulate the electromechanical relay [109]. This setting of the reset curve is required where different relays have different methods of resetting (e.g. electromechanical vs. numeric) so that selectivity can be maintained. If the relay technology type is similar, all the reset curves on the relays can be set to reset instantaneously (e.g. numeric relays). A general version of an electromechanical relay reset curve is provided in (3.5) [117].

$$\text{Reset curve} \quad OT_{curve} = \frac{tr}{\left(\frac{I_f}{PU}\right)^2 - 1} \quad (3.5)$$

where I_f refers to the fault current (A), PU is the relay PU current (A), tr is the relay reset time (s) and OT_{curve} is the relay operating time curve (s). This means that if a NI IDMT curve was used, the OT_{curve} will be replaced by (3.1).

3.4.4 High-set element

A high-set or instantaneous element resembles a DT curve with a zero second time delay. The relay operating time is in the region of 0.5 to two cycles [58]. A value of one to three cycles is given for AR [23] and value of less than two cycles is provided in [55]. Numeric relays have the ability to delay the issue of the trip signal (DT curve). The main advantage of applying a high-set is that the equipment fault exposure time is low. When applied, it

CHAPTER 3 FEEDER OVERCURRENT PROTECTION PHILOSOPHY AND ELEMENTS

improves the risk profile of the fault as this reduces the damage at the fault point significantly [34]. The reduction in operating time assists with reducing thermal damage such as LTE damage (see Chapter 4) [28], [34], [114], [123].

The reduction in operating time can result in a loss of selectivity between series protective devices. For this reason, it is normally set to not overreach the downstream device. Modern relays do have cold load PU algorithms that can desensitise the OC elements for a certain time period [54], [116], [124]. Inrush current can be greater than the instantaneous element PU current setting. Inrush current can be between eight to thirty times the rated transformer current [54]. Very often a value of six times the rated transformer current is used [124]. Another estimate for the inrush current magnitude and duration is ten times the rated current for 100 ms [54]. The IEEE assumes it to be 100 ms for a magnitude ranging from eight to twelve times the transformer rated current [58]. Inrush restraint functionality can be applied or enabled in certain relays (including AR) [116].

Current transformer and relay errors should also be considered when setting protection devices [34]. These errors can result in a loss of selectivity as two relays may measure the same current differently where the result can be a grading margin that is too small. It may also result in the relay underreaching (becoming less sensitive) and not being able to detect a fault (overreaching can also occur). There are instances where the high-set element is required to over reach the downstream element, but then a time delay will have to be introduced to maintain selectivity. The downstream element will require fast protection such as a high-set element with no time delay to obtain a grading margin). A high-set is an additional curve to the IDMT or DT element on a protective relay. This high-set element can be set to initiate an ARC cycle. It is recommended to initiate auto-reclosing as this improves the availability of the network [16], [29], [34], [65], [99]. When applying a high-set function it can also assist in creating grading margin for downstream protective devices, thus more devices can be placed in series without losing selectivity.

The PU of a high-set element should always be determined in maximum network conditions. If the PU is determined in maximum network conditions, the setting is more secure. With

CHAPTER 3 FEEDER OVERCURRENT PROTECTION PHILOSOPHY AND ELEMENTS

the setting determined in this condition, if the network status changes from maximum to minimum, the high-set PU will appear to move closer to the source end of the feeder. This is due to the overall network fault level being reduced (minimum condition) and the PU setting on the relay not changing with this. If the PU is determined in minimum network conditions and the network fault levels change to maximum, the high-set PU will appear to move further into the network. This can lead to a loss in selectivity (grading error) with downstream devices.

When determining the high-set PU the first priority is that it should not overreach the downstream protection device as this will lead to a loss of selectivity (TD set to zero seconds). When determining the PU, the fault level at the downstream device can be used in maximum network conditions. The PU should be increased to a value higher than this fault level to compensate for the transient overreach of the relay. This transient overreach condition will make a fault that is beyond the downstream protective device appear closer to the source than what it actually is. This is due to the DC offset [121]. The fault level on the feeder will increase as the fault position is getting closer to the source. Certain relay technology filters for the fundamental item [58]. For these relays the high-set PU can be set closer to the downstream device fault level. It is recommended to apply a PU value larger than 126 % of the downstream device fault level for numeric relays and 192 % for electromechanical relays [124]. A value of 130 % is used in [61] and a value of 125 % in [103]. If the resulting PU is more than the fault level (maximum network conditions) at the relay position where the high-set element is applied, there will be no benefit in applying this element. This is due to the fault level being too low for this element to PU.

Whenever possible, a high-set element should be enabled as the reduction in operating time minimises network damage and risk [34]. This is especially applicable for protection relays at the source busbar where the fault currents are high and operating times are slow [119]. If the high-set element is set to PU on a value where it will not overreach the downstream device, the time delay can be set to zero seconds. This is due to the relay knowing that the fault is on the feeder and not beyond the downstream protection relay. The PU of the upstream device is thus insensitive to faults below the downstream device.

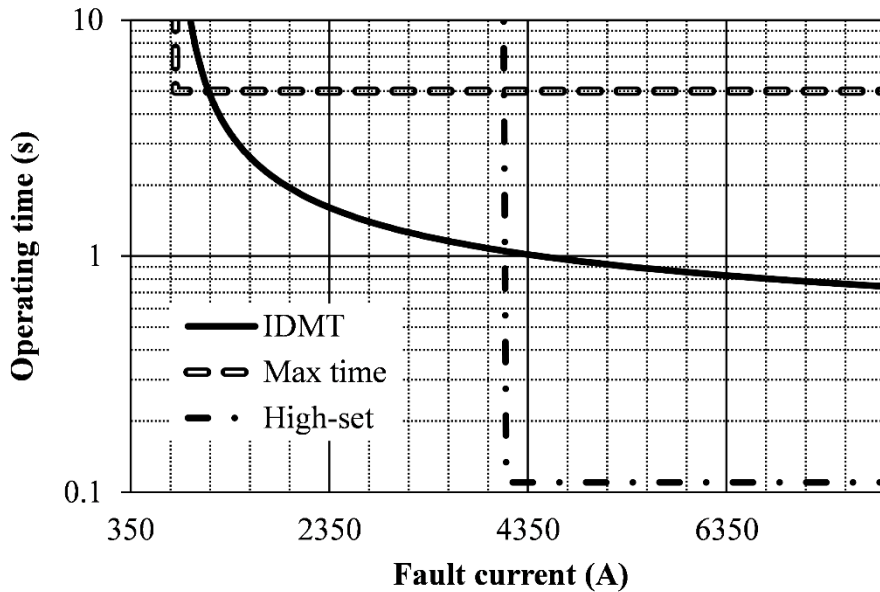


Figure 3.4. A relay operating curve consisting of a maximum time function, IDMT and a high-set element.

A maximum time function, IDMT curve and high-set element is applied in the grading graph of Figure 3.4. The time delay of the high-set element is set slightly higher than zero so as to show it on the logarithmic graph (would normally reside at zero). The resulting operating curve will be the minimum of the three curves at any fault current that is higher than the curve or element PU. The resulting operating curve will clear faults with high fault current quickly (know the fault is on the feeder), allow for grading in the IDMT part of the curve and limit the operating time for low fault levels (fault current to PU ratio).

3.5 AUTO-RECLOSING

The ARC function allows the CB to close automatically once a trip signal was sent to the CB and it opened. The main elements that will have to be set on the ARC function for MV feeder applications are the number of shots, deadtime and reclaim time. The operating curves associated with each attempt can also be set depending on the relay technology applied.

3.5.1 The number of attempts

Two main categories for faults are transient and permanent faults [23], [54], [109]. A broken conductor is a good example of a permanent fault [54]. A permanent fault requires some human intervention to repair the network [125]. Isolating the permanent fault (faulted part of the network) and then reconfiguring the network can be automated. The most common type fault is a transient type fault [20], [25], [29]. An example of this is lightning striking the feeder [44], [124]. When there was lightning the operation of the CB (open and then close) will re-establish the dielectric integrity of the feeder [121], [126]. Except for lightning, a transient fault can also be caused by animals, wind and trees [34], [54]. Another fault classification type is a semi-permanent fault [34]. A semi-permanent fault example is a tree branch touching the bare overhead conductor [34], [125]. The philosophy that is applied to try and clear this fault is to burn away the fault with a longer fault exposure time [34]. This will then not result in the lockout condition of a permanent fault, thus promoting the continuity of supply. The continuity of supply is a requirement for customers [23]. When considering the protection philosophy principles and objectives stated early in this chapter, increasing the trip time will increase the fire risk [79]. The literature differs to the exact occurrence percentage of the three fault categories but there is overwhelming consensus in that transient faults account for the majority of faults [29], [34], [54], [97], [107], [112], [121], [126], [127]. For the transient type fault, a fast type curve (low exposure time) can be applied and slower operating curves can be applied for subsequent ARC attempts [23].

A study done in [128] evaluated 905 protection event records (2044 individual trips) detailing 547 months of data on radial MV overhead feeders. These networks were resistively earthed (limited to 360 A per source transformer). In this study it was found that L-G faults accounted for 44 % of all faults, L-L faults accounted for 34 % of all faults and three-phase faults accounted for 22 % of all faults. In [29] the frequency of fault types is reported as 80 % for L-G faults, 17 % for L-L-to-ground faults, two percent for L-L faults and one percent for three-phase faults. These values are dependent on factors such as tower design and dominant weather phenomenon. The 905 protection events were classified into the three main fault categories of transient, semi-permanent and permanent. The transient

CHAPTER 3 FEEDER OVERCURRENT PROTECTION PHILOSOPHY AND ELEMENTS

faults accounted for 83.5 % of all faults and this corresponds well to existing literature on this topic [24], [29], [34]. Permanent faults accounted for 9.5 % and semi-permanent faults accounted for 7 % of all the faults. An important finding in this article was that the probability of having a successful ARC attempt decreased with the increase in ARC attempts [99], [107]. A successful attempt is an ARC attempt that results in a closure of the CB without the need for more ARC attempts. An ARC success rate of 89 % for the first attempt, 5 % for the second and only 1 % for a third is reported in [107]. An increased number of ARC attempts also increase the probability of customers experiencing more power quality incidents such as voltage dips [99]. It is reported in the IEEE std C37.104 that a third ARC attempt is seldom used [109].

A possible ARC philosophy can be to disable the ARC function completely, but based on the study above, it can be seen that by enabling the ARC function the availability of the network can be improved due to the majority of the faults being transient in nature [24], [29], [34], [58]. Another philosophy can be that the maximum number of ARC attempts should be applied, but this is detrimental to the long-term reliability of the network. An example of this is that the source transformers get exposed to cumulative damage every time there is a fault of sufficient magnitude (or then ARC attempt) [109]. With the probability of having a successful ARC diminishing and the possible damage to the source transformers increasing with an increase in ARC attempts a maximum number of ARC attempts are not advisable. If the maximum number is used (e.g. four attempts), the CB duty cycle (number of open and close attempts) have to be considered to ensure the CB can actually sustain these many attempts. Especially for substation-based CBs where the fault level is generally high and slow operating times can be expected.

When developing an ARC philosophy, the basic concept is to maximize network availability by enabling the ARC function, but minimize the unnecessary closure on to permanent faults. Also, an ARC cycle should not be the cause of equipment damage [127]. When considering the classification percentages in the previous paragraph and then the decline in ARC success with an increase in ARC attempts, a two trip to lockout (one ARC attempt) philosophy is recommended [109], [127], [128]. The first trip is then for transient faults which is most

CHAPTER 3 FEEDER OVERCURRENT PROTECTION PHILOSOPHY AND ELEMENTS

common. The second then assumes that the fault is permanent and the protection relay goes into a lockout condition. Lockout means the protection relay will not issue another close command unless it is instructed to do so either via a SCADA interface or then manual closure. If provision were to be made for semi-permanent faults, the fault will have to be left on the network for a longer period. By leaving the fault on the network for longer, the risk in the network increases and this goes against the initial objectives (beginning of this chapter) set for the feeder protection philosophy. If those objectives are changed, then the ARC philosophy can be changed.

The study in [128] identified that some faults do clear if the CB open time was more than 10 minutes. This accounted for 3.3 % of the 905 incidents. Based on this, the control centre can try to close the CB if it is controllable by the control centre using a SCADA system. If the CB is not controllable by a control centre, the number of ARC attempts can be increased from two trips to lockout to three trips to lockout so as to try and improve the network availability and avoid sending field personnel to investigate unnecessarily [37]. This would be an economic and safety consideration where personnel should not be sent to investigate and be placed in harm's way unnecessarily (traveling and live apparatus). It is mentioned in [29] that utilities may apply up to three ARC attempts (four trips to lockout).

3.5.2 Dead and reclaim time

Deadtime refers to the time that the CB is open, but it is actually measured from the time that the trip signal is sent to the CB [34]. On some relays (not ARs) the deadtime timer can also be started once the fault current has stopped flowing through the CB after a trip signal was sent (can also declare a CB fail condition if the current does not stop). The items that will influence the deadtime are the deionisation of the air in the fault path, the required reset time of the protection relay, CB characteristics, type of loads being supplied beyond the CB, and then system stability and synchronism [34]. When a fault occurs, the air gets ionised, thus creating a path for the flow of current. The deadtime should allow sufficient time for the ionised air to disperse after the fault, otherwise the fault will restrike through the same ionised air path [109], [119]. The voltage level and weather conditions do influence how

CHAPTER 3 FEEDER OVERCURRENT PROTECTION PHILOSOPHY AND ELEMENTS

quickly the air disperses. For MV networks a value not less than 100 ms is sufficient [34]. A minimum value of 300 ms is recommended in [107]. Deadtimes greater than ten seconds are required to allow conductors to settle and birds to fall clear if small conductors are used on the feeder [127].

The protection relay reset time should also be considered. Electromechanical relays do not reset instantaneously whereas numeric devices can be set to reset instantaneously. If the fault is beyond the downstream numeric device and both the upstream electromechanical and the downstream numeric device detects the fault, both will start to time on its operating curve. If the numeric device trips, the fault current will drop off and the disk on the electromechanical device will start to return to its starting position. If the numeric device closes again before the electromechanical relay's disk is at its starting position, selectivity between the two devices can be lost. Thus, when different relay technologies such as electromechanical and numeric are used, this can be compensated for in the deadtime of the numeric device [109]. Deadtime settings of at least ten seconds are recommended [34].

The characteristics of the CB should also be considered [34], [109]. If more than one ARC cycle is applied, then a minimum deadtime of 15 s is recommended to ensure that the CB interrupting capability does not have to be de-rated [109]. Some of the CBs can take up to 300 ms to close. Modern vacuum CBs can close in less than 100 ms. Industrial customers are more likely to be affected by the deadtime. If there are motors and systems running, sufficient time should be allocated for the system to shut down or to reset. Residential customers are not that affected by the deadtime. The interruption is more of an inconvenience to residential customers. Traditionally system stability and synchronising were not a concern for MV networks as it generally supplies load from a single source. Modern MV networks do have DG installations and bidirectional power flow that can occur on these feeders. To accommodate generators on these networks, deadtimes should be kept to a minimum. In [37] a minimum deadtime of three seconds and maximum combined deadtime (each deadtime of ARC attempt) of 30 s is recommended. A value of 10 s is recommended in [37], a value of one to five seconds is recommended in [29] and a value of 3.5 s was used in [52]. The IEEE

CHAPTER 3 FEEDER OVERCURRENT PROTECTION PHILOSOPHY AND ELEMENTS

reported typical deadtimes of zero to five seconds, 11 s to 20 s and ten to 30 s for the first, second and third attempt [109]. It can be seen that there are various deadtimes applied.

The reclaim timer is measured from the time the closing command is sent to the CB. The reclaim timer is there to ensure the duty cycle of the CB is not exceeded (number of open close cycles in a certain time period) [34]. When the timer times out, it resets the ARC trip number. If another fault is detected before the reclaim timer has timed out, then the CB will trip and not close automatically again if the maximum number of ARC cycles are reached (lockout condition). The minimum reclaim time that should be used is 30 s and the maximum is three minutes [127]. If the reclaim time is too long, then the availability of the network will be impacted negatively as a new fault will be perceived to be part of the previous fault. An example of this might be a thunderstorm where there can be multiple transient faults in a short span of time. If the reclaim time is too short, then the fault can be on the network permanently. The type of protection (e.g. IDMT or DT operating curves), the spring rewind time and CB duty cycle can also influence the reclaim time [34]. Reclaim times can be as much as 180 s.

In the actual event record evaluation done in [128] the reclaim time was optimized based on the 905 fault record evaluations. It was recommended there to use a reclaim time of 75 s for CBs that can be controlled via a SCADA system (with one ARC cycle). If a three trip to lockout ARC philosophy is used for a CB that cannot be closed via a SCADA system, a reclaim time of 90 s is recommended for MV feeders.

3.6 PROTECTION ELEMENT APPLICATION

When setting the protection devices using IDMT operating curves on a feeder there are a number of steps to follow. These settings should reflect the protection philosophy. For an IDMT element, there are only three elements that can be set (basic settings). These are the operating curve, PU and TM. In addition to this, the element can then also be set to ARC. The main steps involved when setting the IDMT element on a protection relay for a radial feeder are listed below [39].

CHAPTER 3 FEEDER OVERCURRENT PROTECTION PHILOSOPHY AND ELEMENTS

1. Choose an operating curve.
2. Determine the IDMT element PU.
3. Determine the high-set element PU and TD and test if this can be applied.
4. Determine the upstream device OT.
5. Determine the OT of the element being set.
6. Determine the TM.
7. Set the ARC element.

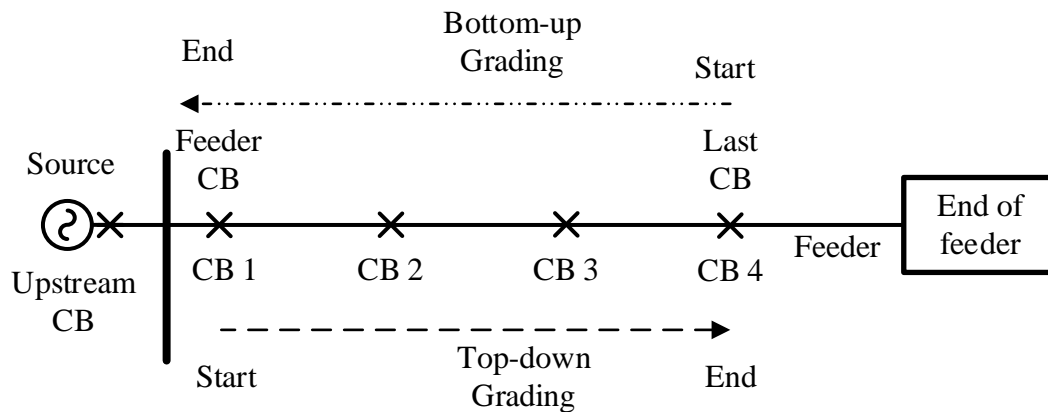


Figure 3.5. The start and end positions for the top-down and bottom-up grading methods on a radial feeder.

There are various grading methods. This includes two of the most common methods of a top-down and then bottom-up approach [40]. Top-down refers to a method of starting at the source or device that should trip last for a fault in the network, and then working your way down the series protection devices towards the end of the feeder [39]. The major steps in the top-down approach are listed above in step one to seven. A bottom-up approach is applied by starting at the last device in the series of protection elements on a feeder, and then setting each device in turn, moving back towards the source or last device required to trip [39], [91]. Figure 3.5 illustrates at which CB to start and then end when grading the protection on a feeder for a top-down and a bottom-up approach. For the top-down approach the protection at CB 1 will be set first, then CB 2 down to CB 3. For the bottom-up approach the protection at CB 4 will be set first and then CB 3 up to CB 1.

The major steps (step one to seven) when setting the protection relay at CB 1 for the top-down method are illustrated in Figure 3.6. The first step of selecting an IDMT operating curve was discussed from its effect on operating time and grading with up-and-downstream protection elements in the initial part of this section (see Section 3.4.1). It can be seen that the chosen grading curve in Figure 3.6 for CB 1 has the same shape as that of the upstream protection which will allow for good grading across the complete fault current range (with upstream curve) [34], [121].

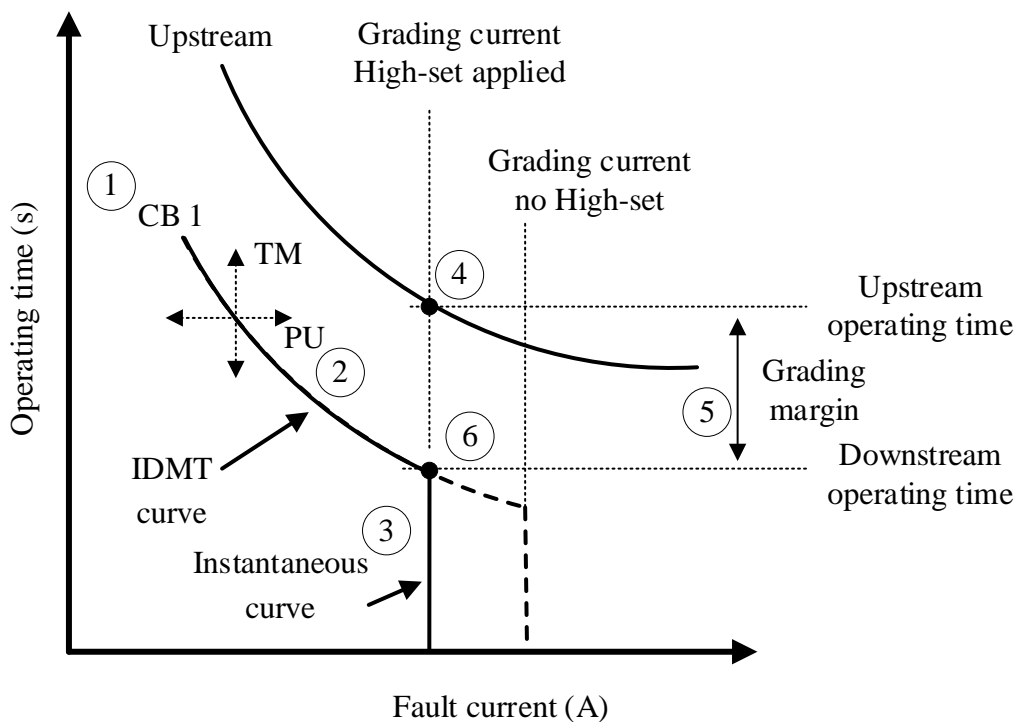


Figure 3.6. The steps of the top-down grading method is illustrated when setting the feeder CB.

The second step is to determine the OC PU of the IDMT element. There are three considerations for this [37].

- Firstly, the PU should be set above load current.
- Secondly, the PU should be sensitive to detectable faults.
- Thirdly, the PU should allow for current grading with the upstream device.

When setting the PU, the minimum of the above criteria (one to three) should be used.

Firstly, the protection PU should be set above load current [29], [34], [54], [114], [121],

CHAPTER 3 FEEDER OVERCURRENT PROTECTION PHILOSOPHY AND ELEMENTS

[127], [129]. Balanced load current resembles positive sequence current and if the phase OC protection PU is set less than this, the protection can operate for load current. This will impact the protection security as it is operating for a current (load) which is not fault current. A method of estimating the load current is to make use of the conductor ratings [37]. If errors such as modelling, measuring and relay errors are considered, a 20 % value can be added to this conductor rating. This also assists with not exceeding the conductor continuous current rating. A value of 20 % above load current is also used in [29], a value of 25 % is used in [21], a value of 150 % to 300 % in [54] and a value of 25 % to 50 % is used in [61].

Secondly, it should be sensitive to faults. In MV networks there are only OC protection devices due to its simplistic nature [27] and because it is relatively inexpensive. Thus, there is only one OC relay (or AR) at each position on the feeder. To provide back-up to downstream devices, the upstream device should back-up all the immediate downstream devices (overlap protection) [34], [130]. This should be determined in minimum network conditions for a L-L fault [54] [57], [87], [121]. This is because the protection device can fail and require maintenance (device out of service then). The PU under this criterion should not be set greater than 80 % of this L-L fault to allow for errors. It should be noted that there can be a conflict between setting the PU above load and being sensitive to a fault when determining the PU current [54]. There are a number of sensitivity percentages used at various utilities [74]. The sensitivity of the PU is broken down further based on the relay technology and whether it is providing main and backup protection in [102]. For electronic relays configured as main protection the PU should be less than 50 %. For numeric relays this is less than 60 % and for any relay providing backup it should be less than 66 %. A sensitivity value of 80 % is applied in [37]. A value of 50 % and 67 % approach is applied in [74]. The sensitivity of the OC element for L-L faults can be improved when making use of negative phase sequence components for detection [54], [131].

A residual voltage element can also be applied to improve sensitivity for the OC PU. With this voltage element applied, it can supervise the OC PU when the PU is set less than the maximum load current. Setting the sensitivity of the PU is a very important step in setting the protection. The reason for this is that protection is reactive, it will only operate if it can

CHAPTER 3 FEEDER OVERCURRENT PROTECTION PHILOSOPHY AND ELEMENTS

detect a fault (sensitivity). The concept of determining the sensitivity of the PU is illustrated in Figure 3.7 for a network consisting of multiple downstream CBs. The required sensitivity reach of the PU is shown by means of the PU sensitivity arrows. Negative sequence elements can also be applied to allow for a sensitive PU towards L-L faults [118]. Arc resistance can be included as well. This will reduce the fault level further and make the required PU more sensitive to faults (at the cost of security). A value of two ohm is recommended [113]. This has a large effect on closeup faults but a small effect on remote faults.

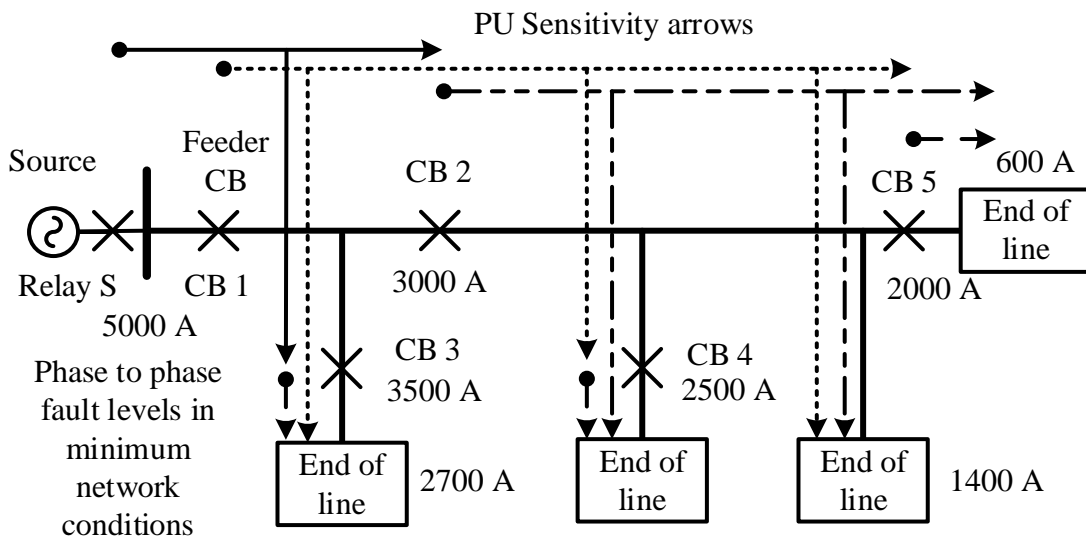


Figure 3.7. Determining the pick-up sensitivity of circuit breakers on a feeder.

For feeders where there is only one protection element at a specific position, the upstream device is required to provide backup protection to all the immediate downstream protection devices (the zones overlap each other) [17], [54], [58], [105]. For the feeder CB (CB 1) the immediate downstream devices are CB 2 and CB 3. These two CBs will be bypassed when determining the sensitivity of the PU (so as to provide backup). CB 1 is not required to be sensitive to faults beyond CB 4 and CB 5. With the 80 % criterion is applied as per [37], the maximum PU current for CB 1 in Figure 3.7 will calculate to 80 % of 1400 A. When considering the PU sensitivity arrows in Figure 3.7, it can be seen that there is a minimum of two arrows reaching all positions in the network. If the PU is set to sensitive, then the feeder may not meet the load requirements.

CHAPTER 3 FEEDER OVERCURRENT PROTECTION PHILOSOPHY AND ELEMENTS

Thirdly, the PU should allow for grading with the upstream protection device PU [119]. This is current grading. A maximum of 90 % of the upstream device PU is recommended in [37]. This allows for relay measuring errors and also the PU-drop-off ratio that can result in a loss of coordination. Measurement errors can be up to 5 % [119]. The PU drop-off ratio is where the relay will PU at a current, but only drop off or release the PU state at a lower current than the PU value. This is also called hysteresis [34]. The PU drop-off ratio of a typical relay is 95 % [34], [55].

The high-set or instantaneous element PU and TD are determined in step three of the seven listed earlier. A check has to be done to see if this instantaneous element can be applied to determine the time delay (zero seconds or higher) when compensating for transient overreach. With the high-set active, it can change the grading current to use as shown in Figure 3.6. This grading current will be the current that is used to set the minimum grading margin with the upstream device. The upstream device operating time at the grading current is determined in step four. The grading margin is subtracted from this upstream operating time and the result is the required operating time of step five. A typical value used for grading is 400 ms [34], [35], [58], [102]. A value of 200 ms was used in [21], a value of 300 ms is recommended in [103], a value of 300 ms to 400 ms is recommended in [55], a range of 200 ms to 500 ms is recommended in [123] and a range of 400 ms to 500 ms is recommended in [25]. In [32] the grading margin is specified as 100 to 200 ms for numerical relays and 300 to 600 ms for electromechanical relays. The IEEE recommends a minimum grading margin of 200 to 300 ms when static OC relays are applied [58]. The grading margin allows for selectivity to be maintained by compensating for setting errors, CT errors (and saturation), relay errors, CB operating time and relay overshoot [31], [58], [114]. CT errors may be up to 10 % [54]. High fault currents can cause the CT to saturate and this may slow down protection and cause a loss of selectivity [54], [114].

The required operating time can be limited to a maximum value by applying a maximum time function. This will keep the time a fault is on the network to a set maximum (see Section 3.4.2). The required TM for the IDMT operating curve can then be determined in step six. For the top-down method, if sensitivity has a bigger priority than security, the PU

CHAPTER 3 FEEDER OVERCURRENT PROTECTION PHILOSOPHY AND ELEMENTS

have to be rounded down when setting the relay. If security is the focus, the PU should be rounded up. Lastly, in step seven the required ARC cycles, dead and reclaim time is set.

At this point most of the key settings for the current based protection elements are set and the settings can be evaluated so as to ensure that the equipment such as the conductors are actually protected. Thus, a LTE evaluation has to be conducted next to ensure the conductor energy exposure is less than the conductor limit.

3.7 CHAPTER SUMMARY

Section 3.2 introduced the protection philosophy elements of speed, selectivity sensitivity, security and dependability. The typical layout of a radial feeder with protection equipment was shared in Section 3.3. Only substation-based relays and ARs were considered for the work going forward in this thesis as they have configurable settings. This excludes the application of fuses and sectionalisers (can be included in future work if required). Section 3.4 identified the key protection elements required and applied to protect a radial feeder. This included the choice of operating curve, the PU, TM (or time delay), maximum time, the reset curve and the high-set element. The concept of ARC with the main settings applicable to this functionality was discussed in Section 3.5. The main ARC elements to set includes the number of attempts, the dead time and reclaim time. The application of the OC elements (or functions) was illustrated by means of a radial feeder in Section 3.6. A top-down grading method was applied. This application showed how the applied protection philosophy of Section 3.2 influence the choice of protection settings applied to the ARs. This example application also showed how slow protection is becoming with a number of series protection devices installed. The settings determined by making use of the top-down grading method can now be tested to see if they will protect the feeder by making use of LTE as a measure.

CHAPTER 4 LTE APPLICATION IN DISTRIBUTION NETWORKS

4.1 CHAPTER OVERVIEW

In the previous chapter the basic philosophy and principles required to protect a MV feeder with OC protection elements were introduced. In Section 4.2 conductor damage, minimum and maximum network conditions and the concept of LTE are defined. Background on conductor resistance and the heating effect of current flowing through a conductor is provided in Section 4.3. Section 4.4 shows how to calculate the conductor energy limits when the conductor is exposed to fault current. Section 4.5 explores the difference between a radial and a multisource interconnected network from the potential LTE risk areas on the evaluated feeder. Fault current flow within radial and multisource networks are also explored. This fault current concept of Section 4.5 is further expanded in Section 4.6 to include the contribution from wind and PV DGs. The OC relay operation and mathematical model for operating curves are investigated in Section 4.7. Section 4.8 takes the typical relay operating curves that were defined in Chapter 3 and explores the effect of these on the conductor LTE exposure. Many MV feeders may consist of more than one type of conductor in series and multiple ARs in series. The effect of this multiple conductor types and ARs in series are investigated in Section 4.9. ARC has an impact on the conductor LTE exposure. This is shown in Section 4.10. Finally, in Section 4.11 the concept of energy-area and Energy-Volume is are introduced for quantifying the conductor LTE exposure.

4.2 LET-THROUGH ENERGY DEFINITION

4.2.1 Conductor limit and damage

All conductors have resistance (R) associated with them. The power (P) that will be dissipated over a conductor is equal to the square of the current (I) passing through the conductor times this resistance of the conductor [132], [133]. For AC, the root mean square (RMS) value will be used [134]. If we add a time component to this, the power will be changed into energy [3], [133], [134]. Based on the aforementioned we can then write (4.1) for energy dissipated in a resistor. For the application in this thesis, this resistance is the resistance of a conductor.

$$Energy = I^2Rt \quad (4.1)$$

where *Energy* is the energy calculated in watt-hour, I is the fault current (A), R is resistance (ohm) and t is time (s). Joule can also be used to represent the energy as 1 watt is equal to 1 Joule-per-second and 1 W·s is thus equal to 1 Joule.

As the current passes through the conductor, heat will be generated in the conductor based on the resistance of the conductor [135]. The higher the current, the greater the resistance or a longer time exposure, the more heat will be generated. The assumption is made that all the heat that is generated by the flow of current is contained within the conductor during a fault [58], [80], [81], [122], [135]-[137]. Thus, this is an adiabatic process with no heat loss to the environment. This heat loss can be due to radiation, convection to the surrounding environment, conduction to clamps, etc [135]. The convection and radiation loss can be ignored if the fault is cleared within 5 s [81], [137]. By making the adiabatic process assumption, we can set the heat energy generated by flow of current equal to the heat energy gained by the conductor [135], [137]. This is also a worst-case approach when setting protection for conductor damage. With this adiabatic process, it allows for the calculation of a conductor limit (more info on this is given in the next section). This limit will specify how

much current the conductor can carry for a specific time period before it gets damaged. Generally, a current value is specified for a given time period of 1 s [138], [139]. Some conductor short time ratings are shown in Table 4.1 [138].

Table 4.1 Conductor short time ratings.

Conductor	Short time rating for 1 s (kA)
Squirrel	1.79
Fox	3.14
Mink	5.4
Hare	8.97
Oak	9.59

From Table 4.1, Mink conductor can carry 5400 A for 1 s. If we look at this in terms of energy, it is an I^2t energy. Because the assumption is made that this an adiabatic process, the energy rating for one instance can be set equal to the energy for another instance [81]. This is shown in (4.2).

$$I_1^2 t_1 = I_2^2 t_2 \quad (4.2)$$

$$t_2 = \left(\frac{I_1}{I_2}\right)^2 t_1$$

where I_1 is the fault current (A) for instance one, I_2 is the fault current (A) for instance two, t_1 is the fault current withstand time (s) for instance one and t_2 is the fault current withstand time (s) for instance two. By using (4.2) it can be determined how long the conductor can sustain a fault current before it gets damaged. This is if the current and withstand time is known for one instance. As an example, if the Mink conductor is exposed to a fault current of 2500 A, it can sustain that current for 4.67 s before it gets damaged. If the fault current was equal to 8000 A, the conductor will be able to sustain this current for 0.456 s before it's damaged. If this Mink conductor is used and the times are calculated over a range of fault currents, a damage curve (limit of conductor) can be created for the Mink conductor. But if

we plot this as an I^2t energy it will result in a straight line instead of a curve. As an example, the energy rating for Mink conductor will be equal to 29.16 MA²s (5400 A for 1 s). This is the LTE rating of the conductor. It is easier to work with the energy rating than the short time rating as the energy rating is constant, whereas the short time rating varies with the fault current.

In Figure 4.1 the short time and LTE rating for a conductor is shown over a current range. A similar approach towards showing the I^2t energy across a current range for a fuse was used in [140]. The equipment damage curves over a current range were shown in [141] where simulation software is used to adjust the time-current curves. This conductor has a LTE rating of 4500 A for 1 s or 20.25 MA²s. Both of these are damage curves for this conductor. One is expressed in terms of LTE and the other in terms of time at a specific current and the time the conductor can sustain the current (short time rating).

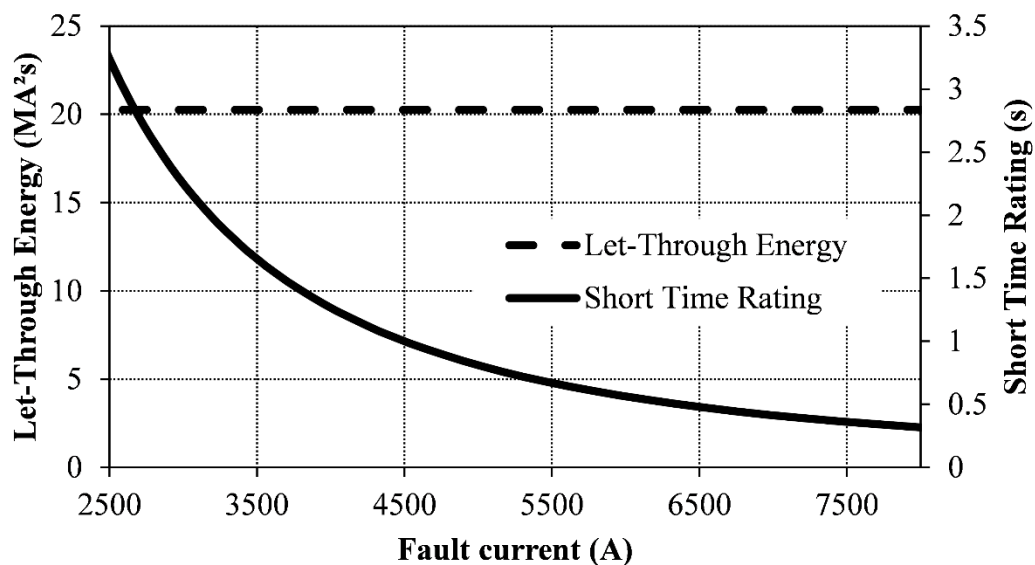


Figure 4.1. Let-through energy and short time damage curves for conductor (4500 A for 1 s).

Conductor damage in the context of this work refers to the annealing effect on the conductor material. This should not be mistaken for the conductor melting. Aluminium melts at a temperature of 660 °C and annealing starts if the temperature exceeds 100 °C [135]. Conductor burndown is not considered for this work. This is a I-t function and occurs much faster than the annealing mechanism [135]. Above 200 °C there is a fast increase in the

annealing mechanism [135]. When the conductor is manufactured, the conductor strands are strain hardened [135]. When the conductor is heated, this material is relaxed and then anneals [54], [135]. This damage is permanent, cumulative and can result in other mechanical failures [54], [113], [135]. These mechanical failures can then be due to stress from weather and wind [54]. This is due to heat generated by the flow of current in the conductor during a fault. [54]. If the change in the conductor material stress is proportional to the change in the material strain, the conductor is said to undergo an elastic deformation [142]. The slope of the stress-strain graph for the material is called the modulus of elasticity. For an elastic deformation the modulus of elasticity of the material will be constant [142]. For an elastic deformation, the material will return to its original profile if the stress is removed. The time it takes for the material to return to its original profile is called the anelasticity of the material. For metals, this time is most often neglected due to it being small [142].

If the change in the stress and strain quantities is not proportional, the material (or then conductor) is said to undergo plastic deformation [142]. This means that the modulus of elasticity is not a constant any more. The electrical resistivity of the conducting material will increase when the conductor has undergone plastic deformation [142]. For plastic deformation there is a small bit of recovery back to the elastic deformation region, but the material will not recover back to its original profile [142].

If this concept is applied to an overhead conductor, the conductor may encroach on its minimum clearance from the ground when heated due to current [54]. This means the conductor will sag towards the ground. An increase in length of 30 % and a loss of strength of up to 58 % may occur when the conductor annealed fully [135]. Normally, the three conductors of a three-phase system will have a similar profile. If the conductor is exposed to a cross wind with this profile, all three conductors will swing a similar amount, thus maintaining the phase clearance. However, if one phase conductor of the three-phase system was damaged, the damaged phase may swing more and this can result in an increase in L-L and L-G faults. The damaged conductor can stay in service, but in time the damaged conductor material can result in a failure [54], [113]. On an actual feeder, the whole

conductor will carry the same current up to the fault point. This means that the entire conductor up to the fault point is subjected to the same potential LTE damage [143].

It is recommended that a safety margin be applied to the material to ensure that plastic deformation does not occur. This margin is with reference to the yield strength of the material. It is recommended to use a safety margin of 1.2 to 4 times for the yield strength. If the safety margin is too big, it will result in the overdesign and then increase in cost of the material [142]. For this work a safety margin of 120 % will be applied to the conductor LTE damage curve or limit to ensure that the conductor is not damaged. If a conductor on a feeder is exposed to excessive faults, it can lead to a reduction of the life expectancy of the conductor due to fatigue [142]. If the conductor is exposed to higher stress levels the number of cycles required to cause severe conductor damage is reduced [142].

Conductors can also be placed in motion due to fault current it will have to carry [108], [143]. This is owing to the electromagnetic forces generated around the conductors when fault current is passing through the conductor [108], [143]. This may result in the conductors touching each other (or get close enough) when they are swinging, resulting in a L-L fault. Thinner or lighter conductors may experience more motion than thicker conductors [143]. The swing motion is a function of the magnitude of the fault current and the exposure time period [108], [143]. This means that by minimising the I^2t energy, the possible conductor swing and possible L-L faults are also minimised [143]. Longer spans are more susceptible to conductor motion and L-L faults [143]. Typical spans are 90 m to 120 m in rural areas and 30 m to 45 m in suburban environments [135]. The swing direction is a function of the fault type (e.g. three-phase vs. L-L) [108], [143]. If the circuit is set to initiate ARC, the swinging motion may be fuelled by the new current when the CB closes, resulting in another potential L-L fault [108]. The most important factor that influences the possible swing is the conductor sag [108]. This means that if the conductor gets damaged due to the prolonged fault current it carried (plastic deformation), it may result in increased L-L faults due to the increased conductor sag [108]. A conductor that has undergone a plastic deformation sag is damaged permanently [108]. This condition can present itself in all of the upstream spans to the original fault position [143]. The contact positions for L-L faults on an aluminium

conductor can be identified by looking for shiny regions on the conductor [143]. Aluminium will normally have a dull look to it due to oxidation [143].

4.2.2 Let-through energy

As stated in the beginning of this section, the I^2Rt -energy is used to ensure the conductor is protected. The resistance is incorporated in the calculation of the conductor limit and hence we are only looking at the I^2t part of the equation. This calculation is shown in the next section. The current part of the I^2t calculation is the fault current. The time part of the I^2t calculation is the fault clearing time [136]. This fault clearing time consists of the protection operating time and then the CB operating time [107], [144]. The CB operating time can be in the range of three to eight cycles [10], [58]. When a fault is cleared on the IDMT protection element further down the feeder, the CB operating time influence is minimal as operating time can be as slow as five seconds (example). However, close to the source where the high fault current region is (see Figure 3.3), the CB operating time influence can be significant. This is even when an instantaneous curve (or high-set curve) is applied.

The LTE equation is shown in (4.3). From a protection perspective, the fault current cannot be changed as this is dependent on the source impedance to the fault (voltage at rated value). The time the conductor is exposed to the fault current is influenced by the protection system. By extension, this is the protection philosophy of Chapter 3 and the application thereof. The behaviour of the protection (e.g. operating time) can be changed by changing the protection settings. From a protection settings perspective, the operating curve can be adjusted, the PU, the TM or time delay, a combination of curves can be used and the ARC philosophy can be changed.

$$LTE = I^2t \quad (4.3)$$

where LTE is the LTE (A^2s), I is the fault current (A) and t is the fault clearing time (s). To ensure the conductor is protected, the LTE exposure should be less than the conductor limit [25], [81], [123]. The fault clearing time is the sum of the time before the fault is detected,

the relay operating time and the CB time [106]. In Figure 4.2 the LTE exposure for the conductor of Figure 4.1 (4500 A for 1 s) is shown over a large fault level range and distance as a radial feeder. The conductor limit is 20.25 MA²s. Radom protection settings applied to a NI curve are used to illustrate the concept of LTE protection. For the graph in Figure 4.2 the distance from the source busbar is used instead of fault current. This approach is applied as it provides a better feel for where on the feeder (position) damage is most likely to occur. The fault level is however also shown as this helps with the calculations and to visually determine possible setting values such as a high-set PU. The LTE was calculated by applying (4.3). The IEEE recommends that the conductor short time heating limits should be graphed [58]. The IEEE further recommends that conductor damage should be considered when coordinating protection [54].

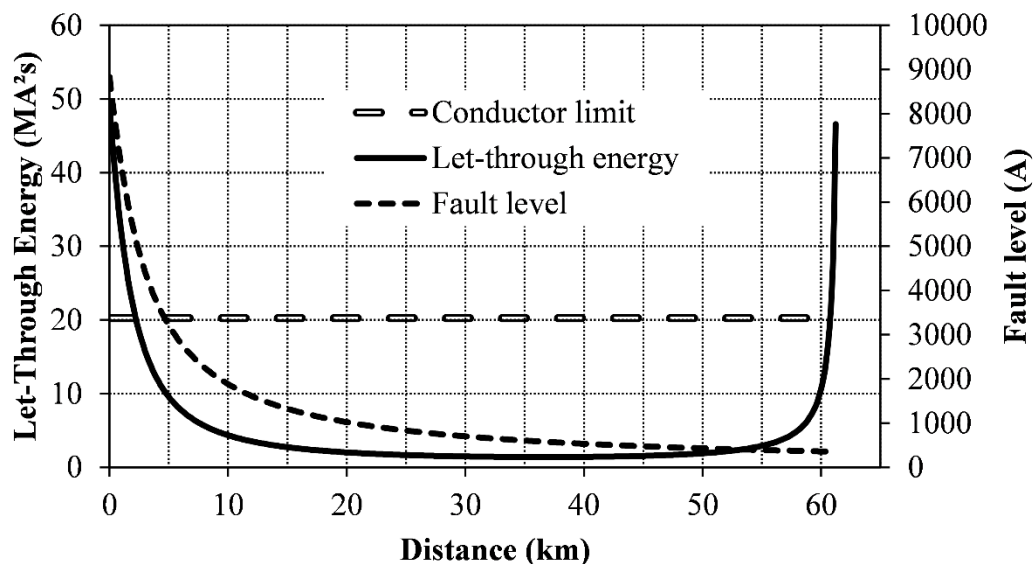


Figure 4.2. Conductor damage curve and the let-through energy exposure for a radial feeder.

In Figure 4.2 it can be seen that the conductor limit is exceeded for the first 2.35 km of the feeder. This means that any fault within this area will result in conductor damage with the current applied protection settings and conductor type. This is also the high fault current region of the conductor. Close to the source, the fault current will be the dominant factor in the LTE calculation. This is for the IDMT protection operating curves of (3.1) to (3.3). As the fault level reduces (move further away from substation) the ratio of the fault level (I_f) to the PU current will get closer to one. As this happens, the time part of the LTE calculation

will become the dominant factor. This is the second damage curve exceedance from about 61 km onwards. This means that even though the fault current is low in this area, the time the conductor is exposed to this will cause the conductor damage. This low magnitude, long duration fault may even cause more damage than the high current short duration fault [103], [106].

To reduce damage the operating time (or fault exposure time) has to be kept to a minimum [36], [103], [106], [114], [145]. This operating time reduction can be managed by the protection when determining the protection settings [103]. The operating time can also be reduced by not using excessive grading margins [103]. This reduction in operating time can be achieved further by grading at the downstream high-set element PU as was shown in Chapter 3. By reducing the fault current, this can also reduce the damage. The faster protection (reduction in operating time) will also aid in increasing the equipment life expectancy [131]. Changing the fault current is not that feasible always [103]. Some methods that can be used are to introduce current limiting reactors, applying current limiters based on electronics, reduce the supply transformer size, increase the supply transformer impedance, reconfigure the network (or operational limitations) [103].

4.2.3 Maximum and minimum network conditions

The current and time parts of the LTE equation (I^2t) have to be evaluated under different network contingencies. As was shown in Figure 4.2, there are two energy peaks when considering the LTE application with IDMT operating curves. As the first peak in the radial network application is dominated by the current, this should be evaluated under a high current contingency. This high current contingency is named maximum network conditions. For maximum network conditions the network is switched in such a way so as to result in the maximum fault current on the part of the network being evaluated. For a radial network this is dependent only on the upstream source impedance, generally the number of transformers in service at the source substation [54].

For an interconnected network or a network where there is additional generation active, a greater study is required. This is because the current through the conductor section under study has to be maximised. This means all the generation may or may not be in service (protection blinding effect of Chapter 2) and then the N/O points will have to be evaluated to determine their effect on the fault level at the study point. As was discussed in Chapter 2, when DG is installed, it may result in lower fault levels in different parts and higher fault levels in others. This can make it difficult to determine the minimum and maximum network conditions. If the DG is a wind, double fed induction generator (DFIG), it may actually become a motor load if the terminal voltage drops below a certain value [69]. The time before this happens is determined by the fault ride through criteria. The fault ride through time and criteria is determined by the various network regulators and is normally published in the grid code for that country. As an example, in South-Africa this is the National Energy Regulator of South Africa (NERSA). This work is detailing OC protection for MV feeders. This work is not aimed at EF protection, even though the concept should also be applied for EFs. To obtain the maximum fault current for phase faults (not EFs) when the network is correctly switched (maximum network contingency), a three-phase fault should be used.

In Figure 4.2 there is a second LTE peak further down the feeder at a low fault level. This fault level is low with reference to the protection PU current value (a protection setting). Minimum network conditions then refer to a network contingency that result in the minimum current at the network point under study. Generally, for a radial MV feeder, only the source transformers will have to be switched as they have the largest impact on the source impedance (also under minimum load) [54]. Similar to maximum network conditions, if the feeder is interconnected or there are multiple points of generation on it, additional evaluations are required to find the minimum network condition. For minimum network conditions a L-L fault will be used as this will result in the minimum fault current where there is no earth path involved. In addition to using minimum network conditions with a L-L fault, suitable fault resistance has to be included [121]. When fault resistance is included in the fault level calculation, it will reduce the fault level further. For a L-L fault this fault resistance is associated with the arc that can exist between the faulted phases [58]. The arc can increase in length over time [121]. As such it is recommended to use the minimum

distance between phases or the minimum L-G distance when determining a suitable distance for the arc [121]. Fault resistance values used for these evaluations range from 0 Ω to 40 Ω [54]. A fault resistance value of 3 ohm is recommended in [41]. for MV feeders (11 kV to 33 kV) with phase clearances as specified in [146]. A fault resistance value of 2 Ω or less was determined by [113].

4.3 RESISTANCE BACKGROUND

Resistance in terms of Ohm's law is defined as voltage (V) divided by current [132]. Ohm's law takes a holistic view on a conducting material. This means that the current passing through a conducting material is dependent on the potential difference between the two ends of the conducting material and the resistance of this conducting material between the two ends. If the length of the material increases, the resistance will increase. The resistance is thus proportional to the length (L) of the conducting material. When the effect of current within a material conducting the current is considered, the resistivity (ρ) of the material can be used [132]. The resistivity of a conducting material can be calculated by dividing the electric field (E) with the current density in a vector format [132]. Current density has units of ampere per square meter. Thus, if the area (A) of the conducting material is increased, the resistivity will decrease if the electric field is kept constant. Conductivity (σ) is a measure of how good the conductor is at conducting current and this is the reciprocal of the resistivity [132]. Resistivity is dependent on the type of material used in the conductor and resistance is a property of the conductor itself [132]. The relationship between resistance and resistivity is defined by (4.4) [3], [38], [132], [134].

$$R = \rho \frac{L}{A} \quad (4.4)$$

where R is the resistance (ohm), ρ is the resistivity of the material ($\Omega \cdot m$), L is the length of conducting material (m), and A is the cross-sectional area of conducting material (m^2).

The temperature coefficient of resistance (α) is a measure of how much the resistance of the conductor will change when there is heating or a change in temperature within the material [132]. The relationship between the temperature coefficient of resistance and the resistivity of the material for a change in temperature (T) is shown in (4.5) [132], [134]. The resistivity of a metal such as aluminium will increase if the temperature increases [132].

$$\alpha = \frac{1}{\rho} \cdot \frac{d\rho}{dT} \quad (4.5)$$

where α is the temperature coefficient of resistance (per °C), ρ is the resistivity of the material ($\Omega \cdot m$), $d\rho$ is the change in the resistivity of the material ($\Omega \cdot m$), dT is the change in the temperature of the material (°C). Equation (4.5) can be rewritten into the form shown in (4.6). In this form the equation is shown with the initial resistivity (ρ_0), final resistivity (ρ_1), initial temperature (T_0) and final temperature (T_1). If (4.6) is multiplied on both sides with the length (L) and divided by the area (A), it will result in (4.7). In this equation it can be seen that the resistance of the material (Ohm's holistic approach) will change with a change in temperature [3], [134], [135].

$$\rho_1 = \rho_0 [1 + \alpha(T_1 - T_0)] \quad (4.6)$$

$$R_1 = R_0 [1 + \alpha(T_1 - T_0)] \quad (4.7)$$

When an AC current is passing through a conductor, there will be eddy currents forming, trying to oppose the flow of current. This will tend to push the current to flow towards the outside of the conductor, in a smaller surface area [135]. This is called skin effect [135]. The skin effect will increase the resistance as the conduction area is reduced (application of (4.4)). This increased resistance due to eddy currents can be termed the AC resistance of the conductor and is a function of the applied frequency [137]. This will be present in both the aluminium and steel strands [135]. Manufacturers normally specify the DC resistance of the conductor. The method used in [137] to determine the conductor LTE rating did not include skin effect for the short circuit rating, it was included for normal operating current rating

(conductor ampacity). Within this work the skin effect is not included either, but this can be included in initial calculations when determining the conductor resistance.

4.4 CONDUCTOR SHORT TIME AND LET-THROUGH ENERGY LIMIT

To determine the conductor short time rating the heat energy generated by the flow of current has to be set equal to the heat energy absorbed in the conductor. It is assumed that this process is an adiabatic process [81], [122], [135], [137], [147]. Due to this being an adiabatic process with no heat loss to the environment, (4.8) can be used to calculate the short time rating [137].

$$I^2 R \cdot t = \left(\frac{W \cdot S}{\alpha \cdot 1000} \right) \log_e \left(1 + \alpha(T_f - T_i) \right) \quad (4.8)$$

where I is the fault current (kA), t is the fault duration (s), W is the mass of conducting material (kg/km), S is the heat capacity of conducting material (J/°C·g), R is the resistance of the conductor at T_i (Ω/km), α is the temperature coefficient of resistance (per °C), T_i is the conductor temperature before the fault (°C), T_f is the conductor temperature after the fault (°C). The heat capacity of a material (S) is a measure of the energy required to increase the temperature of a unit mass of the material by one degree Centigrade [134].

Equation (4.9) and (4.10) is similar to that of (4.8) where the short time rating is determined for copper and aluminium conductors respectively [53]. A similar equation to that of (4.9) is provided in [58], [148] and a similar equation for (4.10) is provided in [58]. In (4.9) and (4.10) the left side of the equation is the heat generated in the conductor and the right side is the heat absorbed as the conductor temperature rises. Both (4.9) and (4.10) make use of an inferred absolute minimum temperature of -234 °C. This is actually material dependent as it provides the temperature where the material resistance would be zero if the gradient of the material resistance vs. temperature curve is extrapolated to zero degree centigrade. For copper the value in (4.9) should be -234.5 °C and for aluminium in (4.10) the value should be -236 °C. The two values are close to each other and that's probably why the author

approximated them to the same value of $-234\text{ }^{\circ}\text{C}$. The constant used for copper (11.5×10^4) in (4.9) and aluminium (5.2×10^4) in (4.10) do distinguish between the two materials. The concept used to derive (4.9) and (4.10) is similar to that of (4.8) where heat energy generated in the conductor due to the flow of current (I^2Rt) is set equal to the energy absorbed in the conductor [53].

Copper:
$$I_f^2 t = 11.5 \times 10^4 \cdot A^2 \log_{10} \left(\frac{234 + T_f}{234 + T_i} \right) \quad (4.9)$$

Aluminium:
$$I_f^2 t = 5.2 \times 10^4 \cdot A^2 \log_{10} \left(\frac{234 + T_f}{234 + T_i} \right) \quad (4.10)$$

where I_f is the fault current (A), t is the fault duration (s), T_i is the conductor temperature before the fault ($^{\circ}\text{C}$), T_f is the conductor temperature after the fault ($^{\circ}\text{C}$) and A is the conductor cross-sectional area without allowing for empty spaces (mm^2).

A similar equation to that in (4.8), (4.9) and (4.10) is provided in [122], [135]. The only difference here is the way the conductor area is defined. In (4.11) the cross-sectional area is defined in a unit of kcmil or thousand circular mils. A mil is one thousands of an inch.

$$\left(\frac{I}{1000A} \right)^2 t = K \cdot \log_{10} \left(\frac{T_f + \lambda}{T_i + \lambda} \right) \quad (4.11)$$

where I is the fault current (A), t is the fault duration (s), T_i is the conductor temperature before the fault ($^{\circ}\text{C}$), T_f is the conductor temperature after the fault ($^{\circ}\text{C}$), and A is the conductor cross-section without allowing for empty spaces (kcmil), λ is the inferred temperature of zero resistance ($^{\circ}\text{C}$) and K is the conductor constant that represent the conductor specific heat, density and resistivity of the material.

Another equation in (4.12) is provided for the same adiabatic conductor limit equations of (4.8) to (4.11) [80]. In (4.12) the instantaneous current is used in an integral form for a

specific time period. To ensure the conductor is not damaged, the LTE should be less than or equal to the heat energy that the conductor material can absorb [80]. The left side of (4.12) is also termed Joule's integral [136], [149], [150].

$$\int_0^{T_f} i^2 dt \leq A^2 k^2 \quad (4.12)$$

where i is the fault current (A), T_f is the fault duration (s), A is the conductor cross-sectional area (mm²), and k is a factor that accounts for the conductor heat capacity, resistivity and temperature coefficient. The rise in conductor temperature is captured within this factor k .

In (4.8), by dividing with the resistance (R) on both sides of the equation, the left side will resemble the LTE equation in (4.3) of the conductor. When looking at the left-hand side of (4.8) the unit is Joule for energy and when dividing by the resistance to obtain the LTE it is changed to Joule per ohm (J/R) [136]. The LTE can also be expressed as ampere-square-second (A²s) [53], [140], [150]. From (4.4), by increasing the conductor size (increase the conducting area) the resistance of the conductor will be reduced. This will reduce the heat being generated in the conductor by the flow of current and hence the short time rating of the conductor will increase. By increasing the short time rating, the permissible LTE rating at that part of the network will be increased. It is thus beneficial to have larger conductor type in high LTE regions on the feeder. It is recommended in [138] that the first kilometres of conductor that leave the substation be strung with a larger conductor (e.g. Mink or Hare conductor). This is based on typical fault levels in the South African MV grid. The term "large conductor" is relative to the fault level at the substation and the typical maximum fault clearing times expected.

Conductors can consist of one type of material or a combination of materials. Aluminium is preferred over copper as it is less expensive, readily available and has a good strength to weight ratio [38]. An overhead conductor consisting of only aluminium is called an all-aluminium conductor (AAC) [38], [135], [137], [139]. If the conductor consists of a steel

core it is called an aluminium conductor steel-reinforced (ACSR) conductor [38], [135], [137], [139]. Another type of overhead conductor being produced is an all-aluminium alloy conductor (AAAC) [38], [135]. Both the ACSR and AAAC conductor types have better mechanical strength and can accommodate a greater span length or higher currents as compared to AAC [135], [137]. The steel does add additional weight to the conductor of up to 18 % [135]. The steel does increase the breaking strength of the conductor as compared to AAC conductor [135].

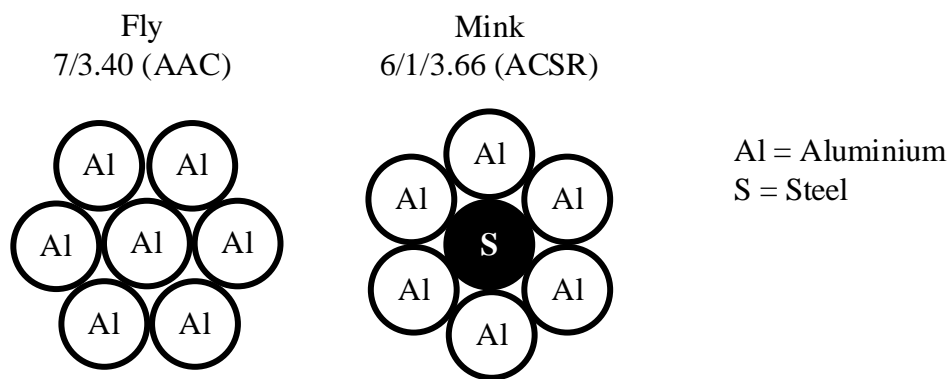


Figure 4.3. Fly AAC and Mink ACSR conductor strand configurations.

In Figure 4.3 Fly (AAC) and Mink (ACSR) conductor configuration are shown [139]. It can be seen that the steel forms the core of the ACSR conductor whereas for the AAC it is only aluminium. The FLY AAC construction is specified by the code 7/3.40. This means that the conductor consists of seven strands, each with a diameter of 3.40 mm. The Mink ACSR conductor is specified by the code 6/1/3.66. Mink conductor consists of six aluminium strands and one steel strand. All the strands have a diameter of 3.66 mm. If there are more steel strands, the conductor strand configuration can be different, but the steel strands form the centre or pass through the centre of the conductor [139]. The steel reinforcement not only assists with the mechanical strength of the conductor, but also improves the short time rating of the conductor [137]. High temperature low sag (HTLS) conductors can operate indefinitely at temperatures in the range of 150 °C to 250 °C [51]. There are other aluminium conductors as well, namely Aluminium conductor composite reinforced (ACCR) and aluminium conductor composite core (ACCC) [51]. ACCR is approximately five times more expensive than ACSR conductor and ACCC is approximately 2.5 times more expensive [51]. These conductors are not considered for this study.

To calculate the short time ratings of conductors, the initial and final temperatures should be known. The initial temperature is the maximum temperature at which the conductor can be operated [80]. Operating temperatures of conductors can vary from 25 °C to 75 °C [108]. The conductor has higher resistance at higher operating temperatures [135]. For the short time ratings of Table 4.1 a prefault (or initial) temperature of 75 °C and a final temperature of 200 °C were used [138]. An initial temperature of 50 °C was used in the IEEE std. 738 [151]. The method that is recommended in [137] made use of an initial temperature of 50 °C for AAC and an initial temperature of 65 °C for ACSR conductor. The final temperature was set to 200 °C for both conductor types [137]. A final temperature of 200 °C is also recommended in [80]. A final temperature of 340 °C was used in [135] and a temperature of 180 °C was used in the IEEE std. 738 [151]. Figure 4.4 illustrates the effect of initial and final temperature choices on the conductor 1 s short time rating. The conductor 1 s short time ratings were calculated by applying (4.8) for Hare, Mink and Fox conductors.

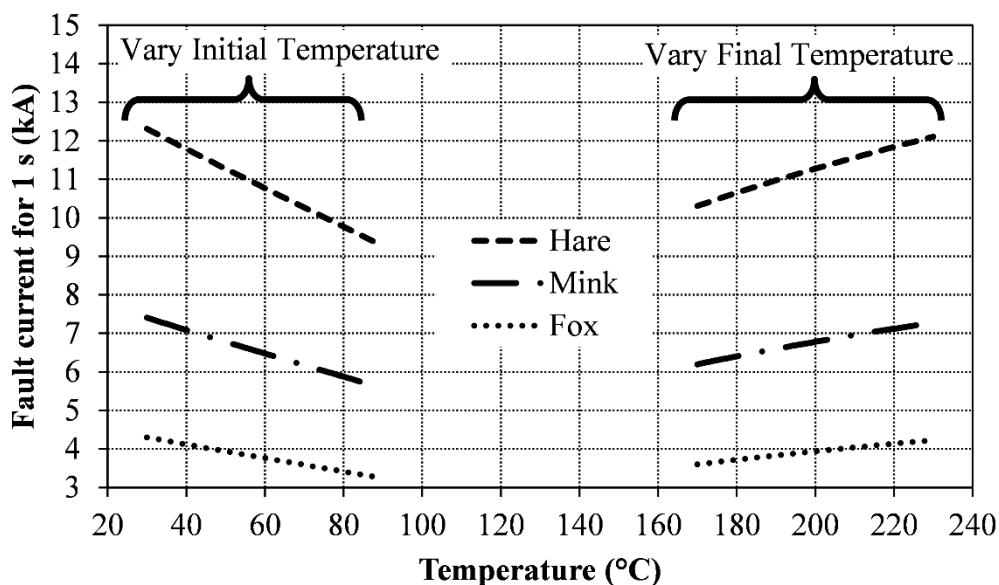


Figure 4.4. The effect on the 1 s short time rating of Hare, Mink and Fox conductors for choices of initial and final temperatures.

Two sets of graphs are shown for each type of conductor in Figure 4.4. The first is where the choice of initial temperature was varied from 30 °C to 90 °C while keeping the choice of

final temperature constant at 200 °C. The second is where the choice of final temperature was varied from 170 °C up to 230 °C while keeping the choice of initial temperature constant at 50°C. This was done for Hare, Mink and Fox conductor types. All three conductors are of ACSR type resembling the Mink configuration in Figure 4.3 with six aluminium strands and one steel strand. Hare has the code 6/1/4.72, Mink 6/1/3.66 and Fox 6/1/2.79 (aluminium strands/steel strands/diameter).

It can be seen that the higher choice of initial temperature, lowers the 1 s short time rating of the conductor (fault current for 1 s). This is the case for all three conductor types. The choice of initial temperature should be based on the highest operating temperature (for load current) of the conductor. For the work done in this Thesis, an initial temperature of 75 °C is used. This initial temperature is the same to the temperature used in [148]. In the final temperature graph of Figure 4.4 it can be seen that the higher the choice of final temperature, the higher the 1 s short time rating of the conductor. This is the case for all three conductor types. The worst case in terms of protection for the choice of final temperature would be to choose a low value. This final value is governed by the conductor material [137]. The maximum value that should be used for aluminium is 200 °C [80]. This is similar to the final temperature value used in [138]. For the work done in this thesis, a final temperature of 200 °C is used. By choosing the highest initial temperature and the lowest final temperature, the temperature delta ($T_f - T_i$ of (4.8)) is small and that results in the low 1 s short time rating. Continuous temperature and short time temperature ratings for insulating mediums are also provided in [58].

Hare conductor has the biggest and Fox the smallest diameter. The results shown in Figure 4.4 further show that the bigger conductor can sustain a larger fault current for the same time (e.g. one second) or a smaller fault current for a longer period. This is expected as the Hare conductor has a greater mass when compared to the other smaller conductors. There is more material to absorb the heat generated.

The change in conductor one second fault current capability is shown in Table 4.2. This is for the conductors from Figure 4.4. It can be seen that the largest change in the current limit

is for the biggest conductor (Hare). This is the case for both a change in initial and final temperature. However, if this change is normalised to the 90 °C (initial temperature graph) and 170 °C (final temperature graph) values the percentage increase is the same for each of the conductors.

Table 4.2 Conductor short time ratings with a change in initial and final temperatures.

	Conductor Type	Temp. (°C)	1 s Fault Current (kA)	Increase (kA)	Normalised Increase (%)
Vary initial temperature (Final at 200°C)	Hare	90	9.27	3.04	32.8
		30	12.31		
	Mink	90	5.58	1.83	32.8
		30	7.40		
	Fox	90	3.24	1.06	32.8
		30	4.30		
Vary Final Temperature (Initial at 50°C)	Hare	170	10.30	1.80	17.4
		230	12.10		
	Mink	170	6.20	1.08	17.4
		230	7.28		
	Fox	170	3.60	0.63	17.4
		230	4.23		

To calculate the conductor one second short time ratings the values listed in Table 4.3 are used for the different material types [137], [139]. The resistance of steel conductor used for the calculations is 192 $\Omega \cdot \text{mm}^2/\text{km}$ at 20 °C [137]. This steel resistance will be divided by the steel cross-sectional area. From the manufacturers datasheets the following information are obtained: overall conductor diameter, conductor stranding configuration, aluminium area, conductor diameter over steel, steel area, the mass of each material type per km, ultimate tensile strength, the DC resistance per km, coefficient of linear expansion, initial

modulus of elasticity, final modulus of elasticity and the continuous current rating [139]. All of this information is not used for calculating the conductor one second short time rating but is mentioned here to indicate what is typically obtained from a manufacturer.

Table 4.3 Conductor material constants used for calculating the conductor short time rating.

	Aluminium	Galvanised steel	Aluminium alloy
Heat capacity of conducting material (J/°C·g)	0.904	0.488	0.904
Temperature coefficient of resistance (per °C)	0.00403	0.00537	0.0036

If the conductor consists of only one material type, the conductor material constants can be used as is for (4.8). But, if there is more than one material type used in the construction of the conductor (e.g. ACSR), some of the elements in (4.8) have to be averaged or combined [137]. The quantities that will have to be averaged or combined are the total weight of the conductor, the heat capacity of the conducting material, the temperature coefficient of resistance and the resistance of the conducting material. Equation (4.13) to (4.16) can be used to average or combine these quantities for two material types in a conductor [137]. The subscript of “1” and “2” for the variables in (4.13) to (4.16) are for the two different materials that the conductor consists of.

$$W = W_1 + W_2 \quad (4.13)$$

$$S = \frac{W_1 S_1 + W_2 S_2}{W_1 + W_2} \quad (4.14)$$

$$\alpha = \frac{A_1 \alpha_1 + A_2 \alpha_2}{A_1 + A_2} \quad (4.15)$$

$$R = \left(\frac{1}{R_1} + \frac{1}{R_2} \right)^{-1} \quad (4.16)$$

where W is the mass of conducting material (kg/km), S is the heat capacity of conducting material ($J/^\circ C \cdot g$), R is the resistance of conductor at T_i (Ω/km), α is the temperature coefficient of resistance (per $^\circ C$), A is the cross-sectional area of conductor (mm^2).

In (4.13) the total weight of the conductor has to be determined and this is simply the sum of each material type used within the conductor. The heat capacity of the conducting material (S) is averaged by the ratio of the mass of each type of material to the total mass of the conductor. In (4.7) it was shown that the resistance is a function of temperature and in (4.4) it can be seen that the resistance is also influenced by the conductor cross-sectional area. The temperature coefficient of resistance is averaged for the conductor by using the ratio of each material type's area to the total cross-sectional area of the conductor. The conductor materials can be considered as resistors in parallel with each material type is parallel to the other along the length of the conductor. Thus, the total conductor resistance is calculated by applying (4.16). The equations provided in (4.13) to (4.16) can be expanded to more than two conductor material types.

Wasp conductor is an AAC with an aluminium area of 105.95 mm^2 [139]. When applying an initial temperature of $75 \text{ }^\circ C$ and a final temperature of $200 \text{ }^\circ C$ to (4.8) the 1 s short time rating calculates to 8982 A. When applying (4.10) with the same initial and final temperature the 1 s short time rating calculates to 9280 A. This was done with an inferred absolute minimum temperature of $-234 \text{ }^\circ C$ as shown in (4.10). If an inferred absolute minimum temperature of $-236 \text{ }^\circ C$ is used the 1 s short time rating calculates to 9255 A for 1 s when applying (4.10). When comparing the 1 s short time rating results from (4.8) to that of (4.10) it can be seen that it compares well. The small difference in inferred absolute minimum temperature does not make a significant difference to the result when applying (3.10). Equation (4.8) will be used to calculate the conductor short time ratings in this thesis. It allows for the application to conductors consisting of more than one type of material such as ACSR conductor.

In Table 4.4 the conductor information is shown that is used for the calculation of the 1 s short time rating of ACSR Fox conductor. By applying (4.13) to (4.16) the following results

are obtained. The total mass of the conducting material (W) calculates to 149 kg/km. The heat capacity of the conducting material calculates to 0.7703 J/°C·g. The temperature coefficient of resistance calculates to 0.00422 per °C. The resistance at 20 °C calculates to 0.7632 Ω/km. This resistance is now moved to the conductor operating or initial temperature of 75 °C by using (4.7) with the average temperature coefficient of resistance. The resistance value calculates to 0.9404 Ω/km at 75 °C. All of these values are now applied to (4.8) so as to calculate the conductor short time rating when the conductor temperature increases from 75 °C to 200 °C. This calculation results in a LTE rating for ACSR Fox conductor of 12.253 MA²s. To calculate the 1 s short time rating for ACSR Mink conductor, the square root of the LTE rating has to be divided by 1 s. Thus, the 1 s short time rating for ACSR Fox conductor calculates to 3.50 kA.

Table 4.4 Fox conductor information from the manufacturers datasheet [139].

	Area (mm²)	Mass (kg/km)	Temperature coefficient of resistance (per °C)	Heat capacity (J/°C·g)	Resistance at 20 °C (Ω/km)
Aluminium	36.68	101	0.00403	0.904	0.7822
Steel	6.11	48.1	0.00537*	0.488*	31.424*

* These values were obtained from [137]

In Table 4.5 results are shown for the 1 s short time rating calculations and then the associated LTE rating of each conductor. The values provided in Table 4.1 compares well to the calculated values using (4.8). Short time ratings for all the conductors are not available in [138]. The calculated 1 s short time rating as listed in Table 4.5 will be used for the work in this thesis.

Table 4.5 Conductor short time and let-through energy ratings.

Conductor	1 s Short time rating [138] (kA)	1 s Short time rating calculated (kA)	Let-through energy calculated (MA ² s)
Fox	3.14	3.50	12.25
Gopher	No value	2.50	6.27
Hare	8.97	10.02	100.39
Mink	5.40	6.03	36.31
Oak	9.59	9.52	90.68
Rabbit	No value	5.04	25.38
Squirrel	1.79	2.00	4.00

4.5 NETWORK CONFIGURATIONS

Two network configurations are being discussed in this section. The first being a radial MV feeder and the second being a multi-source MV feeder.

4.5.1 Radial medium voltage network

In Figure 4.5 a simplified radial feeder is shown. On a radial feeder there will be high fault levels close to the source. The fault level will drop as the fault position moves further into the network on a radial feeder. This means that the fault level in section A will be greater than the fault level in section D. There are many operating curves (see Chapter 3) that can be applied to the protection on AR 1 (and AR 2 and AR 3). If an IDMT type operating curve is used, the operating time will increase as the fault level reduces further into the network. In Figure 4.2 a LTE curve and conductor damage curve are shown. A replica of this is also shown within Figure 4.5 (with high risk areas added).

For AR 1 two LTE high risk areas can be defined when a single IDMT curve is applied. The first being close to the source where the current is dominant and the later at a position where the fault level to PU ratio becomes close to one. This is where the operating time tends to infinity. All of the protective devices will have high risk areas. Depending on the operating curve or curves that are applied, there might be more than one high risk area. When considering the LTE-distance graph. This LTE-distance graph can be used to identify where the potential high-risk areas are. A high-risk area is an area where there is a LTE peak with the potential of exceeding the conductor limit. If there is a fault within this high-risk area it can result in damage not only to the conductor there, but all the sections of conductor that have to carry the fault current. With reference to Figure 4.5, if the fault is in section E and the conductor type in section A to E is the same, all of those conductor sections will get damaged the same. The high-risk area XX is common to all protection devices. This means that the protection device AR 2 will have a similar XX region close to that CB. If there are multiple devices to grade with, not only will the fault current be high in region XX but the operating time will be slow as well [119], [123].

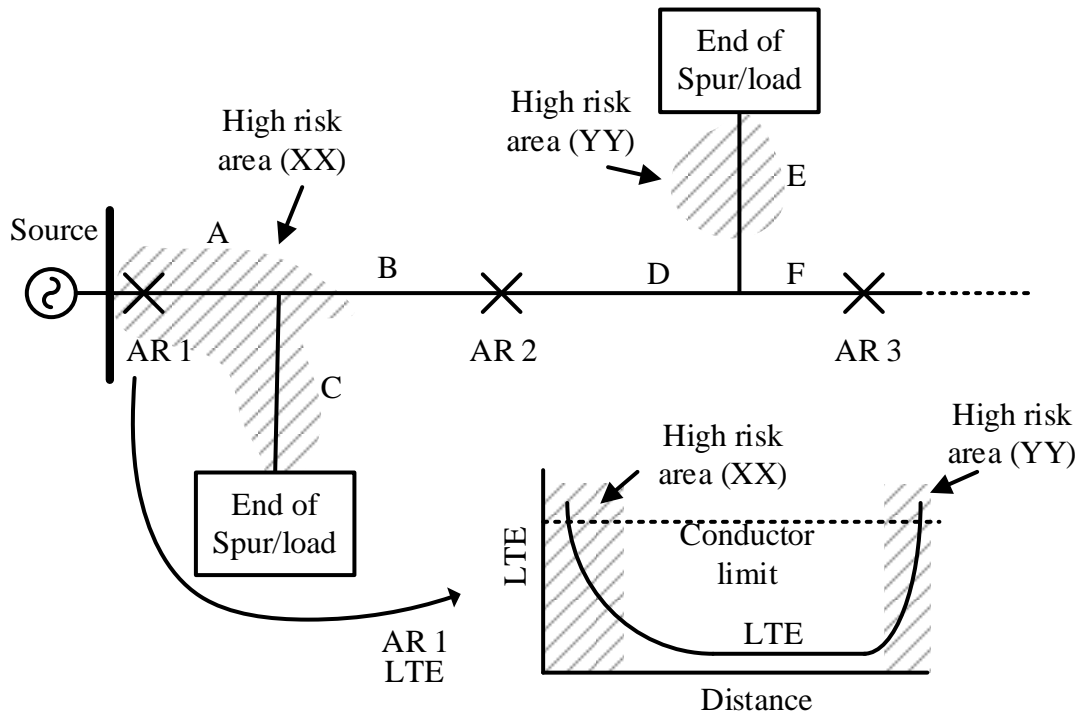


Figure 4.5. Let-through energy high risk areas on a radial feeder.

The high-risk area YY will also be present if an inverse type curve is used and there are long protection operating times. If the protection philosophy was different in that AR 1 did not have to provide backup protection to the downstream AR 2, then the second high-risk area (YY) can move to section B (just before AR 2) from where it is in section E. This depends on the protection philosophy (see Chapter 3) that the utility is applying. If DG or an interconnection is added to the feeder beyond AR 3, bidirectional current flow will be present on the feeder. The high-risk areas XX can then be present in both section B and D for AR 2. AR 2 can also have a second high-risk area YY on both sides (forward and reverse) of the CB (or AR). In general, a minimum of two protection devices are required to detect a fault (main and backup protection) [37], [102]. Additional curves applied to the IDMT operating curve can result in additional high-risk areas. A similar LTE-distance plot can also be made for AR 2 and AR 3 to show how they will protect the conductors within their protective reach. All of the ARs LTE plots can be added to the same plot to look at the feeder as a whole [40], [41].

In a radial feeder the current flow (fault current) is only in one direction from the source to the fault. As such, the OC protection applied to these types of feeders are usually non-directional current based protection. To isolate a fault in a radial feeder, only one CB has to operate, but all supply will be lost to any downstream loads (below the AR that operates). If a fault was present in section B of the network in Figure 4.5, only AR 1 have to operate to isolate the fault.

For a radial feeder, there is no need to have a large backbone conductor throughout the length of the feeder as bi-directional current flow is not possible. In Figure 4.5 the backbone conductor can be defined as section A, B, D and F. A large backbone conductor will assist with reducing losses, improve the voltage profile and for future expansion on the feeder. A larger conductor is however required close to the source where the conductor can get damaged [51], [138]. This is high risk area XX in Figure 4.5. This may not be required for AR 2 as the fault level reduces from AR 1 and the protection operating time may be faster in a radial feeder. From the backbone conductor there are spurs radiating from the conductor to the various loads. In Figure 4.5 spurs can be seen as section C and E. These conductors

can be much smaller in size based on the load they carry. If the spur conductor is located in a high-risk part of the network (such as close to the source) then the spur conductor size should be increased (sized for fault current) as this conductor can also get damaged by the LTE. If we consider the first spur from the source side in Figure 4.5, this falls within the high-risk area.

4.5.2 Multi-source medium voltage network

Multi-source MV networks refer to MV networks where there are two or more possible points of supply. These supply points can be due to the feeder being operated as in a loop configuration, or as a result of N/O points closing creating another supply point on the feeder, or as a result of DG that is installed in the feeder, or a combination of this.

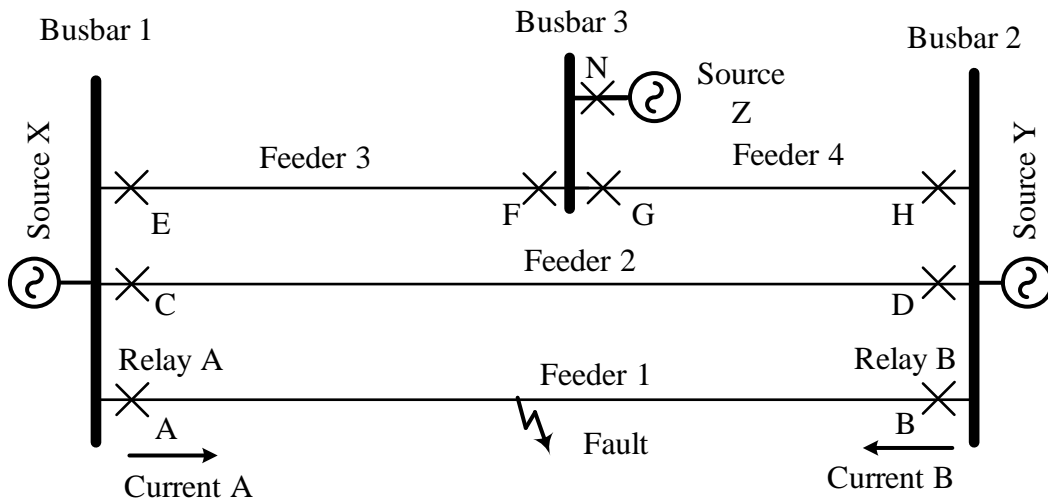


Figure 4.6. An interconnected network consisting of multiple sources.

With DG installed on the feeder, there are more possible simultaneous points of supply on the feeder. This means that not only is the utility supplying the load on the feeder, but other generation points are supplying at the same time. To isolate the fault, a minimum of two CB's are required to operate on either side of the fault (except if the fault is on a radial spur with a CB). Some of these generators may contribute to the fault current. To explain the effect of additional sources on the OC protection of a feeder, the interconnected network with multiple sources of Figure 4.6 is considered. In this network (Figure 4.6) it can be seen

that there are three busbars with a source connected to each of these busbars. Busbar 1 to Busbar 3 is also interconnected to each other using the four feeders. For a fault on the network (Feeder 1), fault current will be supplied from both ends of the feeder (Busbar 1 and Busbar 2). These fault currents will be limited by the source impedance, the impedance of the feeder and the fault resistance.

The conductor from Busbar 1 up to the fault point will be exposed to fault current associated with the Kirchoff sum at Busbar 1 (Current A). The conductor from Busbar 2 up to the fault point will be exposed to the Kirchoff sum of fault current from Busbar 2 (Current B). At the fault position an arc will form between the faulted phases. At the fault position plasma will form [152]-[154]. Within the plasma there will be fault streamers moving from the conductor to the arc [152]-[154]. The assumption is made that the fault current will thus not combine on the feeder. This means that the conductor will not be exposed to the combined fault current from both ends of the feeder. The plasma and streamers are illustrated in Figure 4.7 for the fault of Figure 4.6 on Feeder 1. The duration of fault current from Busbar 1 will be determined by the protection settings applied to Relay A. The same will be for the current from Busbar 2 and Relay B.

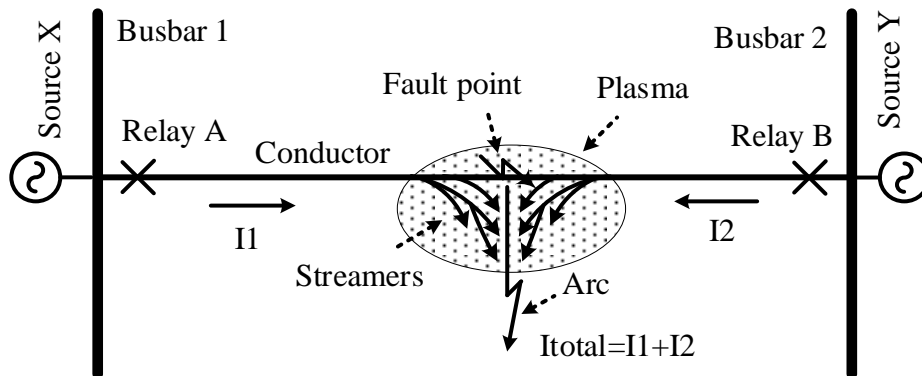


Figure 4.7. The fault current, streamers and plasma at the fault position.

One of the advantages of having DG installed on a feeder is that it reduces the network investment and operational cost [73], [88]. This is due to the load being situated closer to the generation. The losses associated with transporting power to loads at the end of the feeder can reduce [21]. The requirement for large conductors to meet the load demand for the total feeder from the main utility source can be minimised. This is under the assumption that the

DG will have reasonable availability on the feeder. The drawback of these multiple sources and interconnected networks are that the complexity of protecting the network and finding protection settings that are applicable to a wide range of network contingencies become difficult. The smaller conductor, possible increase in fault levels (due to DG) in some parts of the network and potential protection blinding in other parts increases the risk of conductor damage.

4.6 FAULT CURRENT AND DISTRIBUTION

Within an interconnected network, the measured RMS fault current can change if a CB is to open or close (e.g. ARC) within the interconnected network during the fault. This is due to the network impedance (or source impedance to the fault) changing. The opening and closing of CBs will change the current distribution within the network during the fault period. For the fault shown in Figure 4.6 the current measured at A can change if the CB at D opens before A. The same can happen if the CB at B opens before A trips and if A trips before B. This means the IDMT relay equations of (3.1) to (3.3) cannot be used in this form to determine the relay operating time as the equations in this form assume a constant current being measured until the CB opens.

The source Z or Y shown in Figure 4.6 can be a distributed generator. There are many forms of generation such as wind generation, PV, concentrated solar power plant, small hydro power plant, landfill gas power plant, biomass power plant and a biogas power plant [75]. Each of these generators have their own characteristics during normal operating conditions and during faults. The wind and PV generators are the two most common types of generators implemented at present [2]. Wind turbines can be broken down further into four types. Type 1 is a squirrel cage induction generator [4], [69]-[71]. This type of generator connects to a step-up transformer directly. Type 2 is a wound rotor induction generator with resistors that are used to maintain the turbine speed [4], [69]-[71], [155]. Type 3 wind generators are asynchronous wound rotor machines [4], [69]-[71]. An AC-DC-AC converter is used to supply the rotor field. The frequency of the AC excitation can be varied on type 3 generators. A Type 3 generator is known as a DFIG [4], [69]-[71], [155]. The advantage of Type 3

generators is that it the reactive and real power can be controlled separately [4], [70], [71], [155].

A Type 4 wind generator is an asynchronous machine with the stator windings connected to the supply grid through an AC-DC-AC converter [4], [69]-[71]. This generator type offers the greatest benefit as the machine can rotate at the best aerodynamic speed (can be less or more than synchronous speed) [69]-[71]. A Type 5 wind generator is also defined in [70] for turbines where a variable speed drive chain is connected to a torque or speed converter [70]. A synchronous generator is connected to the speed or torque converter. This Type 5 generator connects to the grid directly and makes use of an automatic voltage regulator to regulate the output voltage [70]. For a PV generator rows of generating DC panels are connected together and the output is fed through a controlled DC-AC converter [69]. The fault current contribution from PV generators may vary based on the time of day [9].

The fault contribution from wind generation and PV generators are highly dependent on the control algorithm driving the power converter [69]. Type 1 and Type 2 wind generators do not use power electronics for power conversion and control [69]. The fault current produced by these wind generators (Type 1 and Type 2) are similar to large induction machines [4], [70]. These generators can produce large fault currents (similar to lock rotor value) that will decay after a number of cycles [70]. Type 3, Type 4 and PV generators fault current contribution is dependent on the speed of the converters and control philosophy [69], [70]. Generators making use of a full converter can be set to produce negative phase sequence current for unbalanced fault types [69]. These generators (Type 3, Type 4 and PV) can produce 1.2 p.u. of fault current [69]. This 1.2 p.u. value falls within the range of 1.1 p.u. to 1.5 p.u. specified in [10] for PV generation. In [71] the Type 3 wind generators can inject reactive current up to 1.3 p.u.. For DFIG a crowbar can be added to improve the fault current ride through capability of the generator [69], [156]. With the crowbar applied, the generator can then switch between motor and generator modes [69]. Table 4.6 is showing the fault current contribution for different types of wind turbine generators. The results from [70] and [4] are shown and they compare well with each other.

Table 4.6 Wind turbine fault current contribution.

Wind turbine type	Fault current [70] (p.u.)	Fault current [4] (p.u.)
Type 1	5 to 6	Up to 6
Type 2	5 to 6	Up to 6
Type 3	1.1 to 2.5	Up to 3
Type 4	Just above 1	1.1
Type 5	4 and greater	-

The required duration of this fault current is dependent on the fault ride through capability imposed by the grid code [69], [70]. The embedded generators have to meet the operating regulations as stipulated by the network authority. Within South Africa this is NERSA and the operating regulations are stipulated in the South African Grid Code [75]. Within New Zealand this is the Electricity Industry Participation Code [76]. Within each of these codes there is a generator fault ride through criteria defined. This means that if there is a fault within the network (not the generator), it is required to remain stable and connected to the network [75], [76]. In these codes a no trip zone for the generator is defined based on the measured grid voltage at the point of connection and the duration of the fault. This does not mean that the generator is not allowed to trip for the fault, it means that the generator should remain connected to the grid for the minimum period defined in the grid code. Depending on the severity of the voltage dip during the fault, the required fault ride through time can increase or decrease. During this fault period certain generator types can support the grid by injecting reactive power for voltage support [71]. The response time of modern wind generators is one cycle and then they can provide full reactive support within 3 cycles [71].

The time the generator is connected to the grid can thus vary based on fault type and position. Further, the fault current capability and behaviour of generators are different. The source Z or Y shown in Figure 4.6 can trip before the relay at A has issued a trip signal to the CB at A. This means the measured current will change and result in a change in the operating time.

Again, the relay operating equations as shown in (3.1) to (3.3) cannot be used in this form. For the work done in this thesis, the specific generator behaviour is not studied. In this section it is shown that there are many forms of the most common type of DG, each with its own characteristics. The focus is placed on the fault current that is being measured by the protection relay on the faulted feeder. This section also shows that the measured fault current can change over time when there is DG installed, or when an interconnected network is present or a combination of both additional generation and interconnections. For the results generated in this thesis the source will be modelled as an external grid and CBs will be opened based on protection settings applied to the various CB relays in the model under study. The effect of different embedded generators on the LTE capability of a conductor can be studied further in future work by modelling specific generator types and control strategies in the network simulation software.

4.7 OVERCURRENT RELAY MODEL

The IDMT OC relays make use of RMS current [157], [158]. The operating equations for IDMT type operating curves are shown in Chapter 3. These equations are all applicable when the RMS fault current has reached its steady state condition. By applying them the relay operating time can be determined. As an example, apply a NI curve, with a PU of 250 A and a TM of 0.3 to a relay measuring 1000 A of current. The trip time can then be determined as 1.49 s by applying (3.1). If the fault current was lower at 500 A the trip time would be 3 s. If the fault current is higher at 1500 A the trip time would be 1.15 s. This is true only if the measured RMS fault current did not change. To explain the effect of a change in fault current, an induction disk electromechanical relay is considered. An induction disk electromechanical relay with a NI operating curve is shown in Figure 4.8.



Figure 4.8. An induction disk electromechanical protection relay.

If the RMS fault current stays constant, the relay disk will rotate at a constant speed and the relay operating time can be determined using (3.1) for a NI curve. However, if the RMS fault current reduces before the relay issues a trip signal, the speed of the rotating disk will be impacted and this will change the relay trip time. The same is happening with numeric relays trip time for a change in fault current [157], [158]. To determine the operating time for a change in measured RMS fault current, the relay IDMT operating equations of (3.1) to (3.3) have to be changed.

The basic induction disk electromechanical relay operating equation as derived from differential equations is shown in (4.17) [117].

$$K_I I^2 = m \frac{d^2 \theta}{dt^2} + K_d \frac{d\theta}{dt} + \frac{t_F - t_S}{\theta_{max}} \theta + t_S \quad (4.17)$$

where K_I is a constant relating torque to current, I is the input current, m is the moment of inertia of the disk, K_d is the drag magnet damping factor, θ is the disk travel, t_F is the spring torque at maximum travel, t_S is the initial spring torque and θ_{max} is the maximum disk travel. In [117] and [159] (4.17) is simplified by neglecting the disk inertia. The simplified version of (4.17) is shown in (4.18) [55], [117], [118], [129].

$$1 = \int_0^T \frac{1}{t(I)} dt \quad (4.18)$$

where T is the relay trip time (s) and $t(I)$ is the time-current equation. There are various time-current equations available. To determine the operating time using (4.18) the actual RMS fault current over time signal has to be known. This is the relay measured fault current. In essence, (4.18) is determining when the inverse of the area under the relay characteristic curve is equal to one. To implement this in real time a discrete sample version of (4.18) has to be used. The integrator can be replaced with a summation function in a discrete form (using samples) [131], [158]. This discrete version of (4.18) is shown in (4.19).

$$1 = \sum_{n=0}^{n=\infty} \left(\frac{Tstep}{t(I)} \right) \quad (4.19)$$

where $t(I)$ is the time-current equation, n is the sample number and $Tstep$ is the sample time step size in (s). In (4.19) the inverse of the area under the relay characteristic curve is determined by adding the area of each sample together and checking at which sample number the sum is equal to one. This sample number multiplied by the time step ($Tstep$) is the relay trip time.

Another method to determine the relay trip time was also developed in the course of this thesis using the concept of the rotating disk of an electromechanical relay. The assumption is made that the disk angular speed is constant if the input RMS measured fault current is constant. When considering an object moving in a straight line, the average speed of the object can be determined if the distance is known and the time it took to travel the distance [132]. This average speed formula is shown in (4.20), but it is applied to the rotating disk of an electromechanical relay.

$$v = \frac{s}{t} \quad (4.20)$$

where v is the speed of the disk (m/s), s is the distance travelled by the disk (m) and t is relay trip time is (s). For a rotating disk the distance should be stated as angular distance, as the linear distance is a function of the radius of the disk. As discussed in Chapter 3, the TM will increase or decrease the operating time. In the application of (4.20) to a relay, the TM is proportional to the distance the disk has to travel or rotate before a trip is issued to the CB.

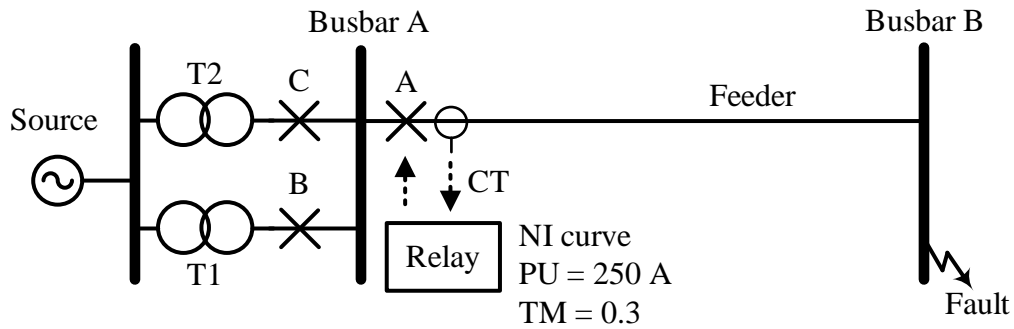


Figure 4.9. Simulation network model for relay operating time illustration.

To show how to apply (4.18), (4.19) and (4.20) a radial feeder is modelled with one source and two transformers (T1 and T2) in a simulation package. An IDMT relay is applied to the feeder CB at Busbar A (on CB A) and a three-phase fault is placed at Busbar B. The relay is programmed with an IDMT operating curve, a 250 A PU and a TM of 0.3. The network diagram is shown in Figure 4.9.

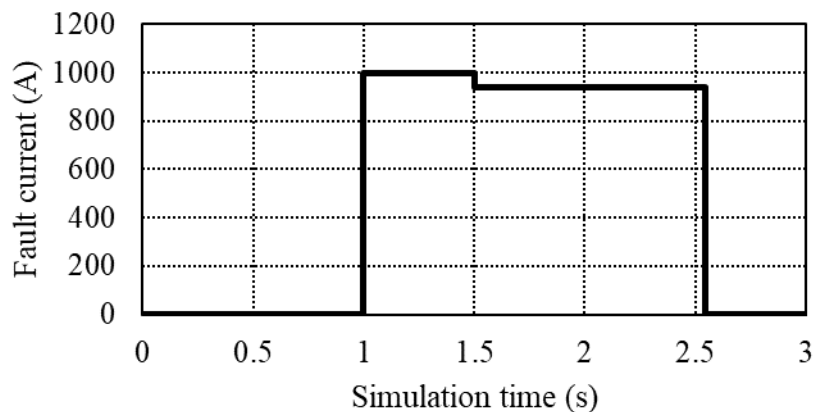


Figure 4.10. Simulation result for the relay operating time simulation.

For the simulation, a three-phase fault is placed at Busbar B at one second, and after 1.5 s CB C is opened to change the current passing through the measuring CT on the feeder at

Busbar A. The relay is set to open CB A once the relay has finished timing. The result of this simulation is shown in Figure 4.10. A similar approach towards testing a relay was applied in [157]. In the result of Figure 4.10 it can be seen that when the fault occurs at one second, the fault current is 999.3 A (from simulation). At 1.5 s when CB C opens the fault current drops to 938.6 A (from simulation) until CB A finally gets tripped by the relay at 2.54 s (from the simulation). If the relay operating time was calculated using (3.1) the trip signal would have been sent at 1.495 s if the fault current was 999.3 A and the relay would have tripped at 1.566 s if the fault current was 938.6 A. As the fault current have changed at 1.5 s into the simulation, (3.1) cannot be used to calculate the relay trip time. The simulation has shown that the trip time occurs at 2.54 s, which means the relay took 1.54 s before it issued the trip signal.

Equation 3.1 and (4.18) is combined to give (4.21). Equation (4.21) is set up for the fault current signal as shown in Figure 4.10. To apply the equation to the current signal it has to be split into two regions to accommodate the change in fault current. This is similar to the Joule integral application for fuses consisting of a minimum melting and total clearing time regions where the fault current is different in each region [149]. If there were more changes, then these have to be accommodated with additional time terms in the equation. In (4.21) $T1$ is the time when the current change from the fault inception time. This is 0.5 s. The value of $T2$ will be the trip time of the relay. Equation (4.21) also solves to the simulation value of 1.54 s.

$$\begin{aligned}
 1 &= \int_0^{T1} \frac{\left(\frac{I_f}{PU}\right)^{0.02} - 1}{0.14 \cdot TM} dt + \int_{T1}^{T2} \frac{\left(\frac{I_f}{PU}\right)^{0.02} - 1}{0.14 \cdot TM} dt & (4.21) \\
 1 &= \int_0^{0.5} \frac{\left(\frac{999.3}{250}\right)^{0.02} - 1}{0.14 \cdot 0.3} dt + \int_{0.5}^{T2} \frac{\left(\frac{938.6}{250}\right)^{0.02} - 1}{0.14 \cdot 0.3} dt \\
 T2 &= 1.542 \text{ s}
 \end{aligned}$$

Similar to the combined integral version of (4.21), (3.1) can be combined with (4.19). This was done in separate code where the fault current signal of Figure 4.10 was programmed into the code and the current was then sampled at 1 kHz (0.001 s time step) to determine the trip time. The sample time can be made faster, but for this purpose 1 kHz is sufficient. This was done in Python. From the result of the code it is found that the trip time is 1543 samples or then 1.543 s at a time step of 0.001 s. With this method a small error is introduced as it makes use of a Riemann calculation approach. This error can be decreased by increasing the sample rate. Generally, an IDMT OC element can be set to issue a trip from roughly 20 ms onward (depends on relay manufacturer and protection element). The times applied depends on the protection philosophy that is applied. From experience this can be in the range of 0.5 s to 3 s for an IDMT element applied to a feeder relay at the busbar.

The trip time for the fault signal can also be determined using the average disk speed method using (4.20). The distance is set equal to the TM of 0.3 (unit of meter). For an RMS fault current of 999.3 A the required disk speed is 0.201 m/s to have the relay sending a trip signal in 1.495 s. For an RMS fault current of 938.6 A the required disk speed is 0.192 m/s to have the relay sending a trip signal in 1.567 s. The relay disk would have travelled a linear distance of 0.1004 m in 0.5 s at an RMS fault current of 999.3 A. The disk still has to travel a linear distance of 0.1996 m of the 0.3 m (TM) before a trip signal is issued. After 0.5 s from fault inception, the RMS fault current changed to 938.6 A. At this current level the disk speed is 0.1915 m/s and the disk will complete the remaining distance of 0.1996 m in 1.0425 s when applying (4.20). The total trip time is 1.5425 s. This is the sum of each section, thus 0.5 s added to 1.0425 s.

It can be seen that the same operating time result is obtained using the simulation, the integral calculation of (4.18), the discrete version of (4.19) and the average disk speed method. Other IDMT operating curves equations such as (3.2) for a VI or (3.3) for an EI curve can also be applied in the relay models (to calculate the operating time) in place of (3.1) for an NI curve.

4.8 CURVE SELECTION

LTE consists of a current and time component. From a protection perspective, the exposure time is the only part that can be influenced without switching healthy equipment out of service or additional equipment into service. The fault clearing time is dependent on the protection operating time (if we neglect CB operating time). The time the protection relay takes to issue a trip signal to the CB is dependent on the fault current, the PU current, the operating curve and the time settings related to the operating curve. There are probably an infinite number of protection operating curves available. These curves consist of predefined curves (IEEE, IEC and relay manufacturers), a combination of predefined curves and user definable curves. The IEEE (IEEE std c37.112) and IEC (IEC 60255) define standard operating curves such as the NI IDMT curve [34], [117].

Figure 3.1 shows the operating time curve for the NI, VI, EI and DT curves. All of them with the same PU current (600 A) and TM (0.25). The DT curve has the same PU current but with a time delay of 0.25 s. In Figure 3.1 it can be seen that the EI curve results in the fastest operating time at high fault currents and the slowest for low fault currents. The opposite is happening to the NI IDMT curve. Thus, the more inverse the curve, the faster the operating time for high currents and the slower for low currents.

In Figure 4.11 LTE curves are shown for the operating curve equations of (3.1) to (3.4). Similar to the operating time curves of Figure 3.1 the settings applied to each equation had the same PU (350 A in this case) and the same TM of 0.25 (except for the DT curve with a time delay of 0.25 s). A conductor energy limit of 4500 A for 1 s is also shown in Figure 4.11. The best curve to use where the fault current is high is the EI curve. Not only does it operate the fastest (Figure 3.1), but it also keeps the conductor LTE exposure to a minimum (Figure 4.11). Another advantage of the EI curve is that the LTE exposure curve (EI curve in Figure 4.11) is almost parallel to the conductor damage curve in the high current region. Thus, it grades well with the conductor damage curve.

The drawback of the EI curve however is that there is a rapid increase in the operating time as the fault current is decreasing. This increase in time can be used when a number of close devices (small change in fault level) are to be time graded. This rapid increase in time does mean that the EI curve is not well suited for applications where the ratio of fault level to PU is close to one. In these cases, the conductor LTE exposure is more likely to be exceeded than for a NI curve. This can be seen in Figure 4.11 when comparing an NI and an EI curve to each other. The NI curve can sustain a fault level to PU ratio closer to one. The NI curve does not grade as well as the EI curve with the conductor damage curve in the high current region. But the NI curve does provide a very horizontal profile when the operating time is considered (as the fault current drops). A small adjustment to the PU current may result in a big reduction in this increased exposure time for faults at the end of the feeder [25].

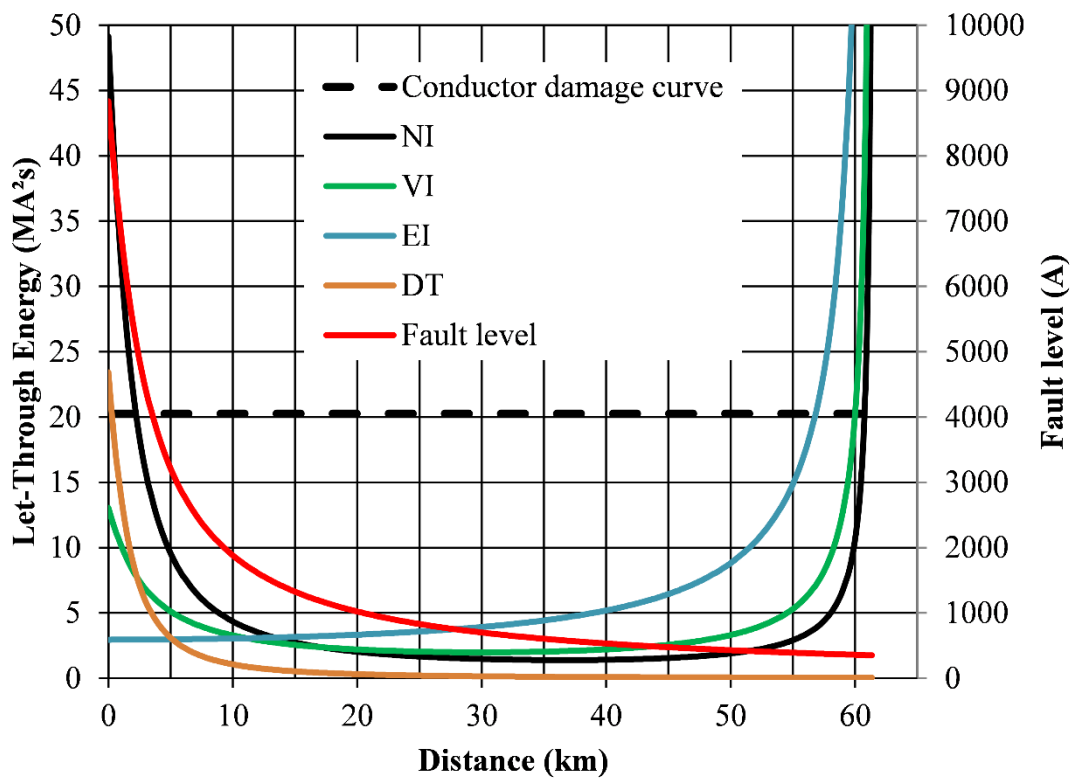


Figure 4.11. Let-through energy curves using different IEC IDMT operating curves.

The DT curve is different to the other IDMT curves as it will only have one energy peak on a radial feeder with one source. This will be in the high current high-risk region close to the source busbar (see Figure 4.5). The operating time will remain constant for this curve as long

as the fault current is larger than the PU current. Due to this constant operating time characteristic it will not produce another energy peak at lower fault levels (low compared to the PU value). This can be seen in the LTE curves of Figure 4.11 and also in the operating time curves of Figure 3.1. The change in LTE for the DT curve is due to the change in fault current across the feeder. The same signature (as DT curve) will also be present for impedance and differential protection.

The DT curve can be applied as an instantaneous element or high-set element if the time delay is set to zero. Under very high fault currents, even this element might not be able to protect the conductor from damage as the CB operating time still has to be considered [36]. In Figure 4.12 the potential conductor LTE exposure is shown for CB operating times ranging from 25 ms to 100 ms. A CB operating time of 83.3 ms is reported in [31], a time of 100 ms (5 cycles) is reported in [103], [106] and a range of 3 to 8 cycles in [10], [58]. From these curves it can be seen that under low fault levels CB operating time is negligible. However, if the fault levels are high the CB operating time is considerable and from a design perspective it is advisable to use faster CBs to minimise the LTE exposure. Larger conductors that can sustain the potential LTE exposure within the first high risk area close to the busbar may also be applied [138].

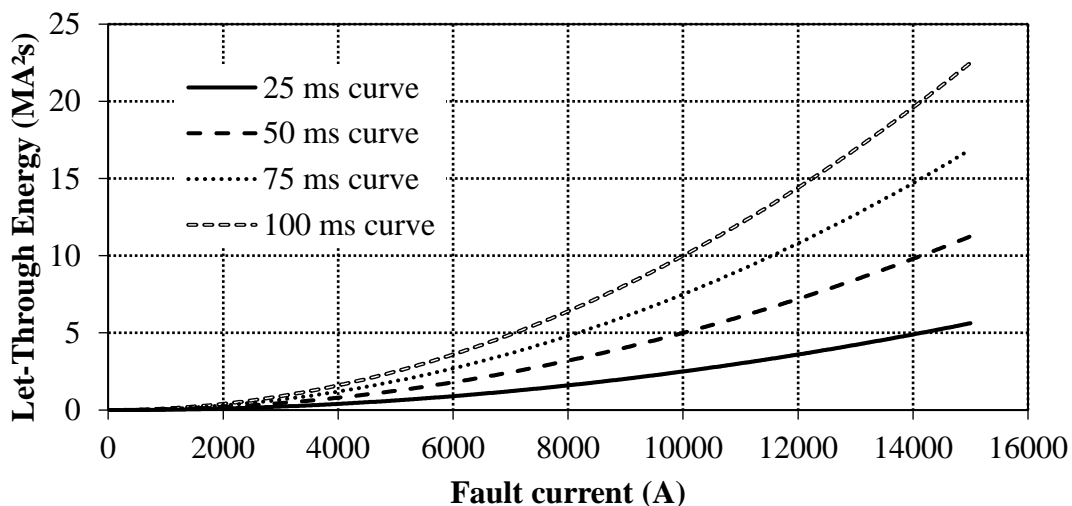


Figure 4.12. The effect of circuit breaker operating time on potential conductor LTE exposure.

For combination curves, the most commonly used and best example is a high-set curve on top of an IDMT curve. This high-set curve will reduce the LTE exposure in the high fault current region close to the source busbar [40], [103]. On top of this IDMT and high-set curve a maximum time function can also be applied (see Chapter 3). This will not only help to limit the maximum operating time of an IDMT curve, but it will also limit the second energy peak at low fault levels for the IDMT type curves. When setting the protection relays, not only should the maximum protection operating time at low fault levels be considered, but also the conductor LTE exposure. This may reduce the applied maximum time setting even further.

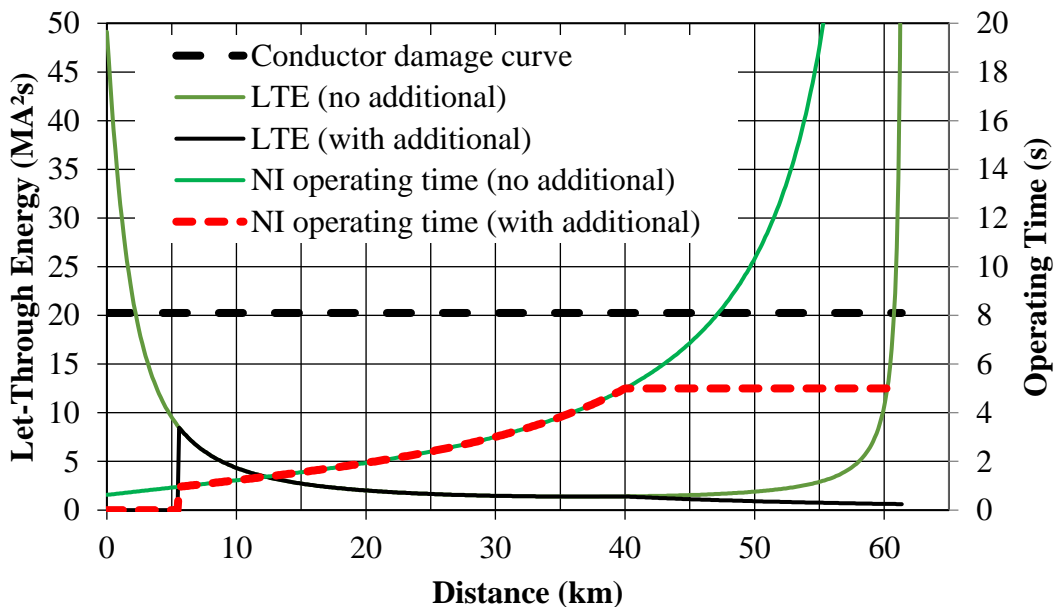


Figure 4.13. The LTE and relay operating times with high-set and maximum time curves applied.

Figure 4.13 is showing the NI curve used in Figure 4.11 on the same fault levels with and without additional curves applied. A high-set curve with a PU of 3000 A and a time delay of zero seconds is applied to the NI curve. Further, a maximum time function is applied with a PU of 350 A and a time delay of five seconds. This maximum time is similar to actual protection philosophies applied in networks [37], [102]. It can be seen that the high-set function is reducing the potential conductor LTE exposure in the high-risk area (high current) close to the source. The high-set curve is also pushing the first high current energy peak further into the network [40], [41]. The maximum time function can be seen to limit

the NI curve operating time to five seconds. The effect of this time limit is reducing the conductor LTE exposure in the second high-risk region in the low fault level part of the feeder. Based on this work it is thus recommended to include a high-set function where possible and always include a maximum time function when an IDMT type curve is used. This will bound the potential conductor LTE exposure to manageable limits in most applications.

The use of EI curves for conductor LTE protection is recommended in [40]. For a strong (high fault currents) network, EI curves will be best suited to protect the conductor. It might not always be possible to use this curve when considering the grading requirements for upstream protection. The DT function may influence grading (selectivity) with downstream devices (lower fault levels). In a weak network NI and DT curves will be better suited if the settings are to be set securely (above load current, see Chapter 3). This is however governed by the protection philosophy that is applied and the priority set by the utility (grading vs. conductor protection).

4.9 MULTIPLE CONDUCTOR TYPES AND CIRCUIT BREAKERS

MV feeders may have many different conductor types in series. The feeders may also have multiple CBs and relays in series. In Figure 4.14 two feeders are shown, one with multiple conductor types (Feeder A) and one with multiple relays (Feeder B). The conductor(s) LTE exposure across the feeder distance is also shown for each feeder.

The same protection settings (PU, TM and operating curve) are applied to Relay A and B. Relay C is set to grade with Relay A with the same operating curve but a lower PU current and TM (see Chapter 3). In the network of Figure 4.14 conductor Type L is smaller than conductor Type K. The conductor LTE exposure from the busbar to point Z is exactly the same as the settings and conductor types are the same. From point Z onward the exposure is changing again. On Feeder A the smaller conductor will have a new conductor limit it has to be evaluated against. On Feeder B the change in LTE is due to the change in applied protection settings at Relay C (compared to Relay B). The new LTE exposure from point Z

onward may be less than the LTE exposure leading up to point Z initially, but my result in an increase towards the end of the feeder (point M) due to the fault level to PU ratio on an IDMT curve. This may exceed the conductor LTE limit again. The effect of LTE exposure on multiple series conductors was discussed in our earlier work [40], [41].

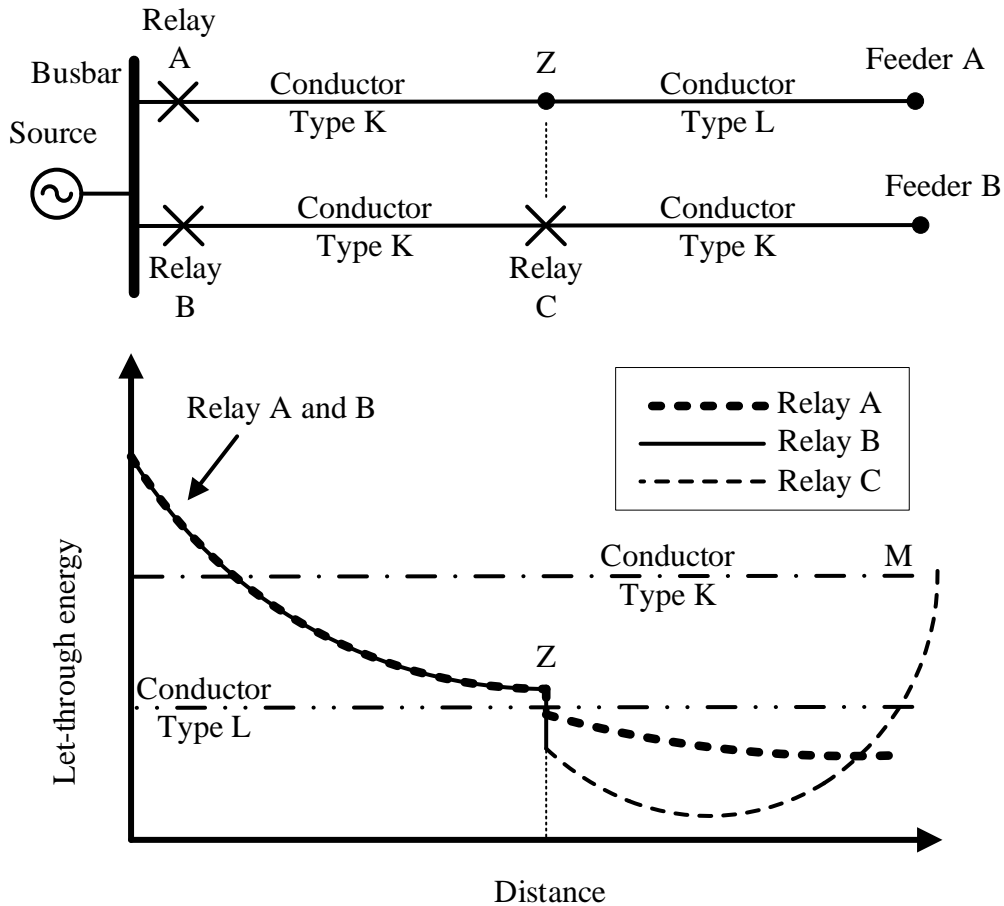


Figure 4.14. Multiple series conductors (Feeder A) and multiple series circuit breakers (Feeder B). The first high-risk region close to the busbar should be evaluated in maximum network conditions and the second high-risk area should be evaluated in minimum network conditions. In general, the LTE exposure of every conductor type and protection relay (or CB) should be evaluated in minimum and maximum network conditions under different fault types as the peak exposure may occur at different places on the feeder, highlighting potential high-risk areas.

4.10 THE EFFECT OF THE AUTO-RECLOSE FUNCTION

Most faults in the network are transient in nature [25], [29], [49], [54], [65], [119]. A good example of this is lightning. This means the fault is non-permanent and as such the CB can be closed to restore supply once the fault is removed [119]. By applying an ARC cycle the availability of the network can be improved [29], [65], [119]. There are many theories on how many ARC cycles should be applied. If the objective is to keep the LTE exposure to a minimum, then no ARC cycles should be applied. If the objective is to maximise the availability, then the maximum number of ARC cycles should be applied. The probability of having a successful ARC attempt decreases with the increase in ARC cycles. Cable faults are normally permanent in nature and as such ARC cycles are not normally applied to them as it will only increase the damage at the fault position [34], [54]. In Chapter 3 background was provided to the ARC function and the three main settings associated with this function. They are the number of attempts, deadtime and reclaim time.

4.10.1 A radial network

In [25] it is mentioned that ARC may have a bearing on the I^2t conductor heating effect. The approach is that during the first ARC trip, the conductor will be heated by the flow of fault current. With the deadtime being short, the assumption is made that the conductor does not lose significant heat energy [40], [54]. This means that for the second shot, the LTE is added to that of the first ARC trip. This same concept is also applied to ARs [57]. The exposure time of each ARC attempt was also added together to attain the total exposure time in [122]. To ensure the conductor does not get damaged, this total energy should be less than the conductor LTE limit. The conductor does not cool down significantly in the deadtime between ARC cycles. A value of five seconds is used as negligible in [81], [136]. When setting the protection devices, this assumption will result in a worst-case scenario when evaluating the settings. As a worst-case scenario, the LTE level attained during the first ARC attempt is thus maintained to the start of the next ARC attempt. This means that the deadtime influence on the conductor LTE exposure is negligible (radial feeder application).

In Figure 4.15 the conductor LTE and fault current time exposure are shown for a radial feeder. The protection settings applied to the feeder CB (operating curve, PU and TM) are not changed. Only the number of trips is changed from one trip to two trips (one ARC cycle) and a highest element is applied. A time delay of 50 ms is applied to the highest element for CB operating time. A conductor LTE limit of 4500 A for one second is applied in this example.

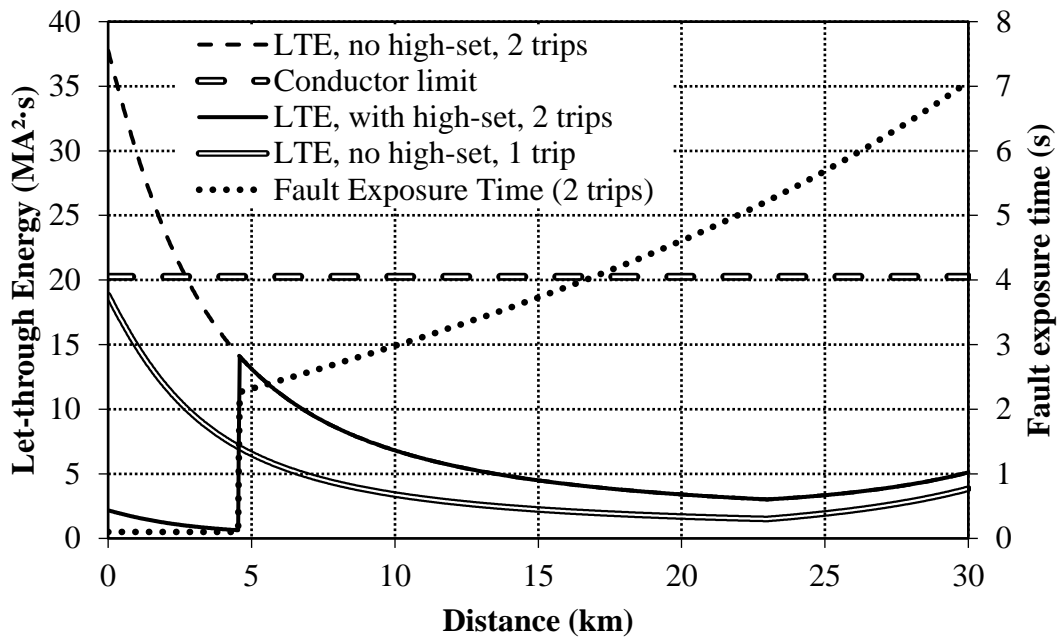


Figure 4.15. The conductor let-through energy and fault current time exposure on a radial feeder with ARC and high-sets applied.

In Figure 4.15 the LTE curve with one trip and no highest is used as a reference. It can be seen that the maximum LTE occurs at the busbar (zero km) and it is less than the conductor limit. Towards the end of the conductor the LTE does increase. When the protection is set to initiate an ARC cycle, the conductor LTE is doubled due to the fault exposure time being doubled. The fault current remains the same. This LTE curve (LTE, no highest, two trips) now exceeds the conductor limit for the first part of the conductor length. A highest element can be applied to reduce this energy peak close to the busbar so as to meet the conductor limit [40]. This highest element should be set to initiate an ARC cycle so as to improve the availability of the feeder as the total LTE in the first portion of the feeder (up to 4.5 km) is

still below the conductor limit [40]. This fast clearance of the fault will also improve the quality of supply to other feeders connected to the same busbar as it is reducing the time a voltage dip is present on the network [40], [59], [131]. It is thus beneficial to apply a high-set function whenever possible to minimise the exposure and set this high-set element to initiate ARC cycles.

If the conductor LTE exposure were to be exceeded in the high-set operating region, then another high-set element can be applied and this element is named a high current lockout function [116]. This high current lockout function, operates the same as a high-set function, except, it does not initiate an ARC cycle. From my experience, it was found that many utilities do not know the difference between a high-set and high current lockout function. There is not much guidance in literature on when to apply a high current lockout function. It is recommended to use the conductor LTE exceedance with ARC and a high-set applied to determine the application and setting of the high current lockout function [160].

The LTE should also be evaluated at the end of the feeder. It can be seen that the additional ARC cycle does double the potential LTE exposure at the end of the feeder as well.

4.10.2 A multi-source interconnected network

When evaluating the effect of ARC on the conductor LTE exposure in a radial single source feeder it entailed determining the LTE for one trip and multiplying it with the number of trips [40]. This was under the approach of each trip being set the same. The total exposure time can also be used by multiplying this time with the square of the fault current. For an interconnected feeder or feeder consisting of multiple sources this approach for when ARC is applied cannot be followed. The reason for this is that more than one CB is required to isolate the fault, the fault current measured is changing over time, each CB protection is operating independently from each other (set different). When ARC cycles are applied to protection devices in a multi-source network, sequencing becomes key to calculating the conductor LTE exposure.

A feeder (Feeder 1) in a multi-source interconnected network is shown in Figure 4.6. If the three-phase fault profile is plotted across the feeder, it may resemble the profiles in Figure 4.16. For this feeder the length is assumed to be 50 km and the distance is measured from busbar 1 to busbar 2. The current distribution is dependent on the network configuration, impedance values and size of generators. There are an infinite number of possibilities, the one shown here illustrates what can happen on a feeder in an actual network. There are two curves shown for each relay, A and B. The first curve is for when both ends of the feeder are supplying the fault current to the fault on the feeder e.g. (A+B). The second is for when the remote or far end is open (e.g. B open), thus only one end is supplying the fault current, e.g. (A). It appears as if the curves are right on top of each other, but the actual current is different. For the A+B(A)-curve the fault current from the A side at the busbar is 10171.3 A and for the A-curve alone the fault current is 10258.2 A. The reason for the change is that when any of the CBs that are carrying fault current opens, the current distribution is changed due to the change in network configuration. The same is happening to the current measured at Relay B with 233.4 A and 397.1 A being measured for each contingency.

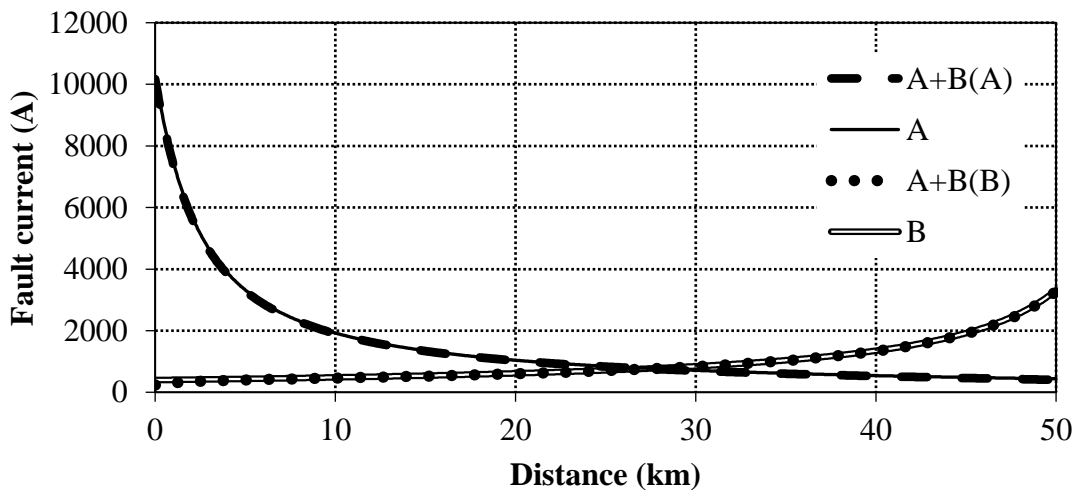


Figure 4.16. The feeder three-phase fault current profile measured from each end of the feeder for different contingencies.

In Chapter 3, the protection philosophy was discussed and the application to radial feeders was used to illustrate the concepts. The philosophy elements included sensitivity and speed

as examples. Even for interconnected multi-source networks that are protected using IDMT type protection these elements are still applicable. When applying protection settings to Relay A and B on Feeder 1 of Figure 4.6 it can be seen that the settings would be different because the fault current measured from either end of the feeder is different. The relay operating time (e.g. time delay before trip signal) may be different depending on the network configuration. For this example, if both Relay A and Relay B was set to operate in 800 ms for a closeup fault on the feeder (for each), the operating time may be the same, but the current that they are measuring is different. This results in a different conductor LTE exposure from each end.

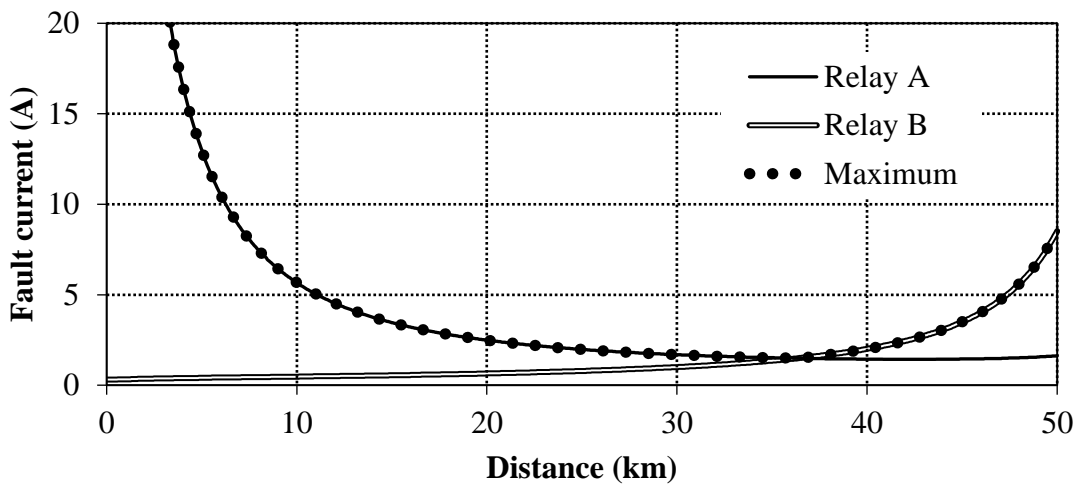


Figure 4.17. The possible feeder LTE exposure showing the potential Relay A, B and maximum of the two ends.

In Figure 4.17 this conductor LTE exposure is shown. It can be seen that the LTE at each end of the feeder is high when considering the maximum curve, which is the maximum of the Relay A and B LTE exposure. The maximum energy exposure does not sum together as the fault current that the conductor is exposed to is either the current from busbar 1 (Relay A end) or busbar 2 (Relay B end). The current is combining in the arc. For the maximum curve shown in Figure 4.17, the protection at both ends of the feeder had to operate at the precise same time. In the actual network, this is not always the case, e.g. measuring errors. When one of the relays trips a CB, it will change the measured current, and this will change the

operating time of the other relay still measuring fault current. To finally clear the fault, both ends have to operate.

If an ARC cycle is added to the protection at either end, it will complicate this clearing of the fault even further as the relay will close at different times. These times depend on the time the deadtime timer is started and then the actual deadtime, time delay. Added to this, if one of the CB has opened and the current have changed, it can change the operating curve the relay is set to if multiple operating curves are applied to the relay. An example of this is if a high-set element is applied to the IDMT curve where the fault current may be just below the highest PU when all the CBs are closed. Then if one end trips, the current increases at the other end to a value that is above the high-set element PU value, thus changing the operating curve from IDMT to the high-set curve.

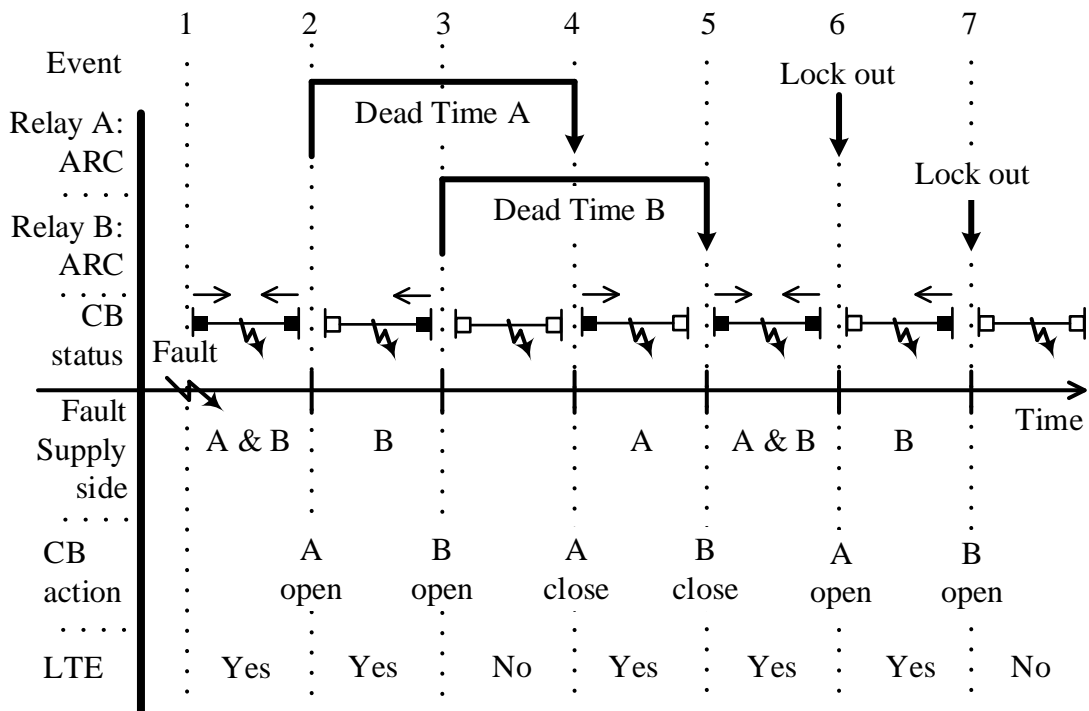


Figure 4.18. A possible sequence of events to isolate a permanent fault on a feeder with ARC applied to the protection at both ends.

In Figure 4.18 a possible sequence of events is shown to illustrate the complexity of sequencing and highlight some of the elements that will influence the conductor LTE exposure. This is in an interconnected or multi-source network when ARC is applied to the

feeder protection. The sequence of events is just a possible sequence of events as there are a multitude of variables that influence this sequence.

In Figure 4.18 the CB statuses (black closed, white open), ARC status, CB action and conductor LTE exposure are shown. Initially there is normal (no fault) and at event 1 a fault occurs on the feeder. As this is a multi-source interconnected network fault current will be supplied from Busbar 1 (Relay A) and Busbar 2 (Relay B) side (see Figure 4.6, Feeder 1). Both Relay A and B will start their respective protection trip timers. During this period the conductor is exposed to LTE from both A and B currents. For this example, Relay A will issue a trip and open the CB at A before Relay B at event 2. At this point the deadtime delay for the CB at A is initiated. From event 2 up to event 3 the fault current is being supplied from the Relay B end. At event 3 the CB at Relay B end is tripped and its deadtime, time delay is started. This is under the assumption that the Relay A deadtime is long enough to allow Relay B to trip first. If it wasn't, then the CB at the Relay A end will close again and the feeder will be exposed to fault current from the A-end as well. This will change the relay operating time for Relay B again as the current is redistributing itself. For event 2 the LTE is dependent on the current from the Relay B end.

From event 3 to event 4 the fault is isolated from both ends of the feeder. At event 4 the deadtime of Relay A is finished timing and the CB is closed. As this is for a permanent fault, the relay will start its tripping sequence again. For the second trip in the ARC cycle the relay may use different relay settings as compared to the first trip. This can change the conductor LTE exposure again. Also, the deadtime of Relay B may not have timed out before Relay A has issued another trip to the CB at its end. This can introduce another change in the sequence of events. Then, if the CB at Relay A has tripped, it will change the relay timing for Relay B again due to the change in fault current at that end. From this, it is better to set the deadtime long enough to allow the relay at both ends to trip and de-energise the feeder, else the fault will just continue to stay on the feeder for the entire ARC cycle. This may result in a lockout condition for non-permanent faults as the arc may be sustained as there is always supply to the feeder.

At event 5 Relay B is closing its CB after the deadtime timer has timed out. Both ends of the feeder will now expose the conductor to LTE. At event 6 relay A timed and opened the CB on that end. Again, the current distribution is changing, changing the relay operating time before the trip signal is sent. Finally, at event 7 Relay B is sending a trip signal to its CB. The fault is finally isolated. For event 6 and 7 the relays could have operated the other way around if they were set differently. For this sequence, the CB open and close time have been excluded, but this can also add additional event steps. The CB operating time can be in the region of 3 to 8 cycles [10], [58]. If there are embedded generation in the network, these generators may also provide initial fault current, but may remove themselves from the network after a time period. In each case this will change the fault current being measured, and change the relay operating time again. Ultimately, the conductor LTE exposure is changed.

When the conductor LTE exposure is to be determined on a multi-source feeder it is much more complicated as compared to a radial feeder. For a radial feeder with no embedded generation the total fault exposure can be determined, multiplied with the square of the fault current and the number of ARC trips to determine the LTE. For an interconnected network the LTE have to be determined between events and this have to be added together to determine the conductor LTE exposure. It was also shown that the number of elements that now influence the LTE exposure have increased with the deadtime now having an impact as well.

To determine the conductor exposure when there is current coming from both ends, the potential LTE from each end has to be determined. The maximum of these two ends have to be used for that specific fault location. In Figure 4.17 the LTE from both ends are shown. If a fault is considered at a position 10 km from Busbar 1, then the LTE from Relay A may be more than the LTE from Relay B end (based on the assumption that the current is squared and there is more current from the Relay A end). The maximum LTE the conductor is exposed to at this point would thus be the LTE from the Relay A side. Energy can be added together to determine the conductor's total exposure. If ARC functionality is added to this,

then the maximum LTE during each event (as seen in Figure 4.18) has to be determined and added together.

With all of these multitude of elements that influence the conductor LTE exposure in a multi-source interconnected network, it is recommended to determine this exposure using computer simulation. If specific elements are to be investigated, this can be included in the model to study its effect. This can be done in future work, for this thesis the LTE evaluation method (following chapters) and the complexity of this evaluation are shown.

4.11 ENERGY-AREA AND ENERGY-VOLUME

It is not easy to quantify the effect of the conductor LTE exposure when making a change to one or more of the influencing parameters. An example of this may be changing the TM from 0.2 to 0.19 or changing the current PU by a small value. To quantify the LTE exposure into a single value the energy-area concept was introduced [40], [41]. This method determined the area under the LTE curve and provided a single number to determine if there was an improvement by making the change. This area was determined by making use of a Riemann calculation [161]. In addition to this the peak exposure value can also be used. This was applied to radial feeders.

For a multi-source interconnected network a LTE surface is created. This surface plots the LTE over the conductor distance (length) to time. As we have shown in the ARC section of this chapter, the energy exposure changes over time and for this reason the energy should be determined over time as well. The LTE peak value at each position on the feeder over all time can be used, but then the dynamic changes contributing to the feeder maximum value are lost. In this thesis we are recommending to rather evaluate the LTE as an energy surface. This will allow for improved evaluation and identification of contributing elements. This is shown in the following chapters.

To quantify the LTE to a single value, the volume under the energy surface is determined. If the energy volume over a specific conductor is to be compared to previous results, the

simulation time will have to be the same. Also, similar to the radial feeder approach the peak LTE value can be used in addition to the energy-volume value.

4.12 CHAPTER SUMMARY

In Section 4.2 the concept of LTE was defined. It was shown how the conductor exposure changes across a radial feeder due to a change in fault level with an IDMT operating curve applied to a protection relay. A way of determining the conductor limit at different fault levels have been introduced based on an adiabatic process. It was also shown that conductor LTE exposure has to be determined at different network contingencies (minimum and maximum) as they influence the LTE equation in different ways. A background on resistance was provided in Section 4.3 where it was shown that resistance is dependent on the conductor material type, the area, resistivity of the material. Further, the resistance changes with a change in conductor (or material) temperature. Methods of calculating the conductor limit were shared in Section 4.4. All of these methods are fundamentally the same with the heat energy generated by the flow of current through a conductor being set equal to the energy absorbed by the conductor. Section 4.5 discussed the high-risk areas for a radial and interconnected multisource feeder. This section also discussed the conductor fault current exposure approach when there is more than one source to a feeder. Section 4.6 provided the potential fault current contribution from different wind and PV generators.

The OC relay equation or model for a relay is discussed in Section 4.6. It was shown the conventional equation cannot be used due to the measured current changing when a CB opens or closes. A discrete version of the equation should be used. Another method of calculating the relay trip time was developed based on the average speed of the disk and this was tested with other calculations and simulations. Section 4.8 explores the effect of different relay operating curves on the conductor LTE exposure. Different curves have different effects on the LTE exposure. Section 4.9 shows that an actual feeder can consist of more than one conductor type and CB in series. The effect of this is on the conductor LTE exposure is discussed in terms of the high-risk areas that was introduced in Section 4.5. Section 4.10 explores the effect of ARC on conductor LTE exposure. It was found that the

exposure is influenced by the number of shots and the deadtime. This section also showed how complex the sequencing can become when multiple CBs are set to ARC in a multisource interconnected network. Finally, in Section 4.11 two methods of quantifying the conductor LTE exposure are introduced. Energy-area is applied to radial feeders where there is no time component (only final operating time). The other is an energy-volume method for applications where the time component can be evaluated from initial fault inception time to the final trip of the CB.

CHAPTER 5 APPLICATIONS FOR EVALUATING LTE PROTECTION

5.1 CHAPTER OVERVIEW

In the previous chapters a focus was placed on protection philosophy, protection elements, the influence of these elements on the conductor LTE exposure, how to determine conductor limits and the effect on relay measurements with a change in measured current. Many software applications were created in the course of this thesis. In this chapter these software applications are discussed. Section 5.2 sheds some light on why these applications were created. Two software applications or tools are discussed in this chapter. All these applications were created with the aim of addressing research questions and then to test the hypothesis. Section 5.3 discusses the full evaluation application consisting of three main parts. Section 5.4 introduces a simplified evaluation method that was used as proof of concept. Results for the simplified evaluation method is provided in Section 5.5 and results for the full evaluation application is provided in the next chapter.

5.2 AIM OF THE SOFTWARE APPLICATIONS

To generate results or explain certain phenomenon software applications were used. One of the key software applications that was applied is a network simulation software package. This allows for the creation of a network model from which quantities such as current and voltage can be determined. The aim of the new program that was created in the course of this thesis is not to create a new simulation tool, but rather a new evaluation method. This

method aims to show why LTE protection should be considered, what factors influence this and how to generate and evaluate results. Depending on the type of study and the size of the results, the output from an existing network simulation package (using scripting) was then imported in other software packages that were capable of handling large volumes of data. Other results were interpreted using the network simulation software visualisation tools or even just the actual numbers.

The main application that was created will be discussed first as this is used for the main results discussed in the next chapter. This application consists of three parts from different software packages. Scripting in each of these allows for them to be added together to create usable results. This is the full evaluation application even though it is not a single piece of software, rather three pieces together. The distinguishing factor of this application is that it allows for results to be evaluated across all simulation time.

The second application that was created also allows for the evaluation of results, but this has some constraints. Again, this application consists of multiple software applications that when put together produced results for evaluation. In this simplified application only the maximum exposure across a feeder is shown. This evaluation method also makes use of the average speed OC relay model developed in Chapter 4 of this thesis.

5.3 FULL EVALUATION APPLICATION

The aim of this application is to evaluate conductor LTE exposure in a network with the presence of multiple supply points or embedded generation. To isolate a fault on a feeder with multiple supply points, a minimum of two CBs have to open. The OC based protection on either end of the feeder will most likely be independent from each other if this is an existing network being converted to an interconnected or multi-source network (no communication). This means that there are no intertrip signals being sent between the relays at either end to reduce the protection clearing time. This is a worst-case scenario and will be applied in the evaluation of these feeders. In this requirement of multiple CB operations for

isolation with independent protection settings lies the complexity of the LTE protection application.

In Chapter 4, the items that influence the LTE exposure were identified. This included changes to source impedance and protection settings related items such as the type of operating curve. Control elements such as the ARC element were also identified as an influencing element. Plant specific constraints such as CB operating time or minimum relay operating time can also influence the LTE exposure. In summary, there are a vast number of factors that influence the LTE exposure. The main network simulation software that was chosen for this thesis allows for many of these items to be simulated and the effect to be studied. Figure 5.1 provides an overview of the full evaluation application in terms of the software used to generate the results. The full evaluation application can be broken down into three parts. The network simulation, data extraction, result calculation with presentation.

For the full simulation application, the network simulation part is used to generate raw data from a network model that has been setup for studying the effect of a specific variable on the LTE protection. The software package that was chosen to do the simulation is DigSilent PowerFactory. This package was also used by [141] to adjust protection settings after a time-current plot has been made, showing that the package is able to perform fault level and protection operation simulations. There is other network simulation software available such as Matlab, Electrical Power Systems Analysis and Operation Software (ETAP), Power System Computer Aided Design (PSCAD) and Power System Simulation and Modelling Software (PSS). The PowerFactory software was chosen as it was able to provide the required output result, it was possible to obtain a full licence for the software and I was familiar with the basics of the software package. The PowerFactory software allows for steady state, transient, network control and protection simulations (there are other capabilities). RMS current and exposure time are the most important raw data obtained from the simulation. There are many other data fields available such as voltage, various angles and CB status, etc. In Figure 5.1 the five parts that make up the network simulation section of the full evaluation application are shown. These are defining the primary plant model,

defining the secondary plant model, creating the required relay model, creating the required simulation code and setting the specific parameters for study in the simulation.

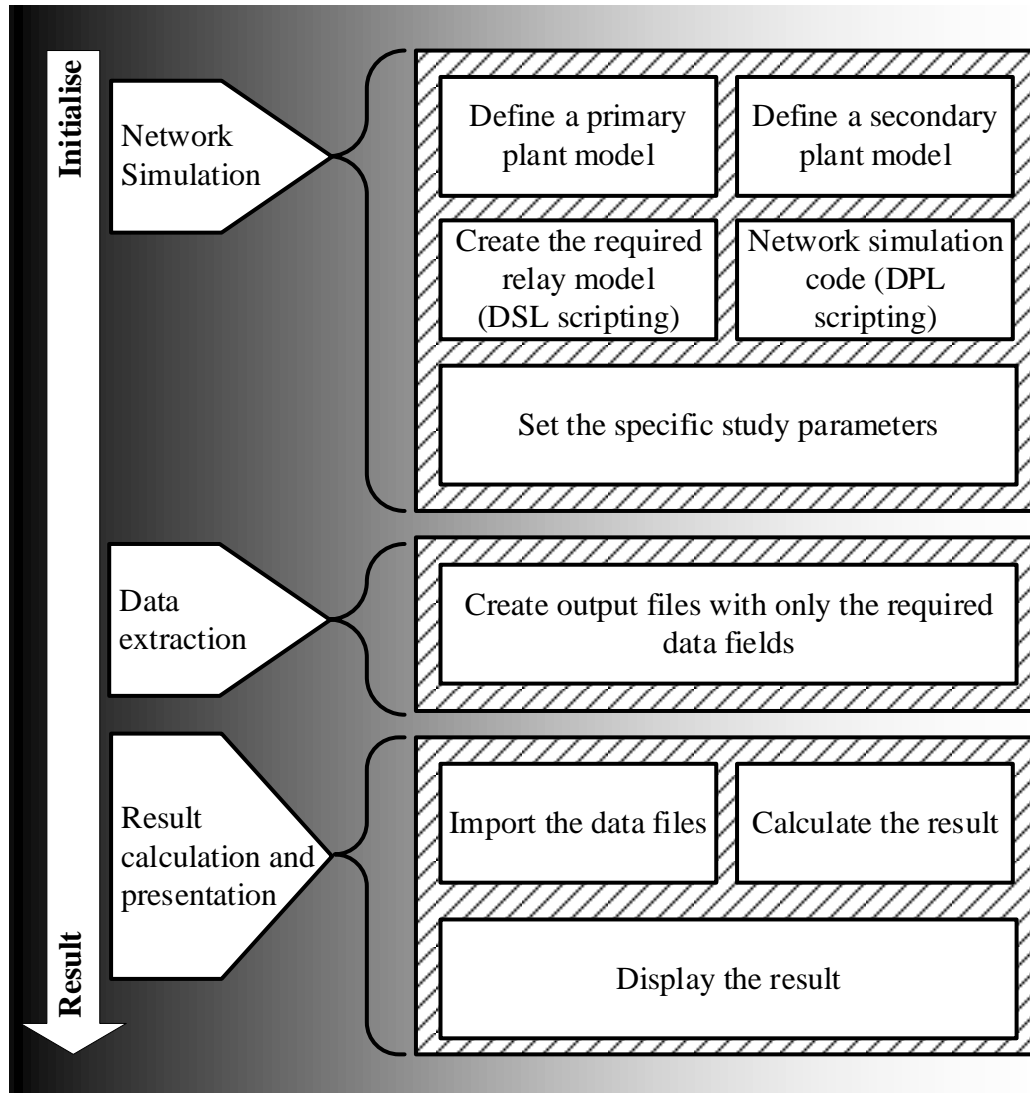


Figure 5.1. Software overview in terms of functionality for the full evaluation application.

5.3.1 Defining the primary plant model

To evaluate the LTE protection in a multi-source network, a network model has to be created. For radial feeders acceptable results can be obtained by simply using source impedance, adding the conductor impedance and solving for the current [40], [41]. The voltage can be assumed at either a high, or low, or rated constant value throughout the feeder (e.g. 1.05 p.u.,

0.95 pu or 1.0 pu) depending on the required result. These may be seen as the upper, normal and lower voltage operating levels for MV feeders. These limits may differ between utilities. For an interconnected multi-source network this uncomplicated analysis method cannot be applied as different protection elements operate independent of each other to isolate a single fault. As was discussed in earlier chapters, the fault current will redistribute itself upon a CB operation until the fault is isolated. This redistribution and change in current influence the voltage in that part of the network. It will also influence the relay timing as the measured RMS current has changed. The complexity of the simulation is increased significantly when it is compared to a radial network application. The modelling software and then the network model in this software take all of these changes into account. This can be done by hand, but it will be very time consuming. In the simplified evaluation application, some of these evaluations were done manually.

Primary plant can be defined as equipment in the power network that carry actual load current (including structures). They may also be connected to the primary voltage. Secondary or control plant can be defined as equipment that does not carry load current and they are used to monitor and control the primary plant equipment. The secondary plant obtains information from the primary plant through instrument transformers such a current transformer [27]. When defining the model for the interconnected multi-source network there are an endless number of network configuration possibilities. The model in this context refers to the primary plant equipment and network configuration. If this model is to be classified as interconnected, there has to be another path for current to flow to the fault if one CB opens. For this network to be a multi-source network, another supply source has to be connected to the network under study. This can be in the form of DG (e.g. wind or PV) or conventional base generation (e.g. coal or nuclear power plants). The generation can also be embedded into a customer plant or distributed on the actual MV network. By modelling this network, these items can be added or removed with relative ease when studying their influence on the LTE protection. In terms of the network requirements for this thesis another external source is required. Specific studies can be done to determine how a certain type of generator will impact the LTE protection exposure using this proposed method (this thesis).

This LTE protection concept can, and should also be applied for EF [162]. This is future work. An example of an interconnected multi-source network is shown in Figure 4.6.

In the network simulation software, the feeders are modelled using a tower configuration and then the conductor type is added to this tower configuration. Any conductor type can be chosen for the studies. The choice of conductor in an actual network is dependent on factors such as the expected loading, fault levels, voltage levels (level at end and start of feeder) and loss optimisation [138]. For the work covered in this thesis conductors were chosen based on typical conductors used in MV networks. Some of these conductor types include Squirrel, Fox, Hare, Mink, Chickadee, Tern and Oak [138]. Any conductor and the LTE protection thereof can be evaluated if it is modelled in the network simulation software.

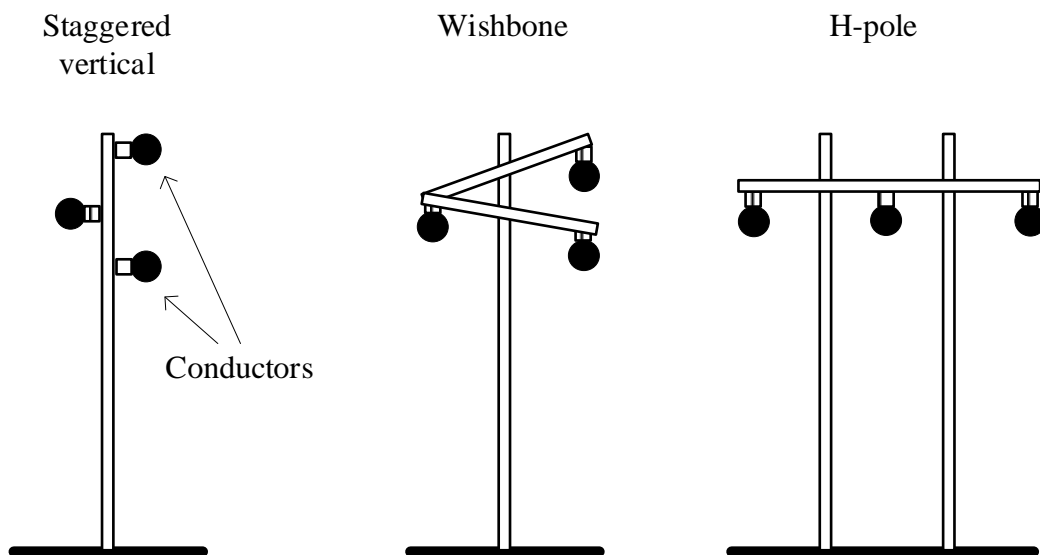


Figure 5.2. Some tower or pole configurations in medium voltage networks.

Different tower or pole configurations are shown in Figure 5.2. These structures are normally made of wood. For the modelling in this research all the towers were modelled using a staggered vertical configuration. This is a very common configuration type used in the Eskom MV grid in South Africa. There are other configurations such as an H-pole and wishbone (delta) too [138]. Each of these do have their own set of advantages and disadvantages. To minimise some of the variables impacting the LTE protection study, the tower configuration is kept the same (staggered vertical) for all the models in this research.

This can however be changed to another structure if the effect of the structure was to be investigated.

5.3.2 Define the secondary plant model

A secondary plant model is not required if the objective was simply obtaining a current magnitude and not the time at which the magnitude is present. This is the case for a radial network where only one CB is required to clear or isolate the fault. The protection relay operating time can be calculated from the current magnitude. It allows then for the LTE to be determined. For an interconnected multi-source network more than one CB has to operate to isolate the fault. Generators will remove themselves from the network by making use of protection if the fault is left on the network for a period of time (fault ride through) [75], [76]. All of these will result in the measured fault current changing at the protection relay position. By modelling the protection relays (and CB trip signals) into the required places of the network under study, this current redistribution due to network dynamics can be included in the result.

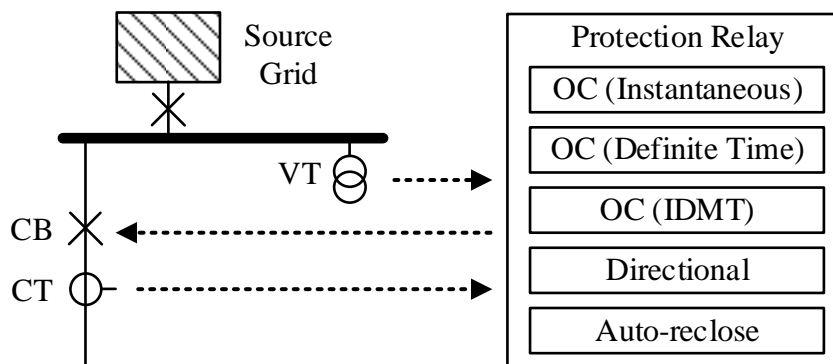


Figure 5.3. A network with the secondary plant equipment modelled.

In Figure 5.3 a feeder that forms part of a larger network is shown with the relevant secondary plant equipment modelled. The CB is used to break the current based on the signal received from the protection relay. The current transformer (CT) and voltage transformer (VT) are used to transform the large primary values to a smaller measurable quantity that is suitable for use by the protection relay [27], [34]. It also provides insulation from the large primary voltage. The CT and VT provide both magnitude and angle values. The VT does

not have to be situated on the busbar as shown in Figure 5.3. It can also connect to each of the feeders at the substation. This is a more expensive design and can be used so as to allow for synchronisation in the grid for islanded schemes (with a busbar VT). The protection relay can consist of many protection elements applied simultaneously. This can be elements such as an OC instantaneous and an IDMT protection element. All of these elements are dependent on the same measurement input (CT and VT).

For the simulation it is not required to model a CT, VT and protection relay at every CB in the network. It is only required to model them at positions where that specific CB is to be controlled based on the parameters set in the protection settings and the current being measured. By modelling the protection relays at other places in the network, the effect of other CBs opening on the conductor LTE (specific feeder) can be evaluated. A relay can also be modelled at certain generator CBs to simulate the relay removing itself from the grid if the fault is present for a prolonged period. By modelling the protection, a holistic evaluation method to the conductor LTE exposure can be achieved. This holistic evaluation method includes the effect of other protection devices (open and close CBs) and generation installed in the network. Generally, if the network is graded, the protection at either end of the feeder should clear the fault first before other protection is required to provide backup clearance (may exclude DG protection from Chapter 2).

5.3.3 Create the required relay model

DigSilent PowerFactory allows for the modelling and simulation of the protection relays. There are many relay models available in the software. Some of these relay models cover specific functions or algorithms that relay manufacturers have implemented in their relays. For the protection relay modelling in this research a generic OC and EF relay was used. This generic relay consists of a phase OC IDMT, phase OC instantaneous and directional protection elements. It does however not have ARC functionality nor a dedicated relay that can be added from a library. This ARC functionality was added to the relay by making use of DigSilent Simulation Language (DSL). The DSL code allows for the dynamic modelling and control of the power system components in the network model. In Figure 5.4 a simplified

relay model logic diagram for a generic OC relay is shown. This relay model was used to model the protection applied to the network model. The additional logic blocks that were created in DSL code to facilitate the auto-reclosing function are shown as well. They are the ARC and CB control output (Close) blocks.

The VT obtains a voltage input (A) and the CT a current input (D). These are the only quantities that the relay has to make a decision on for tripping. Both of these have a model and user settings associated with them. Key settings that should be specified for the VT at (B) include the physical connection (e.g. star connection), the primary and secondary voltage levels. For the CT input at (E) the primary connection (e.g. star), the CT ratio and rated secondary current is required. There are other settings such as errors that can be specified for the CT and VT as well. Different CT types such as class X and class P have different errors associated with them [34]. For this work the errors defined in the instrument transformer models are left on the default values as this is a function of the type of applied CT.

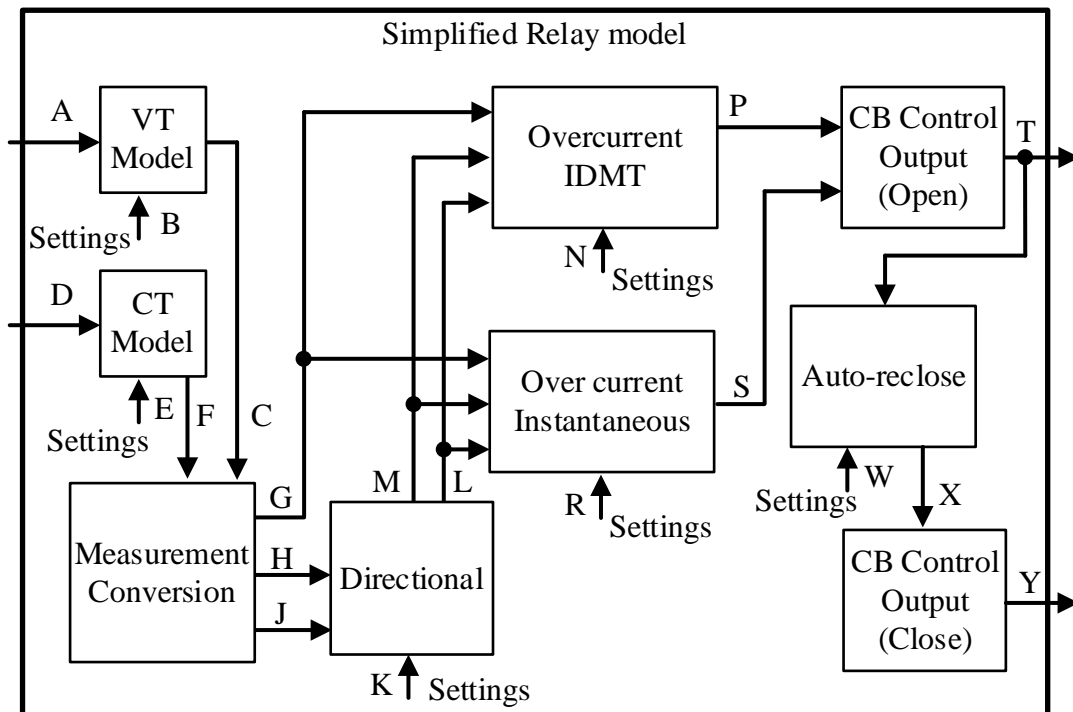


Figure 5.4. The simplified logic diagram of the generic overcurrent relay that was used with the additional DSL logic blocks.

The output from the VT (C) and the CT (F) are the inputs to the Measurement and Conversion logic. These outputs from the CT and VT are the real and imaginary values for each phase it measured. The Measurement and Conversion logic produces the RMS imaginary and real values for each input phase it received (from CT and VT). This is a current (H) and voltage (J) output. The magnitude of the red, white and blue phase RMS currents is then sent to the OC IDMT and the OC Instantaneous logic via signal (G).

The voltage (H) and current (J) are also sent to the directional element. This element is responsible for determining if the direction of the fault is in the forward or reverse direction and then to provide the required forward (M) or reverse (L) signal flag to the OC IDMT and the OC Instantaneous logic. The directional element can be set to provide a tripping signal for forward or then a reverse fault. If both forward and reverse are required, another relay will have to be modelled on to the same CT, VT and CB. The one relay can be set forward and the other reverse. If a non-directional element is required, the directional element can be disabled inside the relay logic. Other settings that can be set in this directional block are the polarising settings.

The OC IDMT and OC Instantaneous logic blocks are where the CB trip decision is made. This is also where the bulk of the protection settings are housed with relay operating curves, PU values, TMs and time delays. It is required to set these so as to set the behaviour of the protection (N and R). There are additional advanced settings available on the generic model to better simulate relay behaviour. This is a function of the protection relay that is applied. These settings include delay times before a PU is registered and the relay reset ratio. These are left at their default values of 20 ms and 95 % respectively. The output from the OC IDMT (P) and OC Instantaneous (S) logic blocks are connected to the CB Control Output (Open). This logic block is an OR-gate that is used to trip the CB (T) from either the IDMT or Instantaneous logical outputs.

The output from the CB Control Output (Open) logical block is also used as an input to the new ARC logic block. This ARC logic block is not present in the standard application of the relay model. This was created using DSL code. This ARC logic gets triggered when the CB

open signal (T) is asserted. The output from the ARC logic (X) will go to the CB Control Output (Close) logic. The output from the CB Control Output (Close) logic (Y) is used to close the CB. This CB control logic is used so as to make it possible in future to add additional logic when closing the CB.

Fundamental blocks that are used in protection logic include flip-flops, latches, timers and conventional gates. Flip-flops are used in protection relay design to store the status of a signal that can change. This means that once the output is set by a certain signal or condition, the output will remain set irrespective of the change in state of the input signal (set input) [163]. Only when the reset condition is met and a signal is placed on the reset input of the flip-flop will it change the output of the flip-flop. This is the basic functioning of the SR-flip-flop. The function of a latch can be compared to that of a gate. While a physical gate is open, anything can pass through it. For a latch, when it is enabled (signal), it will allow the input to change the output. While it is disabled, the input will be blocked from influencing the output. Figure 5.5 shows the symbols for an on-delay, off-delay and an on-off delay timer (with its functioning definition). The on-off delay timer is a combination of the on-delay and the off-delay timers. When considering the on-off delay timer function in Figure 5.5 it can be seen that the input and output signals are not in synchronism. Initially (before A in Figure 5.5) the input and output are both zero. At point A the input rises and this triggers the on-delay timer. After the on-delay timer has timed out, it will release the output to change its state. When the input then falls away (point C) it will trigger the off-delay timer. The output will keep its state until the off-delay timer has timed out (point D).

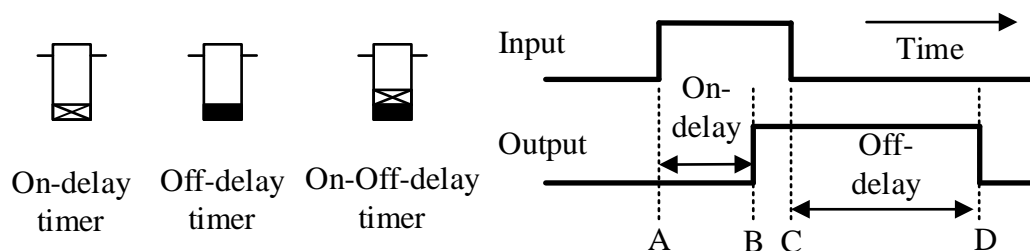


Figure 5.5. The symbols and functioning diagram for an on-delay, off-delay and an on-off delay timer.

The SR-flip-flop, on-delay and on-off delay timers are all used in the DSL code that was generated for the ARC function. The functionality of the code is explained using a logic diagram instead of a flow diagram. The ARC function consists of four major parts, the trip counter, deadtime timer, trip register and lockout function. For an ARC function in a relay, there will be a reclaim timer as well, but for this application of the ARC function this is not required as the CB is not closed again after the lockout condition. The logic diagram in Figure 5.6 is showing the operation of the ARC function (DSL code) as applied to the relay model in the simulations.

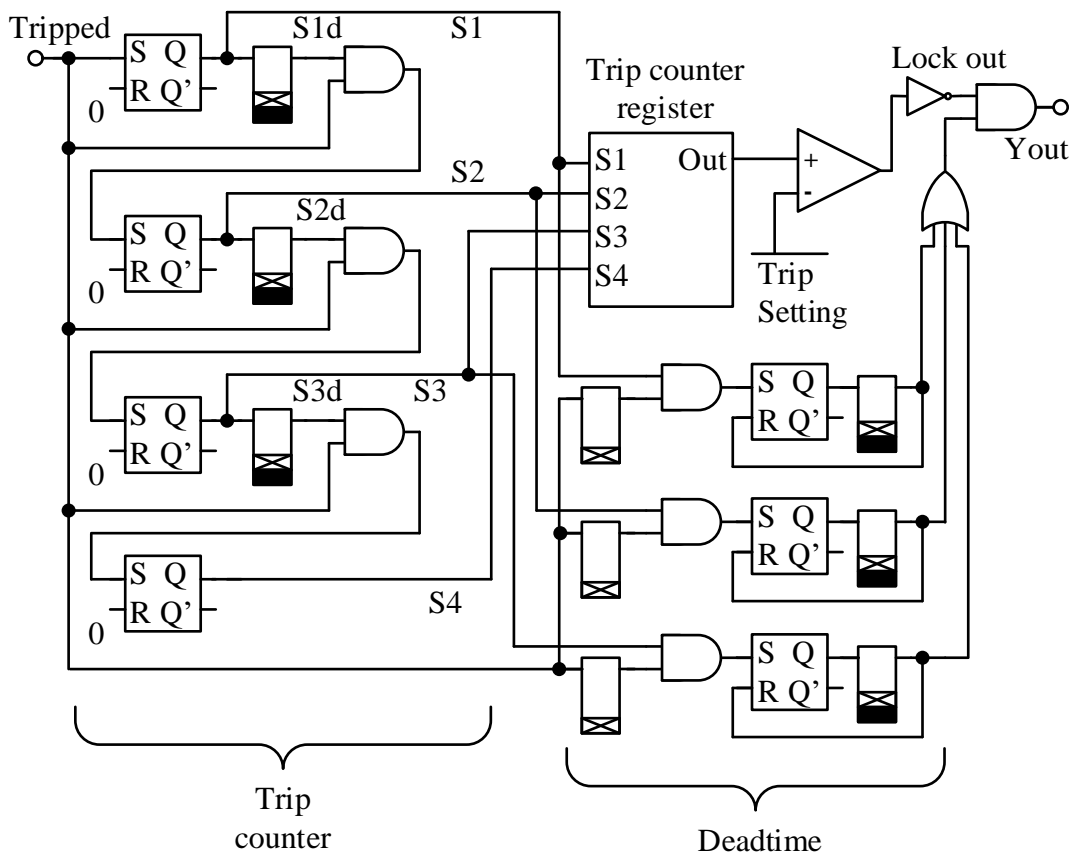


Figure 5.6. A logic diagram of the additional auto-reclose DSL code created for the relay model.

This ARC logic function allows for a maximum of four trips to lockout. The input to the function is the ‘tripped’ signal. This gets routed to both the trip counter and the deadtime timer functions as a trigger for the function. The trip counter function is required to count the trip number and to provide the required trip signal for the correct trip number. An SR-flip-flop is used to provide a logic one output on the rising edge of the trip signal. The trip

signal can then fall away with the status being captured in the SR-flip-flop. It is not required for the SR-flip flop to be reset as the ARC function is only used once (for up to four trips) in the simulation. The reset input signal can be set to a logic zero indefinitely. The output from the SR-flip-flop (S1) is taken to the trip counter register and the deadtime timer. It also starts an on-off delay timer which are set to an on-delay of 15 ms and the off delay to 60 s. The 15 ms on-delay is used for other gates further in the logic to register the current ‘tripped’ and ‘S1’ status before it gets routed to the rest of the logic functions. If this is not done, the first ‘tripped’ signal can also be seen as a second ‘tripped’ signal due to the gates taking time to process their respective logic states. The ARC function will move into a lockout state with the first ‘tripped’ signal. The 15 ms time delay does not influence the overall timing of the deadtime as the deadtime start signal (e.g. ‘S1’) is taken from a position before the time delay. The 60 s off-delay keeps the output set for a period longer than the simulation time. In this case a value of 60 s is chosen, but this can be set longer or shorter. If this function was required to be reset automatically so that it is capable of restarting the ARC functionality the output from the second trip (S2) can be set to reset the SR-flip-flop in the first trip stage (R input on SR-flip-flop). If both the output from the on-off delay timer and a ‘tripped’ signal is present, the output will be routed to the next set input of the following SR-flip-flop. This will then enable the next SR-flip flop to be set using the AND-gate as a gatekeeper when the next ‘tripped’ signal is received. This same approach is used for the second and third trip signals. The fourth is similar except that it does not require the on-off delay timer as it will not enable more trips (or ARC cycles).

The deadtime can be specified differently for each trip in the ARC cycle. For this reason, three deadtime timers are required for a four trip to lockout capability. The ‘tripped’ signal is delayed by 1 ms using an on-delay timer to ensure the correct deadtime timer is started. The correct deadtime timer is selected using the AND-gate and the ‘tripped’ signal when the respective output signal from the trip counter (e.g. ‘S2’) is asserted. The output from the AND-gate is used to set the SR-flip-flop. A flip-flop is used again as the tripped signal can fall away and the flip-flop makes use of the rising edge of the signal to set the output. The output from the SR-flip flop starts the on-off delay timer. The on-delay time is set by the user as the required deadtime. The output from the timer will be passing through an OR-gate

to the lockout section of the ARC function. The output from the SR-flip-flop will have to be reset, else the OR-gate will remain set. To reset the RS-flip-flop the off-delay part of the on-off-delay timer is used. It is set to a delay of 50 ms. This will create a pulse timer that is activated for 50 ms when the deadtime timer times out. The same concept is applied to second, third and fourth trips.

The last part of the ARC function that is shown in Figure 5.6 is the trip counter with the lockout function. The trip counter register is a register that counts in a numerical way when it receives the corresponding trip signal (e.g. ‘S3’ for number three). This trip counter register provides a signal to a comparator. The comparator is a software version of an ‘if’ statement used for decision making in conventional programming. The trip counter output is compared to the user defined trip setting which is the trip to lockout setting in an actual ARC function. While the trip to lockout value is not reached, the output (after the inverter) will remain at a logic one, thus enabling the output from the OR-gate to generate a close pulse to the CB. Once the required trip value is reached, the output via the AND-gate is disabled. The CB is then left open and in the lockout state.

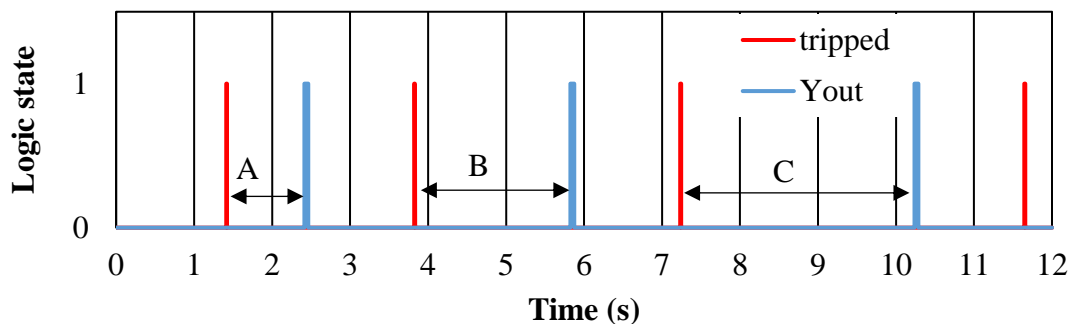


Figure 5.7. The trip signal and circuit breaker close output from the auto-reclose logic.

Figure 5.7 shows the simulation results for the tripped input and CB close output (Yout). It can be seen that both the ‘tripped’ input and the ‘Yout’ output signals are pulses by nature. In this simulation the first deadtime (A) is set to 1 s, the second (B) is set to 2 s and the third (C) to 3 s. For this ARC simulation the first trip input to the recloser is at 1.411 s. This starts the first deadtime timer of 1 s and at 2.412 s the CB close output signal is sent (‘A’ in Figure 5.7). This gives a deadtime of 1.001 s. The 1 ms deadtime timing error is a constant

timing error as a result of the 1 ms on-delay timer used in the deadtime logic. This can be compensated for by subtracting 1 ms from the user setting for the deadtime as it is constant. The second deadtime of 2 s (B) and third deadtime of 3 s (C) can also be observed in Figure 5.7. The relay deadtime timing can be seen in the periods between A, B and C. The tripped signal in Figure 5.8 is the tripped signal from Figure 5.7 at time 1.411 s (time is expanded). This input-output signal from the AR shows that the 15 ms on-delay timer is not added to the overall timing of the deadtime. In Figure 5.8 the reason for the 15 ms time delay is shown using the simulation results for the logic. It can be seen that the ‘tripped’ output falls to a logic ‘0’ before the ‘S1d’ ascends to a logic ‘1’. This is similar for the other signals ‘S2d’ and ‘S3d’.

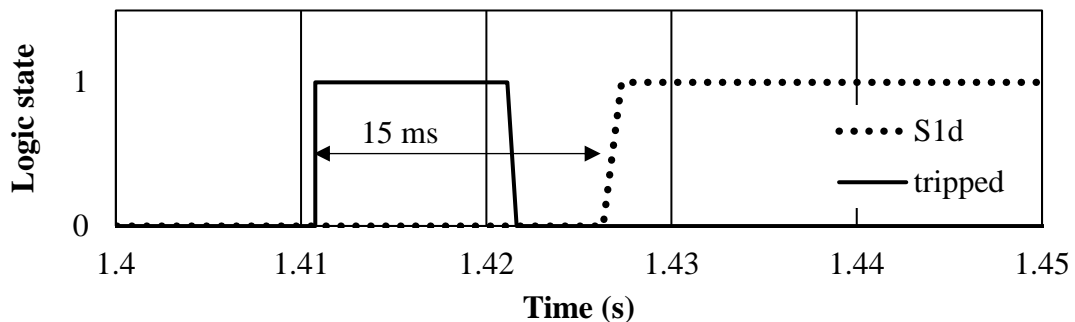


Figure 5.8. The trip signal input and on-delay timed output in the trip counter.

5.3.4 Create the required simulation code

DigSilent Powerfactory was used to generate the network simulation results. Other network simulation software could have been used, but this software did allow for user defined relay modelling (the DSL code) and then to also automate result generation using DPL code. To generate the results for this work, two variables are being changed to create different simulation data points. These are the distance or fault position on the feeder and then the simulation time. The DPL script is not required for the generation of a small number of results from simulation data points. When using a course step size, results can be lost due to the data being smoothed. This smoothing is illustrated in Figure 5.9 for two signals. The one signal has large time steps (A to B) and the other small (A to C). With the small step size

more detail can be shown with the signal decreasing to C, then increasing to D and then decreasing to B again. With the larger step size this is lost. The time steps cannot be made too small either, as this will result in simulation time that is increased and the size of data file being generated will be very large. A time step of 1 ms was used for all of the simulations. This was used based on sampling rates used in existing OC protection relays. Cosine filtering is normally applied for numeric protective relays [118]. This cosine filter allows for a bandpass region to be created, for DC to be removed and to reduce the effect of harmonics on the measured signal [118]. The analogue to digital converter used within the relay cosine filter usually samples at 16 samples per cycle [74], [118]. This is a sample every 1.25 ms for a 50 Hz signal, which is then similar to the 1 ms chosen. Typical trip times for IDMT protection elements on MV feeders can be in the region of 0.5 to 1.5 s depending on the CB position. The 1 ms time step is then well below the relay time, the expected operating time and the resulting file size with data points are acceptable for processing. The same concept is also applied to the other main data variable which is the distance or fault position. If the step size is too coarse data will be lost and if it is too fine the number of result data points and execution time becomes impracticable. A distance step size of a 100 evaluation points per line or feeder segment was applied (one percent step size). For a distribution feeder the line distance can be anything from a couple of meters to a 100 km's as an example. The latter being not that common. If a distance of 15 km is used the distance step size will be 150 m and if the distance was 50 km it will result in a step size of 500 m. All of this will produce acceptable results when considering how the fault levels will change across the feeder distance.

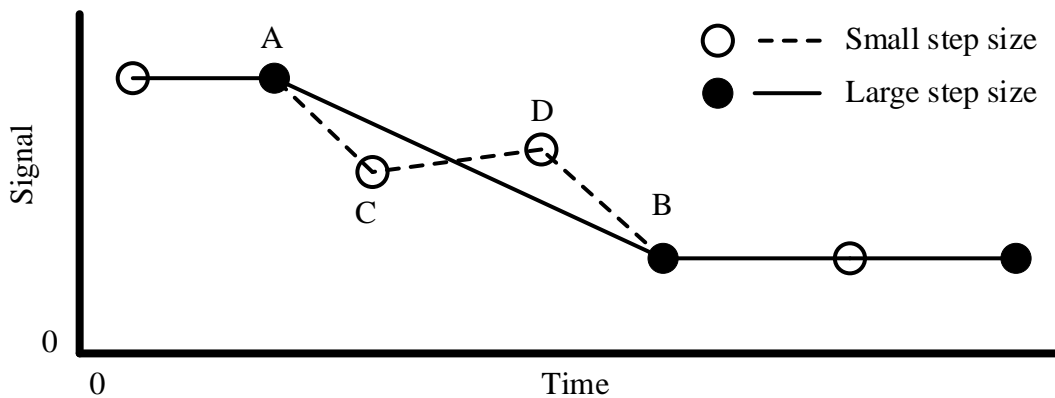


Figure 5.9. The trip signal and circuit breaker close output from the auto-reclose logic.

The feeder simulation concept as applied to a multi-source feeder in a network is illustrated in Figure 5.10. The feeder has two points of supply, being Source A and then Source B. To isolate a fault the protection at both ends of the feeder have to operate. The feeder is divided in 101 evaluation positions across the feeder. This is based on the original 100 that was decided upon and then also the fault level at 0 % (busbar termination) of the feeder distance. At each of these fault positions, a time simulation is done with a step size of 1 ms. Then at every distance and time step intersection a simulation data point is created. At these data points the RMS current from source A (Current A) and that of B (Current B) are sampled. Other variables can be sampled as well, based on the available variables in the network simulation software. The value of these result variables at the various simulation data points are then written to an output file.

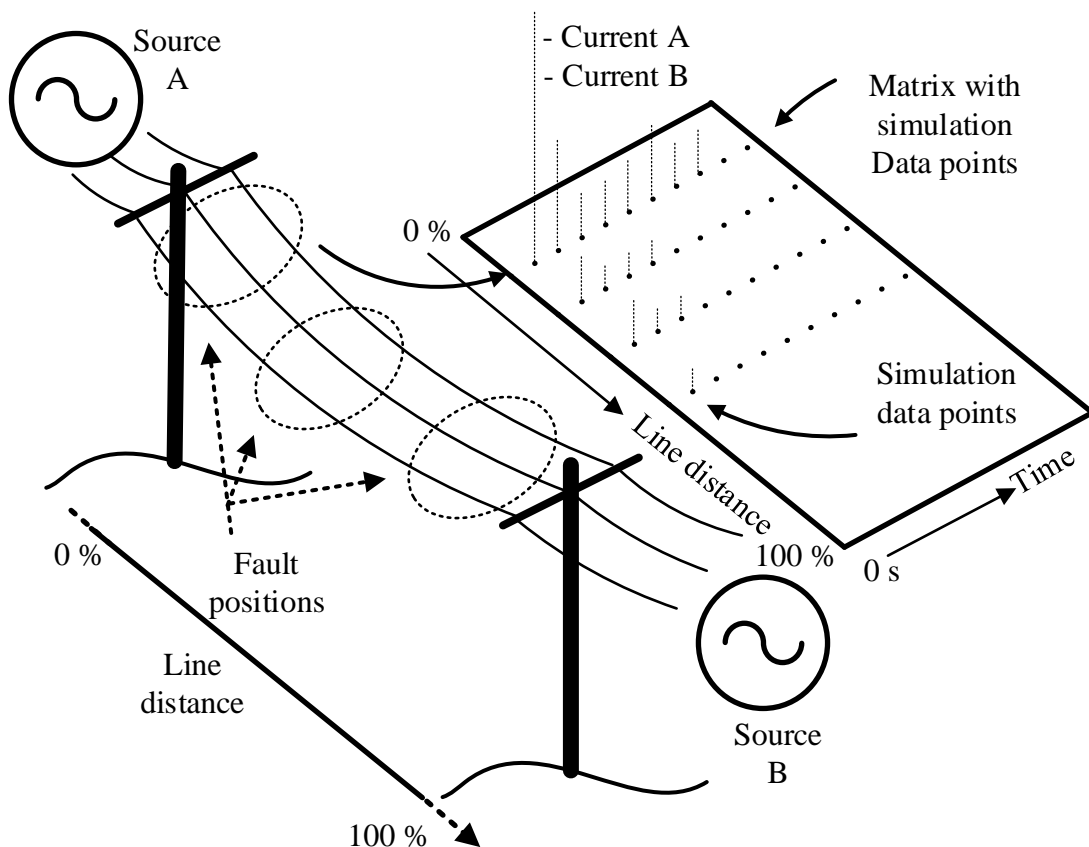


Figure 5.10. Multi-source feeder simulation concept with data points.

The file type or format that is used for the results is the Common Format for Data Exchange (COMTRADE) file type [164]. This type of file is used for storing transient power system

disturbance data. It can provide information on both analogue and binary data. COMTRADE files consist of four files and all of these files are of a text-based file type. The files are a header, configuration, data and information file. Header files provide extra information such as substation name and the faulted phases. The information file is an optional file that can provide extra information when analysing the event. The information file is not used in this simulation. The data file consists of a number of columns of data. When considering a single row of data, it will have a sample number, then a time stamp for the sample and a number of columns with analogue data. The timestamp data is in microseconds. To determine the time from the first sample, the time stamp data has to be multiplied with the sample number. The binary data is typically used to indicate the status of flags in relays. An example of this can be an external trip signal that is received by the protection relay.

The last file type is the configuration file type. Without the configuration file the data file cannot be interpreted. The configuration file consists of a number of data fields that have to be specified. These fields are the substation name, the kind of channel, how many channels there are, the name of the channel, the measuring unit, and factor used for converting the data to the required magnitude or value. The frequency of the power system, the sample rate and then also the date and time of the first data point. There are other fields too but they are not used here. For every analogue quantity that is measured and logged in the data file, there is a corresponding line of data in the configuration file describing what it is, what the value is, when it was measured and how to convert the measured datapoint in the data file to a value. To obtain the measured value, there are four values in the config file that have to be used for each analogue channel, they are the unit, the channel multiplier, the offset adder and the time skew. The unit sets the type of data and overall size multiplier of the data. To get the actual value the data point is multiplied with the channel multiplier, the offset is added to this value and finally the skew is subtracted. The skew time allows to compensate for processing time when one analogue to digital converter is used for multiple channels (multiplexed).

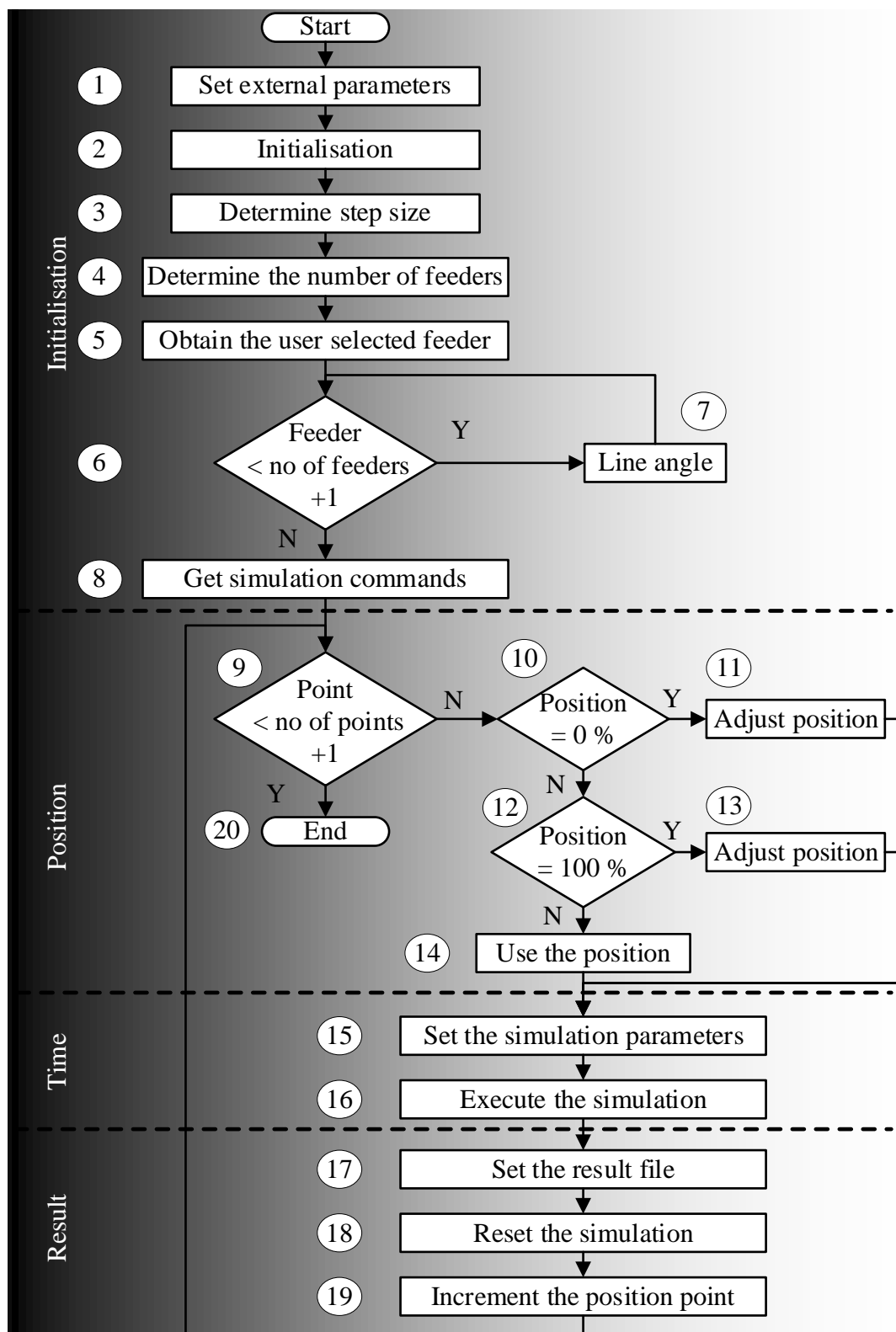


Figure 5.11. The network simulation code (DPL scripting) flow diagram.

In Figure 5.11 a flow diagram is shown for the DPL script that was written to automate the data generation and archiving of the network simulation results. This increased the rate at which results can be generated and evaluated considerably. The four key steps in this program are the initialisation, determining the fault position, obtaining results at time intervals and storing the result data.

The first step when running the network simulation code is to initialise the external variables by the user. These are the required time step, the number of evaluation points, the start and end time. The next step (step 2) is to initialise the variables and objects that are used in the program. This includes defining the objects and for the variables their type and initial value. Based on the number of distance steps required over the feeder length by the user, the step size in percentage is determined in step 3. The number of feeders in the model is determined in step 4. These lines (or feeders) are all saved as an object so as to access the data inside the feeder during the simulation. When starting the simulation, a specific feeder has to be selected by the user. This feeder will be the main feeder that is evaluated for LTE protection. In step 5 this feeder is set to the faulted object. For step 6 the program is cycling through the feeder objects that were created in step 4 and while the last feeder object is not reached it will determine the line angle for each of these in step 7. This angle is required if directional protection is to be applied.

The last step (step 8) in the initialisation phase of this script is to create four more objects for the commands that have to be used when executing the simulation. By using the object, specific fields can be set (e.g. fault position or maximum time step) when executing the simulation. The type of simulation that is used is an RMS simulation. This removes the DC offset and filters for other harmonics. The RMS simulation allows for the DSL script to be executed during the simulation. This means that the protection relay can be modelled and CBs can be opened or closed based on the relay function and the configuration thereof. The next command object is the actual RMS simulation command where the maximum simulation time and time step can be specified. This is specified in step 1 so that it can be automatically populated for each instance the simulation is required to run. Then there is a result command object used to save results. A COMTRADE file format was selected with a

sampling rate of 1000 Hz or then a 1 ms time step. Again, this is specified in step 1. Lastly there is a reset command object that is required to reset the RMS simulation results before the program moves on to the next position on the feeder.

The next part of this DPL script is to set the position on the user selected feeder where the fault will be placed. This starts at step 9 where a test is done to determine the current position on the feeder. If the position is equal to 0 %, the position has to be increased slightly into the feeder so that it is not equal to exactly zero (or then on the busbar). With the position equal to zero the simulation software might not show all the current that is passing to the feeder for a fault on the feeder. This concept is illustrated in Figure 5.12.

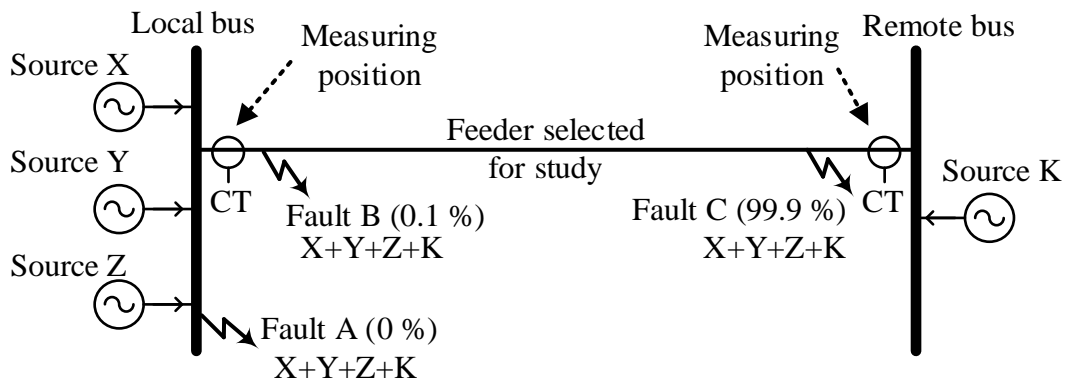


Figure 5.12. Illustration of the 0 % and 100 % fault positions.

There are three fault positions and four sources in the network. For every fault position the total current will be the sum from Source X, Y, Z and K. However, what the feeder is measuring, and what the conductor is exposed to is different. For the fault at A, only the current from the remote bus (Source K) of the feeder will pass to the fault position through the measuring point (CT). The correct place for the fault will be on the feeder at position B so that it will measure the sum of currents from Source X, Y and Z at the local bus and then at the opposite end it will measure the current from Source K. Both currents (local and remote end) will be captured in the results as this is used when determining the LTE exposure. For the simulations the 0 % position is changed to 10 % of the original step size. This means that if a step size of 1 % is used on a 50 km feeder, the first fault position will be at 0.1 % or 50 m. This is then used as the original zero percentage step. The next step will

be at 1 % or then 500 m and the second step at 1 km (counting from zero). The same is also applied to the remote end in step 12 of Figure 5.11 where a test is done to determine if this is the last position or then 100 % of the feeder length. This 100 % position is then changed to 99.9 %. This is also indicated in Figure 5.12 for a fault at position C. The local end will measure the sum of Source X, Y and Z with the remote end measuring only the current from Source K. If the fault is not at 0 % or 100 % the position can be set to the percentage in step 14.

In step 15 the simulation parameters are set using the simulation command object defined earlier. The user set values that were defined in step 1 are used for the start time, maximum time step and end time of the simulation. The type of simulation and type of loadflow study that should be used is also set here. The simulation is executed in step 16. This will then step the time starting at the time specified by the user and determine the status or value of the various elements that were specified as result variables. An example of this would be the current measured at a specific point or the CB status (open or closed).

The last phase of the DPL script is to store the results that are generated for each of the positions on the feeder. In step 17 the result file name is specified and then the results for each step is stored as a COMTRADE file. This means that if 100 steps are specified, there will be 101 files (including position zero) with the required result variables at each time step. The COMTRADE result file will consist of two files for each position on the feeder. They are the data and the config files. The simulation results will then get reset in step 18. The last step in the script (step 18) is to increment the position and then test if the end of the feeder has been reached in step 9.

5.3.5 Set the specific parameters for study

In the second step of the network simulation phase of the full evaluation application the secondary plant model had to be defined. In this the secondary equipment such as a CT, VT and protection relay was placed at points of interest in the network. All of these protection devices require protection and ARC settings. These settings include items such as the type

of curve, the PU, TM, number of ARC attempts, deadtimes, etc. These settings have to be calculated beforehand based on the protection philosophy that were discussed in the earlier chapters. Setting the protection devices includes grading the network so as to obtain selectivity and ensuring that the protection is sensitive to faults. Once these devices have been set, the RMS simulation parameters can be set such as the total required simulation time. Finally, the network model is ready to generate data in the form of COMTRADE files for study.

5.3.6 Data extraction application

After the network simulation part of the full evaluation application is done, the data extraction part can commence. The data that are being extracted are from the config files of the COMTRADE output files. The config files do not have a fixed length as it is dependent on the number of variables that have been defined as output variables in the network simulation part of the program. The Python data extraction program allows the user to specify which rows of data is required and then also which columns should be used. This user setup is then applied to all the result files (e.g. 101 files of the line distance). The data extraction program will create a new text file for each of the position files. This new file consists of a single row vector with the required fields. Fields that were used in the generation of results for evaluation are the channel multiplier and the offset adder. The time skew was zero for all the results generated in the network simulation application. The unit was known beforehand and as such this was not stored in the row vector.

A flow diagram of the data extraction program with step numbers is shown in Figure 5.13. The first step is to initialise the variables that will be used. For this a default file name is defined. This file name is modified with a file number representing the physical position on the feeder being evaluated. Then there is also a new data list that is being created. This list is used as an intermediate variable when constructing text (data) that is written to the new text file from this data extraction program. In the second step a test is done to ascertain if the maximum number of files are reached. These are the result files that were generated in the

output from the network simulation software (e.g. 101 files). If the maximum number was reached, the program would end.

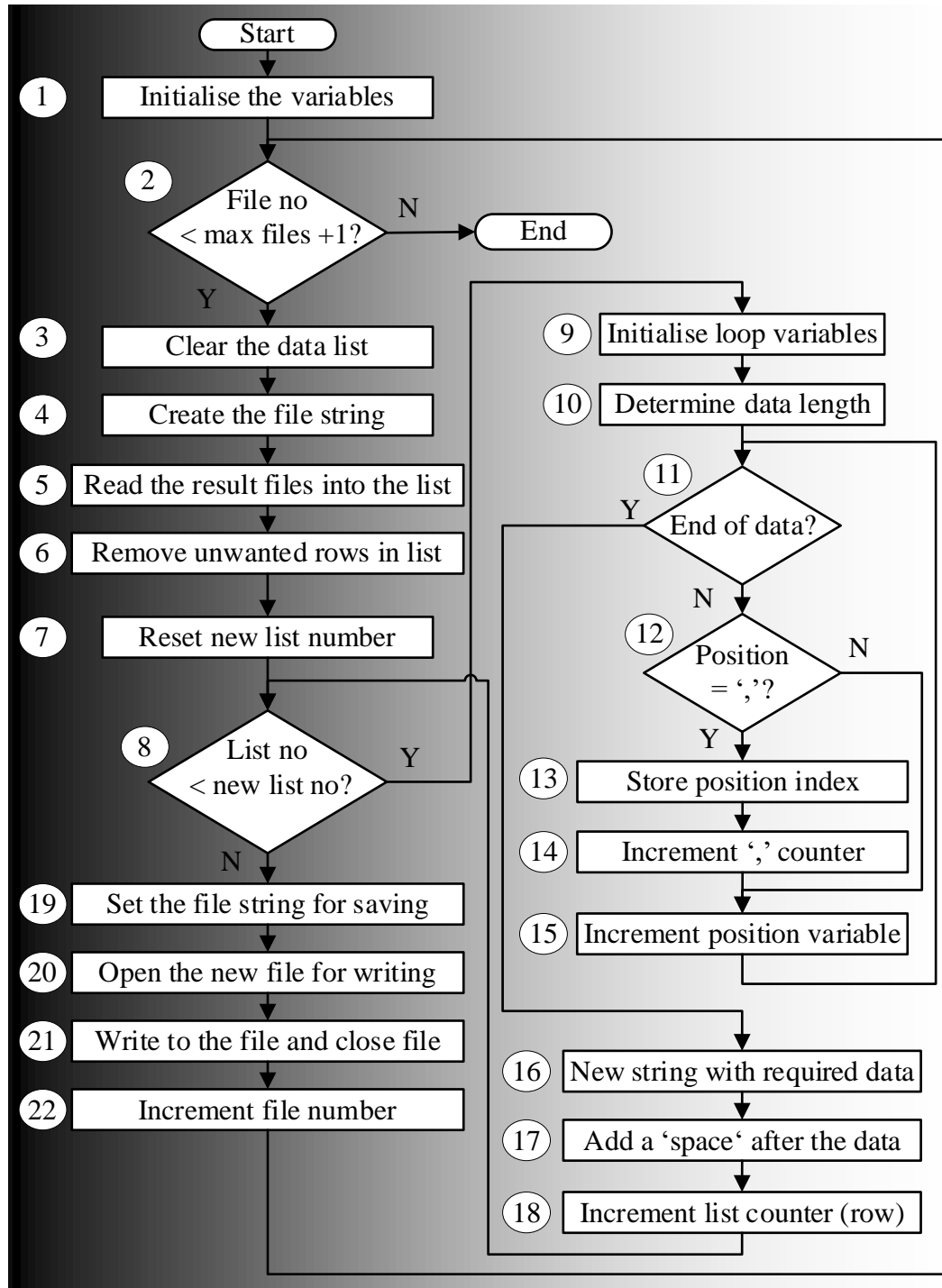


Figure 5.13. A flow diagram of the data extraction Python script.

In the third step the new data list is cleared. This is required to ensure that every time a row of data is read from a new config file, the data list is clean so that once it is written to the output text file the previous row's data is not included. If this was not done a copy of the previous data can be created in the output folder. In the fourth step the default file string is used and then modified to match the name of the config file that is to be opened for reading. The result config files are then read into a list variable in step 5 and after this the original config file is closed. This list variable can now be used to extract data from the original text file (e.g. multiplier).

In step 6 the rows in the list that do not have the required variable information are removed. For a COMTRADE file format a row is inserted into the config file for every variable defined as an output variable. For this application, four rows were used. They represented the current magnitude and angle measured at either end of the line that are being evaluated. In the network simulation software, this line was selected by the user when the network was simulated. The list or then row counter variable is created and set to zero in step 7. In step 8 the list counter variable is used to determine if the data have been extracted from all the required rows. If the last row has been used it will move to creating a new string in step 19 for writing to the result text file. If this is not the last row, it will move towards initialising new loop variables in step 9. These variables are used to determine the start and end position of every data field in the specific row string. There is a row string (now in a list from step 5) for every variable required for evaluation. Two additional counters are also initialised in this section. The first counter will be used to keep track of the character position in each row (each row consists of a string of characters). The second is a comma counter (or ','). Each of the columns in the row of characters are delimited by a comma (','). If the user knows the column of data that is to be extracted, the start and end position of the column is determined by testing for the character comma (',').

In step 10 the number of characters in a row (or length of row) is determined. This is used in step 11 to determine when the end of the row is reached and to break then from the loop. If this is the end of the row, it will move to step 16 where a string is created with the required data columns from the original config file in the list. It will copy characters starting at the

positions determined in step 13. In step 17 a space is added after each column to delimit that column. In step 18 the list counter (or then row counter of the config file) is incremented. The script returns then to step 8 where it is testing to see if the final row has been reached. If this was the final row, a new string (file name) will be created for the new config text file for that position on the feeder. The text that was created for the default file name string (step 1) is used. A number is added to this string that shows the position on the feeder and an additional character is added to show that this is the new config file. In step 20 this new file is opened for writing. The data (required columns) that was stored in the list is now written to the new text file and the text file is closed in step 21. In step 22 the file counter is incremented. This counter then moves to the next position on the feeder where a fault was placed. The script then jumps back to step 2 where it is testing if this was the last file (or position) on the feeder. If it was, the program ends.

5.3.7 Result calculation and presentation

In the last section of the full evaluation application the LTE is calculated and resulting graphs are plotted for evaluation. The flow diagram of this result calculation and presentation part of the full evaluation application is done in Matlab. Matlab was chosen for its ability to handle a large matrix of data and for its ability to display data as three-dimensional graphs. The flow diagram detailing the last part of the full evaluation application is shown in Figure 5.14 and 5.15. The various steps are numbered in the flow diagrams.

In the first step the user inputs are obtained for setting up the required result graph. The user has to provide the feeder length, indicate if the line limit should be shown and also specify the LTE line limit. In the second step the variables can be initialised. Two variables to mention here is the number of files to import and the time step value. Both these values are known and are programmed as a constant for this application. For this application the number of files is equal to 101. This is for 100 steps of 1 % across the feeder length and includes the position zero. The time step is set to 1 ms based on the sampling rate used in the COMTRADE file generation. The size of the result matrix is also determined as this is used to find the last element in the matrix when working with the data.

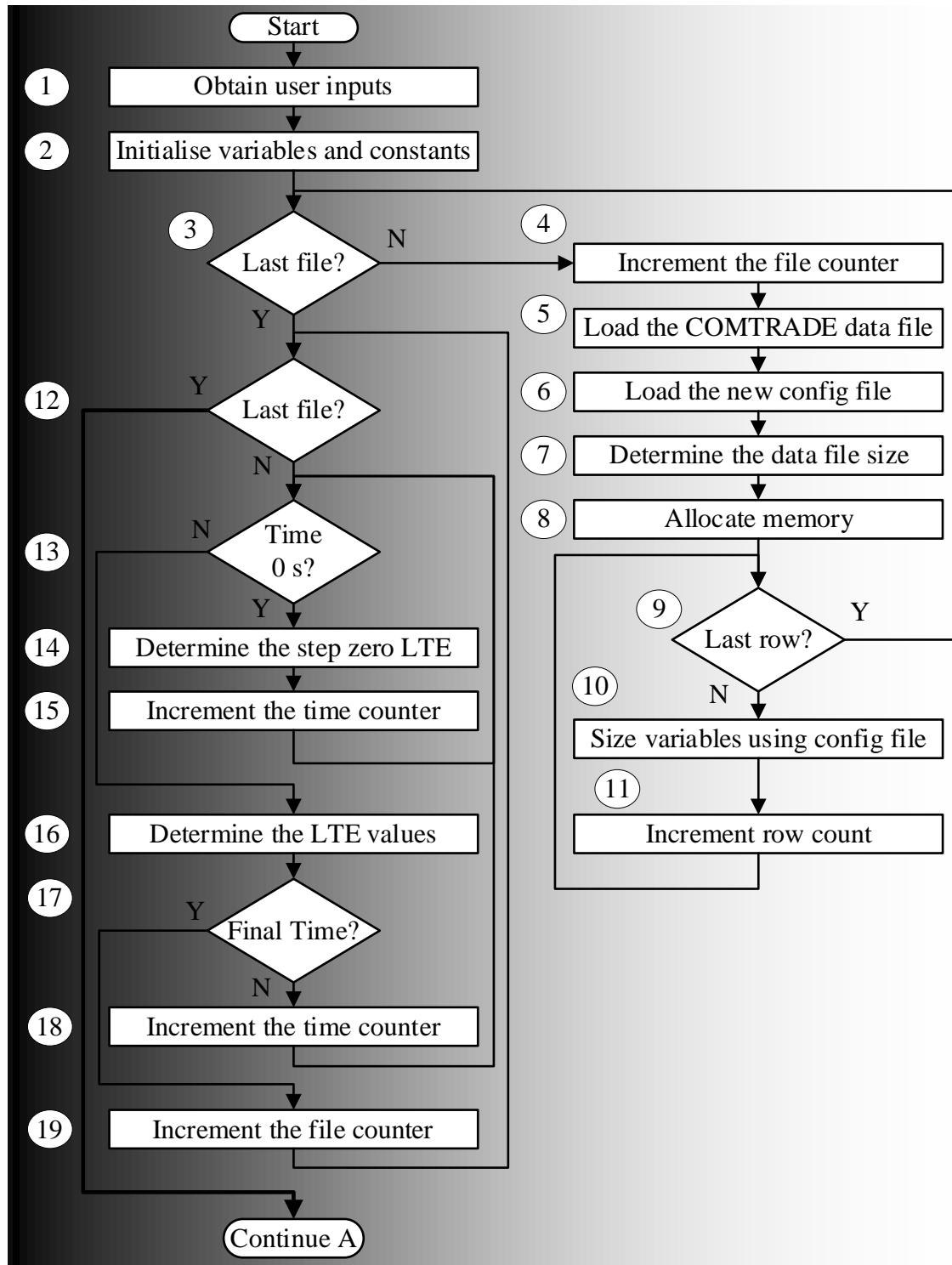


Figure 5.14. The full evaluation application flow diagram (part A).

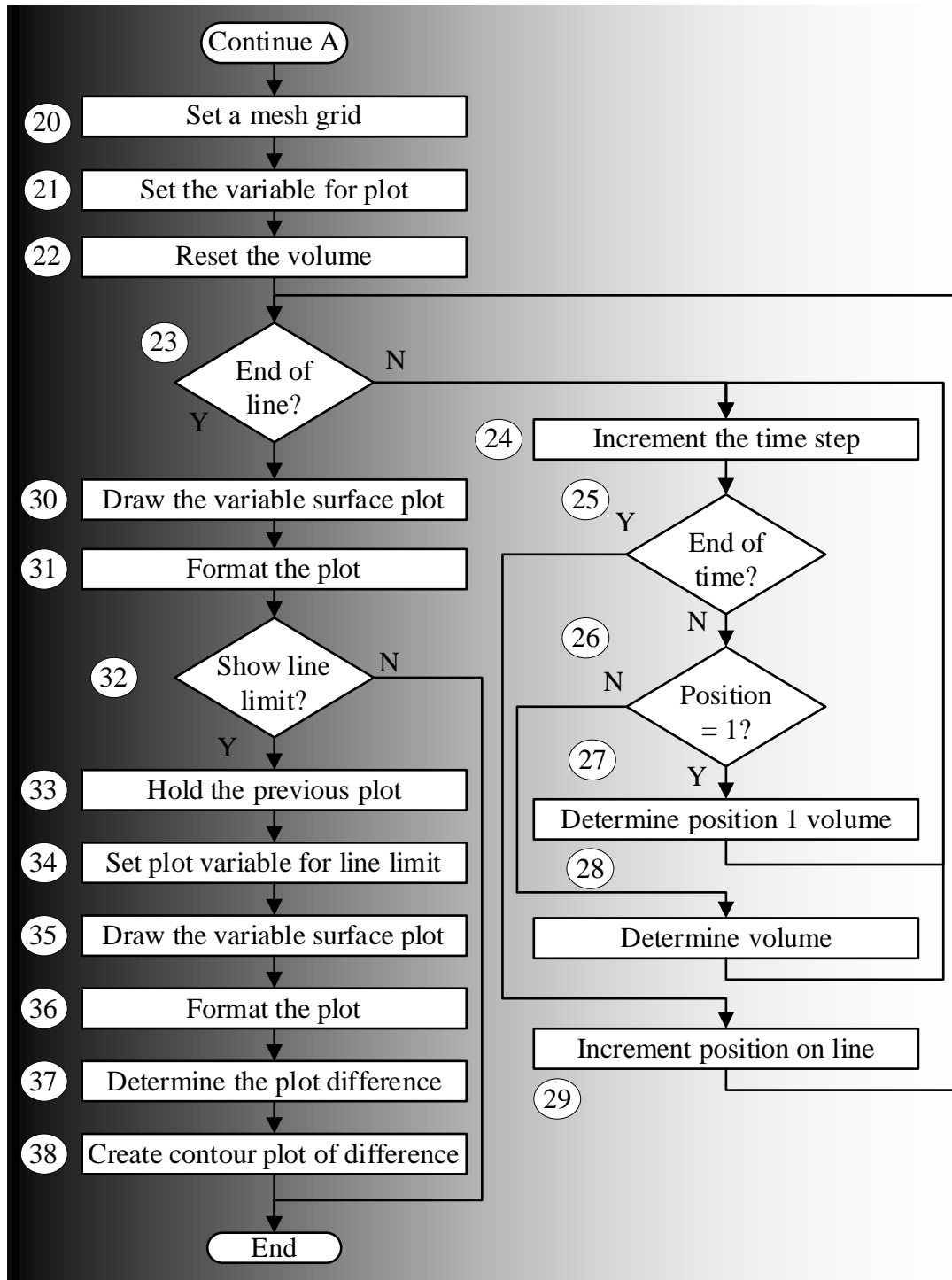


Figure 5.15. The full evaluation application flow diagram (part B).

In the third step a test is done to determine if this is the last file. If this is not the last file, the file counter is incremented in step 4. The first time this is done the file counter is incremented to one from zero. In step 5 the COMTRADE data file that was created in the network

simulation phase is loaded into Matlab. In step 6 the new config file that were created using the Python script is loaded.

The size of the data file is determined in step 7 so as to know when the end of the data file is reached. They are now stored in a matrix form when the text file is loaded in step 5. In step 8 a multidimensional array is created and the memory for this is allocated to reduce the program execution time. This array consists of rows, columns and pages (become a three-dimensional array). Each row corresponds to a row of data in the data file. Each row is then the data from that time step during the original network simulation. Each column corresponds to the required data that are identified in the new config file that was created during the data extraction phase (Python script). The page corresponds to each of the data files that are created for every step taken on the line during the network simulation (101 files in total). This variable combines all the required results into one variable that eases the handling of the data. In step 9 a test is done to determine if the end of the data row (time part) is reached. If the end was not reached, the required variables are extracted from the data file in step 10 and the magnitude is adjusted with the values in the config file. This is then stored in the new combined result variable, in the correct row and column on this page (distance step). The row or time step is then increased in step 11 and the test for the last row in step 9 is done again. If the last row (or time in the simulation for that distance step) was reached, a test is done again in step 3 to determine if the last file (or distance step) was reached. If not, the same steps will be followed to extract the data, adjust the magnitude with the config file values and store the scaled values in the new multidimensional array. If this was the last file, the program will move to the next phase where the LTE is determined.

The LTE is calculated at every distance step (file number) and then at every time step. In step 12 a test is done to determine if the last file (distance step) was reached. If this is not the last file the program will move to step 13 where a test is done to determine if this is time zero. If it is, the LTE is set to zero in step 14 as no time has passed. In step 15 the time counter or step is increased and the program moves back to step 13 to determine if this is time zero. If this is not time zero, the LTE can be calculated for that time step in step 16. The LTE for the feeder under study is calculated for both the source (local bus) and the load end

(remote bus) individually (see Figure 5.12). This means that there will be a LTE exposure value for the feeder conductor based on the current from the local bus and then the current from the remote bus. Each of these are multiplied with the time step. The maximum LTE exposure for the conductor is determined by using the maximum LTE from either the local or the remote end at that position for that time period. These LTE values are stored in the result multidimensional array (Matlab column, row and page).

Once the LTE exposure is determined, the time step will be increased and a test will be done again at step 17 to determine if the final time was reached. The program will not test for “time +1” as you cannot calculate energy in the future with no time to calculate with. If this was not the final time, the time step or counter will be increased in step 18 and the program will test again if this is time step zero in step 13. If this was the final time, the file counter (or distance step) will be increased in step 19 and the same process will repeat itself until the last distance step and time step were reached.

With the LTE results available, the results can be used in a plot variable consisting of three parts. The first being the distance, the second being the time and the last variable is the required LTE. In step 20 an X-Y mesh grid is created consisting of the distance and time steps as variables. The variable required for the plot is then set in step 21. This is extracted from the result variable and placed in the plot variable. This plot variable will be used later when the actual surface is created.

In the next phase the LTE volume is determined so as to quantify the LTE exposure and make it possible to compare LTE exposure. In step 22 the volume is set to zero. To determine the volume under the LTE surface, the surface is divided into a grid and the volume of a rectangular cuboid is determined by using the grid dimensions and then the height to the LTE surface. The volume of each of these cuboids are added together to determine the total volume under the surface. In step 23 a test is done to determine if the last file or then distance step is reached. If not, the time step is increased in step 24 and a test is done to determine if this is the end of the time simulation in step 25. In step 26 A check is done to determine if this is position zero. If this is, the first distance step is set at 10 % of the normal 1 % step

size in the network simulation part of this full evaluation application. This was done to ensure the current passes through the measuring point (see Figure 5.12). When calculating the volume in step 27 the distance has to reflect this 0.1 % step. The time step is started at step 1 (0.001 ms), thus the bottom area of the rectangular cuboid X-Y coordinates can be determined. This area is then multiplied with the corresponding LTE value, creating a volume. After this first position calculation, the script will return to step 24 where the time step is increased. This is then tested again in step 25 to see if it is the end of time and if not, the position is tested again in step 26. If this is not the first position, then normal 1 % step size will be used in step 28 to determine the LTE volume. After this the time step will be incremented again in step 24 and then a test for the end of time in step 25. If this was the end of time, then the position will be increased in step 29 and all the volume calculations will be done again until the end of the line and time is reached.

The LTE surface plot for the selected variable of step 21 is made in step 30. In step 31 this plot is formatted. This format includes edge colours, axis labels, text styles and adding a colour bar to determine the LTE level in the surface plot.

One of the questions that was asked to the user in step 1 was if the line limit should be shown. In step 32 the user response is tested to determine if the line limit should be shown. If the reply was no, then the program will end. If the user said yes, another surface is shown with the limit of the line. This is a flat surface as the LTE limit of the line does not change. In step 33 the previous LTE surface plot is kept on the same axis so that the new plot can be placed on the same axis. In step 34 the line limit is used as the plot variable in the surface plot. In step 35 the line limit surface plot is added to the original LTE surface plot and his new limit plot is formatted in step 36. This is similar to the format for the previous LTE surface plot. In step 37 the intersection of the two plots are determined by subtracting the two surfaces from each other and then creating a contour plot (step 38) of this difference with a black line so that the intersection can be visualised.

5.3.8 Output from the full evaluation application

In Figure 5.16 a result figure is shown for the full evaluation application. In this result figure the X-axis is the distance across the length of the feeder and the Y-axis is simulation time at every distance step. Together the distance and time create the grid at the bottom. The Z-axis is LTE. The result shown in Figure 5.16 is for a feeder where there is a source at both ends of the feeder. The feeder protection at both ends have been set not to initiate any ARC cycle and no high-set has been applied. Two surfaces are shown, the first is the LTE exposure surface and the second is the line limit surface. Any part of the LTE surface above the line limit curve is an exceedance of the conductor limit. This is the part where the conductor gets damaged due to the thermal effect of the current passing through the conductor.

The initial work done on this topic considered radial feeders. For radial feeders it was possible to determine at what time and where on the feeder the exceedance present itself [40], [41], [165]. In the work done during the development of this philosophy for the application of LTE protection to multi-source networks only the maximum LTE for all time was considered [162]. If the LTE and line limit surfaces in Figure 5.16 were to be observed from only the distance axis and only the top part of the LTE is considered, it would resemble this approach. This is shown in Figure 5.17. The evaluation method in Figure 5.17 is good for making a yes or no call on whether a feeder is being protected, but it is not easy to perform in-depth analysis.

In Figure 5.17 it can be seen that the conductor will get damaged at certain positions. By changing specific protection settings such as the number of ARC attempts or the operating curve, this exceedance may be mitigated. By evaluating this from the full surface perspective of Figure 5.16, it can be determined at what point in time this exceedance occurs. This is taking a holistic approach towards evaluating a large part of the network where DG and other feeder CBs can operate independently. This can aid in determining what should be changed to remove this exceedance. If we consider Figure 5.16 it would be changing the operating curve of the protection so as to reduce the operating time. Or the TM can also be reduced to achieve a similar result.

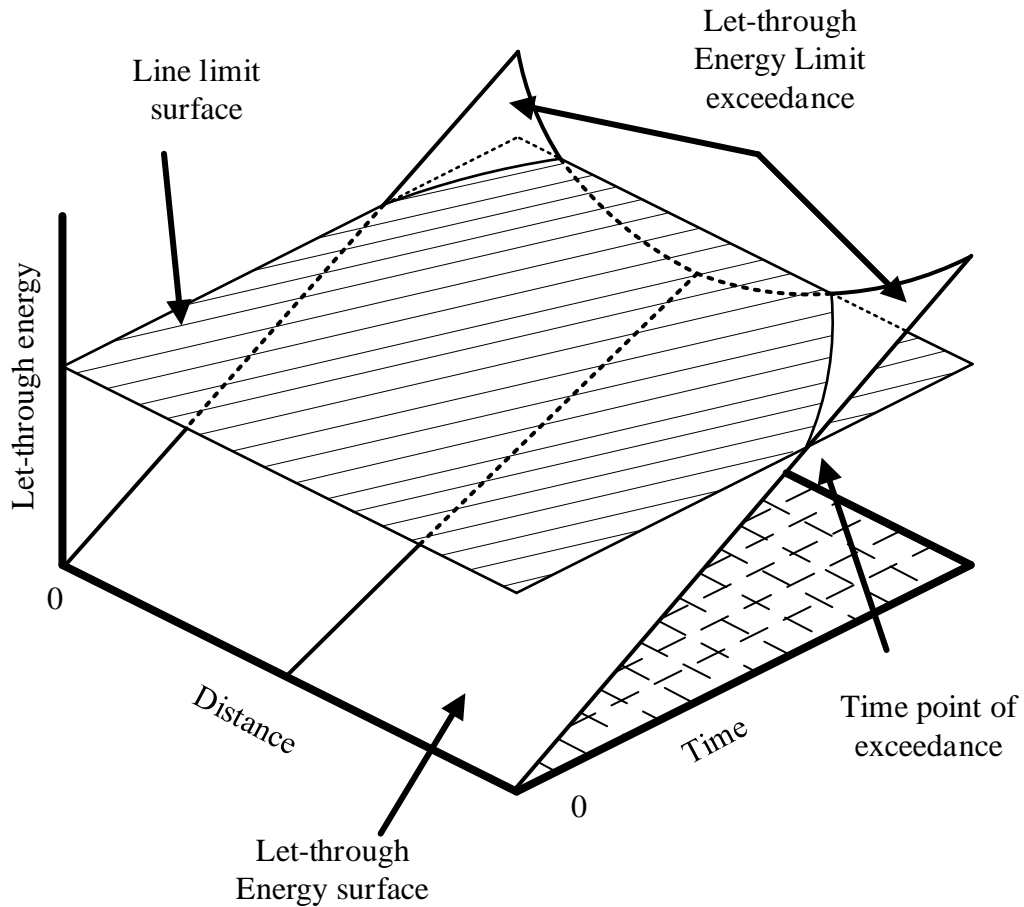


Figure 5.16. Illustration of the expected results for a LTE and line limit surface.

If ARC cycles were applied in these network protection settings, there would be distinct energy levels present in the surface. These levels are where the LTE increases and then level off during the period where the CB is open (deadtime). This cannot be observed in the side on view for a multi-source feeder. The reason for this is that only the maximum is shown. By looking at this from the surface perspective, more insight can be obtained by determining at what time the exceedance occurs so as to apply corrective or mitigating measures. As an example, the time point of exceedance at 100 % of the feeder distance can be determined in Figure 5.16. If this is compared to the side view of Figure 5.17 the time component is lost. This means the dynamic exposure of the LTE is lost. By knowing this time, it may give some design insight for total clearing time of a fault on the feeder (should be less than this).

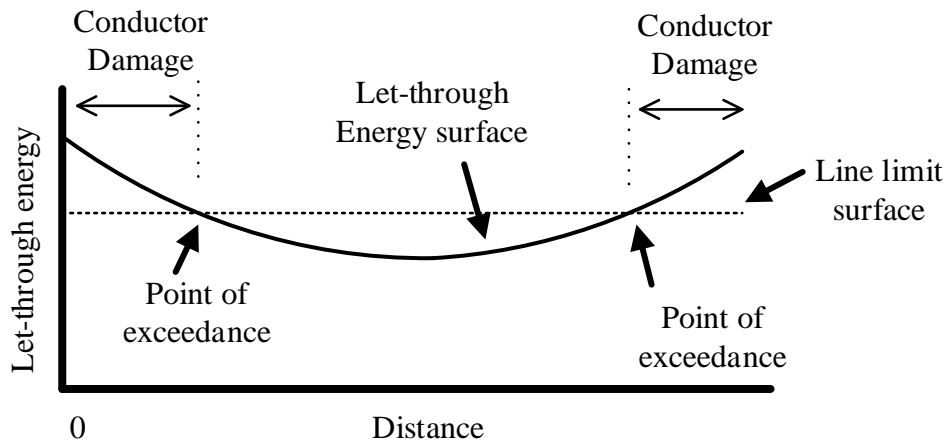


Figure 5.17. The maximum values of the LTE and line limit surfaces viewed from the distance axis.

5.4 SIMPLIFIED EVALUATION APPLICATION

The second application that was created as part of this research is detailed in a journal and a conference article [162], [166]. This simplified evaluation application was the proof of concept to the full evaluation application. The average disk speed relay model that was developed in this research was applied in this application (see Chapter 4). The LTE on a HV feeder is evaluated using an Excel based application with inputs obtained from network simulations in a network simulation tool. The results in this application were created by determining event times. All the relay status elements (tripped, not tripped, how far from tripping) are updated at each of these event times. This method is limited in that it is restricted to the number of variables it is designed with initially. If it is compared to the discrete time method of the full evaluation method, the full evaluation method is only limited by the network simulation software. If the network simulation software allows an element to be modelled, it can be evaluated. This may be accomplished by using predefined elements or additional code as was done for ARC in the relay model for the full evaluation application.

For the simplified application the created output are two-dimensional graphs that details the LTE, fault levels and fault exposure time over the length of the feeder under study. In Figure 5.18 a flow diagram of this program is shown to indicate the steps that were followed.

The simplified application in Figure 5.18 consists of two main parts, simulation and LTE calculation. These are also the same steps that was used for the full evaluation package. The difference is in how the simulation values are obtained. For the full evaluation application all the CB operations and current redistributions were included in the measured quantities obtained. For the simplified evaluation, a simulation has to be done for each possible contingency (separate).

In Figure 5.18 the first step is modelling the network and then in the second step fault levels are obtained from this simulation. These will be the fault levels measured at both ends of the feeder (e.g. A and B-end). The fault levels that are required in this case id for the following:

- When the feeder is supplied from both the A and B-end.
- When the feeder is only supplied from the A-end.
- When the feeder is only supplied from the B-end.

If additional contingencies are to be included such as embedded generation in and out of service, this will increase the number of simulations from three based on the number of CBs that can open (for both DG and N/O points).

These fault levels are determined by placing a fault at different positions across the feeder length. This can (and was) done manually in the initial stages of the program. Later a DPL application was written to automate obtaining the fault levels in Digsilent Powerfactory. This automation program formed the basis for the full evaluation program that was developed in the previous sections. The constraint of this method is that it is only focused on the feeder being studied. It will not consider the other plant (e.g. distributed generator) that might trip due to long fault clearing times. But for the proof of concept, this approach worked well. This application formed the basis of the work to identify aspects that require further investigation culminating in the full evaluation application.

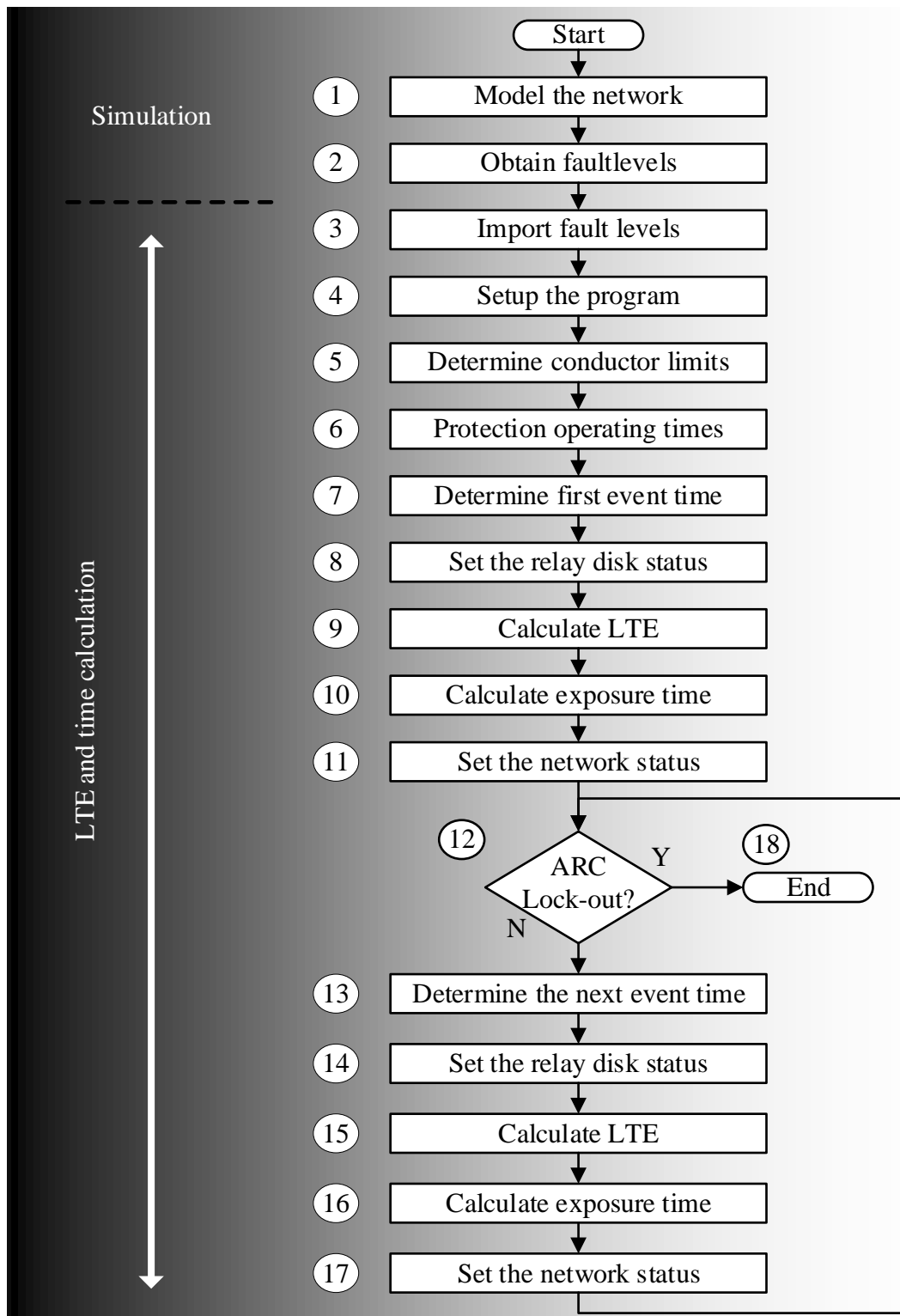


Figure 5.18. Simplified evaluation application.

The second main step in the program is the actual calculation of conductor LTE and time exposure based on the feeder settings and the fault levels obtained. This was done in Microsoft Excel.

In step 3 the fault levels obtained from network simulation are imported into the calculation program and the magnitudes scaled to the required values. The settings that should be applied to the feeder at both ends are set in step 4. This includes the actual settings such as PU, curves and ARC settings. The feeder conductor types and their LTE limits are set in this part as well. The application made provision for more than one type to be used. In step 5 the conductor LTE limits are determined for use in the plotting of results. The program starts with the assumption that the CBs at both ends of the feeder is closed. It will then determine the protection operating time at both ends of the feeder. These operating times are based on the specific settings for each end and the current that it will measure for a fault at that position on the feeder. This is for a specific network configuration. Based on these protection operating times the first event time can be determined in step 7. This will be the shortest operating time of the protection devices.

In step 8 the disc status can be set. The average disk speed model (see Chapter 4) is applied. For this the disk position is set as zero initially, but then the disk position can be determined once the operating time is known and the disk speed. For the relay that has not tripped, the new position can be set based on the time that the other relay took to open. For the IDMT curves in this program no CB time is included. The CB time is only included for instantaneous curves here. In the full evaluation program, all the CB times are included. Once the trip signal is sent, the CB deadtime is started. In step 9 the conductor maximum LTE exposure for a fault at that position is determined. The square of the maximum RMS current (both ends considered) and exposure time is used. This energy value is then stored. In step 10 the exposure time is determined. This is added to the previous value (zero in this case). It was shown that the maximum energy point might not always coincide with the maximum exposure time [40], [41], [162]. The network status in terms of CB open or closed is set in step 11.

In step 12 a test is done to determine if any of the CBs have reached a lockout condition. This method is event driven. If only one trip to lockout was used, then the first CB would have reached this point, but the second still has to open. This means that the program will determine the next event time in step 13. If all the CBs have gone into lockout, then this part of the program will end in step 18.

In step 13 the next event time is determined. This can be a CB that closes or another CB that trips. It is all dependent on the fault position, network (current that is flowing), and the applied protection settings. This complex sequencing is discussed in Chapter 4 where possible sequences are shown. This sequencing was very difficult to implement due to the number of items that can change and then updating the status of all the items concerned as time is moving forward. This is one of the motivations for using the full evaluation application where constraints such as CB operating time was removed by incorporating it in the network simulation software (and model). In step 14 the new disk status is set. This can be for more than one relay if they are both still in service or it can simply be that one CB is closing. But time has passed and the items should be updated with this time. In the full evaluation application, all the network items are evaluated at each time step, whereas in this simplified evaluation application it is only changed at the event time. This makes for faster execution times in the simplified approach, but much more complex programming to keep track of all the variables and network states. In step 15 the new LTE can be calculated again based on the corresponding network current (depends on network state) and this is added to the previous value for a fault at this specific position. The exposure time of step 16 follows the same approach as step 15. Finally, the network status is updated again in step 17 and the program can move back to step 12 for testing if all the CBs are in a lockout state.

Step 6 to 17 will have to be repeated at every fault position on the line. These results are then added together to produce a two-dimensional graph of the LTE across the feeder length. This is similar to the LTE diagram shown in Figure 5.17. The energy area under this two-dimensional curve is also determined to quantify changes made to the network or protection settings. The simplified application was applied to actual 132 kV circuits in an interconnected network [162]. It was shown that the conductor LTE protection should be

considered on HV interconnected networks. This case study based on a circuit in an actual HV network is discussed in the next case study.

5.5 CASE STUDY RESULTS: SIMPLIFIED EVALUATION APPLICATION

The simplified evaluation application was applied to the backup protection of a circuit in an actual HV network. This was done as a proof of concept as the HV network is interconnected and does have supply from both ends of the circuit (multiple supply points). The simplified network diagram is shown in Figure 5.19.

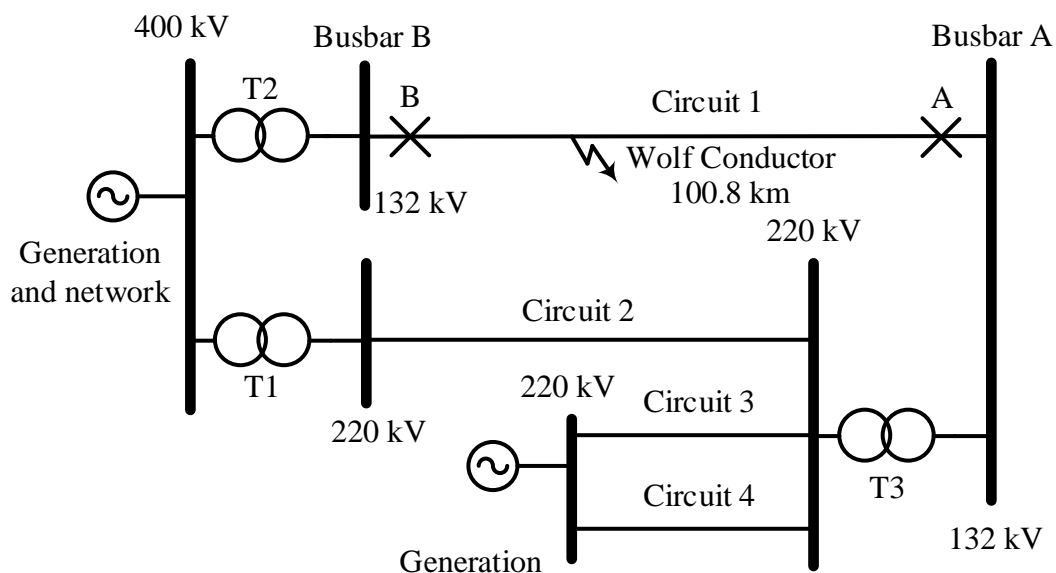


Figure 5.19. Simplified evaluation application case study.

The conductor LTE protection of circuit 1 in Figure 5.19 is being evaluated. This is a circuit at 132 kV consisting of Wolf conductor with supply at each end (Busbar A and B) of the circuit being connected via the network. With this being a HV circuit, both ends have impedance protection applied as main protection and then IDMT relays as backup protection. The backup protection at Busbar A is set to operate on a NI curve with a PU of 600 A and a TM of 0.375. A high-set element is also applied with a PU of 9000 A. At Busbar B the protection on circuit 1 is set to operate on a NI curve with a PU of 600 A and a TM of 0.2. No high-set element is applied to this end of the circuit. There are no ARC attempts applied

to the protection at either end of the circuit. Wolf conductor have a short time rating of 15.72 kA for one second (247 MA²s) when calculated using the method in Chapter 4.

The fault current measured from the A and B ends on the circuit for a three-phase fault at 1 %, 50 % and 99 % are provided in Table 5.1. These fault levels are for three network contingencies. These are when both CB A and B are closed (A and B contributions are listed separately), for when CB B is open and for when CB A is open. The distance is measured from Busbar B (zero km) towards Busbar A (100.8 km).

Table 5.1 Measured fault current for simplified evaluation application case study.

Distance From Busbar B (%)	Fault current	Fault current	Fault current	Fault current
	CB A-closed CB B-closed A-end (A)	CB A-closed CB B-closed B-end (A)	CB A-closed CB B-open A-end (A)	CB A-open CB B-closed B-end (A)
1	3137.689	1502.99	3132.072	1535.896
50	1592.427	2848.32	1623.571	2878.899
99	930.604	20766.582	1086.468	20899.39

When evaluating at the measured fault current in Table 5.1, it can be seen that the measured current change depending on what the CB status (open or closed) is at the other end of the circuit. An assumption is made that the protection in the network is graded. This means that for a fault on Circuit 1, the protection at CB A and CB B will trip before other protection in the network. The conductor LTE protection results are shown in Figure 5.20.

From the results in Figure 5.20 it can be seen that the Wolf conductor is protected as the actual LTE exposure does not exceed the conductor limit. If the high-set element at CB B is disabled, the Wolf conductor will be damaged if a three-phase fault occurs within the first 1.5 % of the feeder length from Busbar B. This high-set is reducing the LTE peak from 387 MA²s to approximately 75 MA²s. The high-set is pushing this lower peak further into

the network from 1.5 % to approximately 11 % measured from Busbar A. It can also be observed that the conductor LTE exposure towards Busbar B is increasing from its minimum value. The energy area value calculated to 1901.95 MA²s·km. More case studies and results using this simplified evaluation method are provided in the conference and published journal articles [162], [166].

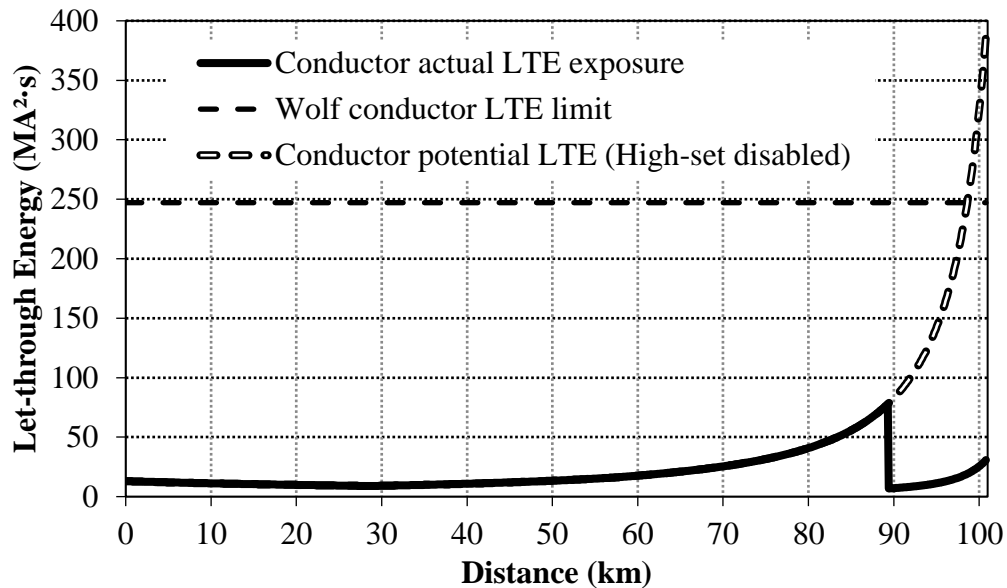


Figure 5.20. Case study results for the conductor LTE exposure in an actual network.

5.6 CHAPTER SUMMARY

In this chapter the simulation applications were discussed. In Section 5.3 the full evaluation application was discussed. The full evaluation application consisted of DigSilent PowerFactory (Simulation, DPL code and DSL code), Python and Matlab code and results are created using discrete time steps. In Section 5.4 simplified evaluation was discussed. The simplified evaluation application made use of DigSilent Powerfactory and the calculations were done in Microsoft Excel. This application was event driven. The event driven method was very complex to program and was limited in the number of variables considered during the simulation. The full evaluation application is only limited by the network simulation programs constraints. In Section 5.5 results for a case study were shared where the simplified evaluation method was applied to an actual HV network as proof of concept. This formed

the basis for the full evaluation application. In the following result and discussion chapter, the full evaluation application is applied to feeders in a radial and multi-source network.

CHAPTER 6 RESULTS AND DISCUSSION OF LTE PROTECTION APPLICATION

6.1 CHAPTER OVERVIEW

In the previous chapter applications were developed to assist with the evaluation of LTE protection in an interconnected multi-source network. In this chapter only the full evaluation application is used to generate results on a feeder. An overview of the case studies are provided in Section 6.2. The case studies are for when the network is configured as a radial feeder in Section 6.3 and then as a multi-source interconnected network in Section 6.4 and Section 6.5. The multi-source feeder is evaluated for different network contingencies (strong and weak network). Section 6.6 provides some insight to the result variables that were generated using the full evaluation application. Results for the discussion were generated from the case studies. Finally, in this chapter the results from all the case studies are combined and discussed in terms of the research questions and hypothesis in Section 6.7.

6.2 CASE STUDY OVERVIEW

The results from three case studies are presented in this chapter. These case studies are:

Case study 1, Radial feeder with ARC and operating curve selection.

Case study 2, Interconnected feeder in a multi-source network with a strong and weak end.

Case study 3, Interconnected feeder in a multi-source network with two strong ends.

In case study two the LTE protection principle is applied to a multi-source interconnected network where one end of the feeder is connected to a strong source and the other to a weak source (sources compared to each other). In case study three the LTE protection is applied to a feeder within an interconnected multi-source network where both ends of the feeder are connected to similar sized strong sources. ARC is applied to all three case studies. For the three-dimensional graphs, a colour bar is provided to assist with identifying the LTE level. The colour used for the conductor limit is also a function of this colour reference bar.

6.3 CASE STUDY 1 – RADIAL FEEDER APPLICATION

6.3.1 The objective of the case study

The objective of this case study is to demonstrate how ARC, curve selection and fault levels influence the LTE protection on a radial feeder. The key elements that will be used to evaluate this is the LTE graph and the energy-volume calculation. An energy-area evaluation (see Chapter 4) can also be used, but in this case the results are to be compared to an interconnected network of case study two. This case study will also demonstrate that the radial feeder can be evaluated using this application and does not have to be a two-dimensional LTE-distance graph such as the one used in [40].

6.3.2 The case study setup

The network that is used for this radial feeder evaluation is shown in Figure 6.1. In this network there is an external source (Source A), connected to a substation consisting of multiple transformers and a radial feeder (Feeder 1). The size and impedance of the transformers and external source is not important as these are used to adjust the three-phase fault level on this radial feeder. No loading is connected on this feeder to minimise the possible influencing variables. CBs are shown on the feeder and they indicate not only the CB position but also the measuring points for current using CTs and the protection relays connected to the CT.

The type of feeder conductor used for this network is Mink conductor. When applying the calculations in Chapter 4, Mink conductor has a short time rating of 6.026 kA. The maximum loading current for a conductor type varies between utilities over the world as this is dependent on factors such as the weather conditions and then the templating temperature [137], [138]. For the work done in this research the continuous loading value for Mink conductor of 285 A at a templating temperature of 50 °C is used [138]. The voltage at the busbar is set to be within the limits of 0.95 p.u. to 1.05 p.u. for a rated value of 22 kV. These bus voltage limits are within the standards specified by NRS-048 standard of 10 % of the rated voltage [60].

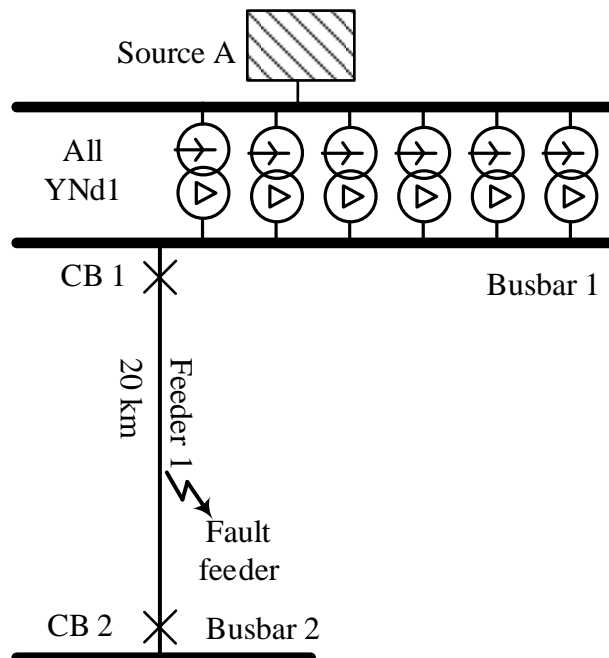


Figure 6.1. A radial network diagram for case study 1.

6.3.3 Protocol

The following protocol is applied for this case study.

1. Do the initial setup of the network so as to resemble that of Figure 6.1 with a three-phase fault level of 6 kA and busbar voltage at Busbar 1 set to the rated value of 22 kV.
2. Create the control case for a radial feeder (Result 1). The network is simulated in maximum network conditions with only IDMT NI protection applied (no ARC, high-

- sets or other protection curves). Set the protection to operate in 1.1 s for a three-phase fault close to Busbar 1.
3. Evaluate the effect of source impedance on a radial feeder (Result 2). The network is simulated in minimum network conditions with only IDMT NI protection applied (no ARC, high-sets or other protection curves). Set the three-phase fault level at Busbar 1 to 3.5 kA.
 4. Evaluate the effect of ARC and a high-set element on a radial feeder (Result 3).
 - 4.1. The network is simulated in maximum network conditions with IDMT settings of step 1. A two trip to lockout ARC philosophy is applied. The ARC deadtime is set to 1 s.
 - 4.2. The same network conditions and settings are applied as that of step 4.1 except for a high-set element that is added. The high-set element is set to initiate ARC.
 5. Evaluate the effect of operating curve selection on a radial feeder.
 - 5.1. The network is simulated in maximum network conditions. The NI IDMT curve is changed to an EI curve. Set the operating time the same as that of the protection in step 2 for a fault at the remote busbar (Busbar 2). The ARC functionality is applied from step 4. No high-set elements are applied in this step.
 - 5.2. In this step the same highest element from step 4.2 is applied with ARC that is initiated by the element.
 6. Compare results

6.3.4 Experimental parameters

The protection settings that are applied to the feeder CB (CB 1) for the required steps in the protocol are provided in Table 6.1. For all of the IDMT type operating curves used in this case study (NI and EI) the PU current is set the same. This is set based on the PU recommendations in Chapter 3. Of the three criteria that should be used to determine the PU, setting it above the expected load current (110 % of the maximum load current) was the limiting factor. It is assumed that the upstream transformer protection at the substation (Busbar 1) is slow enough and the PU is high enough so as to not interfere with the feeder protection. The operating time for the NI operating curve is set to 1.1 s for a fault right in

front of the CB (CB 1) when the network is set to operate in maximum network conditions. The operating time for the EI curve is set to the same operating time as that of the NI curve in step 2 but for a fault at the end of the line (Busbar 2).

Table 6.1 The protection settings set-up to CB 1 in case study 2.

CB	Protocol step	Curve	PU (A)	TM/TD (s)	High-set PU (A)	TD (s)	Trips to Lockout	Deadtime (s)
CB 1	2	NI	315	0.48	-	-	1	-
CB 1	3	NI	315	0.48	-	-	1	-
CB 1	4.1	NI	315	0.48	-	-	2	1
CB 1	4.2	NI	315	0.48	2000	0	2	1
CB 1	5.1	EI	315	0.32	-	-	2	1
CB 1	5.2	EI	315	0.32	2000	0	2	1

The high-set PU is set using the recommendation in Chapter 3. The minimum that it can be set to is 126 % for numerical relay devices. The PU is set to 2000 A with a time delay of zero seconds. This is roughly 200 % of the downstream fault level. For the ARC settings the trips-to-lockout is set to two trips (one ARC cycle). The deadtime is set based on the recommendations in Chapter 3 and 5 and will change from 1 s to 3 s in specific steps.

6.3.5 Case study 1 step 2 results – control case

The control case resulting graph is shown in Figure 6.2. In this result there are only two curves. One is the LTE curve and the other is a flat horizontal plane (or surface) showing the conductor limit. If there were different conductors at different parts of the feeder it would show a plane for each of these conductors relative to their position.

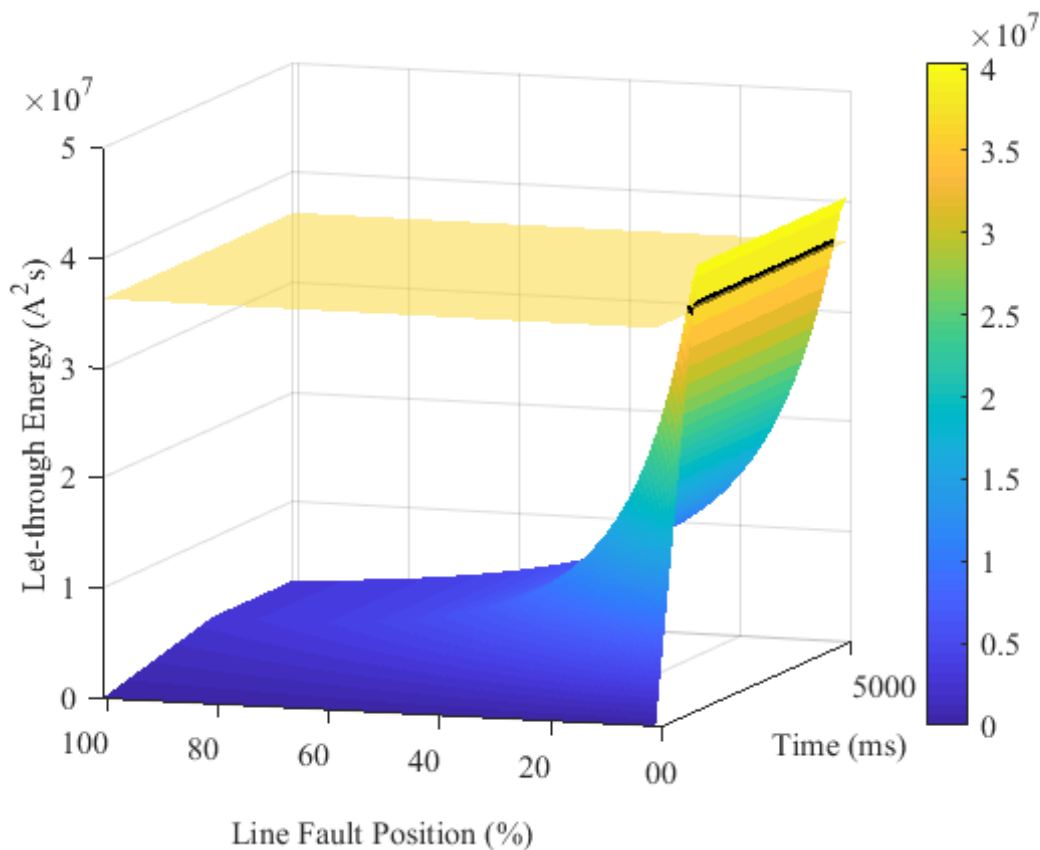


Figure 6.2. The control radial feeder LTE results.

When evaluating the form of the LTE curve in Figure 6.2 it can be seen that the energy starts at zero and it then increases as time pass to a maximum. This maximum decrease as the fault position moves further into the feeder (0 % to 100 % of distance). In this radial feeder application absolute maximum energy will occur close to the busbar in the first high risk area. This relates to a current dominant LTE system. If it was dominated by the protection operating time the high energy point will be at the remote end (second high-risk area) of the feeder (Busbar 2 end) for current flowing from Busbar 1. The LTE is surpassing the conductor limit. This can be observed in the LTE plane intersecting the conductor limit flat plane (dark black line in Figure 6.2). This exceedance will result in the conductor getting damaged if the fault is within the first part of the feeder. This is with the present protection settings applied at these fault levels. In Figure 6.3 the three-dimensional graph is rotated to show a two-dimensional graph of the energy and the fault position on the feeder.

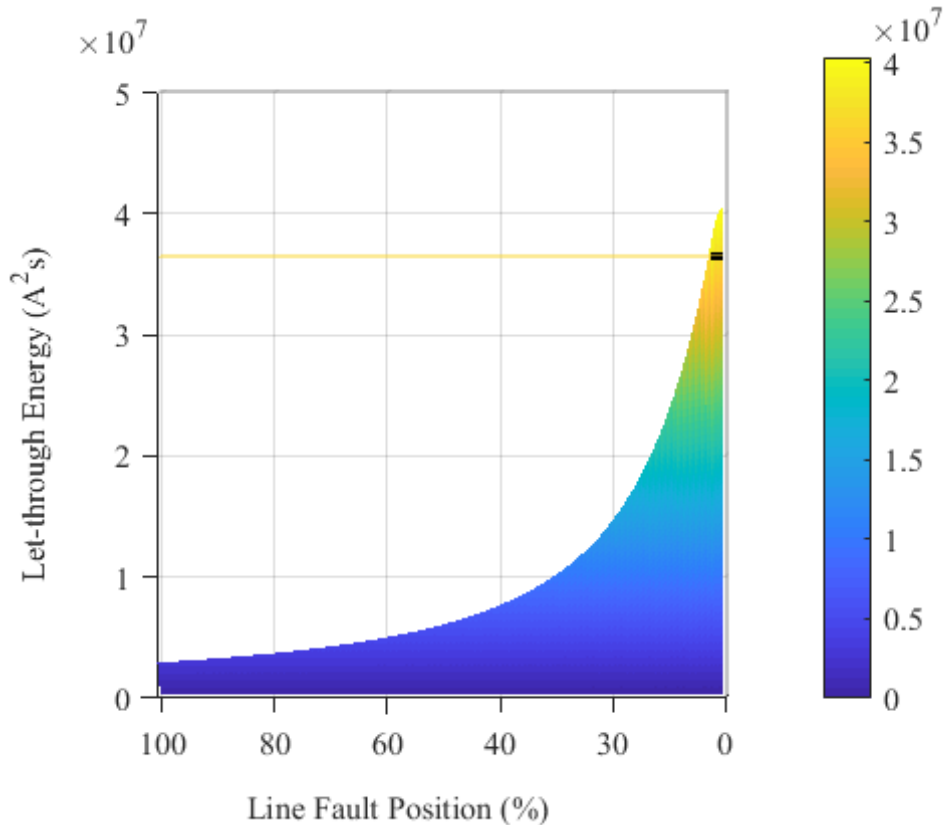


Figure 6.3. The control radial feeder LTE results from the fault position perspective.

The conductor limit is a thin yellow line in Figure 6.3 (based on colour bar level). For this Mink conductor it can be seen that the conductor limit is only exceeded for the first 0.6 km of this feeder. The form of the LTE curve in Figure 6.3 resembles that of previous work done in this field [40]. It also resembles the actual feeder of the case study used for the simplified evaluation application in the previous chapter. The rate of change for this graph (LTE vs. line fault position) is dependent on the source impedance ratio (fault level influence) and applied protection settings (time exposure influence). The source impedance ratio defines how the fault level decreases across the feeder [123].

Figure 6.4 shows the results from a time perspective. This LTE time perspective is novel. Two data points are marked as A and B. These data points show the point in time where there is no more dynamic change in the LTE (stable level reached). This is the time the CB (CB 1) has tripped. A red curve connecting point A and B is drawn to show where the dynamic area stop and static area take over. The dynamic and static area can also be obtained

by evaluating the simulation raw data and looking for the state (time and position) where there is no more increase in LTE. The dynamic area is from the origin to the A-B line and the static area is from the A-B line to the end of simulation time. In the previous work (similar to Figure 6.3) this dynamic area was not seen and the evaluation was made on the final or static time area. This is not incorrect, but the dynamic behaviour of the system is lost.

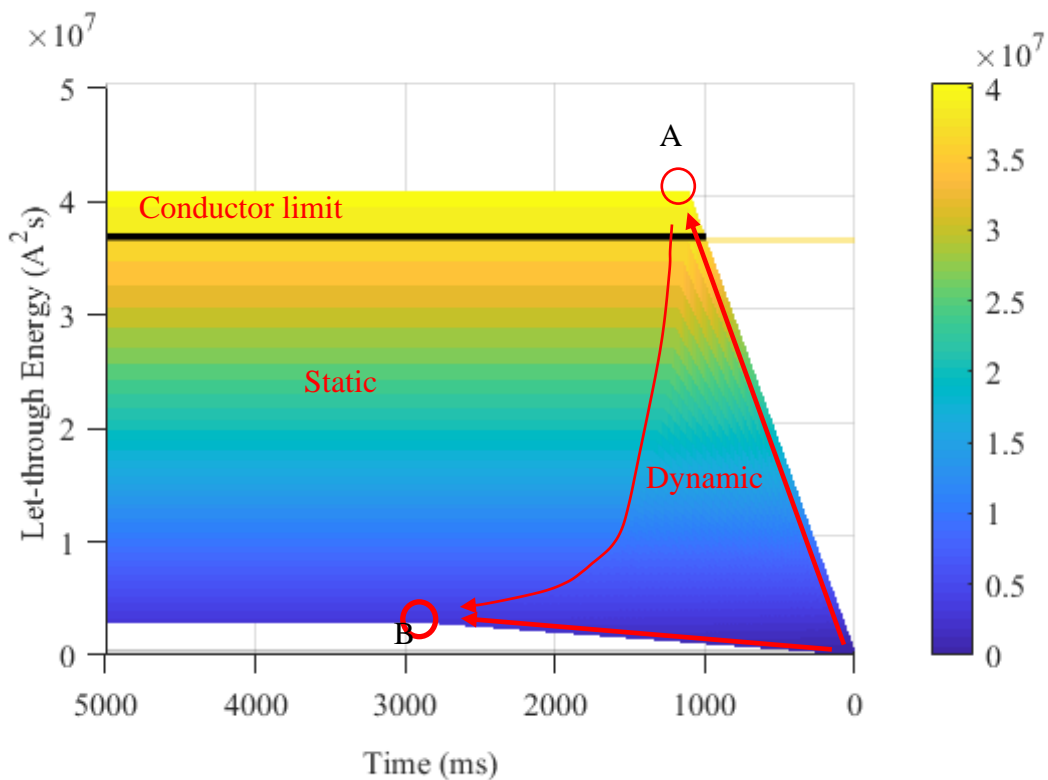


Figure 6.4. The control radial feeder LTE results from the time perspective.

Two additional lines from the origin to point A and from the origin to point B are also drawn. The gradient of these two lines are a function of the source impedance to the fault. This source impedance is the impedance at the source busbar (Busbar 1) for the origin-A line. The LTE level that will be reached is a function of the protection operating time and as such the protection settings. The protection settings define the dynamic area of the LTE surface as this will determine how long and in which form (e.g. operating curve influence) the LTE will reach the static region at the various fault levels. The line starting at the origin to point A has a steep gradient, showing that it has a low source impedance as compared to the line

from the origin to point B. This is valid while the current is the dominant factor in the LTE calculation. The increase in source impedance to the origin-B line is as a result of the line impedance being added to the source impedance at Busbar A. The impedance thus moves through the angle from A to B. It can also be observed that the time to point A and point B is different with point A being much smaller (faster protection) than point B. To protect the conductor, the energy peak defined by point A have to be reduced to a value below the conductor limit. If the operating curve and PU is kept the same, the protection will have to clear the fault within 951 ms. It can be observed in Figure 6.4 that the energy peaks at 1.1 s (based on the setting) and this is past the 951 ms margin. The results in Figure 6.2 combine these two distance and time views.

Table 6.2 The fault levels, expected operating time and LTE levels for case study 1, step 2.

CB	Feeder end	Fault level (A)	Operating time (s)	LTE (MA²s)
CB 1	Busbar 1	6177	1.096	41.8
CB 1	Busbar 2	991	2.9	2.85

The fault levels for a fault close to Busbar 1 and 2 on the feeder with the protection operating time is provided in Table 6.2. These are obtained from the simulation. The applied settings in Table 6.1 and the fault levels are used to determine the protection operating time and the expected LTE. When comparing the expected operating times of the feeder protection in Table 6.2 to the data points A and B in Figure 6.4 it can be seen that they correlate. It can also be observed that the LTE levels correlate. This shows that acceptable results are obtained from the simulation software for further case studies. For this case study the energy-volume calculates to 8.24415×10^8 A²s²·km. This is for a simulation time up to 5 s.

6.3.6 Case study 1 step 3 results – source impedance

For the results shown in Figure 6.5 the source impedance was changed from a maximum network contingency to a minimum network contingency. It can be observed in Figure 6.5 that the LTE surface does not exceed the horizontal conductor limit surface (yellow surface).

Thus, with the lower source impedance and applied settings the feeder will not exceed the conductor limit. The minimum source impedance contingency should be used for evaluating the end of feeder faults where the fault level to PU ratio can result in the LTE increasing towards the lower fault level end of the feeder (see minimum and maximum network conditions in Chapter 4). For this network with these settings it is not a concern. What can also be seen from the results is that if the fault level is lower, it can accommodate slower protection clearing times before the conductor will get damaged. In general, it is recommended to reduce the fault exposure time [33], [92], [107]. This reduction will reduce the LTE exposure and limit potential damage.

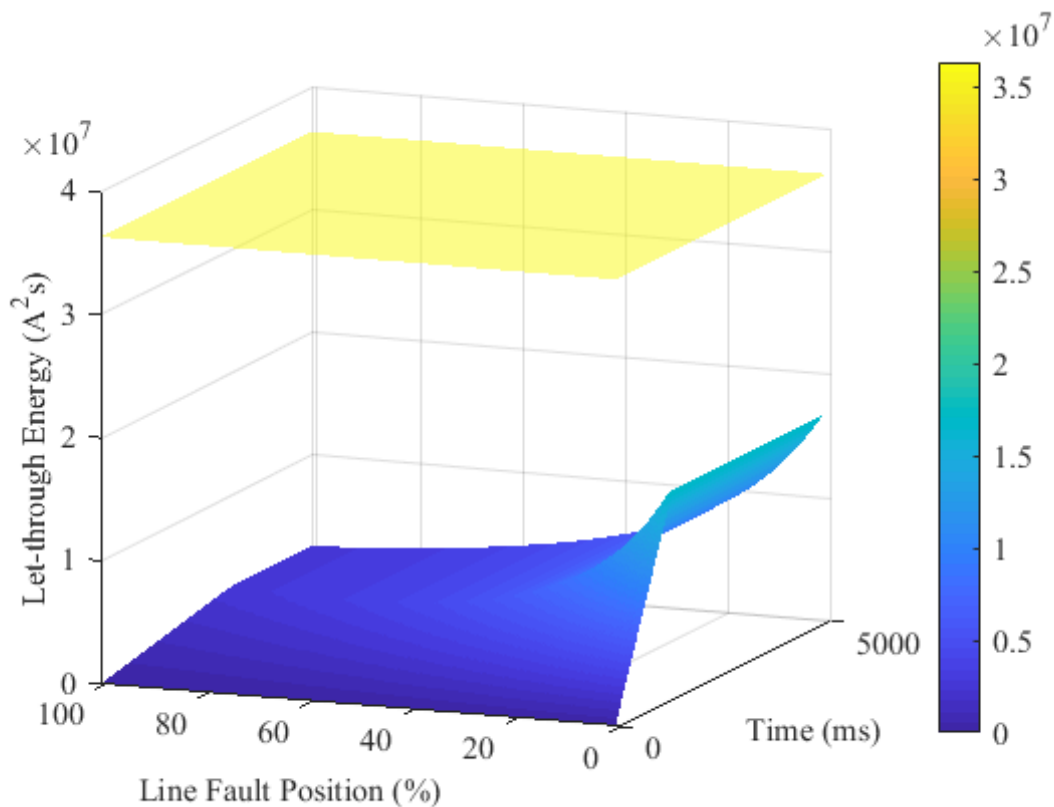


Figure 6.5. The radial feeder LTE results with a change in source impedance.

Figure 6.6 shows the radial feeder result for a change in source impedance from a time perspective. The red line gradients to point A and B are shown for this instance of the results. When comparing the origin-A line gradient from this step to that of step 2 it can be seen that the gradient has reduced which is indicative of an increase in the source impedance if the

settings were kept constant. At a fault exposure time of 1 s the LTE results in Figure 6.4 have reached a value of 36 MA²s whereas only a level of 17 MA²s was reached in the results of Figure 6.6. When the origin to B gradient lines are compared it can be seen that they are almost the same. This indicates that the fault level at the remote end has not changed significantly (dominated by the line impedance). In terms of protection settings, a change to how the protection operates in the high current region will result in a significant change of the LTE exposure as compared to the lower current region of the feeder in this case. The dynamic area of the results can better be observed in the three-dimensional graph of Figure 6.5. It can be seen that there is a graduate increase in LTE exposure up to a time value (constant LTE-static region) value where the CB trips.

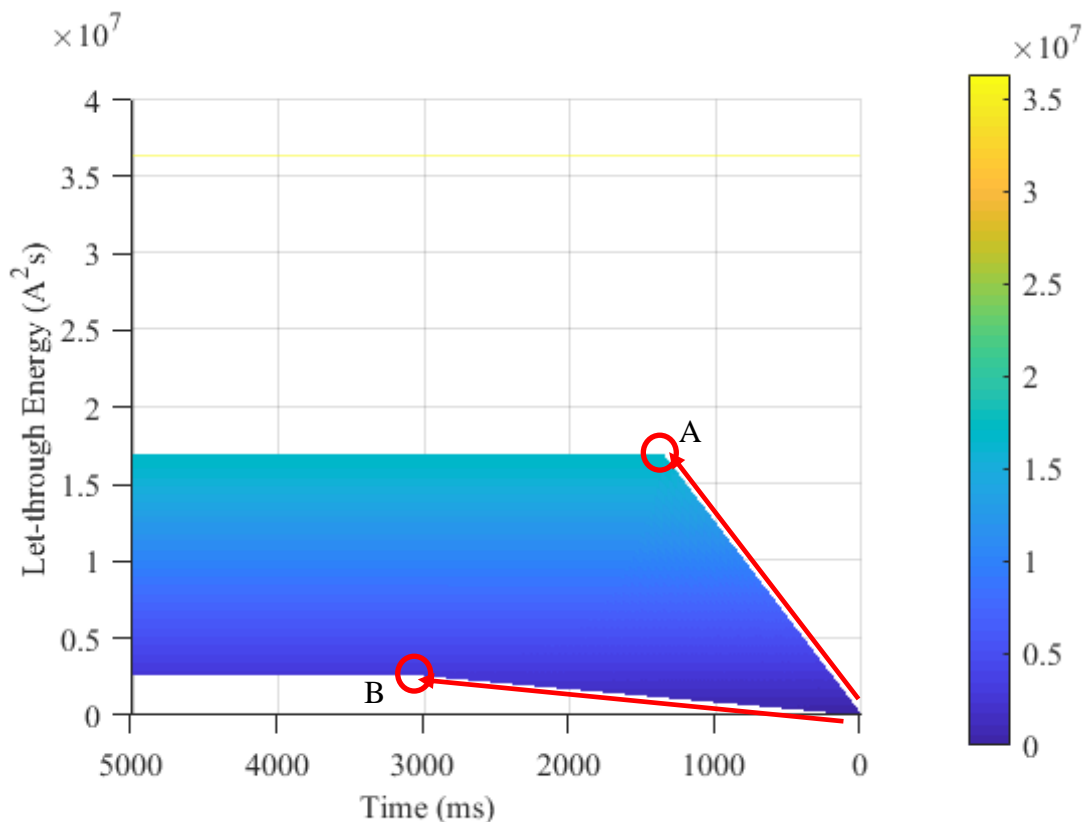


Figure 6.6. The radial feeder LTE results with a change in source impedance from the time perspective.

For this case study the energy-volume calculates to 5.029575×10^8 A²s²·km. This is for a simulation time up to 5 s. When this is compared to that of step 2 it is determined that there

was a reduction in the value. This can also be seen visually when comparing the results in Figure 6.5 to that of Figure 6.2.

The fault levels for a fault close to Busbar 1 and 2 on the feeder with the protection operating time is provided in Table 6.3. These are obtained from the simulation. The expected operating time and maximum LTE is provided in this table. When looking at the actual fault levels it supports the A-B origin line gradient evaluation with a large change in fault level close to Busbar 1 and a small change towards Busbar 2. The operating time and LTE levels compare well to that shown in Figure 6.6.

Table 6.3 The fault levels, expected operating time and LTE levels for case study 1, step 3.

CB	Feeder end	Fault level (A)	Operating time (s)	LTE (MA ² s)
CB 1	Busbar 1	3571	1.35	17.2
CB 1	Busbar 2	918	3.1	2.62

6.3.7 Case study 1 step 4 results – ARC and high-set

For the results in step 4 of the protocol the simulation time is increased from 5 s to 8 s so as to accommodate the increase in fault clearing time with the application of ARC. This is for the results of step 4.1 and 4.2 in the protocol. To simulate ARC, the DSL code developed in Chapter 5 is applied to the protection relay in the power factory model. In step 4.1 of the protocol only the number of ARC attempts are increased to one attempt from zero (see Table 6.1). Figure 6.7 show the LTE simulation results with the LTE surface and the horizontal conductor limit (flat blue plane in Figure 6.7). When evaluating the graph, it can be observed that the conductor limit is exceeded on the first trip and also on the second trip. When no ARC attempts were permitted, the conductor would only get damaged in the first 0.6 kms of the feeder. With an ARC cycle applied, this damage region increases further into the feeder to about 3 km. The magnitude of the LTE exposure is also doubled due to the

additional trip. With the additional trip in the ARC attempt there are now two dynamic regions in the surface.

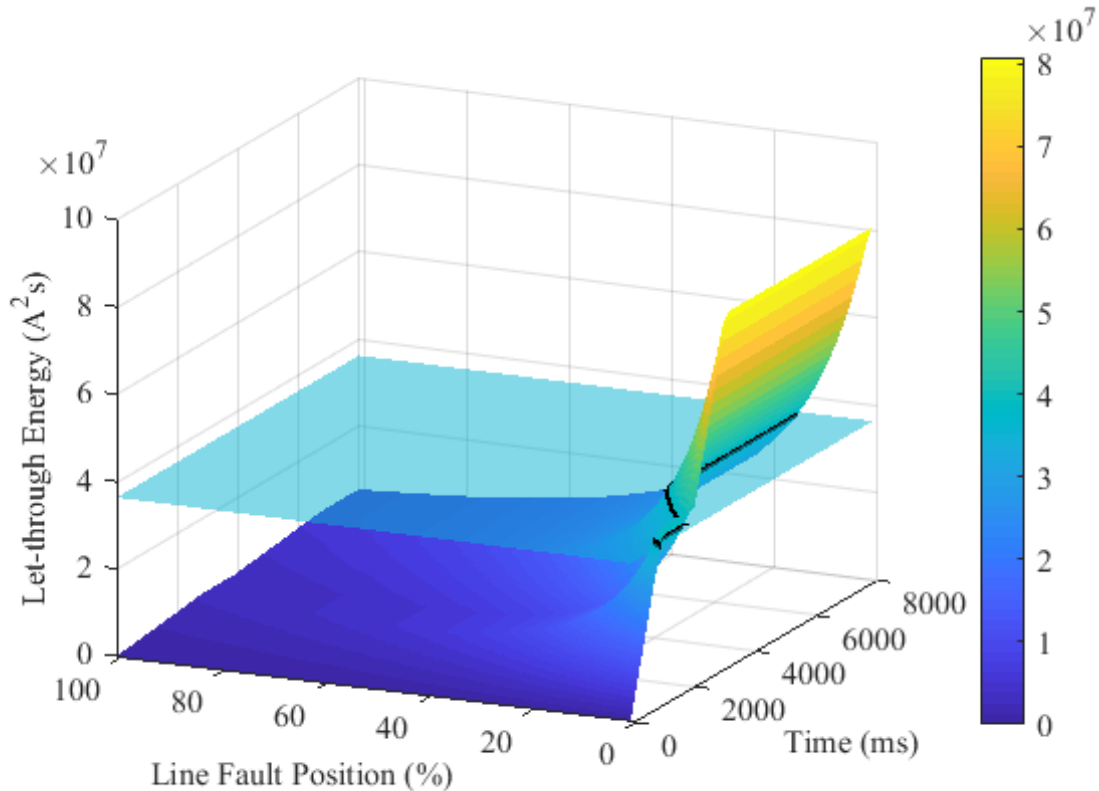


Figure 6.7. The radial feeder LTE results with ARC applied.

The LTE surface is shown from a time perspective in Figure 6.8. It can be seen that the conductor limit (black solid line) is exceeded for all trips in this study. The two dynamic regions can clearly be seen with an increase in LTE from the origin to A1 and B1 and then to points A2 and B2 from the level attained in the previous trip. It can be seen that the gradient of the respective (A1 and A2 then B1 and B2) lines are similar due to them being exposed to the same source impedance. The conductor limit exceedance can be clearly observed when evaluating Figure 6.8. The fault levels are the same as that of Table 6.3 with similar trip times (no change in source impedance). The double LTE can also be observed in Figure 6.8 with a level of approximately 40 MA²s being doubled to 80 MA²s after an ARC attempt. This is all based on the applied protection settings as the source impedance has not changed. For this case study the energy-volume calculates to $23.20365 \times 10^8 A^2s^2 \cdot km$. This is

for a simulation time up to 8 s. With the simulation time longer than that of the previous step, the volume cannot be compared. An improvement that can be made to the diagram and energy-volume calculation is to set the LTE to zero once the CB reaches a lockout state. This will remove the simulation time constraint and then any energy-volume value can be compared without the simulation time having to be the same. This can be applied in future work.

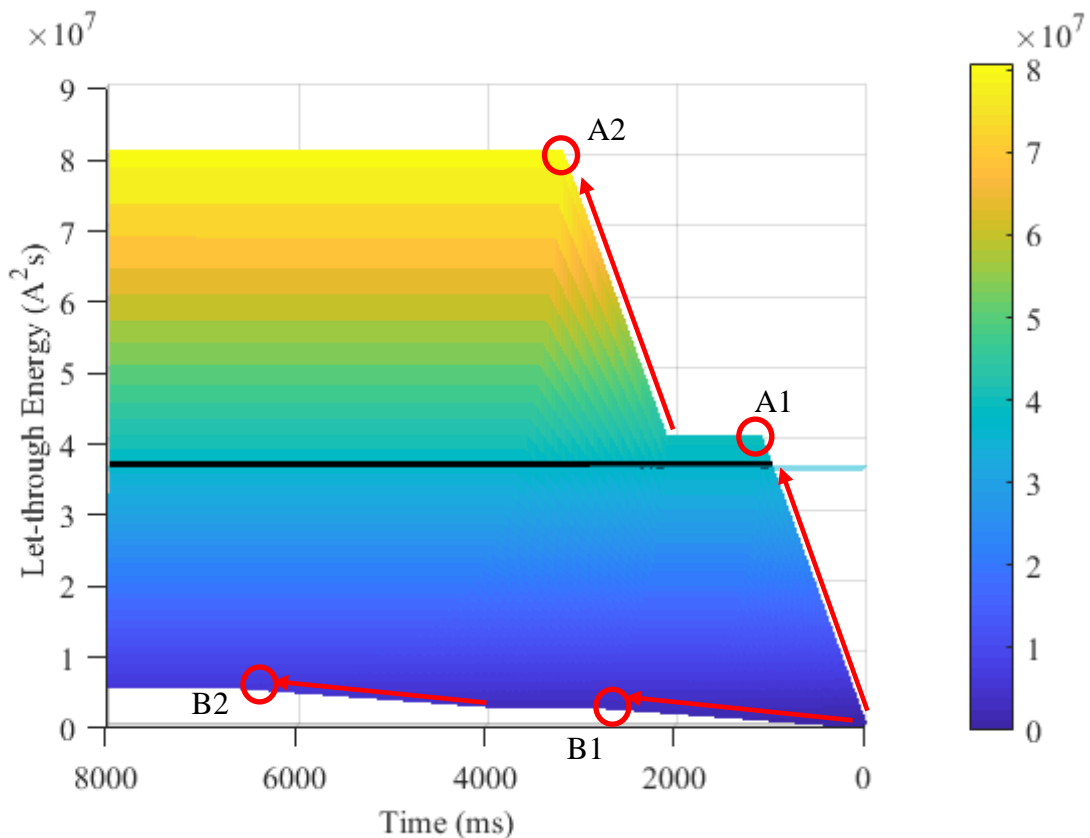


Figure 6.8. The radial feeder LTE results with ARC applied from the time perspective.

In Figure 6.9 the resulting LTE surface graph is shown for when the radial feeder is set to initiate ARC and the high-set element is enabled. It can be seen that the high-set element reduces the conductor LTE exposure significantly within the high current region close to the substation (source). The peak LTE value in this study is less than a quarter of the peak value in Figure 6.8. The LTE surface is not exceeding the conductor limit (horizontal yellow surface based on colour bar). The advantage of applying a high-set element can be observed when comparing the result from Figure 6.9 to that of Figure 6.7. From this it is recommended

to apply a high-set element whenever possible. This confirms results recommended in earlier work [37], [40], [41]. It should be applied even if a small-time delay is to be set (e.g. 100 ms) to ensure selectivity with downstream protection elements. Also, it should be applied even if the high-set element penetration is not that far into the feeder. The fact that the high-set is removing the peak current close to the source has a significant effect on the expected LTE peak as the current part of the LTE equation of (4.3) is squared. The high-set is set to initiate ARC so as to promote the continuity of supply. A high-current lockout function can be applied if the high-set should not initiate ARC [160].

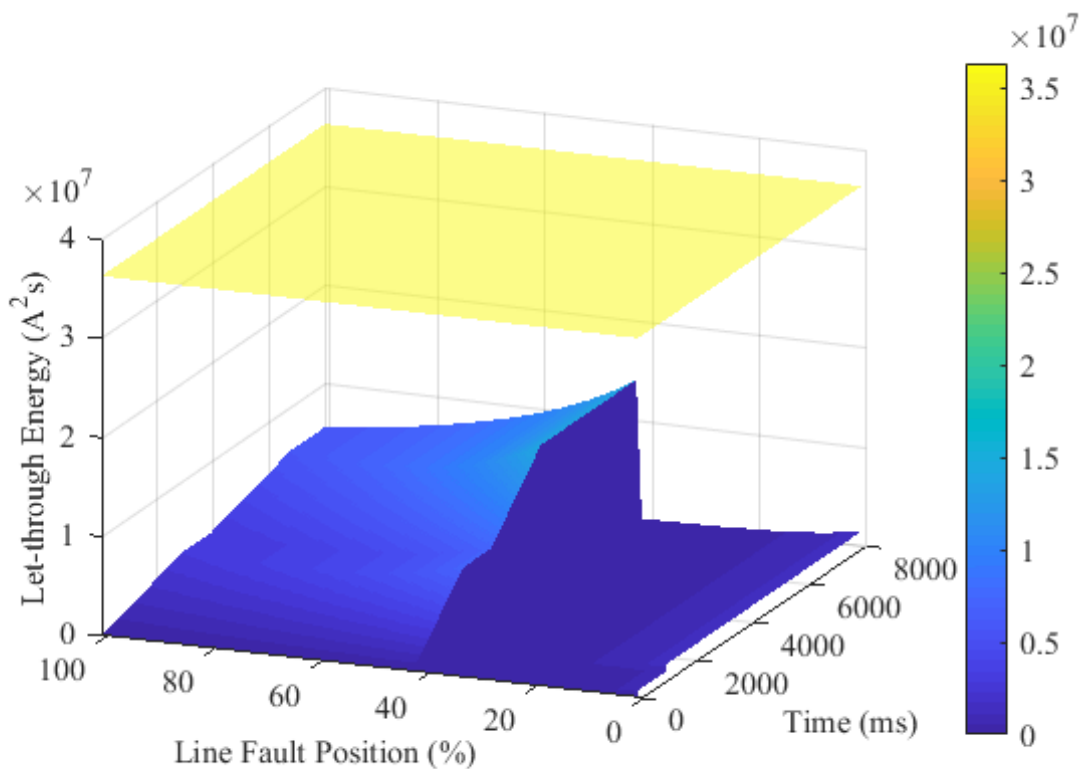


Figure 6.9. The radial feeder LTE results with ARC and high-set applied.

There is still a small amount of LTE in the region where the high-set is active. This is due to the time it takes for the CB to open and the protection relay to process the trip command. CB operating time can be in the region of 3 to 8 cycles [10]. This translates to 50 to 160 ms depending on the frequency of the system. The relay operating time is set to 20 ms for it to get to a trip decision with a time delay of zero seconds applied to the high-set element. In

this simulation only the relay time is reflected, but the CB time can be added if required. The effect of this on conductor potential LTE exposure can be seen in Figure 4.12. During this time fault current is still flowing to the fault. The energy-volume in this study can be compared to that of Figure 6.7 in the previous simulation. The energy-volume calculates to $5.658711 \times 10^8 \text{ A}^2\text{s}^2 \cdot \text{km}$. This is significantly less than that of Figure 6.7.

6.3.8 Case study 1 step 5 results – NI and EI operating curves

For this result, the protection operating curve is changed to that of an EI curve. The PU for this curve is kept the same as this is above load and provides adequate sensitivity for faults. The operating time of the protection (EI curve) is set the same as that of the protection in step 2 of the protocol for a fault at the remote busbar (Busbar 2) with a NI curve applied. There is no change in the network configuration. With the protection settings in step 2 applied to the network, the protection will operate in 2.898 s at a fault current of 991 A when applying (3.3). To set the EI curve operating time to the same value, a TM of 0.32 is applied. The two trip to lockout ARC settings of step 4.1 is kept and the simulation is set to run for 8 s so as to be able to compare the energy-volumes with that of the previous step. The results are shown in Figure 6.10 (step 5.1 of protocol).

The LTE surface of Figure 6.10 show that the change in operating curve made a significant change to the amount of LTE that the conductor is exposed too (blue surface). The LTE surface is very flat (compared to Figure 6.9) which allows for good LTE grading when it is compared to the flat conductor surface (yellow surface). This supports the discussion in Chapter 4 regarding selection of operating curve. In this step the yellow conductor limit is not exceeded. This reduction in LTE is evident in the energy-volume calculation, with the volume calculating to $6.794182 \times 10^8 \text{ A}^2\text{s}^2 \cdot \text{km}$. This is more than the value of step 4.2 ($5.658711 \times 10^8 \text{ A}^2\text{s}^2 \cdot \text{km}$) but it is far less than the value of step 4.1 ($23.20365 \times 10^8 \text{ A}^2\text{s}^2 \cdot \text{km}$).

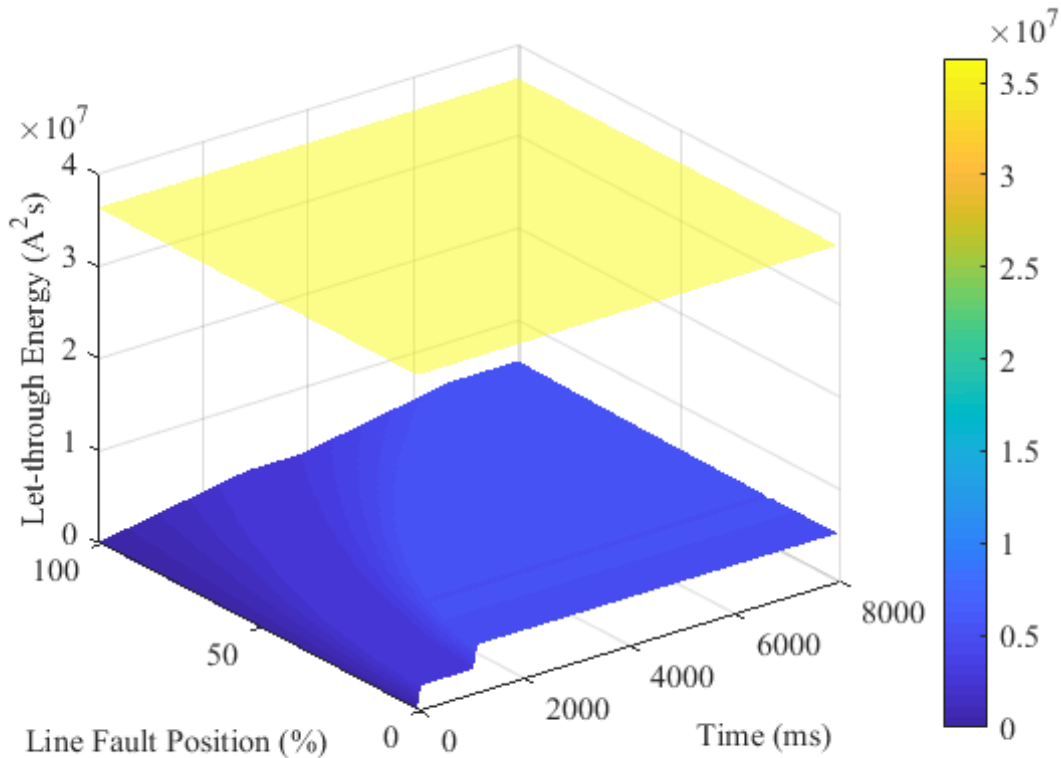


Figure 6.10. The radial feeder LTE results with an EI operating curve applied.

The result of Figure 6.10 is shown from a time perspective (Busbar 2 towards Busbar 1) in Figure 6.11. The operating time for an end of line fault at Busbar 2 can be observed at point B1. This compares well to the designed value of 2.898 s. The angle of the source impedance (origin-A line) is different to that of Figure 6.4 for step 2. The reason for this is the operating curve and TM changed. If the EI curve was set to the same operating time as the NI curve for faults at the source busbar (Busbar 1), then the gradient of the origin-A1 line would be the same. In this application it was set the same as the NI operating time for a fault at Busbar 2. This can be seen when comparing the origin-B and origin-B1 gradients in Figures 6.4 and 6.11. The actual source impedance in the network has not changed. The gradient of the origin-A line is steeper than that of Figure 6.4 due to the protection trip time being less (faster with EI). This supports the discussion in Chapter 3 where rate of change in operating time is discussed for different operating curves with the EI curve having the biggest rate of change between the NI, VI and EI curves. Another way of interpreting this is by considering the line gradients when looking at the LTE-time curves. With the origin-A1

line gradient in Figure 6.11 being steeper than that of the origin-A line in Figure 6.4, it supports the notion of the EI curve having to undergo a greater rate of change so as to reach the origin-B line gradient at the end of the feeder. The feeder (impedance) and source impedance have not changed between when comparing this to step 2.

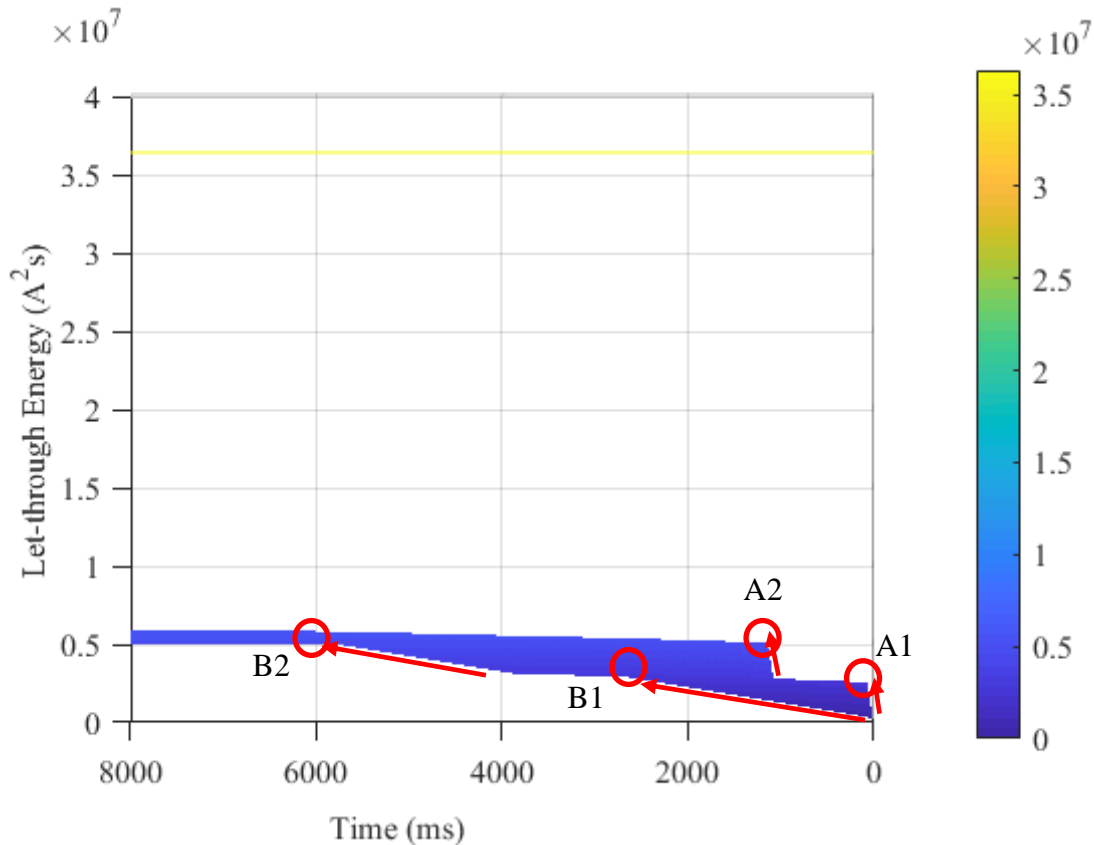


Figure 6.11. The radial feeder LTE results using an EI curve and ARC applied from the time perspective.

There are still two dynamic regions with the two ARC cycles. They first are defined by the area of the origin – A1 – B1 and the origin. The second would be from the start of the A2 line – A2 – B2 – start of the B2 line. The EI curve reduced the operating time of the protection in the high current region. The fault level here for a closeup fault is 6177 A. For the setting applied in step 2, the protection operating time is 1.095 s. With the EI curve applied this time reduces to 6.667 ms. This is the calculated value. This will then be slightly delayed by the CB operating time and the relay operating time.

In Figure 6.12 the results are shown when a high-set element with a PU of 2000 A is applied to the feeder protection. When this is compared to the results of Figure 6.10 it can be seen that the conductor LTE exposure (blue surface) is reduced even further in the high current region close to Busbar 1. The conductor limit (yellow surface) is still not exceeded. When comparing the energy-volume in this step (step 5.2) to that of step 5.1 it is reduced from $6.794182 \times 10^8 \text{ A}^2\text{s}^2 \cdot \text{km}$ to $4.014910 \times 10^8 \text{ A}^2\text{s}^2 \cdot \text{km}$.

This result shows that curve selection does have an impact on the conductor LTE and that a high-set assists greatly in reducing this LTE in the high current region. This is due to the reduction in operating time.

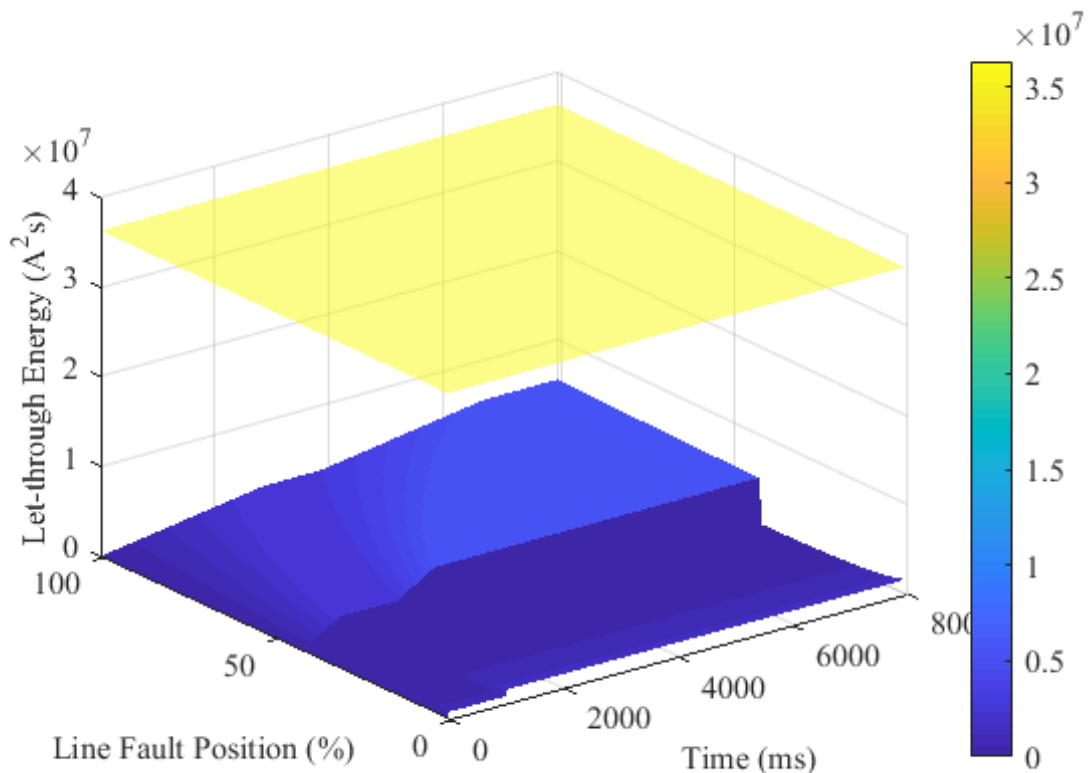


Figure 6.12. The radial feeder LTE results with an EI operating curve and ARC applied.

From this result it can be seen that the choice of protection setting influences the LTE exposure and that similar results can be obtained depending on the choice of settings and desired functions. It might not be possible to apply the desired function such as ARC when

considering the LTE constraint. In such a case other curves and high-set elements may be considered. Then, if the source impedance is considered, different settings can be applied again. As an example, ARC may be applied without having to apply a high-set or change the curve to an EI curve. It is preferable to apply ARC so as to improve the availability of the network [29]. [65], but the effect on the conductor LTE has to be considered to ensure the conductor is protected. By considering the energy, the limit in which the settings have to operate is defined and the elements that contribute to the limit can be identified.

6.4 CASE STUDY 2 – INTERCONNECTED MULTI-SOURCE NETWORK (WEAK AND STRONG SOURCE)

6.4.1 The objective of the case study

The objective of this case study is to demonstrate that LTE protection has to be considered in an interconnected network. As part of this case study, it will be illustrated how to evaluate the applied protection and interpret the resulting graphs. This case study will also illustrate how an interconnected network with multiple sources differs from a radial network. The key elements that will be used to evaluate this is the LTE graph and the energy-volume calculation.

6.4.2 The case study setup

The network used for this interconnected multi-source network case study is shown in Figure 6.13. Feeder 1 will be evaluated. Similar to case study 1, the size of the external sources and transformers connecting them to the interconnected network are not key. The transformers are used to change between minimum and maximum network conditions (high and low fault levels). The sources are there to have another source of fault current besides Source A. The fact that there are multiple fault current paths and sources is key. Different generators have different capabilities and will contribute different fault currents for different times (dependent on generator and protection settings). As the LTE is evaluated and not the generator, all the sources are modelled as an external source. The methods that are presented

and evaluated in this research can be extended to include the effects of different generators and their dynamics. This method of evaluating the conductor LTE exposure allows for a holistic evaluation of the network. To minimise the variables, no load is connected to the busbars. This will help to only consider the effect of fault current. Load current can be included in this method if the effect is to be studied. With bolted three-phase faults being used in this case study, there will not be any load current passing through the faulted feeder. CBs are shown on the feeder and they indicate not only the CB position but also the measuring points for current using CTs and protection relays. Protection will only be modelled on CB 1 and CB 2 as only Feeder 1 in Figure 6.13 will be evaluated.

The three-phase fault level at each busbar is shown in Table 6.4. These fault levels are for maximum network conditions where all three sources are in service and all CBs are closed. The fault is placed on each of the busbars. The voltage at each busbar are kept to within a range of $\pm 5\%$ of 1 p.u (22 kV system). This is within the NRS 048 limits [60].

Table 6.4 The voltage and three-phase fault levels at each busbar for case study 2.

Busbar	Voltage (kV _{L-L})	Voltage (p.u.)	Fault level (kA)
Busbar 1	22.2	1.009	6.709
Busbar 2	21.656	0.984	2.832
Busbar 3	21.496	0.977	9.775
Busbar 4	21.853	0.993	1.871

The three-phase fault current for a fault 0.01 % on Feeder 1 from Busbar 1 and then Busbar 2 is provided in Table 6.5. This is for the network configured with all the transformers, sources and feeders in service. Only the remote end CB is opened or closed for this table. The fault position percentage is measured from Busbar 1 to Busbar 2. This shows that the case study is set such (setup) that the fault current will redistribute itself depending on the network configuration (CBs open or closed). The measured fault current (by the relay) can thus change before a trip signal is issued to the CB. The protection at each end of the evaluated feeder is set and will operate independent of each other. There are an infinite number of

network configurations. For this case study, the network is set as shown in Figure 6.13, with fault levels as depicted in Table 6.4 and 6.5 to illustrate the evaluation method.

Table 6.5 The three-phase fault current measured on Feeder 1 for different CB status.

Circuit Breaker Status		Fault position from Busbar 1	Three-phase Fault current	
CB 1	CB 2	(%)	CB 1 (kA)	CB 2 (kA)
Closed	Closed	0.01	6.090	0.644
Closed	Open	0.01	6.174	0
Closed	Closed	99.99	0.964	1.884
Open	Closed	99.99	0	1.870

The type of feeder conductor used on all the feeders in this network is Mink conductor. There are numerous types of conductors available, Mink is used to illustrate the concept of LTE protection as it falls within the recommended conductors used for MV feeders [138]. From the calculations in Chapter 4, Mink conductor has a short time rating of 6.026 kA. For the work done in this research the continuous loading value used for Mink conductor is 285 A at a templating temperature of 50 °C [138].

For this case study the source impedance will not be changed as this was discussed in case study 1. With a source impedance change in the interconnected network, the busbar fault levels (Table 6.4) and current redistribution (Table 6.5) will change. This will impact the protection operation. The focus is not placed on this change as it is known that this change will be there.

In this case study the applied protection operating curves will not be changed either as it was shown in case study 1 that this influences the conductor LTE exposure.

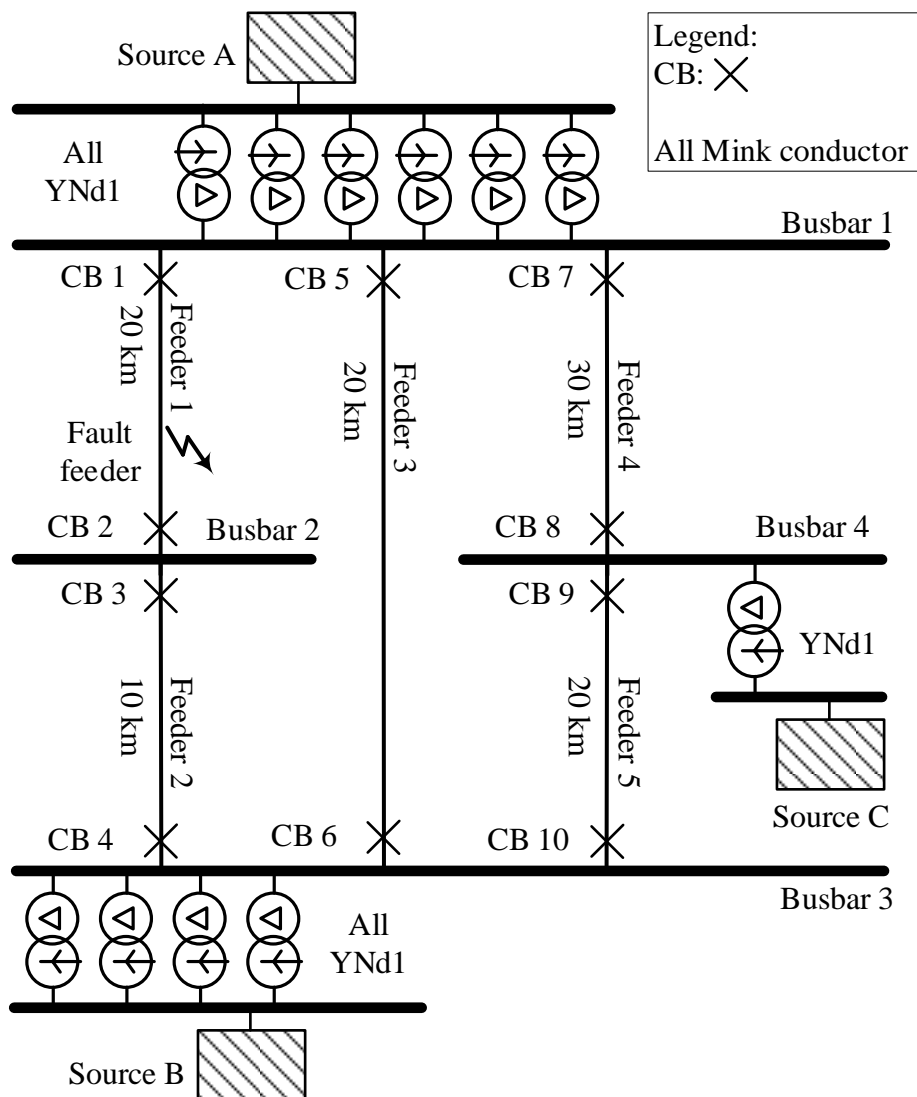


Figure 6.13. The network diagram showing the interconnected multi-source network.

6.4.3 Protocol

The following protocol is applied for this case study.

1. The faulted feeder being evaluated is Feeder 1. Do the initial setup of the network so as to resemble that of Figure 6.13 with a three-phase fault level and voltages at each busbar as provided in Table 6.4 and the fault current distribution as in Table 6.5 for Feeder 1. No loads are connected so as to minimise the influencing variables.
2. Create the control case for a multi-source interconnected feeder (Result 1). The network is simulated in maximum network conditions with only IDMT NI protection applied (no

- ARC, high-sets or other protection curves) For the CB 1 protection on Feeder 1, set the protection to operate in 1.1 s for a three-phase fault close to Busbar 1. Set the CB 2 protection on the remote end of Feeder 1 to operate in 0.4 s for a closeup fault.
3. Evaluate the effect of protection operating time and ARC attempts on an interconnected multi-source feeder (Result 2). The network is simulated in maximum network conditions with only IDMT NI protection applied. The fault levels are the same as step 1 of the protocol.
 - 3.1. Set CB 1 to operate in 1.1 s for a closeup fault to Busbar 1 on Feeder 1. Set CB 2 to operate in 1.1 s for a closeup fault to Busbar 2 on Feeder 1. No high-set element or ARC attempts are applied.
 - 3.2. Use the settings of step 3.1 and apply one ARC attempt (two trips to lockout) to the protection at each end of the feeder (CB 1 and 2). Set the deadtime at each end of the feeder to 1 s.
 - 3.3. Use the settings of step 3.2 and apply a highest to the protection at each end of the feeder (CB 1 and 2). The high-set element is set to initiate ARC.
 4. Evaluate the effect of ARC deadtime on an interconnected multi-source feeder (Result 3). The network is simulated in the same network conditions as Step 1.
 - 4.1. Apply the same settings as that of step 3.2 except for the ARC deadtime at the Busbar 1 end of Feeder 1. Set the deadtime to 4 s for the protection on CB 1 and set the deadtime to 1 s for the protection on CB 2. The high-set element is set to initiate ARC as well.
 - 4.2. Apply the same settings as that of step 3.2 except for the ARC deadtime at the Busbar 1 end of Feeder 1. Set the deadtime to 0.3 s for the protection on CB 1 and set the deadtime to 1 s for the protection on CB 2. The high-set element is set to initiate ARC.
 5. Compare the results

6.4.4 Experimental parameters

The protection settings that are applied to the protection driving the CBs at both ends of Feeder 1 (CB 1 and 2) are provided in Table 6.6. This is for each step of the protocol. Only

NI operating curves are used in this case study. The PU current is set the same for both ends of the feeder. This is set based on the PU recommendations in Chapter 3. Of the three criteria that should be used to determine the PU, setting it above the expected load current (110 % of the maximum load current) was the limiting factor. It is assumed that the upstream transformer protection at the substation (Busbar 1) is slow enough and the PU is high enough so as to not interfere with the feeder protection. The operating time for the NI operating curve is set to 1.1 s for a fault right in front of CB 1 (fault position is 0.01 % from Busbar 1) when the network is set to operate in maximum network conditions. The operating time for the protection driving CB 2 is set to operate in 0.4 s for a fault in front of the CB on Feeder 1 (fault position is 99.99 % from Busbar 1) with all the CBs closed and the network being operated in maximum network conditions (all plant in service).

Table 6.6 The protection settings setup to CB 1 and 2 in case study 2.

Protocol step	CB	Curve	PU (A)	TM (-)	High-set PU (A)	TD (s)	Trips to Lockout	Deadtime (s)
2	CB 1	NI	315	0.48	-	-	1	-
	CB 2	NI	315	0.11	-	-	1	-
3.1	CB 1	NI	315	0.48	-	-	1	1
	CB 2	NI	315	0.29	-	-	1	1
3.2	CB 1	NI	315	0.48	-	-	2	1
	CB 2	NI	315	0.29	-	-	2	1
3.3	CB 1	NI	315	0.48	2000	0	2	1
	CB 2	NI	315	0.29	1000	0	2	1
4.1	CB 1	NI	315	0.48	-	-	2	4
	CB 2	NI	315	0.29	-	-	2	1
4.2	CB 1	NI	315	0.48	-	-	2	0.3
	CB 2	NI	315	0.29	-	-	2	1

The high-set PU is set using the recommendation in Chapter 3. The minimum that it can be set to is 126 % or 192 % of the fault current at the remote end of the feeder in maximum network conditions for numerical and electromechanical devices respectively. For Feeder 1, the high-set PU is set to 2000 A on the busbar 1 side and to 1000 A on the busbar B side. This is roughly 200 % of the downstream fault level for the Busbar 1 end and 155 % for the Busbar 2 end. Both ends are set to a time delay of zero seconds. For the ARC settings the trips to lockout is set to two trips (one ARC cycle) in specific protocol steps. The deadtime is set based on the recommendations in Chapter 3 and 4 and will change from 1 s to 5 s and then to 0.3 s in specific steps for the protection settings applied to the relay at the Busbar 1 end of the feeder.

The simulation time has been set to 12 s so that the results from case study 1 can be compared to later case studies where long ARC deadtimes might be present. For this case study the results cannot be calculated using the known NI equation of (3.1). This is due to the measured fault current that can change when any CB in the network operates. The integral version of the NI equation of (4.18) cannot be used either as the current signal should be defined between boundaries to integrate the curve. As such, the discrete version of the NI operating equation of (4.19) is used (in full evaluation application of Chapter 5). The disk average speed method can be used, but this does have its complexities and constraints.

6.4.5 Case study 2 step 2 results – control case

For this case study the control case resulting graph is shown in Figure 6.14. In this result there is only two curves. The one is the LTE curve and the other is a flat horizontal plane showing the conductor limit. When evaluating the form of the LTE curve in Figure 6.2 it can be seen that the energy starts at zero and it then increases as time pass to a maximum. This is the same across the complete length of the feeder and is similar to the radial results from case study 1. This maximum decrease as the fault position moves further into the feeder, towards Busbar 2. There is an infeed from the Busbar 2 end, but this is less than the LTE contribution from the Busbar 1 end.

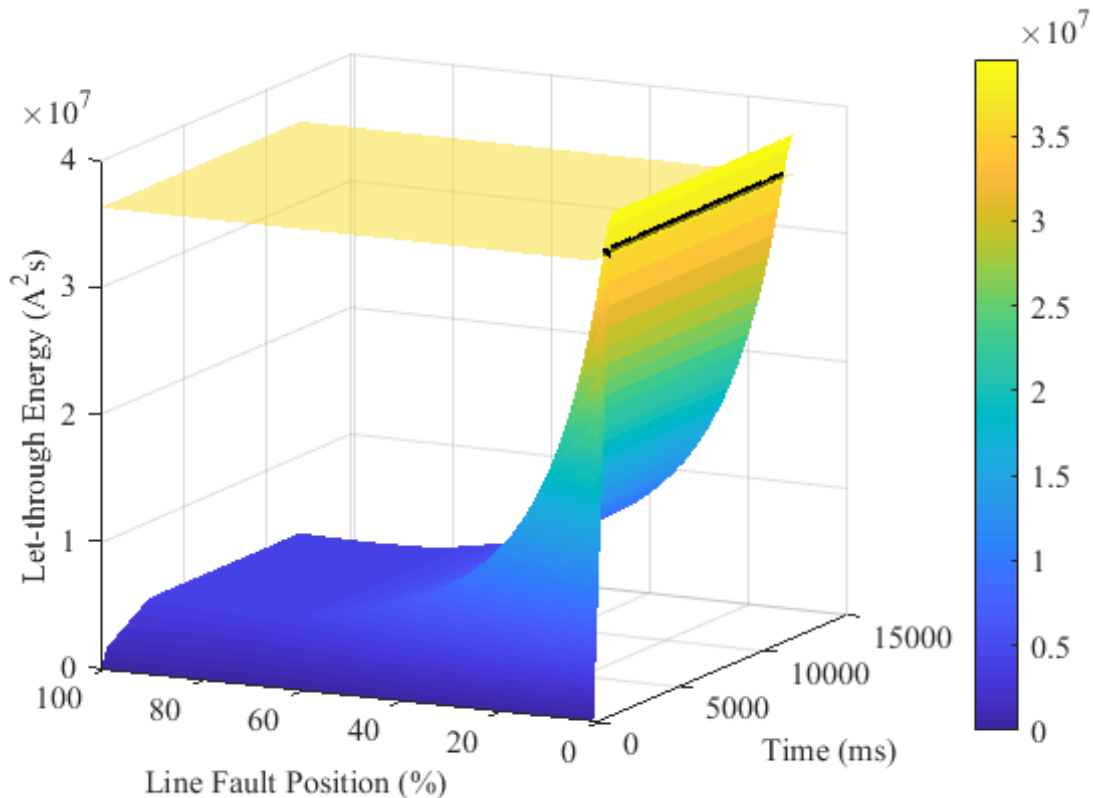


Figure 6.14 The control multi-source interconnected feeder LTE maximum results.

In Figure 6.14 the maximum of the two ends are represented as this would be the maximum that the feeder will be exposed to at that point in time, at that position on the feeder. The fault current from each end of the feeder does not combine on the feeder, but it does in the arc (or plasma around the arc). Figure 6.15 and Figure 6.16 shows the individual contribution from each end of the feeder. This is what each end will contribute if only that end was considered. The maximum LTE value is used between the two ends as this is the maximum that the feeder can be exposed too. It can be seen that the major contribution to the LTE is from the Busbar 1 end and there is a very small contribution from the Busbar 2 end. This is based on both the fault levels and then protection settings applied to the protection relays. If this was a long feeder with low fault levels towards the end of it (Busbar 2 or 100 % side), the LTE may start to increase again towards that end. An increase at the Busbar 2 end can also be as a result of high fault currents and slow operating times for the protection associated with CB 2.

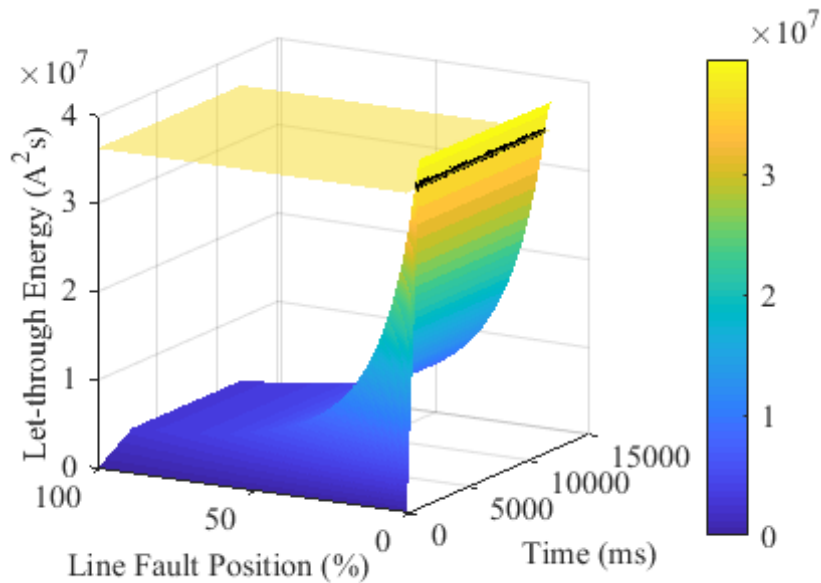


Figure 6.15 The multi-source interconnected feeder LTE Busbar 1 contribution results.

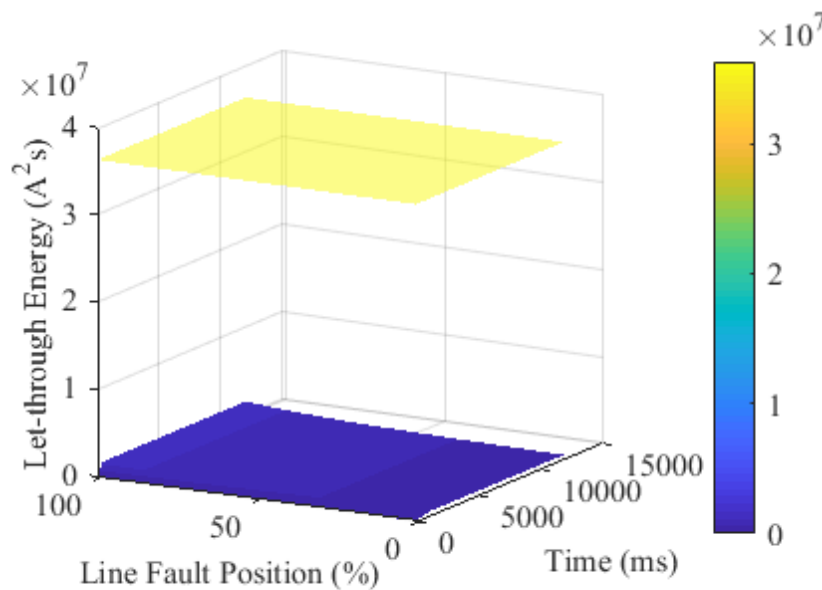


Figure 6.16 The multi-source interconnected feeder LTE Busbar 2 contribution results.

The contribution from the Busbar 2 end is decreasing from the 100 % position to the 0 % position. This only indicate the feeder distance defined with respect to Busbar 1 with 0 % at Busbar 1 and 100 % at busbar 2. The conductor LTE limit (yellow surface) is also shown in each of the individual contributions. The colour of the surface is based on the colour bar

associated with that figure. It is seen that the contribution from Busbar 1 in Figure 6.15 exceeds the conductor limit surface.

In Figure 6.14 there is only one dynamic LTE region. This is for the region where the LTE is changing from zero to its maximum value. The conductor limit is exceeded in the initial part of this feeder. Thereafter the LTE is decreasing before it starts to increase very slightly towards the end of the feeder. To eliminate the conductor limit exceedance, the protection TM on the Busbar 1 end can be reduced slightly. There are other possibilities such as the application of a high-set element, applying a maximum time element (DT element with a time delay) or changing the operating curve to a VI or EI curve. The energy-volume calculates to $21.88761 \times 10^8 \text{ A}^2\text{s}^2 \cdot \text{km}$. This is for a simulation time up to 12 s.

6.4.6 Case study 2 step 3.1 results – operating time increase

The result for an increase in operating time from the protection at the Busbar 2 end is shown in Figure 6.17. The most notable difference between the results in step 2 of the protocol to these results are the increase in LTE towards the remote end of the feeder at Busbar 2. This increase occurs 74 % into this feeder (from Busbar 1) and is purely the result of changes in protection settings. The maximum value attained at the remote end (Busbar 2) is still not exceeding the conductor limit (yellow surface). Close to Busbar 1 the conductor limit is still exceeded (similar to results in step 2). The energy-volume calculates to $22.69773 \times 10^8 \text{ A}^2\text{s}^2 \cdot \text{km}$. This is for a simulation time up to 12 s. The energy-volume has thus increased with the increase in operating time from the protection at the Busbar 2 end. The results in Figure 6.17 still only show one dynamic region as the LTE increase from zero to a maximum value where it stays (static region) once the fault is cleared from both ends (CBs opened).

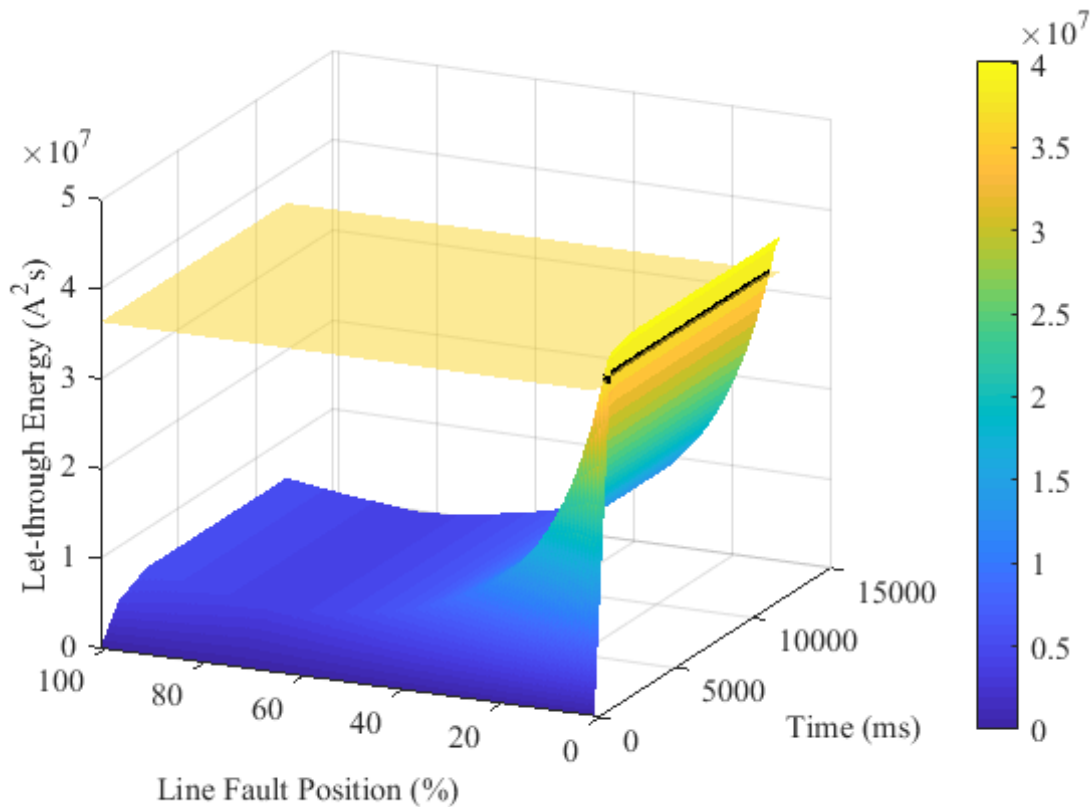


Figure 6.17 The multi-source interconnected feeder LTE maximum results with slow protection on both ends of the feeder.

6.4.7 Case study 2 step 3.2 results – operating time increase with ARC

In this step an ARC attempt is applied to both ends of the protection on Feeder 1. The deadtime is set the same at 1 s for both ends. The results are shown in Figure 6.18. The conductor limit is shown as a flat blue surface (based on figure colour bar) cutting the LTE surface. It can be seen that the conductor LTE exposure has increased across the feeder and there is a step change in the LTE some time into the fault. This increased the region where the feeder can be damaged by pushing the damage region further into the conductor from Busbar 1. When evaluating the LTE curve in Figure 6.18 from a time perspective it can be seen that before the first trip the conductor limit is already exceeded. This means that the recommendations in step 2 have to be applied first. If the high-set element is applied and set to reach at least up to the fault level (or distance) where the conductor limit is exceeded with

the second trip (one ARC cycle) then the conductor may be protected with minimum effort. Downstream elements that impose possible grading limitations may be affected and will have to be reviewed. The effect of ARC from the remote (Busbar 2 at 100 % distance) end did not increase the LTE contribution to a value greater than the conductor limit. The protection from this end will not have to be changed from a LTE perspective.

The energy-volume calculates to $41.36459 \times 10^8 \text{ A}^2\text{s}^2 \cdot \text{km}$. This is for a simulation time up to 12 s. The energy-volume have increased with the application of an ARC attempt at each end of Feeder 1. The results in Figure 6.18 show multiple dynamic regions. These are not easy to observe. Reference is made to the sequence of events as shown in Figure 4.18 for the various possible sequence of events. Every time a CB closes or opens, it changes into a dynamic region.

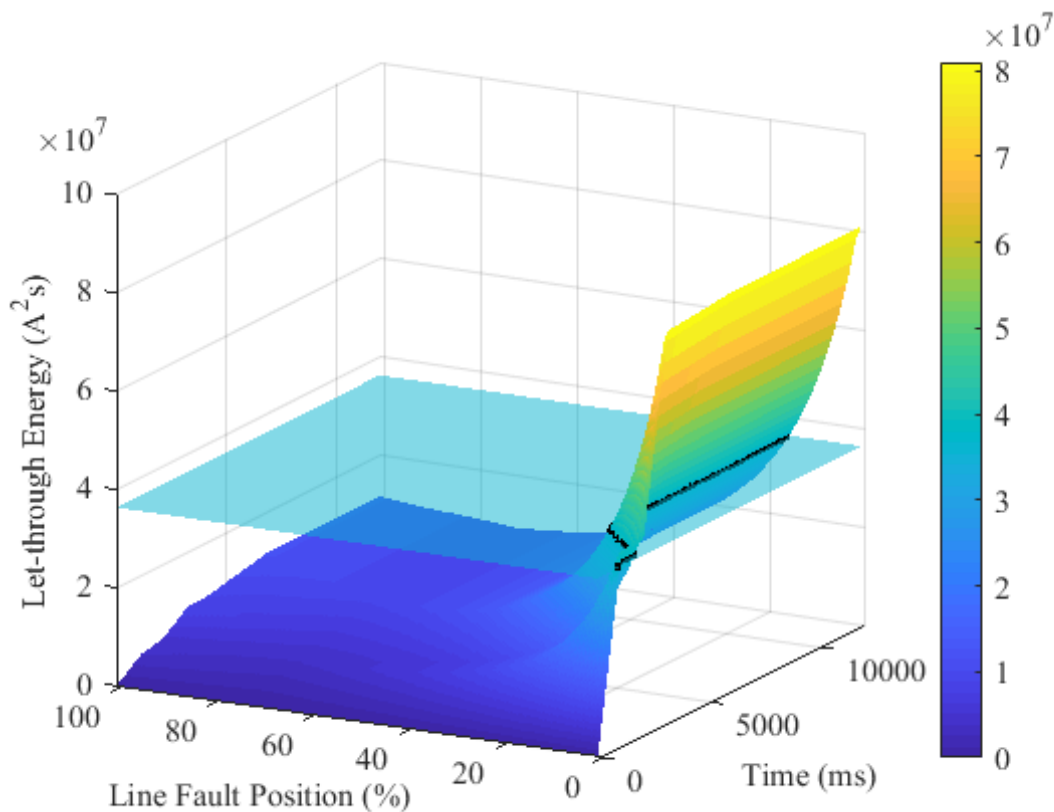


Figure 6.18 The multi-source interconnected feeder LTE maximum results with slow protection on both ends of the feeder and one ARC attempt.

6.4.8 Case study 2 step 3.3 results – operating time increase with ARC and high-sets

In this step an ARC attempt and a high-set element are applied to both ends of the protection on Feeder 1. Both the NI operating curve and the high-set are set to initiate ARC. The deadtime is set to 1 s at both ends. The results are shown in Figure 6.19. The conductor limit is shown as a flat yellow surface (based on the colour bar). It can be seen that the application of the high-set element has reduced the conductor LTE exposure significantly. The peak LTE exposure is now moved further into the network when it is compared to the results in the previous step 3.2 (Figure 6.18).

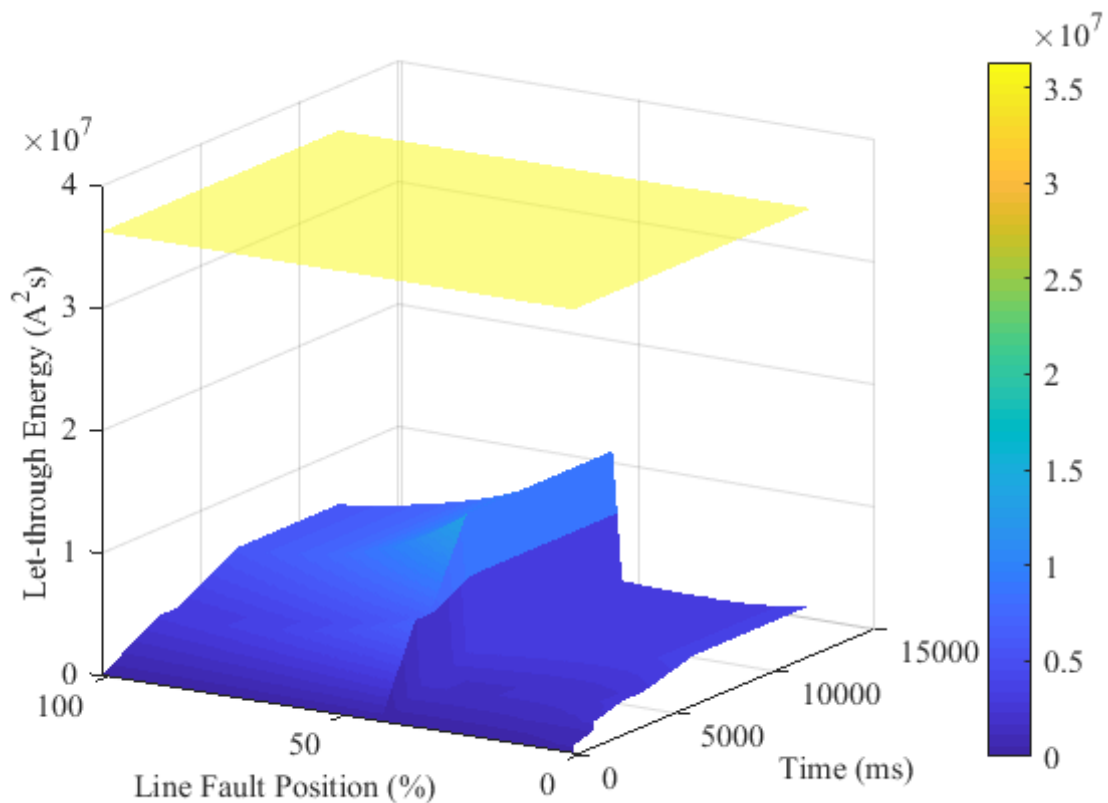


Figure 6.19 The multi-source interconnected feeder LTE maximum results with slow protection on both ends of the feeder, one ARC attempt and high-sets applied.

The maximum value has also decreased and the conductor LTE limit is now not exceeded during any of the trips. With the high-set applied, additional ARC attempts (e.g. three trips to lockout) can be applied without damaging the conductor. The contribution from the

remote end at Busbar 2 has decreased as well with the application of the high-set. Now the contribution from Busbar 1 is the maximum value all through the feeder. If the source impedance was the same on both ends of the feeder, the left-hand side (50 % to 100 %) of the feeder would resemble that of the right side (0 % to 50 %) if the same settings was applied (see case study 3).

When looking at the form of the surface at 0 % across time (in time axis), it can be seen that there are small notches in the curve. This is due to the infeed from the remote end (100 % - Busbar 2) and the LTE being greater than the infeed from the local end (0 % and Busbar 1). As was shown in [162] notches can also be found on the distance axis when the measured RMS fault current is changing in magnitude due to a CBs tripping in the network. This may change the operating curve from its high-set curve to the IDMT operating curve. This tends to happen in the vicinity of the high-set PU value.

For the notches in the time axis at 0 % distance, the remote end is expected to clear the fault in about 2.818 s at a fault level of 644 A. This translates into a conductor LTE exposure of 1.169 MA²s. The local end at Busbar 1 will clear the fault in roughly 20 ms (relay time and ignoring CB operating time). At a fault current of 6090 A and an operating time of 20 ms, the expected LTE is 0.74 MA²s. This estimate excludes the fault current re-routing if a CB is opened. The remote end LTE is thus higher and will be used as the worst-case conductor exposure at that position and at that time. The full evaluation application applies a holistic approach and takes all the modelled aspects into account (e.g. current rerouting) by means of the network simulation. If the individual results (raw data) from each end is considered, this can be determined.

The energy-volume calculates to 12.09630×10^8 A²s²·km. This is for a simulation time up to 12 s. The energy-volume have thus decreased with the application of a high-set at each end of Feeder 1. This is even with the ARC attempts applied. Similar to the results in Figure 6.18, it is not easy to see the number of dynamic regions as any CB operation change the LTE. The time component of the LTE surface can be used to determine which curve should be reduced. If there were two different operating curves for each ARC attempt, the rate at which

the LTE reaches the trip state may be different (depends on protection philosophy applied to determine the settings). By considering the time component in the new surface plots this change can be seen and adjusted if required (by means of protection settings).

6.4.9 Case study 2 step 4.1 results – deadtime 4 s and 1 s applied

In step 4 the effect of deadtime changes on the conductor LTE exposure is investigated. For step 4.1 the same settings as step 3.2 is applied to each end of the Feeder 1 protection (see Table 6.6). While the deadtime of the protection at the Busbar 2 end is kept at 1 s, the other end at Busbar 1 is set to 4 s. The LTE surface result is shown in Figure 6.20. The conductor limit is shown as a flat translucent light blue surface (based on level in colour bar). It can be seen that the conductor limit is exceeded for both the first and second trip. For the results in step 3.2 the deadtime on each end of the feeder was set to 1 s.

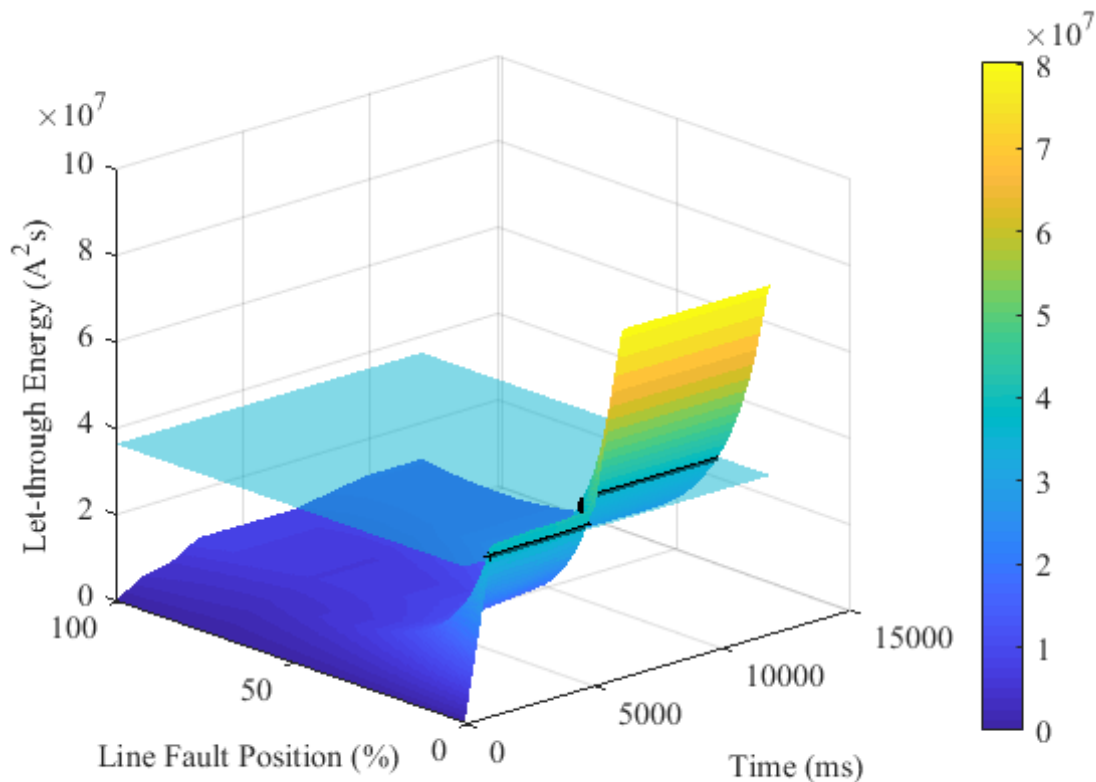


Figure 6.20 The multi-source interconnected feeder LTE maximum results with slow protection on both ends of the feeder, one ARC attempt (deadtimes 4 s and 1 s).

When comparing Figure 6.20 to that of Figure 6.18 it can be seen that the two surfaces are different and the longer deadtime can be observed in the increased static region (can be seen at 0 % position across the time). By changing the deadtime, it is changing the time a CB is open. This can change the current distribution and the LTE exposure of the conductor (change in protection operating time as well). If the deadtime was very long, the opposite end may go through its ARC cycle and lockout before the local end has closed again. There are many permutations as was discussed in Chapter 4 and shown in Figure 4.18. The energy-volume for this surface calculates to $36.72098 \times 10^8 \text{ A}^2\text{s}^2 \cdot \text{km}$. This is for a simulation time up to 12 s. If this is compared to the value in step 3.2 ($41.36459 \times 10^8 \text{ A}^2\text{s}^2 \cdot \text{km}$), it can be seen that the value has decreased. For a radial feeder application (e.g. case study 2) deadtime does not influence the LTE as only one CB is required to open for isolating the fault (not a source from the other end). The actual volume is not that significant on its own, only when it is compared to another volume is there value in it.

6.4.10 Case study 2 step 4.2 results – deadtime 0.3 s and 1 s applied

For step 4.1 the same settings as step 3.2 is applied to each end of the Feeder 1 protection. While the deadtime of the protection at the Busbar 2 end is kept at 1 s, the other end at Busbar 1 is set to 0.3 s. The LTE surface result is shown in Figure 6.21. The conductor limit is shown as a flat translucent light blue surface (based on level in colour bar). It can be seen that the conductor limit is exceeded for both the first and second trip. If this result is compared to the results shown in Figure 6.18 and 6.20 it can be seen that this is different as well. The results in Figure 6.20 and Figure 6.21 confirms that deadtime does influence the conductor LTE exposure. The energy-volume for this surface calculates to $42.13655 \times 10^8 \text{ A}^2\text{s}^2 \cdot \text{km}$. This is for a simulation time up to 12 s. The difference can also be observed and quantified in the energy-volume evaluation.

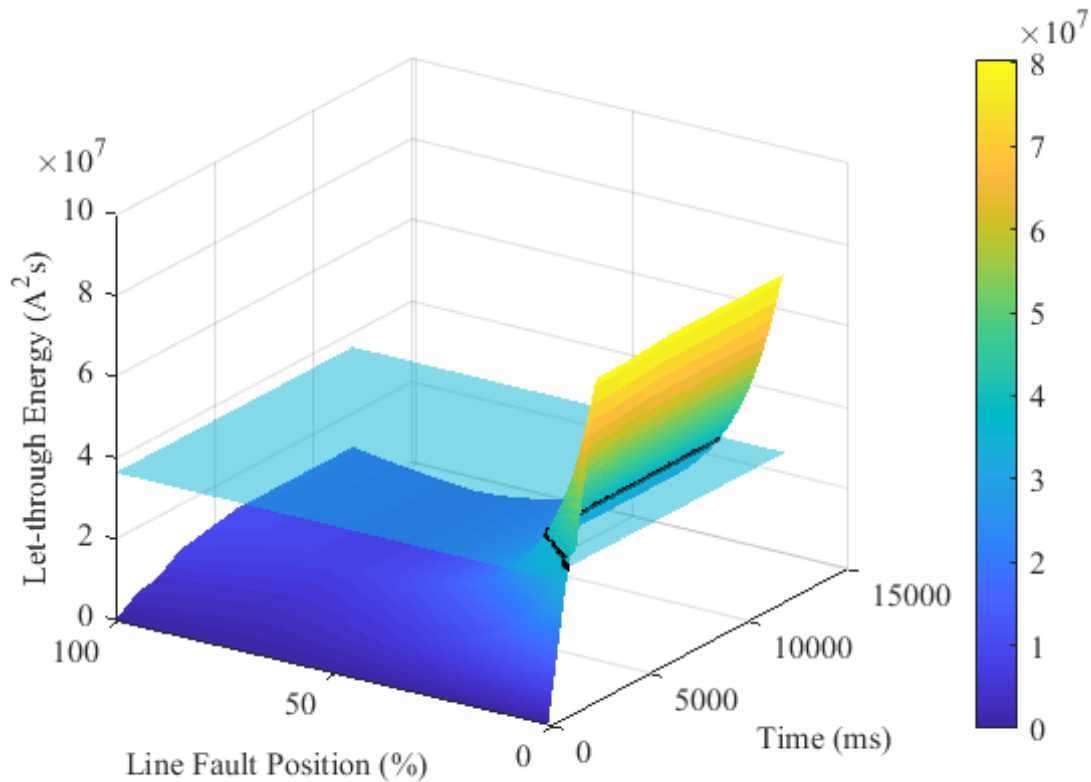


Figure 6.21 The multi-source interconnected feeder LTE maximum results with slow protection on both ends of the feeder, one ARC attempt (deadtimes 0.3 s and 1 s).

6.5 CASE STUDY 3 – INTERCONNECTED MULTI-SOURCE NETWORK (STRONG SOURCES)

6.5.1 The objective of the case study

The objective of this case study is to demonstrate the application of LTE protection in a network where both ends of the feeder have similar fault levels (or source impedance). The network is an interconnected multi-source network. As part of this case study, it will be illustrated how to evaluate the applied protection and interpret the resulting graphs. This case study will also illustrate how the source impedance can influence the conductor LTE exposure in an interconnected network with a multiple source network when it gets

compared to the results from case study two. The key elements that will be used to evaluate this is the LTE graph and the energy-volume calculation.

6.5.2 The case study setup

The network used for this interconnected multi-source network case study is the same as that of case study 2 that is shown in Figure 6.13. Feeder 1 will be evaluated. The source impedance is changed so that the fault levels are similar at each end of the feeder. Like case study 2, the size of the external sources and transformers connecting them to the interconnected network are not key. Similar to the previous case studies, any type or combination of sources can be used in the network as this method allows for the network to be evaluated holistically. If a specific generator is to be studied, it can be modelled and included in the simulation. Similar to this, specific protection can be added at other positions than Feeder 1 to evaluate the conductor LTE exposure on Feeder 1. For this case study, it was kept to only Feeder 1 and external sources. To minimise the variables, no load is connected to the busbars. This will help to only consider the effect of fault current. Load current can be included in this method if the effect is to be studied. With bolted three-phase faults being used in this case study, there will not be any load current passing through the faulted feeder. CBs are shown on the feeder and they indicate not only the CB position but also the measuring points for current using CTs and protection relays. Protection will only be modelled on CB 1 and CB 2 as Feeder 1 in Figure 6.13 will be evaluated.

Table 6.7 The voltage and three-phase fault levels at each busbar for case study 3.

Busbar	Voltage (kV _{L-L})	Voltage (p.u.)	Fault level (kA)
Busbar 1	22.5	1.022	5.724
Busbar 2	21.7	0.985	5.706
Busbar 3	21.6	0.980	11.615
Busbar 4	21.9	0.998	1.878

The three-phase fault level at each busbar is shown in Table 6.7. These fault levels are for maximum network conditions where all three sources are in service and all CBs are closed. The fault is placed on each of the busbars. The voltage at each busbar is kept to within a range of $\pm 5\%$ of 1 p.u. (22 kV system). This is within the NRS 048 limits [60].

The three-phase fault current for a fault 0.01 % on Feeder 1 from Busbar 1 and then Busbar 2 is provided in Table 6.8. This is for the network configured with all the transformers, sources and feeders in service. Only the remote end CB is opened or closed for this table. The fault position percentage is measured from Busbar 1. This shows that the case study is set such (setup) that the fault current will redistribute itself depending on the network configuration (CBs open or closed). The measured fault current (by the relay) can thus change before a trip signal is issued to the CB. The protection at each end of the evaluated feeder is set and will operate independent of each other. There are an infinite number of network configurations. For this case study, the network is set as shown in Figure 6.13, with fault levels as depicted in Table 6.7 and 6.8 to illustrate the conductor LTE evaluation.

Table 6.8 The three-phase fault current measured on Feeder 1 for different CB status.

Circuit Breaker Status		Fault position from Busbar 1 (%)	Three-phase Fault current	
CB 1	CB 2		CB 1 (kA)	CB 2 (kA)
Closed	Closed	0.01	4.911	0.848
Closed	Open	0.01	4.996	0
Closed	Closed	99.99	0.895	4.845
Open	Closed	99.99	0	4.824

The type of feeder conductor used on all the feeders in this network is Mink conductor. There are numerous types of conductors available, Mink is used to illustrate the concept of LTE protection as it falls within the recommended conductors used for MV feeders [138]. From the calculations in Chapter 4, Mink conductor has a short time rating of 6.026 kA. For the work done in this research the continuous loading value for Mink conductor of 285 A at a

templating temperature of 50 °C is used in [138]. The PU current is set to be sensitive to remote end faults and secure in that they are above possible load current (determined by the feeder conductor type maximum load current).

For this case study the source impedance will not be changed from the initial setup values (e.g. remove transformers for specific steps) as this was discussed in case study 1. The applied IDMT protection operating curves will not be changed either as the effect was shown in case study 1 that this influences the conductor LTE exposure.

6.5.3 Protocol

The following protocol is applied for this case study.

1. The faulted feeder being evaluated is Feeder 1. Do the initial setup of the network so as to resemble that of Figure 6.13 with a three-phase fault level and voltages at each busbar as provided in Table 6.7 and the fault current distribution as in Table 6.8 for Feeder 1. No loads are connected so as to minimise the influencing variables.
2. Create the control case for this multi-source interconnected feeder (Result 1) connected to similar source impedance values at each end of the feeder under study. The network is simulated in maximum network conditions with only IDMT NI protection applied. Feeder 1 is set to have two ARC cycles (three trips to lockout) applied at both ends of the feeder. The deadtime for each shot is set to one second at both the CB 1 and CB 2 ends. No high-set element is applied at either end of Feeder 1. For the CB 1 protection on Feeder 1, set the protection to operate in 1.1 s for a three-phase fault close to Busbar 1. Similarly, also set the CB 2 protection on the remote end of Feeder 1 to operate in 1 s for a closeup fault (to Busbar 2).
3. Evaluate the effect of applying a high-set element at both ends of the feeder. No other settings are changed from the control case (Result 2). The network is simulated in maximum network conditions with only IDMT NI protection applied. The fault levels are the same as step 1 of the protocol. Apply a high-set element of 2000 A to the protection at CB 1 and CB 2. Both high-set elements are set to initiate ARC.

4. Evaluate the effect of reducing the number of ARC cycles in the control case to one (two trips to lockout). No high-set elements are applied.
5. Compare the results

6.5.4 Experimental parameters

The protection settings that are applied to the protection driving the CBs at both ends of Feeder 1 (CB 1 and 2) are provided in Table 6.9. This is for each step of the protocol. Only NI operating curves are used in this case study. The PU current is set the same for both ends of the feeder. This is set based on the PU recommendations in Chapter 3. The IDMT element PU value has not changed from that used in case study 2. It is assumed that the upstream transformer protection at the substation (Busbar 1) is slow enough and the PU is high enough so as to not interfere with the feeder protection. The operating time for the NI operating curve is set to 1.1 s for a fault right in front of CB 1 (fault position is 0.01 % from Busbar 1) when the network is set to operate in maximum network conditions. The operating time for the protection driving CB 2 is set to also operate in 1.1 s for a fault in front of the CB on Feeder 1 (fault position is 99.99 % from Busbar 1) with all the CBs closed and the network being operated in maximum network conditions (all plant in service).

Table 6.9 The protection settings setup to CB 1 and 2 in case study 3.

Protocol step	CB	Curve	PU (A)	TM (-)	High-set PU (A)	TD (s)	Trips to Lockout	Deadtime (s)
2	CB 1	NI	315	0.44	-	-	3	1 (all)
	CB 2	NI	315	0.44	-	-	3	1 (all)
3	CB 1	NI	315	0.44	2500	0	3	1 (all)
	CB 2	NI	315	0.44	2500	0	3	1 (all)
4	CB 1	NI	315	0.44	-	-	2	1
	CB 2	NI	315	0.44	-	-	2	1

The high-set PU is set using the recommendation in Chapter 3. The minimum that it can be set to is 126 % or 192 % of the fault current at the remote end of the feeder in maximum network conditions for numerical and electromechanical devices respectively. For Feeder 1, the high-set PU is set to 2500 A (minimum) on the busbar 1 side. This is roughly 280 % of the downstream remote fault level for the Busbar 1 end. With the fault levels the same at each end of the feeder the same will apply to the protection at CB 2. Both ends are set to a time delay of zero seconds.

The simulation time has been set to 12 s as a fault will be cleared in 2.9 seconds by the IDMT element. If the three trips to lockout philosophy with two deadtimes of one second each are added together, it results in a total time of roughly 11 seconds. As was discussed in the previous case study and chapters, the NI equation of (3.1) nor the integral version of (4.18) can be used. As such, the discrete version of the NI operating equation of (4.19) is used (in full evaluation application of Chapter 6). The disk average speed method can be used, but this does have its complexities and constraints.

6.5.5 Case study 3 step 2 – control case

For this case study the control case resulting graph is shown in Figure 6.22. In this result it can be seen that the two ends of the feeder are almost a mirror of each other. Both have a similar source impedance and are set exactly the same. The energy-volume for this surface calculates to $62.62152 \times 10^8 \text{ A}^2\text{s}^2 \cdot \text{km}$. This is for a simulation time up to 12 s. It can be seen that there are two high risk areas on this feeder. These are at the start (0 % Busbar 1 end) and at the end of the feeder (100 % Busbar 2 end). Both of these high-risk areas are due to the current portion of the LTE calculation. This can be seen when evaluating the potential contribution from the Busbar 2 end in Figure 6.23. The detail in Figure 6.23 is not critical, it only shows the profile from Busbar 2 side. It can be seen that the conductor limit is only exceeded close to the Busbar 2 side when only considering the current and protection setting at the Busbar 2 end.

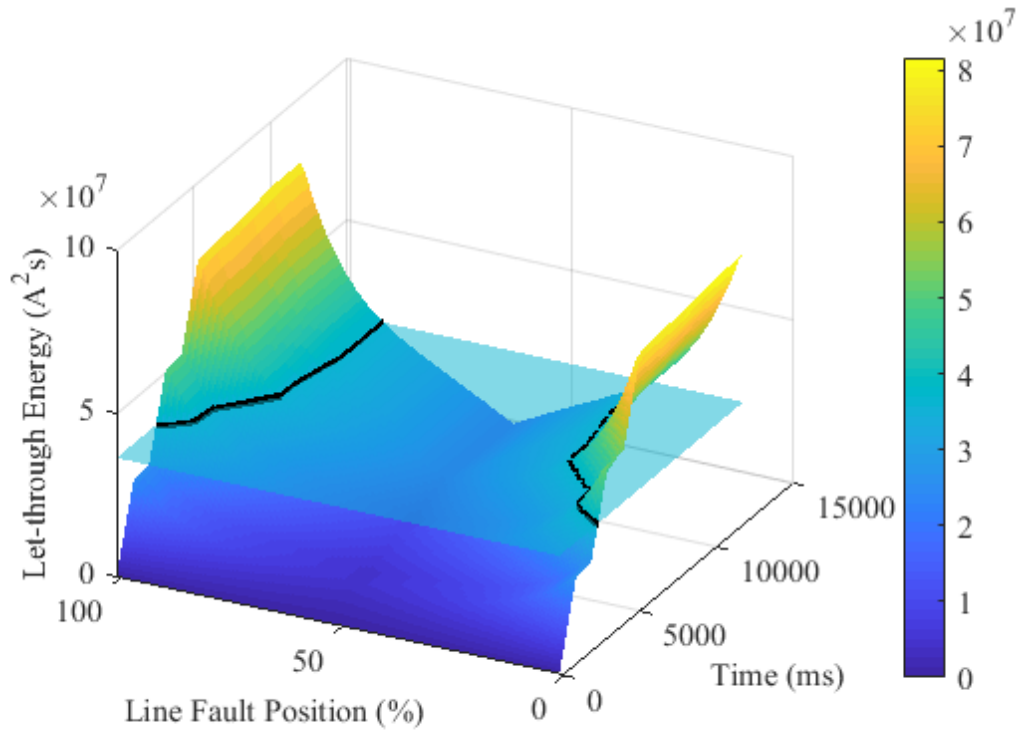


Figure 6.22 The control multi-source interconnected feeder LTE results for case study 3.

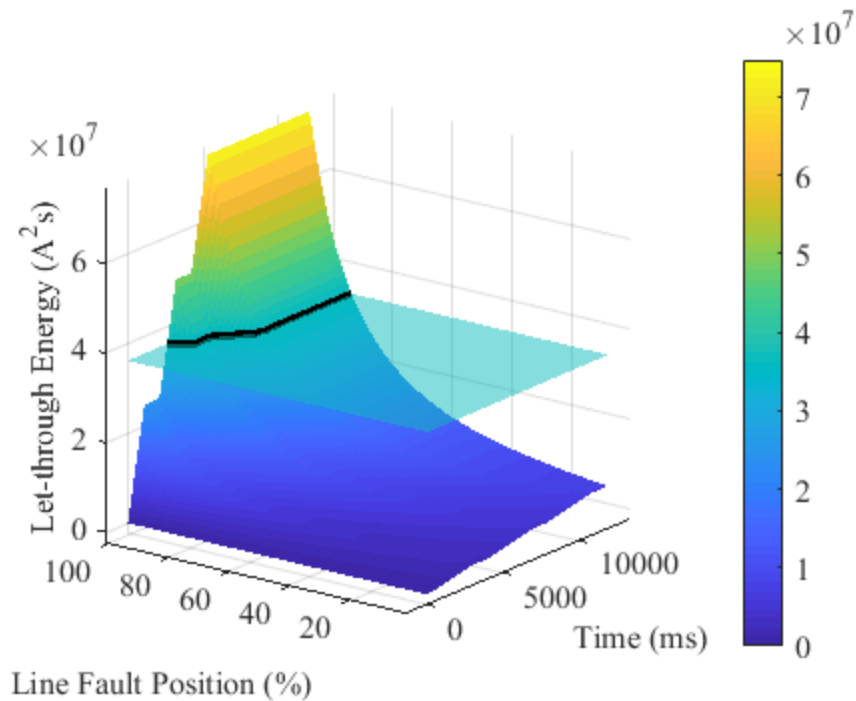


Figure 6.23 The potential feeder LTE exposure from Busbar 2 side.

The contribution from the Busbar 1 end would look similar, but it would be reflected towards the Busbar 1 side. The maximum of these two contributions make up the conductor maximum exposure of Figure 6.22. The conductor limit plane (blue flat surface based on colour bar) is shown in Both Figure 6.22 and 6.23. It can be seen that the LTE from the first trip does not exceed the conductor limit. Partly through the second trip cycle (CB has not tripped yet), the conductor limit is reached. This means that if no ARC cycles were applied to the protection, then there would not be an exceedance. This may be overcome by reducing the number of ARC attempts and setting the protection to operate faster. It can be seen that with every ARC cycle, the potential damage area (distance into the feeder) is increasing.

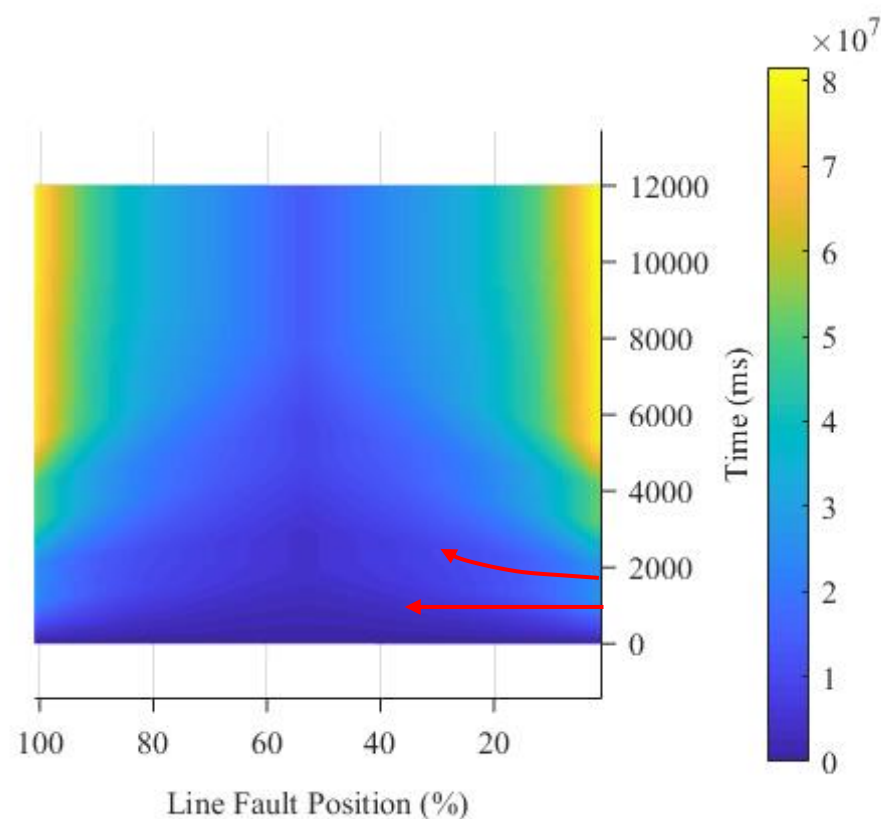


Figure 6.24 The heat map for the results in step 2 of case study 3.

Another method of representing the data is by means of a contour plot or heat map that use colour to indicate the contour. In Figure 6.24 the contour or heat map is shown for the results of Figure 6.22. The colour is indicative of the LTE exposure and the two-axis used are distance and time. The symmetry of the two ends can be observed in the heat map of

Figure 6.24. The source at Busbar 1 is a slight bit stronger than that of the Busbar 2 side as the yellow heat or contour is bigger on the zero percent side than the 100 % side. The protection at both sides are set the same.

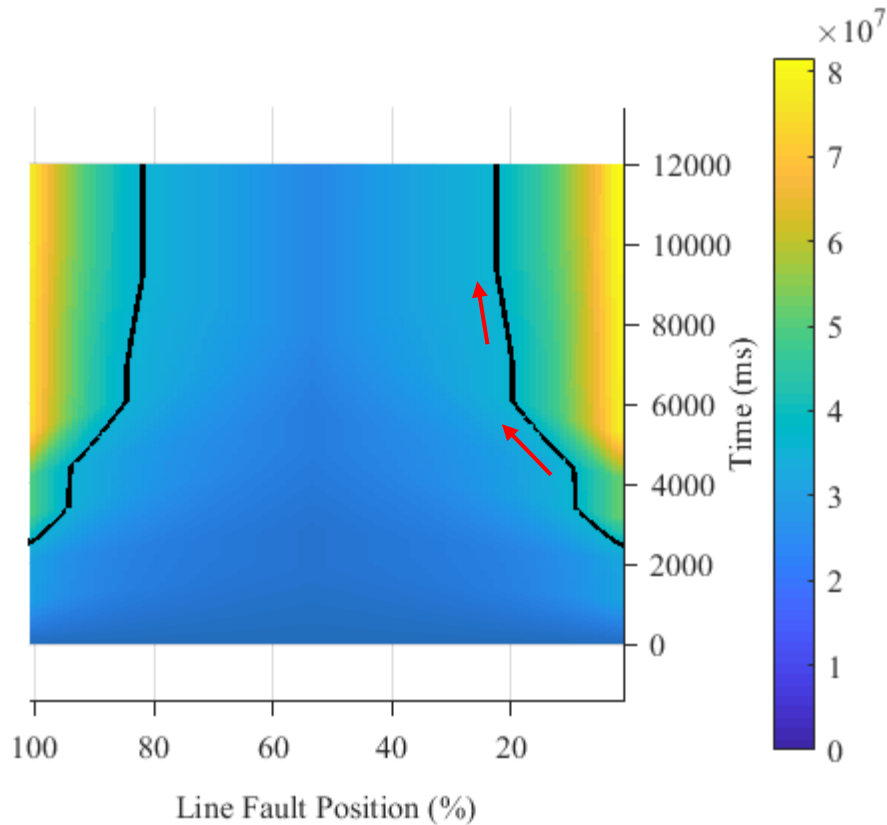


Figure 6.25 The heat or contour map for the results in step 2 (conductor limit applied).

In Figure 6.25 the conductor limit plane is placed on top of the heat map and the intersection of the two planes are shown with the black lines. The high risk area on the feeder is now clearly visible. The effect of prolonged exposure can also be seen clearly. When considering the contour or heat plot the dynamic region can be observed as a function of time. Two red lines are shown in Figure 6.24 to indicate how the dynamic region will expand from the Busbar 1 side. The same will be on the Busbar 2 side. The dynamic region will expand further into the feeder (from zero towards 100 % distance) as a function of the protection operating time (applied protection settings). With the same phenomenon occurring from both ends of the feeder, these two sides will cross each other. In the contour plot it will appear as dark blue lines in Figure 6.24 (shown in between the red lines indicating the dynamic region

from Busbar 1). In the contour plot (heatmap) it appears as if the dynamic region is changing (source impedance) when considering the angles of the black lines. Two red lines are shown in Figure 6.25 to indicate this. The rate of LTE exposure is increasing the same with every ARC attempt, the difference comes in that the starting level (previous trip LTE level) is different and therefore the position where it intersects with the conductor limit (fixed) is changing. From the heat map and conductor limit figure the time component can be used to adjust settings (e.g. the total exposure at zero percent should be less than 2.5 seconds).

6.5.6 Case study 3 step 3 – high-set application

Figure 6.26 is showing the results for when a high-set element is applied to the protection settings at each end of the feeder. The conductor LTE limit is shown as a yellow flat surface based on the colour bar. As the fault levels and settings are similar, the figure would be a mirror image around the 50 % distance line. The first noticeable change when comparing this result with that of the control case of Figure 6.22 is that there is a reduction in the conductor peak LTE exposure. Secondly, the conductor limit is not exceeded. This reduction can also be quantified in the energy-volume. For the result in Figure 6.22 the energy-volume calculates to $26.40312 \times 10^8 \text{ A}^2\text{s}^2 \cdot \text{km}$. This is a reduction of 57.8 % when comparing it to the results of step 2.

By applying the high-set element the LTE peak is reduced and the new peak is pushed further into the network (on the feeder). The high-set element (at this level) also allowed the number of ARC attempts to remain unchanged as the conductor limit was not exceeded.

In Figure 6.26 there are two areas of additional interest. The first red arrow is showing that the energy is decreasing from the 20 % to zero percent distance marks. This means that the energy in this region is actually dominated by the slow protection from the remote end (100 % Busbar 2 end) and not the high current end at Busbar 1. If the high-set element of CB 1 was the dominant element, the curve would start at a high value at zero percent and reduce towards the 20 % mark (see DT curve in Figure 4.11). If the LTE had to be reduced further in this region, the IDMT settings on CB 2 have to be changed (made faster).

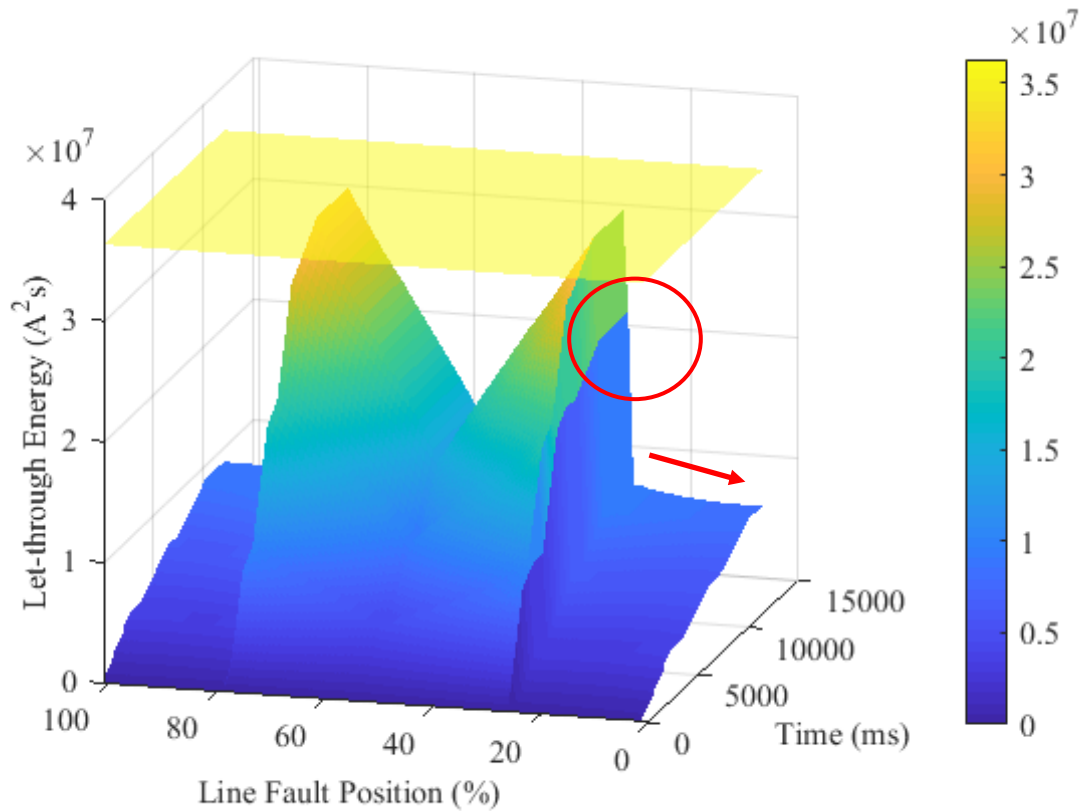


Figure 6.26 The LTE results for case study 3 with high-sets applied.

The second area of interest is shown in the red circle on Figure 6.26. It can be seen that the LTE is creating a boundary line when evaluating the colour change. The LTE colour is changing from a blue to a green and it appears to happen instantaneously. What is happening is that every time a CB (remote end here) opens, the measured RMS fault current is changing. This can be seen in the fault levels of Table 6.8. This phenomenon is happening at the boundary between the high-set and IDMT element. This boundary is based on the high-set PU. Initially the protection will operate on the high-set element up to a specific point (the PU), where it will move on to the IDMT curve (see Figure 3.4). As the remote ends opens, the measured fault current increases, pushing the curve back on to its high-set element with a faster operating time. This will reduce the LTE and create a notch in the LTE surface that appears to be a line or boundary. This was also shown in [162] using the simplified evaluation application (see Chapter 5).

6.5.7 Case study 3 step 4 – reduction in ARC attempts

Figure 6.27 is showing the results of step four of the protocol where the high-set element is removed and the number ARC attempts are set to one (two trips to lockout). The conductor limit is shown as a green flat surface based on the colour bar. With the reduction in the number of ARC attempts, there is a reduction in the peak LTE. This peak is still at the busbar at both ends of the feeder (zero and 100 %). The associated energy-volume for this step four calculates to $47.72669 \times 10^8 \text{ A}^2\text{s}^2\text{-km}$. There is a reduction in the energy-volume when it is compared to that of step two, but it is greater than that of step three of the protocol. This evaluation is specific to this system, with these settings, but the evaluation method is applicable to any system.

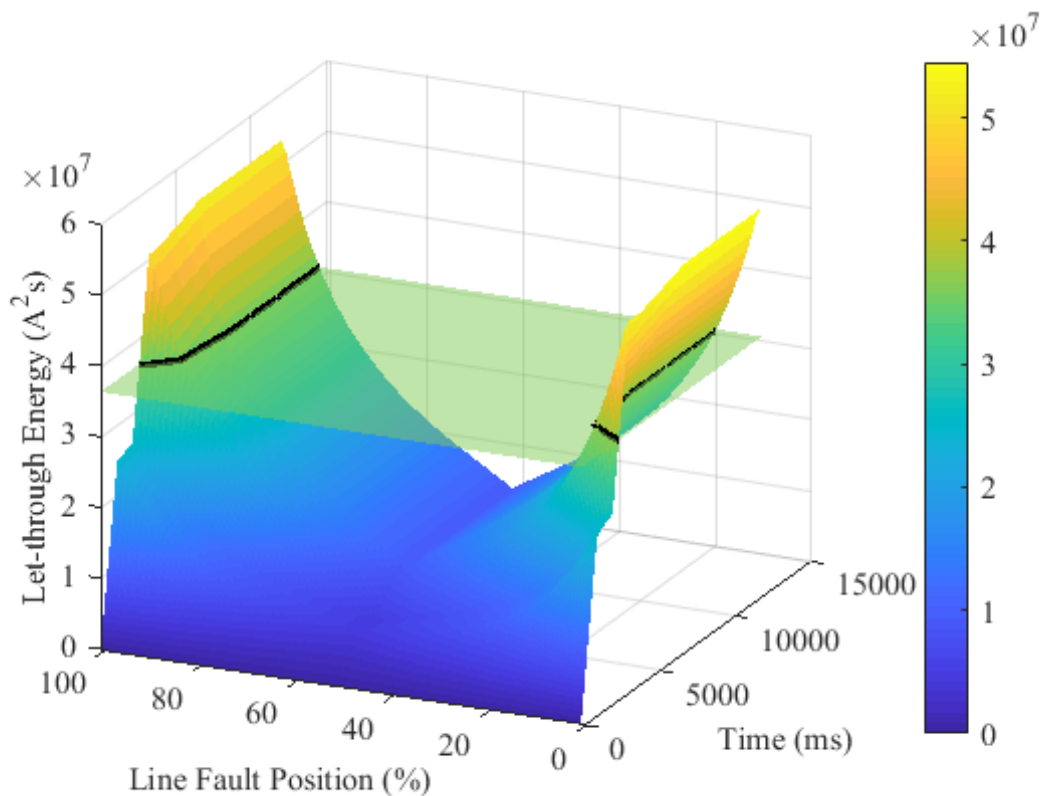


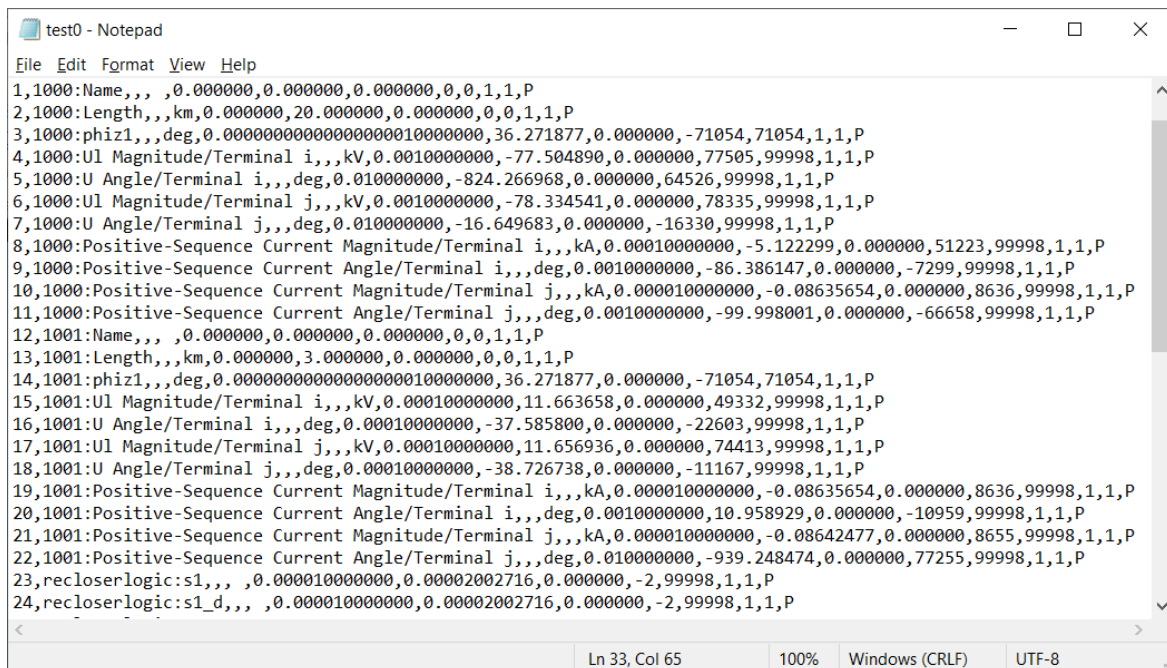
Figure 6.27 The LTE results for case study 3 with a reduction in ARC attempts applied.

It can be seen in Figure 6.27 that the conductor LTE limit is exceeded after the CB has closed for the first ARC attempt. To remove this exceedance, the protection will have to be made

faster if the fault levels remain at these levels. This can be accomplished by changing the operating curve, reducing the TM applied to the operating curve, changing the operating curve for only one of the ARC trips or applying a small high-set element to the protection. The ARC attempt can be removed, but this will reduce the feeder availability for transient faults. Whichever solution is applied, should be affected to both ends of this feeder.

6.6 FULL EVALUATION APPLICATION RESULT GENERATION

The results that were shown in case studies one to three were generated using the full evaluation application of Chapter 5. This consisted of three main parts, network simulation, data extraction and result calculation and presentation. To display the LTE surface of Figure 6.27 a total of 1212000 data points is used for this simulation setup. This accounted for a distance step size of 1 %, thus 101 steps when including zero. The simulation time was set at 12 s and at a sampling rate of 1 kHz the number of time steps calculate to 12000 per distance step. Time step zero can also be included here with the value of zero. The results do not have to be generated at this resolution, but it does provide for smooth surfaces with the probability of losing information due to data smoothing being reduced.



```

test0 - Notepad
File Edit Format View Help
1,1000:Name,,, ,0.000000,0.000000,0.000000,0,0,1,1,P
2,1000:Length,,,km,0.000000,20.000000,0.000000,0,0,1,1,P
3,1000:phiz1,,,deg,0.000000000000000010000000,36.271877,0.000000,-71054,71054,1,1,P
4,1000:U1 Magnitude/Terminal i,,,kV,0.0010000000,-77.504890,0.000000,77505,99998,1,1,P
5,1000:U Angle/Terminal i,,,deg,0.010000000,-824.266968,0.000000,64526,99998,1,1,P
6,1000:U1 Magnitude/Terminal j,,,kV,0.0010000000,-78.334541,0.000000,78335,99998,1,1,P
7,1000:U Angle/Terminal j,,,deg,0.010000000,-16.649683,0.000000,-16330,99998,1,1,P
8,1000:Positive-Sequence Current Magnitude/Terminal i,,,kA,0.0001000000,-5.122299,0.000000,51223,99998,1,1,P
9,1000:Positive-Sequence Current Angle/Terminal i,,,deg,0.0010000000,-86.386147,0.000000,-7299,99998,1,1,P
10,1000:Positive-Sequence Current Magnitude/Terminal j,,,kA,0.000010000000,-0.08635654,0.000000,8636,99998,1,1,P
11,1000:Positive-Sequence Current Angle/Terminal j,,,deg,0.0010000000,-99.998001,0.000000,-66658,99998,1,1,P
12,1001:Name,,, ,0.000000,0.000000,0.000000,0,0,1,1,P
13,1001:Length,,,km,0.000000,3.000000,0.000000,0,0,1,1,P
14,1001:phiz1,,,deg,0.000000000000000010000000,36.271877,0.000000,-71054,71054,1,1,P
15,1001:U1 Magnitude/Terminal i,,,kV,0.000100000000,11.663658,0.000000,49332,99998,1,1,P
16,1001:U Angle/Terminal i,,,deg,0.000100000000,-37.585800,0.000000,-22603,99998,1,1,P
17,1001:U1 Magnitude/Terminal j,,,kV,0.000100000000,11.656936,0.000000,74413,99998,1,1,P
18,1001:U Angle/Terminal j,,,deg,0.000100000000,-38.726738,0.000000,-11167,99998,1,1,P
19,1001:Positive-Sequence Current Magnitude/Terminal i,,,kA,0.000010000000,-0.08635654,0.000000,8636,99998,1,1,P
20,1001:Positive-Sequence Current Angle/Terminal i,,,deg,0.0010000000,10.958929,0.000000,-10959,99998,1,1,P
21,1001:Positive-Sequence Current Magnitude/Terminal j,,,kA,0.000010000000,-0.08642477,0.000000,8655,99998,1,1,P
22,1001:Positive-Sequence Current Angle/Terminal j,,,deg,0.010000000,-939.248474,0.000000,77255,99998,1,1,P
23,recloserlogic:si,,, ,0.000010000000,0.00002002716,0.000000,-2,99998,1,1,P
24,recloserlogic:si_d,,, ,0.000010000000,0.00002002716,0.000000,-2,99998,1,1,P
Ln 33, Col 65 100% Windows (CRLF) UTF-8
  
```

Figure 6.28 A sample of the COMTRADE config file generated in the full evaluation application.

For the results documented here the data points obtained from the network simulation software for one step of the protocol in case study three are 49692000 data points. These data points are captured in the COMTRADE files. This consists of 101 distance step sizes, 12000 time steps at a sample rate of 1 kHz and 41 variables that were monitored (41 is not required for all simulations). A sample of the COMTRADE config file is shown in Figure 6.28. The COMTRADE data file is not shown here as it simply consists of a large collection of comma delimited numbers.

All of the data was not used for generating the results in the final Matlab application. The data extraction Python program was used to extract the required data for the LTE calculation, energy-volume calculation and surface display part done in Matlab. It used the config file where the required values were extracted and then created a new updated config file. This updated config file was used when extracting the data from the COMTRADE data file in Matlab.

The method used to generate results worked exceptionally well. The reason for this is that the results are not limited by the original design of the program. The results are limited by the software that is used to generate the results. Other software can be used to generate results if another special variable is to be monitored. The COMTRADE file interface allows for the required input to be standardised, thus allowing for other simulation programs to be used. Matlab works very well for the purpose of calculating results and displaying them due to its capability of handling large data volumes and being able to display three dimensional graphs. The three-dimensional graphs can be rotated in Matlab to produce different viewpoints or then even contours or heat maps. Python or even a C-program could have been used to work with the large data volumes and calculating the LTE results. But, for plotting the results, Matlab is preferred.

6.7 RESULTS: HYPOTHESIS AND RESEARCH QUESTIONS

The hypothesis that is to be tested in this research is:

A method can be developed to evaluate conductor LTE protection on a MV feeder within an interconnected network and with DG installed.

The research questions that are to be answered are:

- What are the fundamental protection relay elements used to protect a MV feeder?
- How can the conductor LTE limit be calculated?
- What protection elements influence the conductor LTE exposure?
- Determine what present methods or philosophies are used to protect multi-source MV networks?

In this research it is shown that there are many elements that influence the conductor LTE exposure. The number of elements influencing the exposure is different for radial feeders without any additional sources or DG installed. Present methods only recommend that the conductor LTE should be considered when setting the protection devices to ensure the conductor is protected [81]. It does however not indicate that there is any difference between a conventional radial or then interconnected feeder applications with multiple sources. Nor are there any methods recommended for this type of network.

In the problem statement of Chapter 1 it was shown that the traditional radial MV networks are evolving towards multi-source interconnected networks. This is due to the reduction in cost of renewable generation technologies. This can be seen in the rate at which renewable generation is being installed in networks compared to traditional baseload stations (e.g. coal fired power stations). The protection on traditional radial feeders may not be best suited for these new interconnected and multi-source networks. This is due to the protection making use of IDMT elements and being set to grade multiple devices in series. This makes the protection slow and increases the conductor LTE exposure.

In Chapter 2 it was discussed that with multiple sources (DG and interconnections), directional protection may be a requirement. Differential or impedance protection is best suited for an interconnected network. This can be seen in the wide and common application

of this type of protection in HV networks. There is a shift towards installing these types of protection elements on MV feeders as well, but there are limitations when considering network topology (e.g. a feeder with multiple T-offs). As a worst case, there may be only slow IDMT elements applied to the feeder. The LTE evaluation method that was developed can accommodate faster protection such as impedance or differential protection as well. This has to be modelled in the network model for simulation. The LTE exposure is reduced considerably with a reduction in operating time. We have shown in another publication that LTE has to be considered for HV networks when impedance elements are applied [162]. This was done using the simplified evaluation method in Chapter 5. The case study result in Chapter 5 also detail the application to an actual HV circuit in a multi-source interconnected network. This was done as a proof of concept. This simplified method does however have limitations in that the variables that can be studied are limited. The advantage of the simplified method was that it used the average disk speed relay model of Chapter 4. This allowed for change points to be determined with a very high degree of accuracy and with very little data used to generate results.

In this holistic method (full evaluation application) that we have developed for evaluating the conductor LTE exposure, a very large number of variables can be monitored and is limited by the network simulation software. This result is limited by step size, but with a small step size the results are more than adequate for this evaluation. The holistic method allowed for any number of sources and interconnections to be included in the evaluation. In case study two and three we made use of a network consisting of three independent sources and numerous interconnections (see Figure 6.13). In case study two and three it was observed that the current does change when a CB operates. If dependent sources are required, this can be modelled in the network simulation network for study. We aimed to show that if a CB opens, the current will redistribute itself in the network and this may change the RMS current that is measured by the relay that is required to trip for the faulted feeder. This change in current will influence the relay operating time and then influence the conductor LTE exposure. The same effect will happen if a source is tripped. This may add additional steps in the sequence of events before the fault on the feeder is isolated. If we limit the evaluation

to IDMT type protection, the fundamental elements used to protect the feeder would be a relay consisting of IDMT type (or DT) curves, high-set elements and ARC elements.

It was shown that for both radial and interconnected multi-source feeders the ratio of fault current to PU current and the TM setting influence the conductor LTE exposure. It was also shown that the number of ARC attempts influence the conductor LTE exposure [40], [41], [162]. It was discovered that the deadtime setting applied to the protection relay for every ARC cycle also influences the conductor LTE exposure. The conductor was set to reach a specific energy level and maintain this level during the deadtime. This is a worst-case scenario when setting the protection elements to ensure the conductor is protected. The actual conductor may cool down slightly, but is normally neglected for protection operations. In future work, the conductor cooldown can be researched and applied to ascertain how much it does cool down and this can then be used as a starting point when current is passing through the conductor again after an ARC.

For an interconnected multi-source feeder, at least two CBs have to operate to isolate the fault. This is changing the conductor LTE exposure and its profile, creating multiple dynamic and static regions. The complexity increased significantly for an interconnected multi-source network when it is compared to a radial feeder. This is based on the number of possible sequence of events in the network under study where the operation of a CB can change the current distribution in the network (see Figure 4.18). In this new LTE evaluation method, the simulation software takes care of this complex sequencing.

The I^2t calculation for LTE does not take into account the effect of current that can change over time and the effect of this on the relay operating time. For a radial feeder the simplified calculation can be used [40]. For a radial feeder application, the exposure time for one trip can be multiplied with the square of the measured fault current and the number of ARC attempts (trips). For an interconnected multi-source network, the energy has to be determined continuously and this can then be added together as the current may have changed for the specific time period. The energy has to be determined and added together for each time period. The method that we have developed here allows for an approach where

the network as seen from a holistic perspective and the influence of the network on a specific feeder can be evaluated based on small time and distance steps. This was shown with the results of case study two and three. It was shown that this method can be applied to a radial feeder as well in case study one.

For a radial feeder there was a high-risk area close to the source and this was dominated by the current part of the I^2t calculation. The second high risk area is towards the end (low current region) of the radial feeder with the LTE being dominated by the time element. For the interconnected multi-source feeder these two regions are still valid, but they now exist for the protection at both ends. When determining the conductor worst case exposure, the maximum exposure between each end of the feeder is used. The feeder may have two high risk areas that are both dominated by the current part of the I^2t calculation. This was shown in the results of case study three where equal sources were used on both ends of the feeder. There may also be two high risk areas based at each end of the feeder due to slow protection (dominated by the time component).

From this research it is concluded that the conductor LTE exposure is influenced by the fault levels. This is a function of the network layout and the number and type of sources connected in the network under study. The network settings may be set independent of each other (especially DG) with the protection operating at different times, potentially influencing the measured RMS fault current on the feeder under study. This will influence the protection operating time for the feeder protection under study. For the protection on the feeder under study, the same elements are still influencing the LTE as for the radial feeder with the addition of deadtime and multiple paths (and CBs). This includes CB operating time, the operating curve, fault level to PU ratio, operating time (TM or TD), the application of high-set elements and the number of ARC attempts. The difference comes in the way the LTE is calculated with the number of sequence steps (fault current and operating time changes). To determine the conductor LTE exposure on a radial feeder, only the feeder (with its protection) and the source connected to it have to be considered. For an interconnected multi-source feeder, a wider portion of the network has to be considered with the generation included. This extends to the protection applied to the wider network. In Chapter 2 methods

of protecting networks with DG was discussed, but it was found that it is still predominantly current based protection (i.e. IDMT). This answers the questions to what elements influence the LTE and what are fundamental elements used to protect MV feeders?

To evaluate the results, a new three-dimensional LTE surface was developed. This allowed the feeder to be evaluated not only from a LTE to distance perspective, but with the addition of time. The time component allows for more insight into to be gained into the dynamic behaviour of the conductor LTE exposure. It can be seen which ARC attempt may violate the conductor limit (now a flat surface in three dimensions) and at what point in time this occurs. In a two-dimensional representation all this dynamic information is lost and only the peak can be seen. This was observed in the case study results published in [162]. This method is good for a yes or no answer to if the conductor is protected, but it is very limited in determining what caused the exceedance. If this surface is viewed as a contour or heat map the specific points can be determined where the conductor limit is exceeded. This was shown in case study three. For the result here we have included a black line on the LTE surface that indicates where this exceedance occurs. This was achieved by subtracting the conductor LTE exposure surface from the conductor LTE limit (flat surface).

It is difficult to evaluate small changes in protection settings when looking at the LTE graph or all the data in a raw format. To provide a single number that can be used for comparing, the volume under the LTE surface was calculated. This allowed small changes to be evaluated from an improvement or worsening approach. In this version of the software, the simulation time has to be the same for different results to be compared. This can be improved in future by setting the LTE to zero once the CB has reached its final trip, a lockout state. This energy-volume method was applied to all the case studies during the protocol steps. This quantifying method worked well in determining if the result improved the conductor LTE exposure.

The conductor limit was calculated in Chapter 4. To determine this limit, the heat generated by the flow of current through a conductor was set equal to the heat absorbed in the conductor. The process was considered to be an adiabatic process [80], [81], [122], [137],

[147]. From this the conductor limit was determined and the unit for LTE is A^2s or Joule per ohm. Chapter 4 is addressing the research question on how to determine the conductor limit.

Based on this research, the concept of LTE protection should be extended to include EF protection. This method can also be extended towards protection on HV networks as it can accommodate large interconnected networks with multiple sources.

In Chapter 2 the literature indicated that the predominant type of network used for distribution networks are radial networks with OC protection applied. These networks are not designed to accommodate the direction that the world is moving in where DG (especially renewables) are installed and the network is changed from radial to interconnected multi-source networks. When a radial network is changed to this interconnected multi-source network there are a number of challenges introduced, especially towards protecting the network. This includes a change from unidirectional current flow to bidirectional current flow. Other challenges include sympathetic trips, protection blinding, protection under reaching, protection overreaching, decreasing fault levels, increasing fault levels in other parts, islanding, loss of coordination and inability to ARC.

There are a multitude of methods used to protect multi-source interconnected networks. The most common type of protection applied to distribution networks are OC protection. These OC elements can be directionalised to improve its performance against many of the mentioned challenges (e.g. coordination and sympathetic trips). The protection can also be made adaptive. This can allow the protection to adjust to its new network configuration. This may prove to be challenging in that a lot of network analysis is required if this is to be set for many network configurations. This may also require a communication system if adaptive settings are applied that requires inputs (e.g. status of CB) from or to other places on the feeder. The protection can also be made more secure, sensitive and selective by including sequence components and voltage elements. Traditional protection elements used for HV and extra HV can also be applied. This includes impedance and differential protection. Communication infrastructure is becoming a key function for protection of complex

networks. There is a call to install wide area network protection elements such as phasor measurement units. This will allow for a holistic approach towards protecting the network.

The literature did not indicate a clear one solution that fits all application scenarios when it comes to protecting an interconnected multi-source network. The top three approaches are directional protection which is mentioned very often, supervising elements using other parameters is also common and applying protection that requires communication infrastructure. This may be due to most networks being radial as a start with OC protection elements being present. Cost is always a factor. The more elements that are added, the more expensive it becomes.

For the networks consisting of OC elements, optimisation techniques are often used to determine the required settings (PU and TM). Generally, time is minimised. This can be operating time or grading margin. Conductor damage due to LTE is not considered. It was shown in this work that LTE is a concern and it is recommended that this should be included in the optimisation methods. Damage is not only a function of time, but also current and these values change as other CB open and current redistribute. This makes LTE protection a function of the wider network, its infrastructure, applied protection and the protection settings (configuration) and the protection philosophy.

The method that we have developed here for evaluating the conductor LTE exposure can be applied when protection elements such as impedance are used. The software we used can accommodate protection and custom modelling of elements. The reason for this is that the effect of the protection elements and custom modelling is captured in the measured current (and change thereof) at either end of the feeder being evaluated. What should be added to this evaluation is a method to evaluate the sensitivity of the protection PU, prior to evaluating the LTE. This should be done in a similar manner as the LTE evaluation graph where it is evaluated across the feeder for a set time period to ensure protection can detect and isolate all required faults on the feeder. This can be future work.

When considering the results shown in case study one to three and the research questions answered, it can be seen that the method developed in this thesis is capable of evaluating a conductor LTE exposure in a radial and a multi-source interconnected network. This confirms the hypothesis. The traditional time-current curves should still be used, this LTE protection is aimed at providing additional evaluation methods that are better suited for determining if a conductor is protected. This is similar to the recommendation made by [140] for the application of fuses and time-current curves.

The initial distribution systems favoured an AC system due to the losses on the distribution system [9]. Westinghouse won the battle to have an AC system over Eddison's DC system, but with generation being installed close to load centres, DC distribution systems may become the new, old future again...

6.8 CHAPTER SUMMARY

In this chapter the conductor LTE exposure was determined using the full evaluation application of Chapter 5. This evaluation application was developed based on the theory of Chapter 4 and the protection elements in Chapter 3. Section 6.2 gave an overview of the case studies. Results were generated for three case studies, one for a radial feeder in Section 6.3, one for an interconnected multi-source feeder with different source impedances in Section 6.4 and the last one for an interconnected multi-source feeder with similar sources on either end in Section 6.5. The results from the radial feeder application showed how to read the new energy-area graphs. It also showed that the new application can be applied to a radial feeder. The results for the multisource interconnected networks of case study2 and 3 showed that the new method allows for a holistic evaluation of the conductor LTE exposure. Greater insight was obtained to when conductor exceedances occur and possible solutions to mitigate this. Section 6.7 combined the results from the case studies and also the earlier chapters into a discussion. This discussion was centred around the four research questions and the hypothesis. The results confirmed the hypothesis that a method can be developed to evaluate this type feeder. In Chapter 7 a conclusion is made, summary of the results is shared and suggestions for future work based on this research are made.

CHAPTER 7 CONCLUSION

7.1 SUMMARY OF THE WORK

Traditional MV feeders are radial in nature. These networks are changing with different feeders being able to connect to other feeders and there is an increase in the installation of DG within these feeders. This is changing these radial feeders to interconnected multi-source feeders. Many of these feeders still have traditional IDMT protection installed. These protection relays may have the capability of having multiple types of curves, high-set elements and ARC capabilities.

In Chapter 2 the challenges were introduced when a traditional radial feeder with OC protection is changed to a feeder consisting of multiple sources. This included bidirectional power flow, fault level increases, fault level decreases, sympathetic tripping, protection blinding and ARC challenges. Chapter 2 also introduced the various methods that are applied to protect these feeders. Traditional OC protection is still very common. Variations of this are found where the protection is made directional, adaptive and additional supervision is introduced (sequence components and voltage elements). Differential protection and impedance protection are applied as well. Optimisation techniques are used to determine settings for the OC elements, but these do not consider damage (LTE) as a constraint. This is a shortcoming.

There are many protection elements that can be applied in modern numeric relays. Main elements and functions that are applied to protect feeders include the operating curve, high-set element, maximum time element and ARC. Each of these elements have different settings associated with them. Each of these elements were explored in Chapter 3 and the traditional

way of setting these elements was shared. The protection philosophy is what dictates how the protection elements should be set. The philosophy elements consist of speed, security, dependability, sensitivity and selectivity.

The conductor LTE limit can be used to determine if a conductor is protected from the thermal effects of the fault current it must carry during a fault. This LTE is calculated by setting the heat energy that is generated by the flow of fault current equal to the energy absorbed in the conductor as an adiabatic process. This then leads to the LTE value which is the I^2t capability of the conductor. The unit for this is Joule per ohm or A^2s . Each conductor has a limit and in Chapter 4 it was shown how to determine this limit. The concept of minimum and maximum network conditions was introduced and what condition should be used to evaluate the conductor exposure.

The application of LTE protection was discussed in Chapter 4. The difference between a radial feeder and multi-source interconnected network was discussed. Fault current contributions from embedded generation such as wind and PV were shared, but the focus is not placed on the types of generation, more on the fact that there can be generation and that this may influence the conductor LTE exposure. The interconnected multi-source network discussion is centred around fault current that will redistribute itself once a CB has opened. If a single feeder in a multi-source network is considered, the protection at either end may operate at different times and this can result in different LTE exposures at different times during a fault. If ARC is added to this protection setup the complexity increases with a vast number of network configuration possibilities for determining conductor LTE exposure. This is due to the number of protection settings and network permutations.

With the measured RMS current being able to change before the relay trips, the normal IDMT relay equations cannot be used and a discrete version of the equation has to be applied to determine the relay operating time. An average disk speed method for determining the relay operating time was introduced, but the discrete version is preferred. With the fault current and exposure time changing over time due to the operation of CBs, the LTE of each period have to be added together to determine the conductor exposure. This is why the multi-

source interconnected network LTE evaluation has to be performed while considering the time changing from zero to a CB lockout time (fault isolated). Different relay operating curves were discussed from a LTE perspective and it was recommended that the IDMT EI curve is preferred for LTE grading where there are high currents, but this curve has a high operating time rate of change when compared to the NI curve. Lastly, the conductor LTE exposure was quantified into a single number that allows for changes made to settings or the network to be compared. This was done by introducing an energy-volume value.

Two software applications were created to produce results for evaluation. The first is a full evaluation application and the second is a simplified evaluation application. The simplified evaluation made use of the average disk speed relay model. One case study in an actual network is shared and results from this application was published [40]. The full evaluation was discussed. This application consisted of three main parts, the network simulation part, the data extraction part and the result calculation and presentation part. The complete network has to be considered when a conductor LTE exposure is to be determined in a multi-source interconnected network. The advantage of using network simulation software is that the software takes care of the network simulation and if a variable is to be evaluated, it has to be modelled in the network simulation software. In the network software used the ARC function was not available and this was modelled using DSL code. To obtain measured fault currents at either end of the feeder under study for faults across the feeder for a period of time, network simulation software has to be used. The format used for the output from the simulation software is a COMTRADE file with a sampling rate of 1 kHz. All of these measured currents are then fed into the data extraction software where the COMTRADE config file is changed so that certain data can be extracted in the Matlab program. Matlab was used for calculating the LTE and presenting the three-dimensional LTE-distance-time graph.

The full evaluation application was used to generate results for evaluation and discussion in Chapter 6. The results from three case studies were discussed. The first is a radial feeder, the second a multi-source interconnected feeder with a strong and weak source at either end of the feeder. The third case study is for a multi-source interconnected network with two similar

strong sources at either end of the feeder under study. In these case studies the effect of relay operating curve selection, ARC, high-sets, deadtimes, CBs operating at different times and source impedance are shown. The protection elements used and the setting of these elements were discussed in Chapter 3. The method developed in Chapter 5 based on the theory of Chapter 4 and Chapter 3 work well to evaluate the conductor LTE exposure for both a radial and multi-source network.

7.2 SUMMARY OF THE RESULTS AND THE DISCUSSION

From the work leading into the case studies, the results obtained and the subsequent discussion the following conclusions are made:

- The full evaluation application works well for determining a conductor's LTE exposure. The method used is very versatile in that any variable that can be modelled in the simulation software can be evaluated for conductor LTE influence.
- Matlab works very well for presenting the three-dimensional data as the volume of data used is large. It allows the figures to be rotated or focused to observe different points of interest. It also allows for the calculation of the energy-volume value and to determine the LTE and conductor limit intersection.
- The three-dimensional representation of the results with LTE-distance-time provides good insight into what protection element may be responsible for causing the exceedance, where it is occurring on the feeder and from what point in time. This information may be used to adjust the applied protection settings to remove the exceedance.
- The contour or heat map display compliments the three-dimensional surfaces as it provides improved clarity for determining specific positions or times without evaluating the raw data.
- The energy-volume quantification works well for quantifying the conductor LTE exposure into a number that can be compared to other simulations for the purpose of classifying the change as a decrease or increase in exposure.

- The full evaluation application can be applied to both radial and interconnected multi-source networks.
- When evaluating an interconnected multi-source feeder, the LTE contribution from both ends of the conductor has to be considered and it has to be considered at every point in distance and time on the feeder. The maximum of the two ends (or more ends if this is a multi-ended feeder) have to be used for the conductor exposure. These contributions cannot be evaluated individually. The complete network has to be considered and the contribution from each end at the same time.
- The traditional IDMT type equations cannot be used to determine the conductor LTE exposure as the RMS current is changing when a CB is operated. This change in current affects the relay operating time. A discrete version of the IDMT equation is recommended where the required variables are sampled at specific time intervals. The energy can be calculated for each interval and added together.
- It is recommended to apply high-set elements whenever possible. This reduction in operating time significantly reduces the conductor LTE exposure in the first high risk area close to the busbar. The high-set element can be set to initiate ARC to improve availability and a time delay may be added to allow for selectivity with downstream protection. The high-set element also reduces the area that can lead to possible conductor damage.
- LTE is influenced by the type of operating curve, the fault level to PU ratio (for IDMT curves), the operating time (e.g. time before a trip is issued based on TM), other curves that may be used in conjunction with the IDMT curve, deadtime and the number of ARC attempts.
- It is recommended to apply a maximum time function to all IDMT curves as this will stop the operating time from going towards infinity for high impedance faults.
- The CB deadtime setting during an ARC cycle influences the conductor LTE exposure.

- The conductor LTE evaluation should be done in both minimum and maximum network conditions so as to check for both the high-risk areas. The first high risk area is close to the source busbar and is dominated by the fault current (current of I^2t). The second high risk area is towards the end of the feeder and is dominated by the exposure time (time of I^2t).
- The network layout, the type and number of distributed generators can influence the conductor LTE exposure. This can influence the current distribution when any CB carrying fault current is operated (open or close). For a radial single source feeder, the RMS current does not change over time and this keeps the calculation to an uncomplicated level only requiring exposure time and fault current. For a multi-source interconnected feeder the measured RMS current can change over time and this introduces the time consideration and the addition of energy, rather than time to determine the LTE level.
- Elements that cause a possible delay in operating the CB have to be included e.g. CB operating time.
- Multiple CBs are required to open so as to isolate a fault on an interconnected multi-source feeder. These CBs may be set and operate independently. This will influence the conductor LTE profile.

7.3 SUGGESTIONS FOR FUTURE WORK

There are a number of research fields and specific aspects that can stem from this research work documented here. Possible topics are:

- Apply this conductor LTE exposure method in the optimisation techniques used for determining protection settings for IDMT relays in interconnected multi-source networks. The optimisation techniques are skewed towards grading and does not consider protecting the actual conductor.

- A three-dimensional graph may be used similar to the LTE-distance-time graph that allows the PU sensitivity to be investigated. This can then be a graph showing where and when (time) the PU sensitivity criterion is not met. The graph can be of the form sensitivity-distance-time.
- The concept of LTE and the application thereof to feeders may be investigated from a feeder reliability impact. This may provide insight in how the reliability can be improved from a primary and secondary design perspective. The LTE can be used as a measure.
- A three-dimensional graph may be used similar to the LTE-distance-time graph that allows the expected voltage dips to be classified based on the protection applied and the network configuration. This can then be a graph showing where and what type of dip will be experienced. The type can be classified in terms of the NRS-048 standard [60]. This will allow for the protection settings design to also include a power quality element aimed at improving the customer experience. The groundwork for this was done in [40]. The graph can be of the form voltage dip (type or percentage)-distance-time.
- The three-dimensional graph of LTE-distance-time may be changed to exclude the static regions once the CB is open and in a lockout state. This will allow any result from any simulation to be compared to other simulations in terms of energy-volume. At present there is a constraint of the simulation time that has to be the same and that the energy volume may be off-set by large simulation times compared to protection operating times (time up to lockout).
- The effect of specific generator types and their contribution to conductor LTE exposure may be studied. The method developed in this thesis allows for this to be done. This can be extended towards network topologies as well. As a possible hypothesis to be tested, a very interconnected network may accommodate a larger penetration level of DG before conductor LTE damage occurs (just a hypothesis).

- Other fault and relay elements may be included in the model to study their effects on the conductor LTE exposure. A possible topic can be to study the effect of arc resistance, or to look at possible tower (or structure) type changes to remove certain fault types that may cause severe conductor LTE exposure. The effect of communication assisted tripping between relays can aid in reducing conductor LTE exposure. This may require a complete protection philosophy change for certain networks.
- The cooling effect on conductors can be included for the deadtime period during an ARC cycle. This will reduce the final LTE result as compared to the adiabatic approach taken here (worst case for setting protection relays).
- The release of heat energy to the surrounding environment may be included when determining the conductor LTE exposure. This is for the second-high risk area where the conductor is exposed to a lower current for a very long time (can approach infinity). The worst case for setting protection relays is applied in this research.
- Practical experiments may be done to support the theory documented here. This can be based on a controlled environment where a conductor is placed in tension and current is allowed to pass through the conductor. The damage can then be investigated in terms of how brittle the conductor became and when it may lead to conductor failure. Different conductor types and materials can be investigated. This topic leans more towards a material science topic. This can also be extended to an actual feeder for comparison.

REFERENCES

- [1] United Nations, “Net installed capacity of electricity plants by type,” in *Energy Statistics Yearbook 2017*, 2020, ch. 30, pp. 383–417. [Online]. Available: https://www.un-ilibrary.org/content/publication/afa_76179-en
- [2] United Nations, “Net installed capacity of electricity plants by type,” in *Energy Statistics Yearbook 2014*, 2017, ch. 30, pp. 363–397. [Online]. Available: <https://www.un-ilibrary.org/content/publication/5e311f0a-en>
- [3] G. Masters, “Basic Electric and Magnetic Circuits”, “The electric power industry”, “Distributed generation” and “Wind power systems,” in *Renewable and Efficient Electric Power Systems*, 1st ed. Hoboken, N.J., Country: USA, 2004, ch. 1, 3, 4 and 6.
- [4] E. Muljadi, N. Samaan, V. Gevorgian, Jun Li and S. Pasupulati, "Short circuit current contribution for different wind turbine generator types," IEEE PES General Meeting, Providence, RI, 2010, pp. 1-8, doi: 10.1109/PES.2010.5589677.
- [5] I. Ivanova. “It's now cheaper to build a new wind farm than to keep a coal plant running.” CBSnews.com. <https://www.cbsnews.com/news/its-now-cheaper-to-build-a-new-wind-farm-than-to-keep-a-coal-plant-running/> (accessed Sep. 15, 2019).
- [6] B. Henderson, “Lessons from Australia – Understanding the Australian renewables boom and what it means for new generation development in New Zealand,” presented at the *EEA Conf.*, Akl., NZ, 25-27 June, 2019.
- [7] M. Benintende, “Growth opportunities in distributed energy, forecast to 2030.” ReportLinker. https://www.reportlinker.com/p05894509/Growth-Opportunities-in-Distributed-Energy-Forecast-to.html?utm_source=GNW (accessed Oct. 28, 2020).
- [8] Global industry analysts, “Global distributed generation (DG) industry.” ReportLinker. https://www.reportlinker.com/p03329803/Global-Distributed-Generation-DG-Industry.html?utm_source=PRN (accessed Oct. 28, 2020).

REFERENCES

- [9] T. G. M. Alvin, I. Z. Abidin and H. Hashim, "Changes in fault current levels due to renewable embedded generation in a distribution network," *IEEE Conference on Clean Energy and Technology (CEAT)*, Lankgkawi, 2013, pp. 254-258, doi: 10.1109/CEAT.2013.6775636.
- [10] D. Turcotte and F. Katiraei, "Fault contribution of grid-connected inverters," in *IEEE Electrical Power & Energy Conference (EPEC)*, Montreal, QC, 2009, pp. 1-5, doi: 10.1109/EPEC.2009.5420365.
- [11] C. Arderne, C. Zorn, C. Nicolas, and E. E. Koks, "Predictive mapping of the global power system using open data.," *Sci Data*, vol. 7, no. 19, Jan. 2020, doi: 10.1080/15325008.2011.559186.
- [12] S. Abeysinghe, J. Wu, M. Sooriyabandara, M. Abeysekera, T. Xu and C. Wang, "Topological properties of medium voltage electricity distribution networks.," in *Applied Energy*, vol. 210, Jan. 2018, doi: 10.1016/j.apenergy.2017.06.113.
- [13] B. Patnaik, M. Mishra, R. C. Bansal, R. K. Jena, "AC microgrid protection—A review: current and future prospective.," *Applied Energy*, vol. 271, Aug. 2020, doi: 10.1016/j.apenergy.2020.115210.
- [14] *IEEE Recommended Practice for Electric Power Distribution for Industrial Plants*, IEEE Std 141-1993, 29 April 1994, doi: 10.1109/IEEESTD.1994.121642.
- [15] *IEC Standard Voltages*, IEC Std 60038-2009, Jun 2009.
- [16] RSA Grid Code Secretariat: 'RSA distribution code definitions Ver. 6', NERSA, South Africa, July 2014. [Online]. Available at: <http://www.nersa.org.za>
- [17] T. E. Del Carpio Huayllas, D. S. Ramos and R. L. Vasquez-Arnez, "Microgrid systems: current status and challenges," in *IEEE/PES T&D-LA*, Sao Paulo, 2010, pp. 7-12, doi: 10.1109/TDC-LA.2010.5762853.
- [18] I. Almutairy, "A review of coordination strategies and techniques for overcoming challenges to microgrid protection," *Saudi Arabia Smart Grid (SASG)*, Jeddah, 2016, pp. 1-4, doi: 10.1109/SASG.2016.7849681.
- [19] A. Moreno-Munoz, V. Pallares-Lopez, J. J. Gonzalez de la Rosa, R. Real-Calvo, M. Gonzalez-Redondo and I. M. Moreno-Garcia, "Embedding synchronized measurement technology for smart grid development," in *IEEE Trans. on Ind. Informat.*, vol. 9, no. 1, pp. 52-61, Feb. 2013, doi: 10.1109/TII.2012.2209659.
- [20] J. K. Tailor and A. H. Osman, "Restoration of fuse-recloser coordination in distribution system with high DG penetration," *IEEE Power and Energy Society General Meeting - Conversion and Delivery of Electrical Energy in the 21st Century*, Pittsburgh, PA, 2008, pp. 1-8, doi: 10.1109/PES.2008.4596422.

REFERENCES

- [21] A. Waqar, B. Hussain, S. Ahmad, T. Yahya and M. Sarwar, "A communication-less protection strategy to ensure protection coordination of distribution networks with embedded DG," in *PGSRET*, Islamabad, Pakistan, 2018, pp. 1-6, doi: 10.1109/PGSRET.2018.8685935.
- [22] S. A. Gopalan, V. Sreeram and H. H. C. Iu, "A review of coordination strategies and protection schemes for microgrids," *Renewable and Sustainable Energy Reviews*, vol. 32, pp. 222-228, Apr., 2014, doi: 10.1016/j.rser.2014.01.037.
- [23] G. Kangle, C. MyeonSong, L. SeungJea and L. SeongIl, "Coordination method for protective devices of closed-loop distribution system", in *Proc. of the 11th Int. Conf. IEEEIC*, pp. 47 -52, May 18 -25, 2012.
- [24] A. F. Naiem, A. Y. Abdelaziz, Y. Hegazy and M. A. Elsharkawy, "Recloser-fuse coordination assessment by classification technique for distribution systems with distributed generation," *Electric Power Components and Systems*, vol. 39, no. 11, pp. 1077-1096, doi: 10.1080/15325008.2011.559186.
- [25] E. Lakervi and E. J. Holmes, "System protection" in *Electricity Distribution Network Design*, U.K., London: IEE Power Ser. 21, 1995, ch. 7.
- [26] M. Alghassab, "Adaptive protection of distribution networks integrated with DG units," in *ICCAIS*, Riyadh, Saudi Arabia, 2019, pp. 1-6, doi: 10.1109/CAIS.2019.8769536.
- [27] M. P. Comech, M. A. Montanes and M. Garcia-Gracia, "Overcurrent protection behavior before wind farm contribution," in *MELECON - The 14th IEEE Mediterranean Electrotechnical Conf.*, Ajaccio, 2008, pp. 762-767, doi: 10.1109/MELCON.2008.4618527.
- [28] J. J. J Kennedy, P. Ciufu and A. Agalgaonkar, "A review of protection systems for distribution networks embedded with renewable generation," *Renewable and Sustainable Energy Reviews*, vol. 58, pp. 1308-1317, 16 Jan. 2016.
- [29] J. Sahebkar Farkhani, A. Najafi, M. Zareein, R. Godina and M. G. Rodrigues, "Impact of recloser on protecting blind areas of distribution network in the presence of distributed generation," *Appl. Sci.*, vol. 9, no. 23, 25 Nov 2019, doi: 10.3390/app9235092.
- [30] A. Khademlahashy, L. Li, J. Every and J. Zhu, "A review on protection issues in micro-grids embedded with distribution generations," in *ICIEA*, Siem Reap, Cambodia, 2017, pp. 913-918, doi: 10.1109/ICIEA.2017.8282969.
- [31] J. S. Farkhani, M. Zareein, H. Soroushmehr and H. Mortazavi, "Coordination of directional overcurrent protection relay for distribution network with embedded DG," in *KBEI*, Tehran, Iran, 2019, pp. 281-286, doi: 10.1109/KBEI.2019.8735025.

REFERENCES

- [32] R. Tiwari, R. K. Singh and N. K. Choudhary, "Performance analysis of optimization technique for protection coordination in single and multi-loop distribution system," in *UPCON*, Aligarh, India, 2019, pp. 1-6, doi: 10.1109/UPCON47278.2019.8980151.
- [33] S. Mladenovic and A. A. Azadvar, "Sympathetic trip prevention by applying simple current relays," *IEEE PES General Meeting*, Providence, RI, 2010, pp. 1-7, doi: 10.1109/PES.2010.5589955.
- [34] AREVA T&D, "Network Protection and Automation Guide", AREVA T&D, 2011, chap. 2, 6, 7, 8, 9, 10, 11, 13, 14, 22 and 23.
- [35] D. K. Singh and S. Gupta, "Optimal coordination of directional overcurrent relays: A genetic algorithm approach", presented at the *SCEECS*, pp. 1-4, 1-2 March 2012.
- [36] V. Rozine and M. H. Adams, "Protective device problems and solutions", in *Proc. IPEC Conf.*, Singapore, 2010, pp. 789-794, doi: 10.1109/IPEC.2010.5697074.
- [37] *Protection settings philosophy for medium voltage distribution networks*, 240-76628317, Eskom Holdings Ltd, Jhb., Mar. 2015.
- [38] H. Saadat, "Transmission line parameters", "Balanced fault," and "Symmetrical components and unbalanced fault," in *Power System Analysis*, 2nd ed., McGraw-Hill, Asia, 2004, ch. 4, 9 and 10, pp.102-105, pp. 353–425.
- [39] R. Bansal, in *Power System Protection in Smart Grid Environment*, 1st ed., CRC Press, NY, USA, 2019.
- [40] M. J. Slabbert, R. Naidoo, R. C. Bansal and S. J. van Zyl "Evaluating phase overcurrent protection philosophies for medium-voltage feeders applying let-through energy and voltage dip minimization," *Electr. Power Compon. Syst.*, vol. 44, no. 2, pp. 206–218, 2016, doi: 10.1080/15325008.2015.1107862.
- [41] M. J. Slabbert, "Evaluating the effectiveness of phase overcurrent protection on overhead medium voltage feeders," M.S. thesis, Dept., Electrical, electronic and computer Eng. Univ. of Pretoria, Pretoria., GAU, 2014.
- [42] S. H. Horowitz and A. G. Phadke, "Introduction to protective relaying", and "Relay operating principles," in *Power System Relaying*, 3rd ed., West Sussex, UK: John Wiley & Sons, 2008, ch. 1 and 2.
- [43] J. Courtney and A. McDonnell, "Impact on distribution system protection with the integration of EG on the distribution network," *UPEC*, Bucharest, Romania, 2019, pp. 1-5, doi: 10.1109/UPEC.2019.8893563.

REFERENCES

- [44] H. Cheung, A. Hamlyn, Lin Wang, G. Allen, Cungang Yang and R. Cheung, "Network-integrated adaptive protection for feeders with distributed generations," *IEEE Power and Energy Society general meeting - Conversion and delivery of electrical energy in the 21st century*, Pittsburgh, PA, 2008, pp. 1-8, doi: 10.1109/PES.2008.4596856.
- [45] V. Papaspiliotopoulos, G. Korres, V. Kleftakis and N. Hatziargyriou, "Hardware-in-the-loop design and optimal setting of adaptive protection schemes for distribution systems with distributed generation," *IEEE Power & Energy Society general meeting*, Chicago, IL, 2017, pp. 1-1, doi: 10.1109/PESGM.2017.8274178.
- [46] D. S. Kumar, D. Srinivasan and T. Reindl, "A fast and scalable protection scheme for distribution networks with distributed generation," *IEEE Trans. on Power Del.*, vol. 31, no. 1, pp. 67-75, Feb. 2016, doi: 10.1109/TPWRD.2015.2464107.
- [47] A. Dysko, C. Booth, O. Anaya-Lara and G. M. Burt, "Reducing unnecessary disconnection of renewable generation from the power system," *IET Renewable Power Generation*, vol. 1, no. 1, pp. 41-48, March 2007, doi: 10.1049/iet-rpg:20060015.
- [48] S. K. Salman and S. F. Tan, "Investigation into protection of active distribution network with high penetration of embedded generation using radial and ring operation mode," *Proceedings of the 41st International Universities Power Engineering conference*, Newcastle-upon-Tyne, 2006, pp. 841-845, doi: 10.1109/UPEC.2006.367599.
- [49] H. K. Karegar and S. Saberi, "Investigating of wind turbines effects on recloser operation in distribution networks," *IEEE International conference on Power and Energy*, Kuala Lumpur, 2010, pp. 523-526, doi: 10.1109/PECON.2010.5697638.
- [50] S. Mirsaiedi, D. M. Said, M. W. Mustafa, M. H. Habibuddin, K. Ghaffari, "Progress and problems in micro-grid protection schemes," *Renewable and Sustainable Energy Reviews*, vol. 37, pp. 834-839, Sep., 2014, doi: 10.1016/j.rser.2014.05.044.
- [51] S. S. S. Beryozkina, "Evaluation study of potential use of advanced conductors in transmission line projects," *Energies*, vol. 12, no. 5, Mar., 2019, doi: 10.1109/EEEIC.2018.8493858.
- [52] J. A. Martinez and J. Martin-Arnedo, "EMTP modeling of protective devices for distribution systems with distributed generation," *IEEE PES General Meeting*, Providence, RI, 2010, pp. 1-6, doi: 10.1109/PES.2010.5590018.
- [53] T. Wildi, "Generation of electrical energy", "Transmission of electrical energy" and "Distribution of electrical energy", in *Electrical Machines, Drives and Power Systems*, 5th ed. Prentice Hall, 2002, ch. 24, 25 and 26.

REFERENCES

- [54] *IEEE Guide for Protective Relay Applications to Distribution Lines*, IEEE Std C37.230-2007, 2008, doi: 10.1109/IEEESTD.2007.4447926.
- [55] J. C. Tan, P. G. McLaren, R. P. Jayasinghe and P. L. Wilson, "Software model for inverse time overcurrent relays incorporating IEC and IEEE standard curves," *IEEE CCECE2002.*, Winnipeg, Manitoba, Canada, 2002, pp. 37-41 vol.1, doi: 10.1109/CCECE.2002.1015171.
- [56] J. Armas, A. Ivanov and T. Varjas, "Short-circuit currents calculations in street lighting networks," *IEEE RTUCON*, Riga, 2017, pp. 1-9, doi: 10.1109/RTUCON.2017.8124758.
- [57] D. Sweeting, "Applying IEC 60909, Fault Current Calculations," in *IEEE Trans. on Ind Appl.*, vol. 48, no. 2, pp. 575-580, March-April 2012, doi: 10.1109/TIA.2011.2180011.
- [58] *IEEE Recommended Practice for Protection and Coordination of Industrial and Commercial Power Systems*, IEEE Std 242-2001, 17 Dec. 2001, doi: 10.1109/IEEESTD.2001.93369.
- [59] S. Mladenovic and A. A. Azadvar, "Sympathetic trip prevention by applying simple current relays," *IEEE PES General Meeting*, Providence, RI, 2010, pp. 1-7, doi: 10.1109/PES.2010.5589955.
- [60] *Electricity supply – Quality of supply – Voltage characteristics, compatibility levels, limits and assessment methods*, NRS 048-2, 2003.
- [61] D. M. Dy, J. F. Ilarde, H. G. Navarrete, D. X. Valeros, R. F. Bersano Jr., M. C. Pacis and R. V. M. Santiago, "Optimal overcurrent relay coordination of a multi-loop distribution network with distributed generation using dual simplex algorithm," *IEEE Tensymp*, Sydney, Australia, 2018, pp. 180-184, doi: 10.1109/TENCONSpring.2018.8691897.
- [62] J. Leiva, J. A. Aguado, Á. Paredes and P. Arboleyac, "Data-driven flexibility prediction in low voltage power networks," *Int. Journal of Electrical Power and Energy Systems*, vol. 123, June, 2020, doi: 10.1016/j.ijepes.2020.106242.
- [63] Weiqing Tao, Jiayi Li, Zhixia Gu and Leqin Wang, "Study and comparison on standard for interconnecting distributed resources with electric power systems," *IEEE IPEMC-ECCE Asia*, Hefei, 2016, pp. 1000-1005, doi: 10.1109/IPEMC.2016.7512423.
- [64] X. Wang, Y. Li and Y. Yu, "Research on the relay protection system for a small laboratory-scale microgrid system," *IEEE Conference on Industrial Electronics and Applications*, Beijing, 2011, pp. 2712-2716, doi: 10.1109/ICIEA.2011.5976056.

REFERENCES

- [65] S. De Bruyn, J. Fadiran, S. Chowdhury, S. P. Chowdhury and P. Kolhe, "The impact of wind power penetration on recloser operation in distribution networks," *UPEC*, London, 2012, pp. 1-6, doi: 10.1109/UPEC.2012.6398454.
- [66] T. Saksornchai and B. Eua-arporn, "Determination of Allowable Capacity of Distributed Generation with Protection Coordination Consideration," *Eng. J.*, vol. 13, no. 3, pp. 29-44, Nov., 2009, doi: /10.4186/ej.2009.13.3.29.
- [67] H. Al-Nasseri, M. A. Redfern and F. Li, "A voltage based protection for micro-grids containing power electronic converters," *IEEE Power Engineering Society General Meeting*, Montreal, Que., 2006, pp. 7 pp.-, doi: 10.1109/PES.2006.1709423.
- [68] *IEEE Application Guide for IEEE Std 1547(TM), IEEE Standard for Interconnecting Distributed Resources with Electric Power Systems*, IEEE Std 1547.2-2008, 15 April 2009, doi: 10.1109/IEEESTD.2008.4816078.
- [69] Pan European Sub Group on Protection Equipment, "Short circuit contribution of new generating units connected with power electronics and protection behaviour," entsoe, Apr. 2019. Accessed: Jan. 30, 2020. [Online]. Available: https://eepublicdownloads.blob.core.windows.net/public-cdn-container/clean-documents/SOC%20documents/190304_SOC_TOP_7.4_Short%20Circuit%20Contribution%20of%20Power%20Electronics%20Connecting%20Generators%20and%20Protection%20report.pdf
- [70] E.H. Camm, M. R. Behnke, O. Bolado, M. Bollen, M. Bradt, C. Brooks, W. Dilling, M. Edds, W. J. Hejduk, D. Houseman, S. Klein, F. Li, J. Li, P. Maibach, T. Nicolai, J. Patiño, S. V. Pasupulati, N. Samaan, S. Saylor, T. Siebert, T. Smith, M. Starke, R. Walling, "Characteristics of wind turbine generators for wind power plants," *IEEE Power & Energy Society General Meeting*, Calgary, AB, 2009, pp. 1-5, doi: 10.1109/PES.2009.5275330.
- [71] AEMO, "Wind turbine plant capabilities report, 2013 wind integration studies," AEMA, AUS., Rep. ABN 94 072 010 327, 2013.
- [72] R. P. Gallardo, A. M. Rios and J. S. Ramirez, "Analysis of the solar and wind energetic complementarity in Mexico," *Journal of Cleaner Production*, vol. 268, May, 2020, doi: 10.1016/j.jclepro.2020.122323.
- [73] J. Ekanayake, K. Liyanage, J. Wu, A. Yokoyama and N. Jenkins, "Energy storage," in *Smart Grid Technology and Applications*, 1st ed. Chichester, Country: UK.: John Wiley & Sons, 2012, ch. 12, pp. 259–270.
- [74] J. Kennedy, P. Ciufu and A. Agalgaonkar, "Protection analysis tool for distribution networks with a high embedded generation penetration," *Electrical Power and Energy Systems*, vol. 107, July, 2018, doi: 10.1016/j.ijepes.2018.12.001.

REFERENCES

- [75] RSA Grid Code Secretariat, 'Grid connection code for renewable power plants (RPPs) connected to the electricity transmission system (Ts) or the distribution system (DS) in South Africa Ver. 2.8', NERSA, South Africa, Jul 2014. [Online]. Available at: <http://www.nersa.org.za>
- [76] Electricity Authority, 'Electricity industry participation code 2010, Part 8-Common quality', Electricity Authority, New Zealand, Nov. 2010. [Online]. Available at: <https://www.ea.govt.nz/code-and-compliance/the-code/>
- [77] *Standard for grid connection of energy inverter systems via inverter. Part3: grid protection requirements*, AS 4777.3-2005, Standards Australia, Aus., 2005.
- [78] A. D. Stokes and W. T. Oppenlander, "Electric arcs in open air", *Journal of Physics D: Applied Physics*, vol. 24, pp. 26 -35, 1991.
- [79] A. D. Stokes, "Fire ignition by electrically produced incandescent particles," *Aust. J. Electr. Electron.Eng.*, vol. 10, no. 3, pp. 175–187, 1990.
- [80] M. Mitolo and M. Tartaglia, "An analytical evaluation of the factor k^2 for protective conductors," *IEEE Industry Applications Society Annual Meeting*, Orlando, FL, 2011, pp. 1-8, doi: 10.1109/IAS.2011.6074413.
- [81] M. Tartaglia and M. Mitolo, "An analytical evaluation of the prospective I^2t to assess short-circuit capabilities of cables and busways," *IEEE Trans. on Power Del.*, vol. 25, no. 3, pp. 1334-1339, July 2010, doi: 10.1109/TPWRD.2009.2037505.
- [82] J. Horak, "Directional overcurrent relaying (67) concepts," in *Annual Conference for Protective Relay Engineers*, 2006., College Station, TX, 2006, pp. 13 pp.-, doi: 10.1109/CPRE.2006.1638701.
- [83] D. Costello, M. Moon and G. Bow, "Use of directional elements at the utility-industrial interface," in *Power Systems Conf.: Advanced Metering, Protection, Control, Communication, and Distributed Resources*, Clemson, SC, 2006, pp. 283-298, doi: 10.1109/PSAMP.2006.285400.
- [84] J. Roberts and A. Guzman, "Directional element design and evaluation", in *Western Protective Relay Conf.*, Spokane, WA, pp. 1-27, Oct.,1994 (revised Aug. 2006).
- [85] A. C. Enríquez, E. V. Martínez, "Sensitivity improvement of time overcurrent relays," *Electric Power Systems Research*, vol. 77, no. 2, pp. 119-124, Feb., 2007, doi: 10.1016/j.epsr.2006.02.004.
- [86] Advanced distribution automation: Application design guide: Nu-Lec loop automation solution, Eskom 240-71497919, 2014.

REFERENCES

- [87] M. Y. Shih, A. Conde, "Implementation of directional over-current relay coordination approaches in electrical networks," *Electric Power Components and Systems*, vol. 43, no. 19, pp. 2131-2145, Sep. 2015, doi: 10.1080/15325008.2015.1080769.
- [88] M. Farsadi, A. Yazdani Nejadi and A. Esmaeilnasab, "Reducing over-current relays operating times in adaptive protection of distribution networks considering dg penetration," *ELECO*, Bursa, 2015, pp. 463-468, doi: 10.1109/ELECO.2015.7394439.
- [89] H. Nikkhajoei, and R. Lasseter, "Microgrid fault protection based on symmetrical and differential current components," Wisconsin Power Electronics Research Center, USA, Dec. 2006.
- [90] T. Loix, T. Wijnhoven and G. Deconinck, "Protection of microgrids with a high penetration of inverter-coupled energy sources," *CIGRE/IEEE PES joint symposium integration of wide-scale renewable resources into the power delivery system*, Calgary, AB, 2009, pp. 1-6.
- [91] R. Naidoo and M. Zietsman, "An adaptive protection philosophy for embedded renewable distributed generators in low voltage radial networks," *IEEE ISC2*, Casablanca, Morocco, 2019, pp. 465-470, doi: 10.1109/ISC246665.2019.9071666.
- [92] S. M. Mousavi, H. A. Abyaneh and M. Mahdavi, "Optimum setting and coordination of overcurrent relays considering cable damage curve," *IEEE Bucharest PowerTech*, Bucharest, 2009, pp. 1-5, doi: 10.1109/PTC.2009.5281810.
- [93] *IEEE Standard Conformance Test Procedures for Equipment Interconnecting Distributed Resources with Electric Power Systems - Amendment 1*, IEEE Std 1547.1a-2015 (Amendment to IEEE Std 1547.1-2005), 1 May 2015, doi: 10.1109/IEEESTD.2015.7100815.
- [94] *Requirements for micro-generating plants to be connected in parallel with public low-voltage distribution networks*, BS EN 50438:2013, Dec. 2013.
- [95] *BDEW. Technical guideline: generating plants connected to the medium-voltage network*, June 2008.
- [96] *Technical rule for distributed resources connected to power grid*, Q/GDW 480-2010, Aug. 2010.
- [97] A. Fazanehrafat, S. A. M. Javadian, S. M. T. Bathaee and M. -. Haghifamt, "Maintaining the recloser-fuse coordination in distribution systems in presence of DG by determining DG's size," *IET DPSP*, Glasgow, 2008, pp. 132-137, doi: 10.1049/cp:20080024.

REFERENCES

- [98] V. Calderaro, V. Galdi, A. Piccolo and P. Siano, "Adaptive relays for overhead line protection," *Elect. Power Syst. Res.*, vol. 77, pp. 1552–1559, 2007, doi: 10.1016/j.epsr.2006.11.001.
- [99] T. W. Cease, "Protective relaying and power quality", IEEE PSRC Working Group, Dec. 20, 2013, [Online]. Available: <http://www.pes-psrc.org/Reports/PROTECTIVE%20RELAYING%20AND%20POWER%20QUALITY.pdf>
- [100] H. B. Funmilayo, J. A. Silva and K. L. Butler-Purry, "Overcurrent protection for the IEEE 34-node radial test feeder," *IEEE Trans. Power Del.*, vol. 27, no. 2, pp. 459–468, April 2012, doi: 10.1109/TPWRD.2012.2186181.
- [101] D. P. Roth, "Maximizing protection coordination with self-healing technology," *Rural Electric Power Conference*, Milwaukee, WI, 2012, pp. B4-1-B4-12, doi: 10.1109/REPCon.2012.6194568.
- [102] *Feeder and bus coupler protection setting guide*, TP.OP 03.01-2, Transpower NZ Ltd, NZ, 2019.
- [103] J. Simms and G. Johnson, "Protective relaying methods for reducing arc flash energy," *Annual Conference for Protective Relay Engineers*, College Station, TX, 2010, pp. 1-15, doi: 10.1109/CPRE.2010.5469495.
- [104] I. Ramljak, M. Majstrović and E. Sutlović, "Statistical analysis of particles of conductor clashing," *IEEE ENERGYCON*, Cavtat, 2014, pp. 638-643, doi: 10.1109/ENERGYCON.2014.6850494.
- [105] A. Chaly, K. Gutnik, A. Testoedov and A. Astrakhantsev, "Autocoordination of protection settings of series reclosers", presented at the *Int. CIGRE Conf.*, 2008, pp.1-4.
- [106] J. A. Kay and L. Kumpulainen, "Maximizing protection by minimizing arcing times in medium-voltage systems," in *IEEE Trans. Ind Appl.*, vol. 49, no. 4, pp. 1920-1927, July-Aug. 2013, doi: 10.1109/TIA.2013.2255253.
- [107] J. C. Gomez and M. M. Morcos, "Voltage sag mitigation using overcurrent protection devices," *Electr. Power Compon. Syst.*, vol. 29, no. 1, pp. 71–81, 2010, doi: 10.1080/153250001461192.
- [108] E. S. Thomas and R. A. Barber, "Overhead conductor motion during short circuits," in *IEEE Trans. on Ind Appl.*, vol. 52, no. 1, pp. 119-124, Jan.-Feb. 2016, doi: 10.1109/TIA.2015.2477940.
- [109] *IEEE Guide for Automatic Reclosing of Line Circuit Breakers for AC Distribution and Transmission Lines*, IEEE Std. C37.104, 2002, doi: 10.1109/IEEESTD.2012.6232415.

REFERENCES

- [110] *IEEE Guide for Protecting Power Transformers*, IEEE Std. C37.91, 2008, doi: 10.1109/IEEESTD.2008.4534870.
- [111] *IEEE Guide for Electric Power Distribution Reliability Indices*, IEEE Std. 1366, 2012, doi: 10.1109/IEEESTD.2012.6209381.
- [112] S. Jamali and H. Shateri, "Optimal application of reclosers and sectionalisers to reduce non-distributed energy in distribution networks," Presented at *CIGRE*, Turin, Italy, June 6–9, 2005.
- [113] L. L. Grigsby, "Hard to find information (on distribution system characteristics and protection)" and "Voltage sags", in *Electric Power Generation, Transmission, and Distribution*, 2nd ed., Boca Raton: CRC Press, 2007, ch. 23 and 31.
- [114] T. Smith and R. Hunt, "Current transformer saturation effects on coordinating time interval," in *IEEE Pulp and Paper Industry Technical Conference (PPIC)*, Portland, OR, 2012, pp. 1-7, doi: 10.1109/PPIC.2012.6293016.
- [115] A. C. Enriquez, E. V. Martinez and H. J. Altuve, "Time overcurrent adaptive relay," *Electr. Power Energy Syst.*, vol. 25, pp. 841–847, 2003, doi: 10.1016/S0142-0615(03)00059-0.
- [116] Schneider Electric, Rueil Malmaison, Fr. *ADVC Controller range operation manual-R29*, first ed. (2018). Accessed: Sep. 24, 2020. [Online]. Available: <https://www.se.com/ww/en/product-range-download/1966-nulec-n-series/>
- [117] *IEEE Standard inverse-time characteristic equations for overcurrent relays*, IEEE Std. C37.112-2018 (Revision of IEEE Std C37.112-1996), 1996, doi: 10.1109/IEEESTD.2019.8635630.
- [118] E. O. Schweitzer and S. E. Zocholl, "The universal overcurrent relay," in *IEEE Industry Applications Magazine*, vol. 2, no. 3, pp. 28-34, May-June 1996, doi: 10.1109/2943.491383.
- [119] A. R. C. Warrington, "Overcurrent Protection", in *Protective Relays – their theory and practice*, vol. 1, 2nd ed., Fletcher & Son Ltd, Norwich, Great Britain, 1968, pp. 141 -173.
- [120] J. Meppelink and M. Benzin, "Lightning protection of metal roofs", in *28th International Conference on Lightning Protection*, Kanazawa, Japan, pp. 1298–1303, 2006.
- [121] C. R. Mason, "Line protection with overcurrent relays," in *The art and science of protective relaying*, Wiley, 1956, pp. 259–295.

REFERENCES

- [122] E. S. Thomas, "Bonding requirements for conductive poles," in *Rural Electric Power Conference*, Milwaukee, WI, 2012, pp. A4-1-A4-6, doi: 10.1109/REPCon.2012.6194564.
- [123] T. Keil and J. Jager, "Advanced coordination method for overcurrent protection relays using nonstandard tripping characteristics," *IEEE Trans. Power Del.*, vol. 23, no. 1, pp. 52-57, Jan. 2008, doi: 10.1109/TPWRD.2007.905337.
- [124] *Guide for the application and setting of phase instantaneous overcurrent protection*, DGL 34-994, Eskom Holdings Ltd, Jhb., RSA, Oct. 2008.
- [125] A. E. D. C. Tio, I. B. N. C. Cruz, B. M. Malquisto and R. D. del Mundo, "A binary programming model for reliability optimization considering fuse-blow and fuse-save schemes," in *TENCON*, Cebu, 2012, pp. 1-6, doi: 10.1109/TENCON.2012.6412247.
- [126] *Electrical transmission and distribution reference book* (formerly the Westinghouse electrical transmission and distribution reference book), ABB Power T&D Company, Inc., pp. 666–808, 1997.
- [127] S. H. Money and J. Harris, "Autoreclosing switchgear in distribution practice," in *Proceedings of the Institution of Electrical Engineers*, vol. 115, no. 2, pp. 288-300, February 1968, doi: 10.1049/piee.1968.0048.
- [128] S. van Zyl and A. Lubbe, "Characterisation of MV overhead feeder faults using auto-recloser event data," in *Southern African Power System Protection Conf.*, Jhb., RSA, Nov. 12–14, 2014.
- [129] A. C. Enriquez, E. V. Martinez and H. J. Altuve, "Time overcurrent adaptive relay," *Electr. Power Energy Syst.*, vol. 25, no. 10, pp. 841–847, 2003, doi: 10.1016/S0142-0615(03)00059-0.
- [130] P. S. Babu, S. V. J. Kumar and P. R. K. Chaitanya, "Digital relay based adaptive protection for distributed systems with distributed generation," *Int. J. Energy Sci.*, vol. 1, no. 2, pp. 72–77, 2011.
- [131] O. Arreola Soria, A. Conde Enríquez and L. A. Trujillo Guajardo, "Overcurrent relay with unconventional curves and its application in industrial power systems," *Electric Power Systems Research*, vol. 110, pp. 113-121, May, 2014, doi: 10.1016/j.epsr.2013.12.012.
- [132] D. Halliday, R. Resnick and J. Walker, "Motion along a straight line", "Current and resistance" and "Conduction of electricity," in *Fundamentals of Physics*, 6th ed., NY: John Wiley & Sons, 2001, ch. 2, 27, and 42.
- [133] J. W. Nilsson and S. A. Riedel, "Circuit elements," in *Electric Circuits*, 6th ed., Upper Saddle River, NJ: Prentice Hall, 2001, pp. 31–33.

REFERENCES

- [134] J. D. Cutnell and K. W. Johnson, "Temperature and heat", and "Electric circuits," in *Physics*, 4th ed., New York: John Wiley & Sons, 1998, ch. 12 and 20.
- [135] T. A. Short, "Overhead Lines" in *Electric Power Distribution Equipment and Systems*, USA, FL, Boca Raton: CRC/Taylor & Francis, 2006, ch. 2.
- [136] G. Parise and M. Adduce, "Conductor protection against short circuit current: available I²t evaluation," in *IEEE IAS Conference. (Cat. No.98CH36242)*, St. Louis, MO, USA, 1998, pp. 2336-2341 vol.3, doi: 10.1109/IAS.1998.730140.
- [137] B. Wareing, "Conductor characteristics and selection," in *Wood pole overhead lines*, 1st ed., vol. 48, London, UK: The institution of engineering and technology, pp. 114–140, 2008.
- [138] *Network planning guideline for lines and cables*, DGL 34-619, Eskom Holdings Ltd, Jhb., RSA, Nov. 2010.
- [139] Aberdare, RSA. *Overhead aluminium conductors*, (2008). Accessed: Dec. 30, 2016. [Online]. Available: <https://www.aberdare.co.za/product-categories/overhead-conductors/>
- [140] T. Papallo and M. E. Valdes, "Traditional time - current curves are not enough, adding I²t considerations," in *IEEE Trans. on Ind Appl.*, vol. 49, no. 1, pp. 264-274, Jan.-Feb. 2013, doi: 10.1109/TIA.2012.2231659.
- [141] S. Nikolovski, M. Havranek, P. Maric, "Numerical relay protection coordination using simulation software", presented at *Information & Communication Technology Electronics & Microelectronics (MIPRO)*, pp. 869 -873, May 20 -24, 2013.
- [142] W. J. Callister, Jr., "Mechanical properties of metals", "Failure", and "Electrical properties," in *Materials Science and Engineering an Introduction*, 6th ed., NY: John Wiley & Sons, 2003, Ch. 6, 8, and 18.
- [143] D. J. Ward, "Overhead distribution conductor motion due to short-circuit forces," *IEEE Trans. on Power Del.*, vol. 18, no. 4, pp. 1534-1538, Oct. 2003, doi: 10.1109/TPWRD.2003.817818.
- [144] C.-R. Chen, C.-H. Lee and C.-J. Chang, "Optimal overcurrent relays coordination in power distribution system using a new approach," *Electr. Power Energy Syst.*, vol. 45, no. 1, pp. 217–222, Feb. 2013, doi: 10.1016/j.ijepes.2012.08.057.
- [145] J. A. Kay, J. Arvola and L. Kumpulainen, "Protecting at the speed of light", *IEEE Ind. Appl. Mag.*, vol. 17, no. 3, pp. 12-18, May-June, 2011.
- [146] Overhead power lines for conditions prevailing in South Africa, SABS 0280, 2001.

REFERENCES

- [147] F. Kussy and J. L. Warren, "Effects of short-circuit currents on conductors" in *Design Fundamentals for Low-Voltage Distribution and Control*, New York: Marcel Dekker, 1987, ch. 5.
- [148] C. D. Hughes and E. C. Strycula, "Sizing equipment grounding conductors based on thermal damage curves," in *IEEE Industry Applications Magazine*, vol. 6, no. 3, pp. 42-44, May-June 2000, doi: 10.1109/2943.838039.
- [149] I. Balabozov, "Prototype of a microcontroller system for defining joule integral of fuse," in *Electrical Engineering Faculty Conference (BULEF)*, Sozopol, Bulgaria, 2018, pp. 1-3, doi: 10.1109/BULEF.2018.8646920.
- [150] G. Parise, "The magic of the conductors current density in the time and in the space," *IEEE Industry Applications Society Annual Meeting*, Cincinnati, OH, 2017, pp. 1-6, doi: 10.1109/IAS.2017.8101875.
- [151] *IEEE Standard for calculating the current-temperature of bare overhead conductors*, IEEE Std 738-1993, Nov. 1993, doi: 10.1109/IEEESTD.1993.120365.
- [152] H. -P. Schmidt and G. Speckhofer, "Experimental and theoretical investigation of high-pressure arcs. I. The cylindrical arc column (two-dimensional modeling)," in *IEEE Trans. Plasma. Sci.*, vol. 24, no. 4, pp. 1229-1238, Aug. 1996, doi: 10.1109/27.536570.
- [153] E. Nasser, "Some physical properties of electrical discharges on contaminated-surfaces," *IEEE Trans. Power. App. Syst.*, vol. PAS-87, no. 4, pp. 957-963, April 1968, doi: 10.1109/TPAS.1968.292070.
- [154] M. Arrayás and J. L. Trueba, "Investigations of pre-breakdown phenomena: Streamer discharges," *Contemp. Phys.*, vol. 46, no. 4, pp. 265–276, 2005, doi: 10.1080/00107510500146733.
- [155] B. Babu and S. Divya, "Comparative study of different types of generators used in wind turbine and reactive power compensation" in "*Emerging Research Trends in Electrical Electronics & Instrumentation*" (ERTEEI'17), Mator, Kalady, Kerala, pp. 95-99, Mar 2017.
- [156] Y. H. Yuan; F. Wu, "Short-circuit current analysis for DFIG wind farm considering the action of a crowbar," *Energies*, vol 11, no 2, Feb., 2018, doi: 10.3390/en11020425.
- [157] B. Olejnik, "Selected protective algorithms of modern IED," *Computer Applications in Electrical Engineering*, vol. 11, pp. 389-395, 2013.

REFERENCES

- [158] T. S. Sidhu, M. S. Sachdev and H. C. Wood, "Design of a microprocessor-based overcurrent relay," *WESCANEX '91*, Regina, Sask., Canada, 1991, pp. 41-46, doi: 10.1109/WESCAN.1991.160517.
- [159] E. Sorrentino, "Behavior of induction disc overcurrent relays as a function of the frequency," *Electr. Power Syst. Res.*, vol. 143, pp. 474-481, 2017, doi: 10.1016/j.epsr.2016.10.059.
- [160] M. J. Slabbert, S. J. van Zyl and R. Naidoo, "Using let-through energy to determine the application of a high current lock-out function on MV feeders," presented at the Southern African power system protection conf., Jnb., Gauteng, RSA, Nov. 12-14, 2014.
- [161] J. Stewart, "Integrals", in *Calculus early transcendentals*, 4th ed. London, International Thomson publishing, England, 1999, pp. 367-376.
- [162] M. J. Slabbert, R. C. Bansal and R. Naidoo, "Application of let-through energy to back-up over-current protection on high-voltage feeders," *IET Generation, Transmission & Distribution*, vol. 12, no. 19, pp. 4341-4347, Oct., 2018, doi: 10.1049/iet-gtd.2018.6190.
- [163] R. C. Jaeger and T N. Blalock, "MOS memory and storage circuits," in *Microelectronic circuit design*, 2nd ed. New York, NY, USA: McGraw-Hill, 2003, ch. 8, pp. 551-554.
- [164] *IEEE Standard common format for transient data exchange (COMTRADE) for power systems*, in IEEE Std C37.111-1999, Oct. 1999, doi: 10.1109/IEEESTD.1999.90571.
- [165] M. J. Slabbert, R. Naidoo, and S. J. van Zyl, "Analysing the effectiveness of phase over current protection on overhead MV networks," presented at *PAC World Africa Conf.*, Cape Town, RSA, 30 July to 2 Aug, 2013.
- [166] M. J. Slabbert, R. Naidoo, and R. C. Bansal, "The application of let-through energy protection to the main and back-up protection elements on high voltage overhead feeders," presented at *CIGRE Conf.*, Paris, France, 26-31 Aug. 2018.

ADDENDUM A CASE STUDY INFORMATION

A.1 CASE STUDY 1 FEEDER DATA

The network information used for the network models of case study one in Chapter 6 are provided here. For case study 1 the network consisted of a single radial feeder. The feeder sequence impedance values are provided in Table A1.

Table A.1 Feeder sequence impedance values for case study 1.

Feeder	Length (km)	R1 (ohm)	X1 (ohm)	R0 (ohm)	X0 (ohm)
Feeder 1	20	9.096037	6.674832	12.04378	35.66912

A.2 CASE STUDY 2 FEEDER DATA

The network information used for the network models of case study two in Chapter 6 are provided here. For case study 2 the network consisted of five feeders. Each feeder's sequence impedance values are provided in Table A2.

Table A.2 Feeder sequence impedance values for case study 2.

Feeder	Length (km)	R1 (ohm)	X1 (ohm)	R0 (ohm)	X0 (ohm)
Feeder 1	20	9.096037	6.674832	12.04378	35.66912
Feeder 2	10	4.548018	3.337416	6.021892	17.83456
Feeder 3	20	9.096037	6.674832	12.04378	35.66912
Feeder 4	30	13.64406	10.01225	18.06568	53.50368
Feeder 5	20	9.096037	6.674832	12.04378	35.66912

A.3 CASE STUDY 1 FEEDER DATA

The network information used for the network models of case study three in Chapter 6 are provided here. For case study 3 the network consisted of five feeders. Each feeder's sequence impedance values are provided in Table A3.

Table A.3 Feeder sequence impedance values for case study 1.

Feeder	Length (km)	R1 (ohm)	X1 (ohm)	R0 (ohm)	X0 (ohm)
Feeder 1	20	9.096037	6.674832	12.04378	35.66912
Feeder 2	3	1.364406	1.001225	1.806568	5.350368
Feeder 3	20	9.096037	6.674832	12.04378	35.66912
Feeder 4	30	13.64406	10.01225	18.06568	53.50368
Feeder 5	20	9.096037	6.674832	12.04378	35.66912